JOURNAL OF APPLIED PHYSICS

JOURNAL OF APPLIED PHYSICS

Vol. 22, No. 12 DECEMBER, 1951

In This Issue

	Page
Contact Potential Variations on Freshly Condensed Metal Films at Low Pressures — Leland L. Antes and Norman Hackerman	1395
Volta Potentials of the Copper-Nickel Alloys and Several Metals in Air — Herbert H. Uhlig	1399
Technique for Preparing Beta-Ray Autoradiographs of Metals and Minerals — A. B. Michael, W. Z. Leavitt, M. B. Bever, and H. R. Spedden	1403
Ultrasonic Propagation in Liquids under High Pressures: Velocity Measurements on Water — Gerald Holton	1407
Propagation in a Compressible Fluid of Finite Oblique Disturbances with Energy Exchange and Change of State — Frederick W. Ross	1414
Studies in Nonlinear Vibration Theory — Stanley Fifer	1421
Critical Study of the Circuit Concept — Jesse Gerald Chaney	1429
Free Convection Heat Transfer from Electrically Heated Wires — Erich A. Farber	1437
Finite Difference Treatment of a Helium Cryostat Design Problem — Warren E. Henry	1439
Electron Microscopic Replica Studies of Porosity in Fused Iron Catalysts — J. T. McCartney and R. B. Anderson	1441
Method of Growing Single Crystals of Lead Telluride and Lead Selenide — W. D. Lawson	1444
General Theory of Electromagnetic Horns — A. F. Stevenson	1447
Exact and Approximate Equations for Wave Propagation in Acoustic Horns — A. F. Stevenson	1461
Evaporation Rate of Liquid Helium. I — Aaron Wexler	1463
Studies in Newtonian Flow. II. The Dependence of the Viscosity of Liquids on Free-Space — Arthur K. Doolittle	1471
Convection Currents in Porous Media. IV. Remarks on the Theory — F. T. Rogers, Jr., L. E. Schilberg, and H. L. Morrison	1476
Dosimetry of X-Rays and Gamma-Rays by Radiophotoluminescence — James H. Schulman, Robert J. Ginther, Clifford C. Klick, Raymond S. Alger, and Robert A. Levy	1479
Crystallographic Aspect of Slip in Body-Centered Cubic Single Crystals. II. Interpretation of Experiments — A. J. Opinsky and R. Smoluchowski	1488
Atomic Size Effect in the X-Ray Scattering by Alloys — B. E. Warren, B. L. Averbach, and B. W. Roberts	1493
Propagation of Disturbances in One-Dimensional Accelerated Electron Streams — L. D. Smullin	1496
Capacitance of a Circular Annulus — W. R. Smythe	1499
Letters to the Editor:	
Electron Diffraction Study on the Ordered Alloy Au_3Cu — S. Ogawa and D. Watanabe	1502
On the Reliability of Geiger-Counter Response at Moderately High Rates — L. G. Parratt and C. F. Hempstead	1502
Transmission of Hydrogen through Metals — H. B. Wahlin	1503
Method of Producing an Electric Current from Radioactivity — P. E. Ohmart	1504
New Point of View on Magnetic Losses in Anisotropic Bars of Ferrite at Ultra-High Frequencies — H. G. Beljers, W. J. van de Lindt, and J. J. Went	1506
On the Anomalous Magnus Effect — Itiro Tani	1506
Radioactive Tracers for Rapid Measurement of Cutting Tool Life — M. Eugene Merchant and E. J. Krabacher	1507
Deformation of Body-Centered Cubic Metals — E. A. Calnan and C. J. B. Clews	1508
On the Ratio of the Critical Shear Stresses — A. J. Opinsky and R. Smoluchowski	1508
Problem in Heat Conduction — William Squire	1508
Author Index to Volume 22	1509
Subject Index to Volume 22	1516
Index to Advertisers	xxxii

BOARD OF EDITORS

Elmer Hutchisson, *Editor*

Earle C. Gregg, *Assistant Editor*

Associate Editors

Howard H. Aiken
Lyle D. Borst
James Hillier
Leonard B. Loeb
W. James Lyons
Eric Reissner
Raymond J. Seeger
Frederick Seitz
Charles S. Smith

Publication of the American Institute of Physics

OFFICERS

George R. Harrison, *Chairman*
George B. Pegram, *Treasurer*

GOVERNING BOARD

J. W. Beams
C. Paul Boner
Wallace R. Brode
W. F. Fair, Jr.
S. A. Goudsmit
G. P. Harnwell
George R. Harrison
F. V. Hunt
Rudolph Kingslake
Paul Kirkpatrick
F. W. Loomis
J. R. Oppenheimer
George B. Pegram
I. I. Rabi
Duane Roller
Harold K. Schilling
Frederick Seitz
Francis G. Slack
John C. Steinberg

Consultant on Printing

Melvin Loos

ADMINISTRATIVE STAFF

Henry A. Barton, *Director*
Wallace Waterfall, *Executive Secretary*
Theodore Vorburger, *Advertising Manager and Assistant Treasurer*
Ruth F. Bryans, *Publication Manager*
Betty H. Goodfriend, *Assistant Secretary*
Eileen B. Neuberger, *Circulation Manager*
Kathryn Setze *Senior Accountant*

The Journal of Applied Physics, published monthly at Prince and Lemon Sts., Lancaster, Pa., is devoted to physics in its role as the science basic to other natural sciences and to the arts and industries. Previous to 1937 this publication was known as Physics. The Journal of Applied Physics publishes editorials and reviews, as well as technical papers of applied physics. Articles appearing in it are indexed regularly, according to their field, by Physics Abstracts, Chemical Abstracts, Engineering Index Inc., Industrial Arts Index, etc.

Manuscripts should be submitted to Elmer Hutchisson, Editor, Case Institute of Technology, Cleveland 6, Ohio. Unless otherwise stated, submission of a manuscript is a representation that it has been neither copyrighted, published, nor submitted for publication elsewhere. The authors' institutions are requested to pay a **publication charge** of $8 per page which, if honored, entitles them to 100 reprints without further charge. Instructions will be sent with galley proofs.

Subscriptions, renewals, and orders for back numbers should be addressed to the American Institute of Physics, 57 East 55 Street, New York 22, New York.

Subscription Price	U.S. and Canada	Elsewhere
To members of the American Institute of Physics and Affiliated Societies	$10.00	$11.00
To all others	12.00	13.00

Back Number Prices

Yearly back number rate when complete year is available: $10.00. Single copies: $1.00 each.

Changes of address should be sent to the American Institute of Physics; **corrected proofs** should be sent to the Publication Manager, American Institute of Physics. **Advertising rates** supplied on request. Orders, advertising copy, and cuts should be sent to the American Institute of Physics.

Entered as second class matter January 22, 1937, at the Post Office at Lancaster, Pennsylvania, under the Act of March 3, 1879. Accepted for mailing at the special rate of postage provided for in paragraph (d-2), section 34.40, P. L. & R. of 1948, authorized May 2, 1932.

Copyright 1951, by the American Institute of Physics.

Journal
of
Applied Physics

Volume 22, Number 12 December, 1951

Contact Potential Variations on Freshly Condensed Metal Films at Low Pressures*

LELAND L. ANTES† AND NORMAN HACKERMAN
Department of Electrical Engineering and Department of Chemistry, University of Texas, Austin, Texas
(Received May 7, 1951)

The reason for contact differences of potential is discussed. Since it is purely a surface phenomenon, subject to wide variation as the result of adsorbed and chemically combined surface layers, it is of interest to observe the change of contact potential as a function of time for various freshly evaporated metal films in high vacuums. The results thus obtained indicate characteristically different behavior for each of the six metals studied. Electrical resistance measurements made on similar metal films under similar conditions are correlated with contact potential measurements.

CONTACT difference of potential arises from a difference in the work functions of dissimilar metal surfaces. The work function is defined as the minimum energy required to liberate an electron from a surface at 0° Kelvin. The potential barrier which the electron must overcome is created by the discontinuous array of positive ions at the surface. When two metals are brought into electrical contact, this discontinuity is practically eliminated over the contact area and electrons are exchanged freely. The difference in internal affinity for electrons displayed by two dissimilar metals results in a net shift of charge until the potential difference between the two metals becomes equivalent to the difference in work functions, resulting in an equilibrium. The potential difference which now exists between the free surfaces of the two metals may be measured by electrostatic means and is known as the contact difference of potential.[1]

The measurement of this potential difference is usually complicated by the effects of adsorbed or chemically combined atoms or molecules on the surface which create a potential sheath exhibiting a work function different from that of the pure metal.[2,3] However, a metal film condensed from evaporated molecular rays in "vacuum" should present a perfectly clean surface. In experiments using different common metals and performed inside the bell jar of a commercial high vacuum machine, it has been found that the effect of spontaneous surface contamination quickly alters the contact potential even at pressures as low as 0.01 micron of Hg. Furthermore, the time function of the

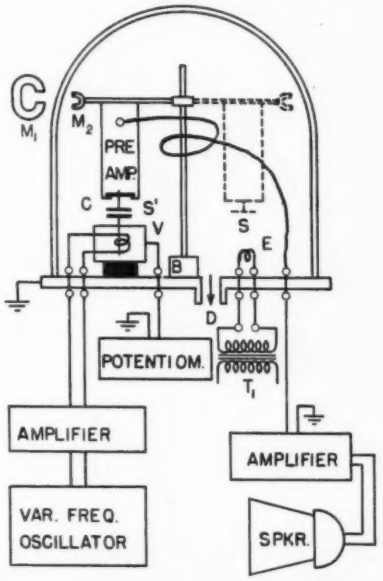

FIG. 1. Schematic representation of apparatus used to produce evaporated metal films and to measure their contact potential *vs* platinum (see text for explanation of symbols).

* Based in part on a dissertation by Leland L. Antes, presented to the faculty of the graduate school of the University of Texas in partial fulfillment of the requirements for the degree of Doctor of Philosophy.

† Now Acting Director, Optical Research Laboratory, Department of Physics, University of Texas.

[1] N. K. Adam, *The Physics and Chemistry of Surfaces* (Oxford University Press, London, 1941), third edition.

[2] Fred B. Daniels and M. Y. Colby, Phys. Rev. **52**, 1200 (1937).

[3] E. Dubois, Ann. Phys. **14**, 627 (1930).

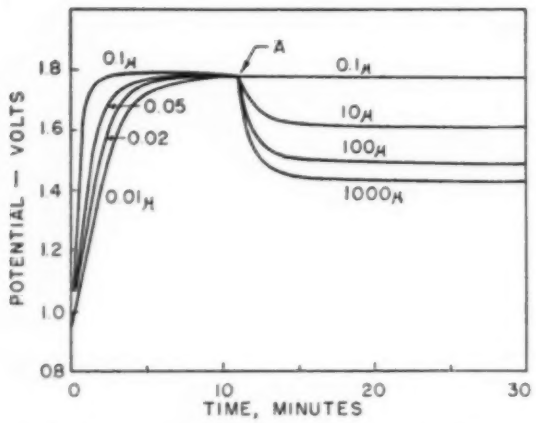

FIG. 2. Contact potentials of aluminum films at pressures shown. Air was admitted at "A."

contact potential change is characteristic of each metal.

The apparatus used for making the determinations in vacuum is schematized in Fig. 1. The metal film to be tested was condensed on the surface S, while this surface was positioned over the evaporating filament E. The test film and connected preamplifier were then immediately swung in place over the vibrating plate V. The two plates then formed a condenser, C. Magnets M_1 and M_2 were used to move S into the desired position, E is the heated filament for metal evaporation, T_1 is the transformer, D is the connection to the vacuum system, and B is the bearing on which the rod holding S pivots.

The vibrating plate was of platinum and served as a standard of reference, because platinum was found to have a very stable surface potential. The potentiometer was used to vary the potential of the platinum plate. When its potential was the same as the surface potential of the test film S, there could be no charge on the condenser, and the continuous variation in capacitance could cause no change in voltage. This furnished a null method of determining the surface potential difference using a vacuum tube amplifier and loud speaker. The useful accuracy of measurement was ±5 mv. This method of measurement was first publicized by Zisman.[4]

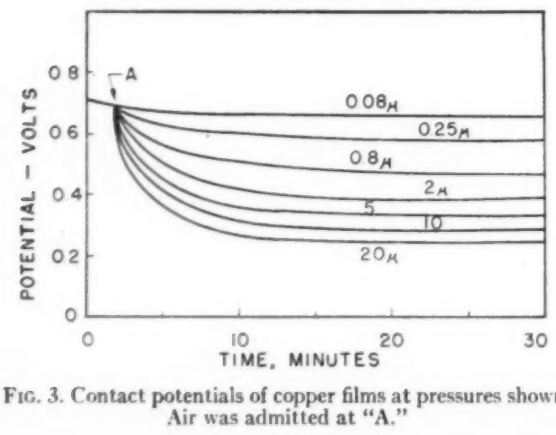

FIG. 3. Contact potentials of copper films at pressures shown. Air was admitted at "A."

Families of curves showing variations of potentiometer bucking potential as a function of time at various pressures for the metals aluminum, copper, gold, nickel, iron, and chromium are presented in Figs. 2 through 7. It should be emphasized that an increase in potential as plotted represents a decrease in work function. These curves show in "slow motion" the initial steps by which oxidation of a clean metal surface proceeds. When the pressure is raised and lowered, partial reversibility of the surface potential is always found, as illustrated by Fig. 6 (center) for an iron film. This indicates that a portion of the molecules on the surface were physically adsorbed, and that they were only slightly adherent and did not rest long on their landing sites, because lowering the number of contacts per unit area by lowering the pressure resulted in a net reduction of the absorbed layer. At the same time, a fraction of the oxygen molecules found and occupied sites of a more permanent nature, either by direct hits or by migration, as evidenced by the incomplete reversibility of surface potential as a function of pressure. Figure 6 (lower) shows the result of applying higher pressures to an iron film. The effect of 99.9 percent pure nitrogen was shown to be comparatively negligible at the same pressures.

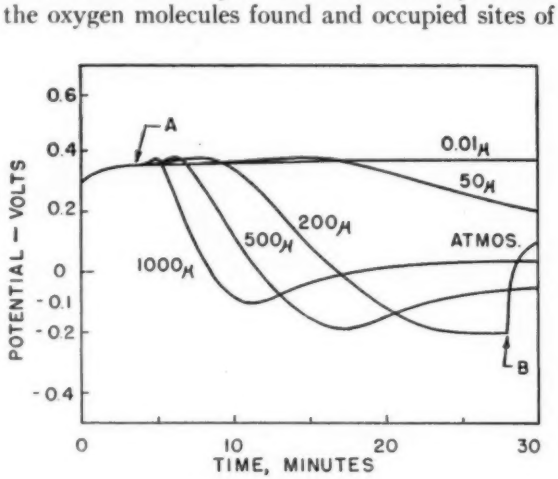

FIG. 4. Contact potentials of gold films at pressures shown. At "B" air was admitted to atmospheric pressure.

ALUMINUM AND COPPER

The reaction of aluminum is quite different from that of copper, as may be seen from Figs. 2 and 3. The affinity of aluminum for oxygen is initially very great. It is assumed that the knee in the curves is the result of complete coverage of the surface area by a monolayer of oxygen molecules. Beyond the knee, where the curves become flat at low pressures, it is supposed that the diffusion rate of the oxygen into the metal is rapid enough to preserve the same surface conditions over a considerable period. This supposition is supported by

[4] W. A. Zisman, Rev. Sci. Instr. 3, 367 (1932).

the rapid and continuous increase in the electrical resistance of very thin aluminum films at the same low pressures. The point of interest, however, is the fact that the work function for aluminum is decreased initially, as shown by a rise in bucking potential, which is to say that the effective potential barrier discouraging the escape of electrons has been lowered by the adsorption of oxygen. The oxygen molecule evidently becomes strongly polarized during this stage, extending electrons elastically toward the aluminum surface, and at the same time partially baring at least one positive nucleus so that the oxygen surface potential is more positive than that of the metal.

At the point *A* on the potential curves for aluminum at low pressures, the effect of suddenly raising the pressure is shown. At higher pressures, or after longer periods of time, the diffusion rate becomes insufficient to remove the oxygen which has passed through the stage of physical adsorption, ionization, and combination with the ions of aluminum. Under this condition

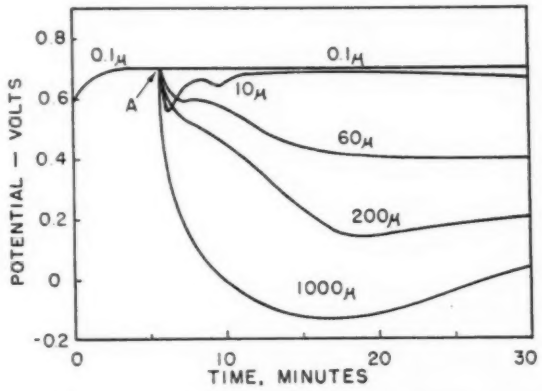

FIG. 5. Contact potentials of nickel films at pressures shown. Air was admitted at "A."

of increasing aluminum oxide concentration on the surface, the work function increases. This is the usual result of an oxidized layer on a metal surface. The process of oxidation and diffusion may be augmented by the presence of water vapor.

With copper, the initial rise in potential, or decrease in work function, was not observed as in the case of aluminum and the other metals, suggesting that strong polarization of the oxygen molecule prior to chemisorption and chemical combination was virtually nonexistent. At point *A*, again, the effect of suddenly raising the pressure a short time after deposition of the film is shown. In common with the other metal films, copper exhibited the usual reversibility of potential with pressure decrease which has been attributed to physical adsorption.

One is urged to the conclusion that the initial binding forces between the copper ions and the oxygen are, besides being of lesser magnitude, different in nature from those existing between aluminum and oxygen.

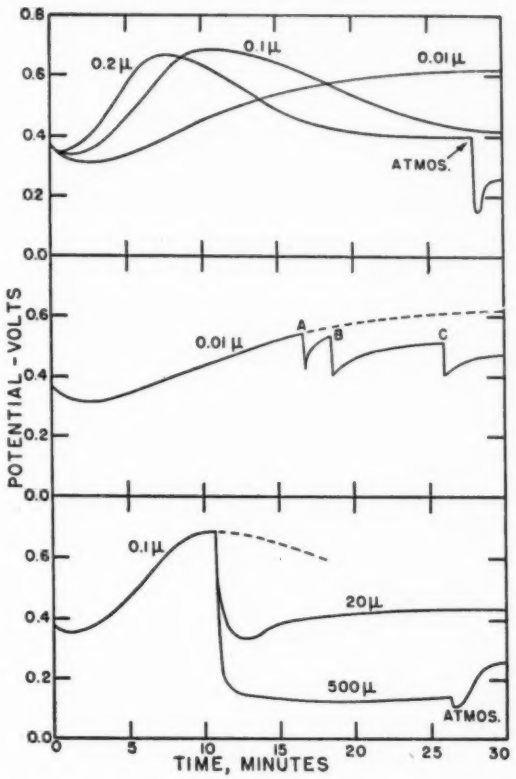

FIG. 6. Contact potentials of iron films. At A, B, C, pressure was 10μ for 15 seconds.

The similarity of the copper characteristics to those of the aluminum after the initial potential rise in the case of aluminum is the main evidence to support the theory that the process by which aluminum binds the oxygen initially is either missing or of very short duration in the reaction of copper and oxygen. The copper evidently combines with the oxygen without first polarizing the oxygen molecule in the manner envisioned for aluminum.

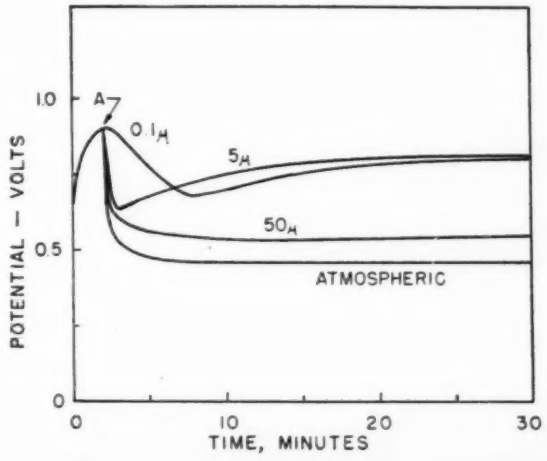

FIG. 7. Contact potentials of chromium films at pressures shown. Air was admitted at "A."

These explanations seem to be in agreement with the basic ideas presented by Mignolet[5] in his discussion of the sorption of various gases on nickel.

GOLD AND NICKEL

At the best vacuums attained, both gold and nickel, after a slight initial rise, showed little change of contact potential, as shown in Figs. 4 and 5. With the admission of higher pressures as indicated, it is evident that similar reactions occurred. Gold, as might be expected, shows a lower reaction rate than nickel, and it is noticeable that the direction of the change in potential immediately after raising the pressure is positive for gold and negative for nickel, but the significance of the difference is unknown. The peculiar double-hump characteristic of the nickel curves at different pressures indicates a more complicated type of reaction than that affecting gold. One may speculate that the concentration of the adsorbed layer is largely responsible for the rate of diffusion and combination but that the time required for some steps in the process may be more or less definite and independent of pressure, so that peculiar potential variations are produced.

Gold films exhibited the greatest reversibility of potential with reduction of pressure, and at any point on the curve prior to long exposure to atmospheric pressure, continued pumping would produce up to 0.2 volt change in surface potential. This is the extreme example of physical adsorption.

Nitrogen up to 200 microns pressure produced no appreciable effect on either gold or nickel films. However, Mignolet,[5] has reported 0.2 volt change in potential for N_2 on Ni at $-196°C$ in the same pressure range.

IRON AND CHROMIUM

Iron and chromium both proved to be quite capricious, experimentally. Considerable difficulty was encountered in reproducing results under seemingly similar conditions. Both were profoundly pressure sensitive, but beyond this it was evident that some obscure factor was responsible for the variation in results, particularly with iron. Figure 6 is typical of averages of the results obtained from iron films, and Fig. 7 gives typical results from chromium. With all of the curves obtained, there is a rapid rise, followed by a slower fall and a still slower partial recovery. As has proved to be the case with all the metal films tested a minimum potential is reached during the reaction process which is lower than the potential in the final, fully oxidized state. The general tendency to overshoot the final minimum may be due to the lack of sufficient diffusion time, under a condition of high oxygen concentration on the surface which results in interference with the required orientation of the oxygen molecules necessary to effect combination with the metal. Also, as usual, no particular effects were noted when nitrogen was admitted to moderate pressures, showing that oxygen is the main affinity of these films when exposed to air.

ELECTRICAL RESISTANCE VARIATIONS

Electrical resistance measurements were made on similar metal films at comparable pressures. With 20A aluminum films, the resistance rise was continuous and rapid at a pressure of 0.06 micron, supporting the theory that rapid oxygen diffusion takes place. A few of the films, and gold in particular, exhibited a negative resistance-time characteristic. This has usually been explained as molecular reorientation, and this it may well be. Such a reorientation should not be expected to affect the contact potential greatly, in view of the minute potential variations reported for different faces of metal-crystals of the kinds used in these experiments. Resistance stability has been reached in all the metals tested within about two minutes, using film thicknesses of 100A or more and vacuums at least as good as 10^{-4} mm of Hg. This indicates that the contact potential effects measured at such low pressures are due to surface conditions which do not penetrate appreciably into the metal film, because, with the exception of gold, almost no change in resistance was found with these thick films.

CONCLUSION

It seems likely that contact potential measurements offer a powerful tool for the study of the fundamental processes involved in the adsorption and combination of oxygen, and possibly other reactive gases, by metal surfaces. The fact that each kind of metal exhibits a characteristically different potential curve seems to offer proof that each metal possesses differences in ionic structure. The extension of this work to include all metals should lead to certain generalizations and correlations with atomic surface layer characteristics.

[5] J. C. P. Mignolet, Disc. Faraday Soc. **8**, 326 (1950).

Volta Potentials of the Copper-Nickel Alloys and Several Metals in Air

HERBERT H. UHLIG
Department of Metallurgy, Massachusetts Institute of Technology, Cambridge, Massachusetts
(Received April 8, 1951)

Volta potentials of various metals approximately parallel the emf series. Metals abraded wet are more noble than when abraded dry, the transition metals changing an average of 0.28 volt compared with 0.07 volt for the nontransition metals. This owes possibly to the greater tendency of the transition metals to chemisorb oxygen, especially in the presence of moisture. All metals change in the noble direction upon aging in air, the average value being 0.3 volt after six days.

Potentials for copper-nickel alloys, plotted with composition, fall on a sigmoid curve, whereas potentials for composite electrodes made up of separate nickel and copper areas are linear with percent area of nickel exposed. Commerical nickel-copper alloys above 50 percent nickel age more rapidly than laboratory alloys. The cause may lie in deoxidizers like magnesium or aluminum, present in commercial alloys, but absent in the laboratory alloys. This suggests a nondestructive method for detecting impurities of this kind in metals.

THE Volta potential or contact potential of two metal surfaces is essentially the difference in work functions. In the same sense, as the thermionic or photoelectric work function is sensitive to substances on the surface, the Volta potential is also sensitive to presence of surface oxides and gases. For example, the completion of a monolayer of adsorbed oxygen on tungsten changes the work function, and hence the Volta potential of tungsten in the order of volts.[1] Since measurements of the Volta potential, described herewith, can be made to ± 0.001 volt, changes on the surface of as little as 1/1000 of a monolayer of adsorbed substance can therefore be detected. This is an advantage from the standpoint of following small surface changes, but also a disadvantage because small changes, difficult to avoid experimentally, produce large fluctuations of potential. Surface preparation, except under high vacuum conditions, is seldom reproducible in Volta potential to better than ± 0.01 volt and variations are sometimes 5 to 10 times this value. Notwithstanding, much useful information can be gained by data reproducible within this range. In this paper, for example, it is shown that Volta potential measurements in air can reliably, and consistently, differentiate between many metals of the Periodic Table. Also, effects of electronic interaction between nickel and copper in alloys of these metals can be detected and reproduced. Furthermore, it is shown that the Volta potential, as usually measured, is an average of surface phases weighted in accord with the area of each phase exposed.

METHOD OF MEASUREMENT

The vibrating condenser method of measurement was used, essentially as described by Zisman,[2,3] supplemented by the use of an oscilloscope as null point indicator, and a filter circuit to increase sensitivity of measurement. An outline of the circuit is given in Fig. 1. We used a Burgess "Vibrotool" as a convenient source of 120-cycle vibration. Either the unknown or the reference electrode was vibrated, the reference electrode being abraded and aged platinum. Gold and silver were also used occasionally, but platinum seemed to change less with time and was more reproducible, as judged by comparison with freshly abraded copper and silver electrodes, employed as standards. If potentials of the reference electrode changed with respect to the latter electrodes, it was assumed that the reference electrode had shifted, since in general the difference in potential of the freshly abraded copper and silver, using a standardized abrading technique, remained reasonably constant from day to day. Despite frequent standardization of this kind, one of the inherent difficulties of Volta potential measurements lies in the lack of a good reference electrode constant to within 0.01 volt or better.

The reference electrode measured one inch square and the unknown electrodes from $\frac{1}{2}$ inch to 1 inch square. Three levelling screws mounted within a Bakelite holder made it possible to parallel accurately the lower electrode with respect to the upper. In addition, the entire levelling device holding the lower electrode could be raised or lowered by means of a precision screw. In operation, the bottom electrode was placed to within 0.01 to 0.005 inch from the top electrode, then the top electrode vibrated. The closer the electrodes the greater the input to the amplifier. Varying the separation sometimes produced a change in Volta potential difference amounting to an increase or decrease of as much as 0.05 volt, but the effect was minimized or eliminated by careful surface preparation, and by making certain the plates of the condenser were parallel.

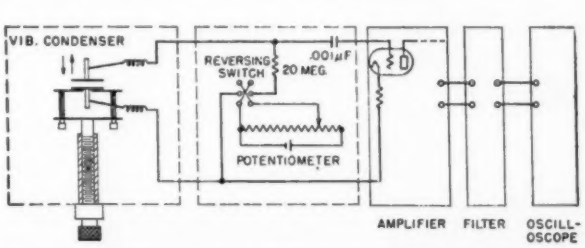

FIG. 1. Sketch of apparatus for measuring Volta potentials.

[1] I. Langmuir, Phys. Rev. **2**, 402, 450 (1913).
[2] W. A. Zisman, Rev. Sci. Instr. **3**, 367 (1932).
[3] W. A. Zisman and H. G. Yamins, Physics **4**, 7 (1933).

TABLE I. Comparison of Volta potentials for abraded surfaces and evaporated films measured immediately in air *vs* Pt.

	Abraded 00 paper, washed benzene	Evaporated films on glass, no further treatment
Cu	0.35	0.34
Fe	0.49	0.46
Ag	0.14	0.21
Al	1.29	1.47

The ac component of the potential across a 20 megohm resistor, generated by the vibrating condenser, was amplified, then passed through a filter designed to amplify a narrow band of low frequencies by a factor of about five while attenuating all others. The amplified and filtered signal was then impressed on the oscilloscope. When the potentiometer exactly compensated the Volta potential difference, the sine wave deflection on the oscilloscope disappeared.

External electrical interference was minimized by mounting the condenser and potentiometer inside grounded metal boxes. In addition, ac power lines to the amplifier passed through a static-elimination filter. Unless external disturbance was excessive, as produced for example by a 15 kw spark-gap oscillator nearby, the electrical circuits performed without trouble. With this arrangement, the Volta potential could be measured to within ± 0.001 volt.

The copper shield surrounding the vibrating condenser was also employed to maintain a controlled atmosphere. Most measurements reported herein, were obtained in a continuous stream of air dried over $CaCl_2$, thereby avoiding the variable effects on potential produced by changes in humidity.

SURFACE PREPARATION

Surface preparation, as mentioned previously, was the most important factor from the standpoint of reproducibility, and least satisfactory of all variables requiring control. Most of our data were obtained for surfaces abraded with numbers 1, 0, and 00 emery paper, followed by swabbing with cotton soaked in benzene, and then washing in several beakers of distilled benzene. For some measurements, specimens were abraded under water using water-proof emery paper 600A. The latter specimens were then washed under the distilled water tap, dried in a stream of air previously passed over $CaCl_2$, and immediately measured, or placed in a glass jar containing air of 100 percent relative humidity. Filing of the specimens was also tried without a subsequent benzene wash, giving some evidence of better reproducibility than abrading. This bears out conclusions reached by Ende.[4] We also confirmed Ende's conclusion that pickling a metal surface causes rather large fluctuations of potential.

The effect of embedded emery on our results was not too serious judging from the proximity of Volta potentials for a few films produced by evaporation in vacuum to similar potentials for abraded specimens. Comparative data are shown in Table I.

TABLE II. Volta potential series in air *vs* Pt volts.

Metal	Source	Abraded 00 paper, washed benzene, aged desiccator 1 hr	Abraded wet, aged over water 1 hr	Difference
Mg	Distilled Dow	1.51	1.67	−0.16
Be	Lab.	1.45	1.21	0.24
Al	Reynolds High Purity	1.16	1.08	0.08
Zr	Bur. Mines	1.10	0.56	0.54
Tl	Lab.	1.09	1.07	0.02
Zn	Commercial	1.08	0.92	0.16
Pb	High Purity	0.79	0.69	0.10
Sn	High Purity	0.69	0.66	0.03
Ti	Bur. Mines (1 Meas.)	0.69	0.50	0.19
Ta	Fansteel	0.63	0.32	0.31
Mn	Electrolytic	0.66	0.45	0.21
Ni	Electrolytic	0.61	0.39	0.22
Cr	Electrolytic	0.58	0.59	−0.01
18–8	Commercial	0.46	0.13	0.33
Fe	Electrolytic	0.44	0.16	0.28
U	Lab.	0.44	0.21	0.23
Mo	Lab.	0.39	0.02	0.37
Hg	Lab. (1 Meas.)	0.29	...	...
Cu	Commercial	0.27	0.12	0.15
Au	Commercial	0.16	0.13	0.03
Ag	Commercial	0.08	0.02	0.06
Pt	Lab.	0.00	−0.16	0.16

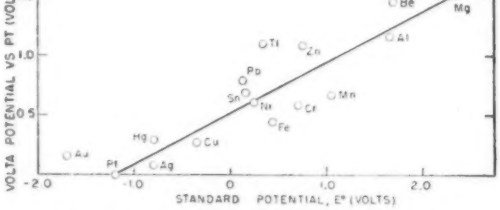

FIG. 2. Relation of Volta series in air *vs* Pt, to emf series for various metals.

VOLTA SERIES

Table II lists values obtained for various metals with respect to a platinum reference electrode. In general, data were averaged for two to six sets of measurements obtained on different days with exceptions as specified. The metals, including the platinum reference electrode, were abraded, as previously described, finishing with 00 emergy paper. Reproducibility of measurements was frequently ± 0.01 volt but sometimes as poor as ± 0.06 volt, the variations reflecting not only changes in value for the metal, but also possible changes in the platinum reference electrode. The second series of measurements was obtained for metals abraded under water with water-proof emery paper. A platinum electrode abraded dry as above was again used as reference. Maximum variations for this series reached ± 0.1 volt.

Volta potentials for metals abraded in air show some degree of correspondence with the standard potentials of the usual emf Series as shown in Fig. 2. Since the emf Series for metals also parallel, to some extent, the order of metals arranged according to work function values, and according to the first ionization potentials,

[4] W. Ende, Physik. Z. **30**, 477 (1929).

as shown by Michaelson,[5] the Volta series in air also show a general correspondence to the latter data.

It appears that abrading metals wet produces a more noble potential compared with metals abraded dry. Magnesium is the outstanding exception. Interesting is the fact that the transition metals, defined as metals with unfilled *d* electron levels, show a greater difference in this respect than the nontransition metals. The average difference for 10 transition metals of Table II is 0.28 volt, whereas for 10 nontransition metals the value is 0.07 volt. Chromium appears to be the only transition metal showing no change, however abraded. This may indicate an unusually stable surface film unaffected by moisture. It was the only metal of the series which behaved in this manner.

Upon aging metal electrodes in dry air, potentials tend toward more noble values. This confirms previous observations.[6,7] For electrodes in a desiccator six days, the average Volta potential decreases toward the value of platinum to the extent of about 0.3 volt. The average change is the same for both transition and nontransition metals (0.28 *vs* 0.26 volt).

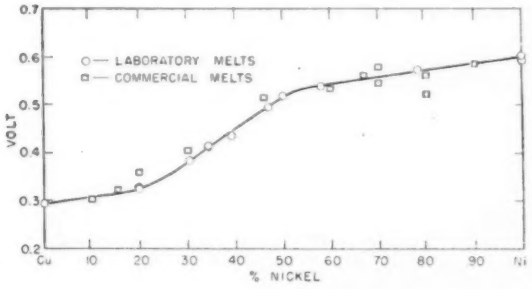

FIG. 3. Volta potentials of copper-nickel alloys *vs* platinum.

THE COPPER-NICKEL ALLOYS

Volta potentials for the copper-nickel alloy series prepared in the usual way with 00 emery are given in Fig. 3. Some of the alloys were laboratory melts, starting with high purity copper and carbonyl nickel, the latter supplied through the courtesy of The International Nickel Company. They were melted and cast in a vacuum furnace using alundum crucibles and a steel mold. After an homogenizing heat treatment, the alloys were rolled and annealed, then cut into sizes suitable for electrodes. Included with measurements of these were commercial sheets of special melts made available by the International Nickel Company. Values compared favorably with the laboratory melts when the electrodes were abraded dry. However, abraded wet and aged over water, the commercial alloys containing more than 50 percent nickel changed in a noble direction to a greater extent than did the laboratory melts. This characteristic behavior often made it possible to pick

[5] H. B. Michaelson, J. Appl. Phys. **21**, 536 (1950).
[6] E. Dubois, Ann. phys. **13–14**, 627 (1930).
[7] H. Neuert and H. Hansel, Z. Angew. Phys. **8**, 319 (1950).

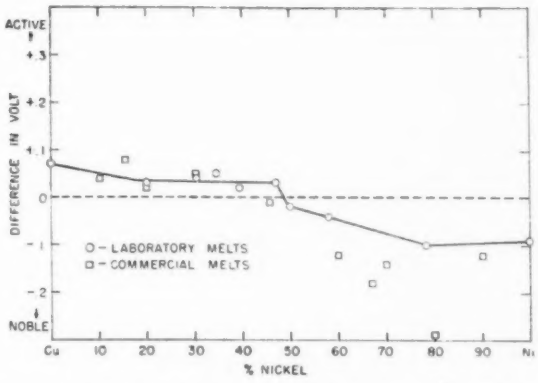

FIG. 4. Change in Volta potentials of copper-nickel alloys aged over water for 1 hour and similarly for 48 hours.

out such alloys according to their source, making use of aging characteristics summarized in Fig. 4. On the whole, the distinction applied only to alloys above 50 percent nickel. Commercial and laboratory alloys under 50 percent nickel, abraded, wet became slightly more active on aging in moist air.

COMPOSITE ELECTRODES

The specific shape of the curve in Fig. 3 was reproduced many times and is considered characteristic of the copper-nickel alloys whether of commercial origin or laboratory purity. The characteristic point of inflection occurs with freshly abraded or aged electrodes. However, Volta potentials of composite electrodes with various area ratios of pure copper to pure nickel vary *linearly* with percent area of nickel exposed. Figure 5 shows this linear relationship for electrodes abraded dry and aged one hour in a desiccator, and also depicts the actual appearance of the electrodes of composite parts soldered together. For example, at 50 percent, two electrodes were used, one for which half the area was nickel and half copper, and a second electrode made up of narrow alternate strips of copper and nickel, again of equal total areas. Both electrodes displayed the same Volta potential within 0.02 volt. The null point for a

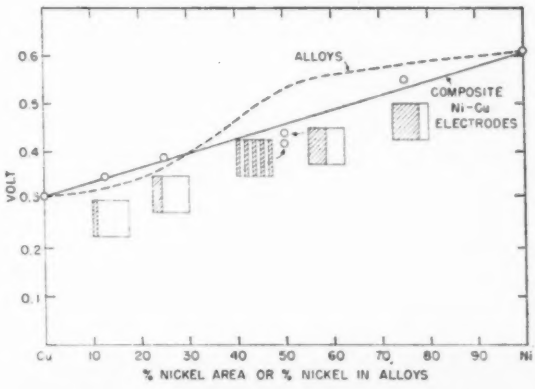

FIG. 5. Volta potentials of composite electrodes of nickel and copper of various area ratios *vs* platinum.

composite electrode was similar to that for a pure metal, in other words, a single sharp value was obtained and not two hazy values. This behavior is expected from previous discussions of the subject in the literature[8] namely, that the measured Volta potential is an average over all the surfaces exposed, weighted in accord with their respective areas. This situation differs from that in electrolytes where the ultimate measured or "corrosion" potential of a composite surface is determined not only by the areas but also by the polarization characteristics of the respective surfaces. It also differs from the situation for the measured thermionic or photoelectric work function which normally exaggerates areas of lowest work function values.

DISCUSSION

Table II shows zirconium to be apparently one of the most active of the transition metals in the Volta series. Its position next to zinc, however, may be the result of impurities (e.g., traces of magnesium, calcium, and aluminum) since a second small sample of high purity metal produced by the Iodide process gave a value more noble by 0.2 volt. This illustrates the extreme sensitivity of Volta potential measurements not only to surface contamination but also to traces of impurities within the metal. The effect may be similar to the well-known influence of the alkali and alkaline earth materials in lowering the work function of tungsten.

The impurities common to zinc, on the other hand, appear to exert an opposite effect. High purity zinc obtained through the courtesy of the New Jersey Zinc Company, abraded dry and aged 1 hour (total iron, cadmium, and lead content <0.0002 percent) gave a value of 1.19 volt compared with 1.08 volt for commercial zinc, the latter being more noble by 0.11 volt.

Amalgamated copper and zinc electrodes were also investigated, the electrodes being prepared by dipping into a solution of mercuric nitrate and nitric acid, then washed in water, followed by acetone. Potentials started out with values appreciably different from mercury. Thirty seconds after washing in acetone, the value for amalgamated copper was 0.45 volt *vs* platinum as reference; three minutes later the value was 0.30 volt, marking a trend in the *noble* direction of 0.15 volt. Five days later the Volta potential was found noble by an additional 0.1 volt. The initial value for amalgamated zinc, on the other hand, was 0.95 volt, with no significant change after three minutes. At the end of five days, the value was 1.18 volts marking a trend in the *active* direction of 0.23 volt.

The more pronounced change in potential of the transition metals (e.g. Fe, Mo, Ni, etc.) when abraded under water is probably associated with the tendency of this group of metals to adsorb, or more accurately, chemisorb oxygen. A chemisorbed film of negative oxygen ions can account for the observed change in noble direction; chemisorption, in turn, may be stimulated by the presence of water. Oxidation of metals at the local high temperatures produced by abrasion may also play a part, since oxides are typically more noble than metals. However, in general, the transition metals oxidize less readily at a given temperature than the nontransition metals but chemisorb substances more readily, therefore the factor of surface oxides in accounting for the observations may be less important than adsorbed films.

Pronounced adsorption of water alone on the metal surface is not a plausible reason for the observed noble behavior after wet abrasion because Dubois[6] showed that Volta potentials of metals in vacuum, brought into contact with water vapor, change in the *active* direction. On the other hand, contact with oxygen at room temperature, he found, changed the Volta potential in the noble direction (for iron as much as 0.34 volt). It seems reasonable, therefore, that the effect illustrated by data of Table II is explained by the increased chemisorption of oxygen on the transition metals aided by water. On the nontransition metals (e.g., Cu, Sn, Zn, etc.) chemisorption of oxygen usually is less pronounced or does not occur at all because of immediate chemical reaction to form oxides (zero activation energy for reaction). Hence these metals, on the average, are expected to change less with variation of abrading technique, as observed.

The characteristic shape of potentials for the copper-nickel alloys compared with a linear dependence for composite electrodes indicates an effect of alloying either on the work function of the alloy or on the total electric moment per unit surface area. This means that in the general expression for the work function:

$$\varphi = \varphi_0 \pm 4\pi n\mu$$

effect of alloying is on φ_0, the work function of the metal, or on n, the number of dipoles per unit area, or on μ, the normal component of electric moment for each dipole. It seems likely, since oxygen normally absorbs rapidly in multilayers, that the effect of alloying would be either on φ_0 or μ, rather than on n.

The point of inflection of Fig. 3 falls in the neighborhood of 40 percent nickel which may be ascribed to a change in electronic states at this approximate composition. Mott and Jones[9] pointed out that below 40 percent nickel, the d band of electronic energy states is filled, whereas above 40 percent nickel the d band is not filled. Presumably without an electronic change of this kind the Volta potentials of the copper-nickel alloys would vary linearly with composition instead of according to the nonlinear dependence shown in Fig. 3. Hence the present data may be taken as evidence for such interaction.

[8] K. T. Compton and I. Langmuir, Revs. Modern Phys. **2**, 145 (1930).

[9] N. Mott and H. Jones, *The Theory of the Properties of Metals and Alloys* (Oxford University Press, London, 1936), p. 196.

The difference in aging characteristics of commercial alloys compared with laboratory alloys may be caused by impurities, the exact nature of which is as yet unknown. Deoxidizers, such as magnesium and aluminum, for example, were probably used in melting and casting the commercial alloys, but were not used in the laboratory melts. Whether impurities in this instance affect chemisorption of oxygen, or the rate of chemical combination of alloy components with oxygen to form metal oxides, is not apparent from the present limited information. This point is being explored further with laboratory alloys to which controlled small amounts of impurities are added. The effect of impurities, once established, may have bearing on the mechanism of initial oxidation rate, as well as suggesting a simple nondestructive means, through measurements of the Volta potential, for detecting specific classes of impurities.

ACKNOWLEDGMENT

Assistance in the experimental program by Michael J. Moravcsik, and financial support both by the Office of Naval Research on contract N5ori-07815 and by the Research Corporation are gratefully acknowledged.

JOURNAL OF APPLIED PHYSICS VOLUME 22, NUMBER 12 DECEMBER, 1951

A Technique for Preparing Beta-Ray Autoradiographs of Metals and Minerals

A. B. Michael, W. Z. Leavitt, M. B. Bever, and H. R. Spedden
Massachusetts Institute of Technology, Cambridge, Massachusetts

(Received May 18, 1951)

A technique for preparing autoradiographs of metals and minerals on a microscale is described. Limitations of this technique and possible variations are indicated. Illustrative examples of autoradiographs are presented and interpreted.

THE usefulness of autoradiography for the solution of problems in metallurgy[1–4] and mineralogy[5–8] is gradually being established but several factors have retarded the development of this technique. For most microstructural investigations work on a sufficiently small scale was not possible in the past because adequate resolution could not be obtained. The difficulties of preparing the required thin sections and of applying thin photographic emulsions to such sections also tended to delay this application. Finally, autoradiography depended on the ready availability of radionuclides for preparing synthetic materials or on the possibility of rendering constituents of metallic systems or of naturally occurring minerals radioactive by nuclear bombardment.

Beta-ray autoradiography has been successfully used in the field of biology.[9–11] Knowledge of the technique has also been advanced by a detailed treatment in a monograph[12] and by an analysis of the problem of obtaining high resolution.[13] A thorough review of the entire subject has appeared recently.[14] As a result of these developments it is known that the successful use of the microautoradiographic technique depends on the following requirements:

(1) a thin section of a specimen having suitable radioactive properties; (2) a sufficiently sensitive and fine-grained emulsion, which should also be thin for maximum resolution; (3) close proximity of the emulsion and the specimen during exposure; (4) a separating inert layer between the specimen and the emulsion to prevent chemical fogging of the emulsion and chemical attack of the specimen.

The work reported here was undertaken in an effort to develop a technique of beta-ray autoradiography for the study of metals and minerals on a microscale. The unique features of the new technique are mainly the procedure for manipulating the film and the method of examining the finished microautoradiograph. The technique produces autoradiographs which remain superimposed upon the samples; under favorable conditions an autoradiograph can be compared directly by refocusing with the structure observed by metallographic or petrographic microscopy.

[1] G. Tammann and G. Bandel, Z. Metallkunde **25**, 153–156 and 207–209 (1933).
[2] W. Seith and A. Keil, Z. Metallkunde **26**, 68–69 (1934).
[3] United States Atomic Energy Commission: Fourth Semi-Annual Report, pp. 114, 119 (1948).
[4] A. Kohn, Rev. mét. **48**, 219–235 (1951).
[5] C. Goodman and D. C. Picton, Phys. Rev. **60**, 688 (1941).
[6] C. Goodman and C. A. Thompson, Am. Mineral. **28**, 456–467 (1943).
[7] M. R. Coppens, "Etude de la radioactivité de quelques roches par l'émulsion photographique," thesis, University of Paris (Masson et Cie, Paris, 1949).
[8] L. R. Stieff and T. W. Stern, "The preparation of nuclear-track plates and stripping films for the study of radioactive minerals," United States Geological Survey TEI Rept. 127 (August, 1950).
[9] G. A. Boyd and A. I. Williams, Proc. Soc. Exp. Biol. Med. **69**, 225–232 (1948).
[10] G. A. Boyd and F. A. Board, Science **110**, 586–588 (1949).
[11] R. H. Hertz, Med. Radiography and Photography **26**, No. 2, 46–51, 84 (1950).
[12] H. J. Yagoda, *Radioactive Measurements with Nuclear Emulsions* (John Wiley and Sons, Inc., New York, 1949), IX and 356.
[13] I. Doniach and S. R. Pelc, Brit. J. of Radiology **23**, 184–192 (1950).
[14] Gross, Bogaroch, Nadler, and Leblong, Am. J. of Roentgenol. Radium Therapy **65**, 420–458 (1951).

INTRODUCTION OF RADIOACTIVITY INTO THE SPECIMEN

Radioactive nuclides for autoradiography may be incorporated by chemical synthesis, for example by melting of an alloy, or they may derive *in situ* from irradiation with neutrons or deuterons. In the work reported all samples were irradiated in the finished state. In this way all operations prior to the final autoradiographic exposure are carried out on a sample which is not radioactive. The autoradiographic technique described here, however, would be equally applicable to materials in which radioactive nuclides are present prior to the preparation of thin sections, but in this case proper additional safeguards would be required to prevent contamination and health hazards.

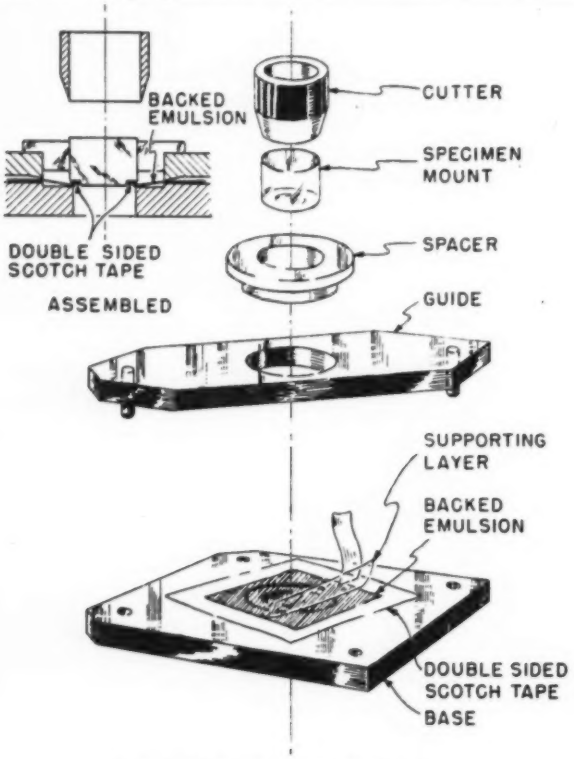

FIG. 1. Diagram of mounting fixture.

Some of the samples used in this work were irradiated in the Brookhaven nuclear reactor with a flux of approximately 10^{12} neutrons per cm^2-sec. The time of irradiation was approximately fourteen hours. Other samples were irradiated for approximately three hours in the M.I.T. cyclotron with a flux of 10^7–10^8 neutrons per cm^2-sec. Still other samples were irradiated with a flux of approximately 10^{13} deuterons per cm^2-sec for ten minutes in the M.I.T. cyclotron. All samples were allowed to decay for sufficient periods before photographic exposures to eliminate undesired short-lived activities.

PREPARATION OF SPECIMENS

Thin sections of the metal to be investigated are prepared by grinding, polishing, and etching one surface of the sample according to usual metallographic techniques. The prepared surface is then cemented with glycol phthalate to a cylinder of plastic which serves as a sample mount. Special precautions are necessary in the selection of the plastic which must be of a chemical composition so that any activities induced therein by neutron capture are of such low intensity or are so short-lived that they do not interfere with the examination of the sample. In the work described, polystyrene was chosen, but in some instances the polystyrene mounts became very active; this rendered the specimens wholly unusable if their own activity was low. This difficulty could be obviated by activating the samples before they are ground and polished into thin sections. There is also some indication that troublesome activation of the mounts may not occur with all batches of polystyrene.

The mounted metallic specimen is machined in a lathe to a thickness of less than 70 microns followed by grinding on abrasive paper until a thickness of approximately 20 microns is attained. The exposed surface of the specimen is then polished and etched.

Polished samples or thin sections of minerals can be prepared by petrographic techniques.[15,16] For a mount, however, a plastic rather than glass is used.

CHARACTERISTICS OF FILM

Eastman Kodak NTB Stripping Film was adopted in this work after an investigation of several other films. This film was satisfactory with regard to resolution, sensitivity and low inherent background. The manufacturerer[17] describes this emulsion as containing 81 percent (by weight) of silver halide, having an average diameter of 0.2–0.3 micron. The density of the emulsion is approximately 3.64 grams per cc. This film is most sensitive to beta-particles in the energy range of 0.06 to 0.07 Mev; the sensitivity curve flattens out fairly rapidly to a steady value at energies above 0.4 Mev.[18]

The film consists of the emulsion, a permanent support, and a temporary support. The emulsion, 10 microns thick, is permanently attached to a 10-micron layer of cellulose nitrate. The composite of these two layers will be referred to as the "backed emulsion." The cellulose nitrate layer is attached to a layer of cellulose butyrate, which is 0.15 mm thick and serves as the temporary support. This support can be removed when the film is ready for use.

MOUNTING AND PROCESSING OF FILM

For stripping the supporting layer from the backed emulsion and mounting the latter on the specimen, the fixture shown in Fig. 1 was developed. This fixture

[15] F. Kennedy, Econ. Geol. **40**, 353–360 (1945).
[16] Charles Meyer, Econ. Geol. **41**, 166–172 (1946).
[17] Eastman Kodak, descriptive bulletin, 1950.
[18] Private communication of Mr. R. A. Dudley.

consists of a base plate, a guide, a spacer, and a cutter. For use, a square piece of double-sided Scotch Tape, having a hole in the center, is placed over the hole in the base plate so that the two holes are in register. A piece of film two inches square is cut and the backed emulsion is then loosened along one edge with a razor blade from the supporting cellulose. The piece is attached to the double-sided Scotch Tape with the emulsion side down, the support is stripped off completely by attaching a small piece of ordinary Scotch Tape and lifting gently. This operation must be carried out quite slowly to minimize fogging.

The locating pins in the guide are then inserted in the holes in the base. A ring of double-sided Scotch Tape is placed in a 0.009-in. groove previously machined in the plastic specimen mount. The surface of the sample and mount is coated with Kodak Film Lacquer.

The mount is placed inside the spacer and pressed down firmly to contact the stripped film before the lacquer dries. The ring of Scotch Tape provides an immediate bond and fixes the emulsion on the specimen before the lacquer can be effective as a cementing agent. The cross section in the upper left of Fig. 1 shows the assembly at this stage of the operation. The spacer is then removed and the circular cutter is brought down to cut the film at the edge of the mount. The mount-film interface is waterproofed along this edge with Cenco Label Varnish to prevent the photographic processing solutions from penetrating between the emulsion backing and the sample mount and attacking the specimen.

The specimen is placed in a desiccator containing phosphorus pentoxide in a light-tight box for the chosen exposure time which may vary from less than one hour to several days. All manipulations are carried out in a darkroom with No. 2 Wratten Safe-light illumination. The exposed emulsion is processed in accordance with the recommendations of the manufacturer.[17] It should be noted that the technique results in fixing the emulsion in place on the specimen.

EXAMINATION OF MICROAUTORADIOGRAPHS

The processed emulsion is examined under the microscope at magnifications of 50 to 1500 diameters. Reflected light is used with metals and opaque minerals, while transmitted light can be used with non-opaque minerals. Because of the small grain size of the emulsion, individual grains cannot be readily observed at magnifications of less than approximately 1000 diameters.

The number of silver halide grains rendered developable is determined by the radioactivity of the sample, the time of exposure of the emulsion and the energy of the beta-particles emitted by the sample. For a given sample the exposure time may be so chosen that the developed grains corresponding to an underlying active area can be resolved only at magnifications of 1000 diameters or more. (See Fig. 3.) If the grain yield, that is the number of the photographic silver halide grains developable per incident beta-particle is known, a count of the developed grains will give an estimate of the activity of the sample in the neighborhood of this area of the film. Longer exposure times may be used so as to obtain patches of high grain density at lower magnifications. (See Figs. 2 and 4.)

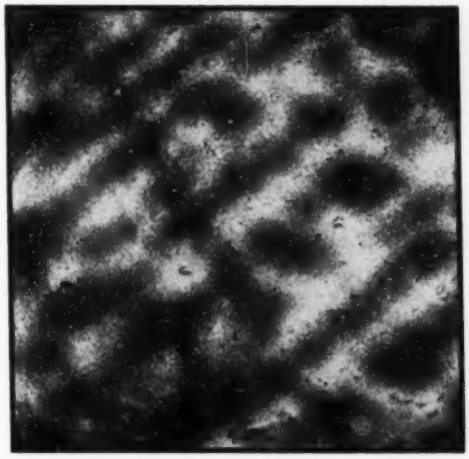

FIG. 2. Photomicrograph of autoradiograph of concentration gradients in aluminum alloy containing 1.5 percent copper, solidified under nonequilibrium conditions. Irradiated for 14 hours with thermal neutron flux of approximately 2×10^{12} neutrons per cm^2-sec. Photographic exposure of emulsion: one hour. Magnification 50×.

ILLUSTRATIVE EXAMPLES

Applications of the technique described are illustrated by the microautoradiographs in Figs. 2, 3 and 4. Figure 2 shows the distribution of copper in a cast aluminum-copper alloy having an over-all copper con-

FIG. 3. Photomicrograph of autoradiograph superimposed on etched metal surface of an aluminum copper alloy containing 3.0 percent copper. Solidified under nonequilibrium conditions. θ-constituent ($CuAl_2$) surrounded by aluminum-rich α solid solution. Irradiated three hours with thermal neutron flux of approximately 10^7 neutrons per cm^2-sec. Photographic exposure of emulsion: 12 hours. Magnification 1500×.

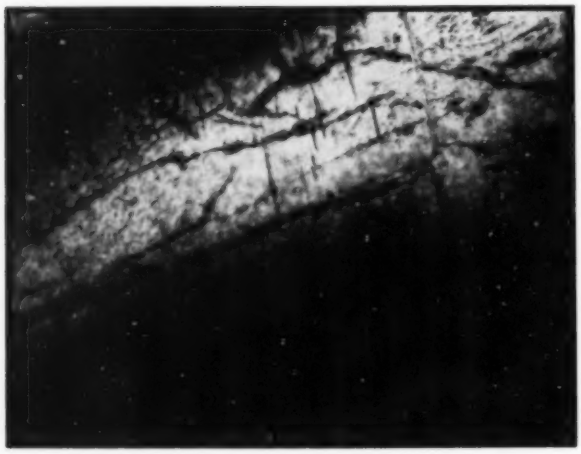

FIG. 4a. Photomicrograph of autoradiograph of intergrowth of albite and microcline. Photographed with transmitted light. Irradiated for ten minutes with a 4-Mev deuteron flux of approximately 10^{13} deuterons per cm^2-sec. Photographic exposure of emulsion: 2 hours. Magnification 250×.

FIG. 4b. Photomicrograph of intergrowth of albite and microcline shown also in Figure 4a. Photographed with polarized light set at extinction for albite. Magnification 250×.

tent of 1.5 percent. This alloy solidified under conditions causing marked concentration gradients in the solid solution (dendritic segregation, microsegregation). The darker areas in the autoradiograph indicate the copper-rich regions in the alloy; aluminum has such a short half-life that its residual activity had fallen to a negligible level at the time of the exposure of the emulsion. The emulsion shown in Fig. 2 was too dark to permit examination of the underlying metal structure at the magnification used, but after removing the emulsion and examining the metal specimen metallographically, the autoradiograph and the metallographic structure could be matched in all significant details.

In Fig. 2 small scar-like marks appear. These marks are probably not connected with either metallographic or nuclear features of the specimen but are due to impurities or foreign matter picked up in the photographic processing of the emulsion. Such effects usually go unnoticed because emulsions are not often examined at high magnification.

Figure 3 shows the developed grains around a particle of θ-phase ($CuAl_2$) in a cast aluminum-copper alloy containing 3 percent Cu. This alloy solidified under nonequilibrium conditions leading to the formation of a small amount of eutectic consisting of aluminum-rich α-phase and the θ-constituent. It was possible to locate a particle of θ-constituent through the developed emulsion by focusing on the metal surface. Figure 3 was made by a double exposure by first focusing on the emulsion and then on the metal surface.

Figure 4 shows an application of the autoradiographic technique to a mineral. The example illustrated is microperthite, an intergrowth of albite and microcline; the former is predominantly a sodium feldspar and the latter predominantly a potassium feldspar. Under the conditions of irradiation the activity produced in sodium is of the order of one thousand times that produced in an equivalent concentration of potassium. The relative concentration of the alkalis in both minerals is such that the albite is defined by the activity (Na^{24}) induced in the high sodium-bearing mineral, albite.

Figure 4a is a photomicrograph of the autoradiograph as taken with transmitted light. The dark areas represent high sodium content (albite). Figure 4b is a photomicrograph of the sample obtained under polarized light. The sample has been so placed that the albite intergrowth is at extinction. Figures 4a and 4b thus permit a comparison of the results obtained by autoradiography and by petrographic microscopy applied to a mineral.

ACKNOWLEDGMENTS

The support of the work reported here by grants of the Aluminum Company of America and of the Research Division of the Atomic Energy Commission is gratefully acknowledged. Thanks are also due to the staffs of Brookhaven National Laboratory and of the M.I.T. Laboratory of Nuclear Science and Engineering without whose cooperation this investigation could not have been made.

JOURNAL OF APPLIED PHYSICS VOLUME 22, NUMBER 12 . DECEMBER, 1951

Ultrasonic Propagation in Liquids under High Pressures: Velocity Measurements on Water

GERALD HOLTON
Lyman Laboratory of Physics, Harvard University, Cambridge, Massachusetts
(Received June 4, 1951)

The problem under discussion is the velocity of ultrasonics in liquids, specifically water, at various temperatures and high pressures. This report deals with the apparatus, and with some representative results obtainable with it.

The electrical apparatus makes use of a presentation unit (Dumont 256 or A/R 'scope) which synchronizes the sequence of operations by internally generated trigger signals at low repetition rates. Three- to five-microsecond pulses at controllable amplitude and approximately 15 Mc/sec carrier frequency are imposed on an X-cut quartz crystal which has been placed inside a pressure-supporting vessel containing the test sample. The resulting ultrasonic pulses in the liquid are reflected back and forth over a definite path length between the transducer and a mirror. After amplification in a receiver strip the complete echo-pattern becomes available for visual comparison on the presentation screen. The timed relative delay (and the measurable amplitude differences) between successive pulses furnish data for velocity (and attenuation) measurements when certain corrections are attended to.

Representative data are given for the velocity in water (to 0.1 percent) as a function of pressure to about 6000 atmospheres. From the data on water, information is derived on the temperature coefficient of sound velocity and on the ratio of specific heats at increasing pressures. The latter results are compared with those obtained directly from purely static experiments, and the advantages of the ultrasonic measurement technique for the derivation of some of the thermodynamic coefficients are cited.

I. INTRODUCTION

WORK on the velocity and attenuation of sound in liquids has been going on widely and vigorously, especially during the past twenty years. Very little attention had been directed toward the higher pressure range; but now some particular questions, e.g., those concerning the association of molecules in liquids, clearly call for experimental work in a wider range. Velocity measurements of sound in liquids at various temperatures and pressures have also been of interest for other reasons: the value of several thermodynamic coefficients may be determined or checked with respect to static measurements; pressure coefficients of sound velocity, and temperature coefficients at given pressures, may be found directly; regions of dispersion may be investigated, even if only a single frequency is impressed on the sound source, and so forth.

The specific problems for which the ultrasonic method was here used are: the measurement of sound velocity as a function of temperature and pressure in liquid samples; the use of such data to compute, in conjunction with independently available static p-v-T measurements, such thermodynamic coefficients as the ratio of the specific heats; the measurement of sound attenuation constants, and the interpretation of these data in terms of the theories of the structure of liquids. The results on attenuation measurements are to be reported on separately.

The fundamental method of measurement can be traced back to the war-time Radar Trainer and its first application to scientific problems by J. R. Pellam and J. K. Galt.[1,2] But as previously reported[3] all information must here be obtained by intercomparison within the set of multiple ultrasonic echoes for fixed path lengths.

II. PREVIOUS APPLICATION OF SOUND MEASUREMENTS IN LIQUIDS AT HIGH PRESSURES

The literature on previous experiments on sound in liquids at high pressures, though scant, did warn of some of the technical difficulties to be expected. J. C. Swanson[4–6] in 1934 had measured the pressure coefficient of sound velocity, $(\partial u/\partial p)_T$, for nine organic liquids to 300 atmospheres at room temperature. Using an interferometer technique developed by Hubbard and Loomis,[7] he attained an accuracy of 1 in 1000 for his velocity data,—a figure generally considered to be the best accuracy reasonably obtainable unless extraordinary labor is put into design and secondary measurements. His measurement technique involved moving a sound mirror to and fro in relation to a stationary traducer, therefore it does not recommend itself at higher pressures; for example, the packing around the rod which guides the sound mirror is likely to leak.

Swanson warned of one problem to be expected in this type of work: "The correlation between the calculated and experimental values (of velocity) is not as good as we had expected. However, considering the uncertainty of the values of many of the thermodynamic coefficients used in the computations, they are in very good agreement. In some instances the values given by different observers varied as much as 20 percent."[5] The disagreement mentioned actually reached 10 per-

[1] J. R. Pellam and J. K. Galt, J. Acoust. Soc. Am. **18**, 251 (1946).
[2] J. R. Pellam and J. K. Galt, J. Chem. Phys. **14**, 608 (1946).
[3] G. Holton, Phys. Rev. **73**, 543 and 1268 (A) (1948).
[4] J. C. Swanson, Rev. Sci. Instr. **4**, 603 (1933).
[5] J. C. Swanson, J. Chem. Phys. **2**, 689 (1934).
[6] J. C. Swanson and J. C. Hubbard, Phys. Rev. **45**, 291 (1934).
[7] J. C. Hubbard and A. L. Loomis, Phil. Mag. **5**, 1177 (1928).

cent for some of his liquids around 250 atmospheres, and points to even poorer correlations at higher pressures.

Another and original method of velocity measurement in liquids under pressure is given by A. C. Talbott.[8] Pressure pulses are generated by squirting a small quantity of liquid into the full pressure chamber. The incidence of the pulse as well as of subsequent echoes is recorded photographically by means of a mirror-and-lever system connected to a terminating membrane at one end of the chamber. The most obvious limitation is the pressure range, which is less than 425 kg/cm² in his model. Finally, P. Biquard[9–12] made measurements of velocity for several liquids of about 7- and 10-Mc/sec sound at ambient temperatures to 800 kg/cm². Since it uses diffraction of light by the density-grating set up by the traveling sound waves, that method has an inherent limitation in the maximum pressure which the essential glass windows in Biquard's arrangement can

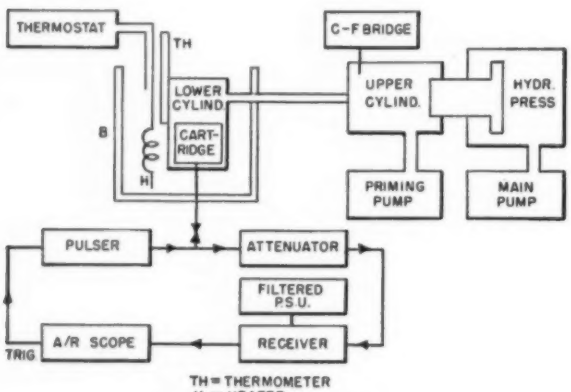

SCHEMATIC DIAGRAM OF ELECTRIC AND MECHANICAL COMPONENTS

FIG. 1.

be expected to endure; but below that point the optical method may be brought to such perfection that the most accurate velocity values for transparent media can be obtained with it.

In Biquard's work the temperature fluctuated during some of the runs, and may have been greater inside the test chamber where continuous operation of the transducer may cause substantial heating of the sample in contact with it. (This point may in fact be of significance in most types of investigations not using short pulses at long intervals, with the exception of Schreuer's.[13]) But in general, agreement with corresponding data in Swanson's publication and in this work does occur within the expected error limits.

[8] A. C. Talbott, Phil. Mag. **19**, 1126 (1935).
[9] P. Biquard, Compt. rend. **202**, 117 (1936).
[10] P. Biquard, Ann. phys. **6**, 195 (1936).
[11] P. Biquard, Compt. rend. **206**, 897 (1936).
[12] P. Biquard, Rev. acoust. **8**, 130 (1939).
[13] F. Schreuer, Akust. Z. **4**, 215 (1939).

Thus, the survey of earlier methods, including work on gases under pressure,[14–16] helped to emphasize certain advantages inherent in the suggested velocity and attenuation measurements by timing and by comparing amplitudes of successive echoes over a known path. These advantages may be summarized as follows:

1. Both sets of required data are immediately and simultaneously available, and few secondary experiments are needed for their reduction. 2. The error corrections, though numerous, are much more easily handled in this procedure than, for example, in resonance methods involving parasitic resonances. 3. The echo method does not depend on precision measurements of changes of distances inside the pressure chamber, and so dispenses with the necessity for rods passing through packings. 4. Large power outputs can be expected from the quartz transducer during the short cycle of its operation. 5. Under favorable conditions, one may expect velocity measurements as accurate as those obtained by almost any other method, and attenuation measurements superior to most. 6. No other method seems to offer fewer inherent limitations to prospective extension of this work to larger pressure and temperature ranges and to measurements on solids.

III. APPARATUS

Figure 1 is a schematic diagram of the relation between the electronic components. The original trigger is a pulse taken from the Dumont 256 'scope. The pulser, essentially a shock-excited oscillator, provides variable pulse height, length, and frequency; the receiver is a broad-banded 120-db amplifier. The single transducer, used as sender and receiver, is a small X-cut quartz crystal disk being driven at its fundamental frequency of about 15 megacycles. The power pulse can be considerable because for such brief applications the voltage difference between the faces of the crystal can be more than 5000 volts. The primary acoustic radiation, released at about 10^{-2} second intervals, is directed down a tube containing the liquid under investigation, and is reflected back toward the crystal from an optically flat steel disk at a convenient fixed distance. If a good acoustic mismatch is provided at the two ends of the sonic path, a great number of multiple echoes will reach the crystal following upon a single power pulse. These echoes arrive at a measurable rate depending on the length of the sonic path and the velocity in the medium, and with a measurable decrement depending, at least in part, on the attenuation constant of the liquid.

Thought has to be given to the Q of the crystal transducer. It would seem to be desirable to keep it as low as possible, if only to obtain faithful reproduction of impressed pulses and some possibility of slight frequency adjustment. A Q of 10 is not unsatisfactory as

[14] A. H. Hodge, J. Chem. Phys. **5**, 974 (1937).
[15] J. C. Hubbard and A. H. Hodge, J. Chem. Phys. **5**, 978 (1937).
[16] D. Bancroft, thesis, Harvard University (1939).

far as operating band width is concerned. From the point of view of "ringing," i.e., persistence of oscillation after cessation of the applied power pulse, this value is not too high if the applied power pulse is sufficiently short compared to the time of travel per echo; but at high velocities (that is, high hydrostatic pressures) and for poorly chosen mirror-crystal distances, the tail-end of the outgoing pulse may beat with the leading part of the returning echo, and so distort it. Indirectly, therefore, this factor determines the shortest distance between mirror and crystal that may be considered for a given liquid, and also warns of possible pulse distortion if the crystal is to be driven at a higher harmonic.

The transducer, tube, and contained liquid (an assembly called *the cartridge*) are immersed in a pressure-communicating fluid. Over a single electrical lead to the external electronic equipment, data on time per echo and decrement per echo under various conditions of temperature and pressure are received simultaneously.

From a purely mechanical point of view the cartridge assembly involved the greatest problems of design and construction, and is still, perhaps, less satisfactory than it might be. Figures 2 and 3 refer to the component parts of a cartridge model that has been used for velocity measurements.

The most severe design consideration, apart from the demands of the theory of sound propagation and the velocities and absorptions expected, are (1) the small inner diameter (0.8″) of the 6000 kg/cm² pressure cylinder which must receive the cartridge; (2) the necessity to obtain very accurate alignment between the mirror and crystal before each run; and (3) the separation of the back of the crystal from the test liquid so as to permit use of conducting liquids.

Under pressure the various components will shrink in varying degrees. For this reason no cement could be relied on to hold the crystal, and placement was secured by spring-clamped edge support. In this connection it will be noted that the whole lower cartridge can be disassembled to allow replacement of the crystal. Even if the very thin and fragile crystal did not break occasionally during a run, a really permanent cartridge cannot be hoped for because the front face of the crystal deteriorates over a period of time by loss of plating and by pitting of the quartz surface in use. Moreover, the rubber washers eventually freeze and crack, requiring periodic replacement. The problem of mirror alignment has always been a difficult one in such research. The pressure changes, which are sometimes uncontrollably sudden, only aggravate this trouble, similar in some respects to the irregularities obtained with piezometers that have undergone a shock. Stainless steel spacers whose lengths are known to within 0.0001 inch can be added below the mirror spacer to increase the sonic path. Dummy blocks can be screwed into the holding nut above the mirror to

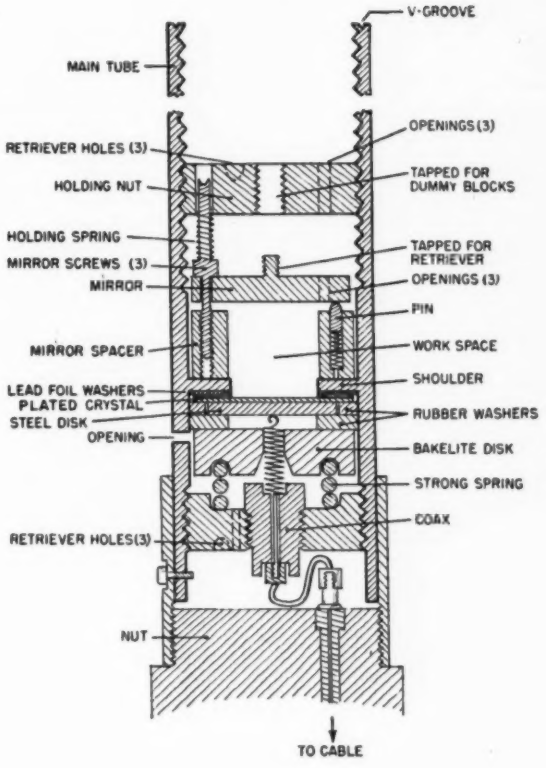

CARTRIDGE AND MIRROR ASSEMBLY

FIG. 2.

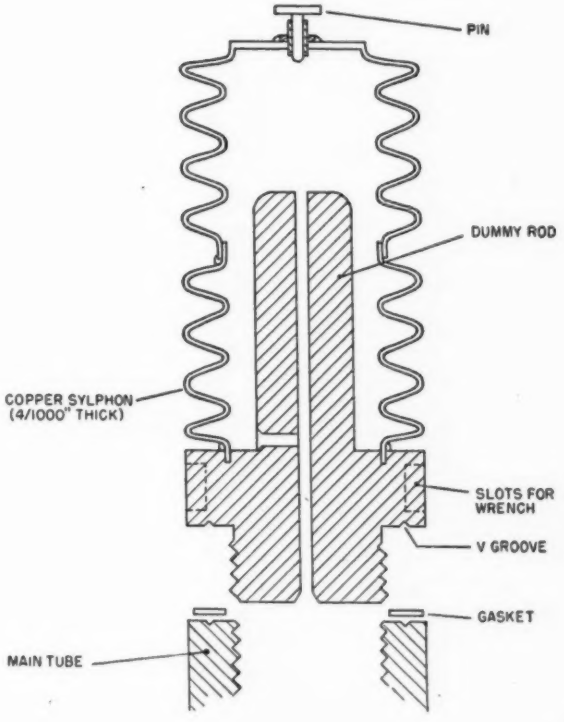

SYLPHON ASSEMBLY

FIG. 3.

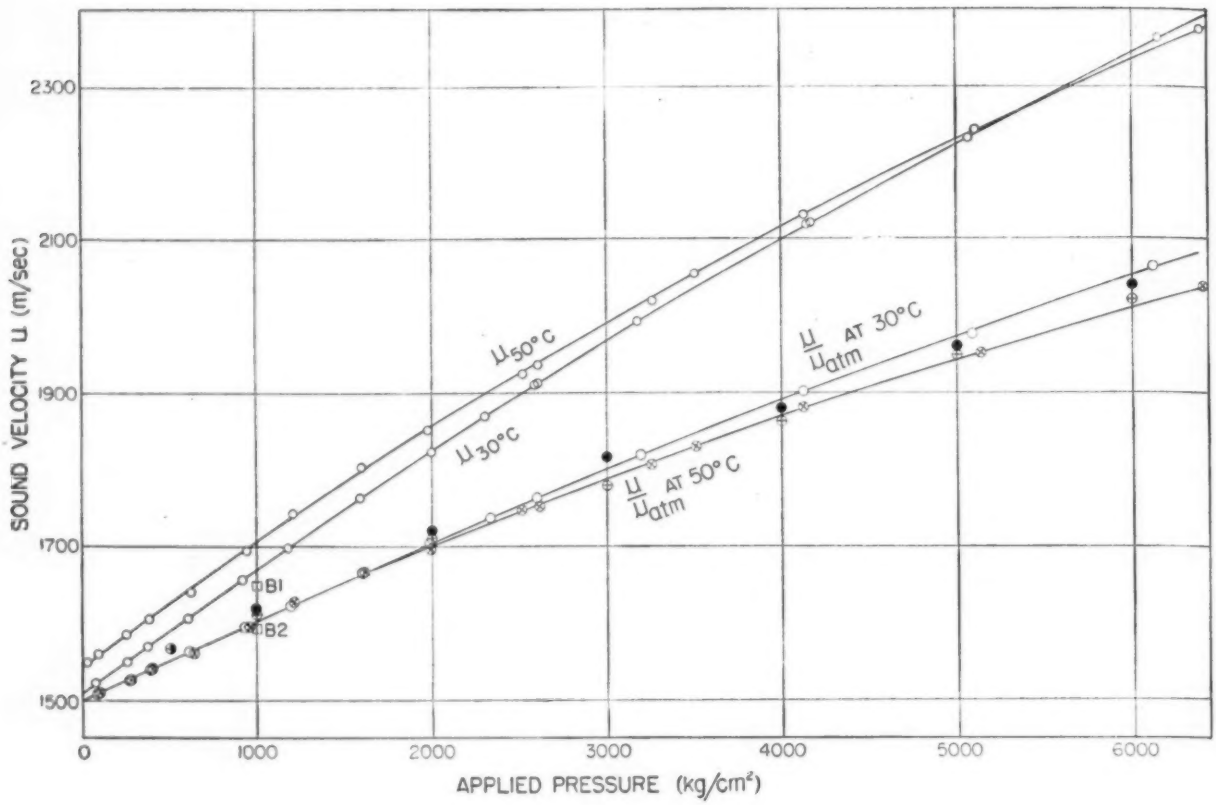

FIG. 4.

fill "dead" space and so to increase the effective maximum compression of the liquid in a given assembly.

The work space above the crystal is sealed off liquid-tight by means of a sylphon assembly (Fig. 3) which screws into the top of the main tube. Leakage past the joint is effectively prevented by lapping the touching shoulders, except for a circular V-groove in each, which is fully packed by a rubber gasket when the sylphon is tightened against the main tube.

Before assembly, the sylphon, made of flexible copper sheet 0.004 inch thick, is filled with the same liquid as the work space itself. The dummy rod indicated in Fig. 3 serves to increase the fractional compression which the total amount of liquid in the upper cartridge can undergo without danger of crushing the sylphon or the crystal. Additional sylphon sections can be added where greater compression is expected. The flexibility of the sylphon assures that the liquid in the work space is at the pressure of the surrounding pressure-conducting medium. It also permits changes in temperature between pressure runs on an unchanged assembly.

The remaining accessories indicated in Fig. 1 include the pressure plant and the thermostated bath. The pressure equipment and its methods of operation are so well known that they need no description, being in fact Professor P. W. Bridgman's own or modeled after it.

The pressure itself is ascertained by measuring on a Cary-Foster bridge, the resistance of a standard manganin wire coil placed in the upper pressure cylinder. The accuracy of the absolute pressure data in this work is at worst 10 kg/cm², a factor which may be ignored until discovery is made either of definite discontinuities and critical points on the velocity (u) curves, or of large values of $\partial u/\partial p$.

The lower cylinder, carrying the cartridge inside, is immersed in an oil bath that is thermostatically controlled to within ± 0.02°C once the desired level is reached. The bath itself was thoroughly and continuously agitated by a motor-driver stirrer.

IV. VELOCITY MEASUREMENTS

Sources of Error

Since the number of secondary effects theoretically expected in these tests was large, it seemed wise to try a preliminary experimental determination of some well-known velocity of sound in a liquid, under conditions corresponding to actual pressure runs, and with precautions based on an analysis of expected errors. The cartridge system discussed above was filled with distilled water at atmospheric pressure and 26.20°C. The delay of a convenient high order (39th) echo was noted with respect to the first echo before and after a spacer of 0.5000-cm length was introduced below the mirror assembly. In the first case, the result was 21.82 μsec/echo; in the second, 15.15_8 μsec/echo. Since the difference in sonic paths was just 1 cm, the velocity of sound

in the liquid comes to 1.501×10^5 cm/sec, the same value obtained by Willard[17] (within his accuracy of ±1 m/sec).

Nevertheless, there is good reason to mention that careful allowance must be made for the following list of error sources:

(1) Alleged factory calibration of time delay circuit.

(2) Pulse distortion, owing to (a) phase distortion or insufficient recovery in the receiver circuits; (b) selective attenuation of high frequency components of pulse; (c) temperature gradients across the wave front; (d) deviation of the vibrations of the X-cut crystal from the theoretical pure piston motion; (e) deviation of the crystal and mirror surfaces from ideal plane parallelism; (f) ringing of crystal after cessation of the applied pulse; (g) mixing at the crystal of echoes with stray reflections, from walls, back of mirror, etc.; (h) diffraction effects causing large phase differences across the wave front.

(3) Effect of viscosity and thermal conduction to the walls.

In practice, the errors in velocity measurements can either be prevented by a proper choice of experimental conditions, or can be allowed for by exact calculations, or are by nature below the limit inherent in individual delay readings—which is at present 1 in 1000.

Experimental Results

Representative results on the velocity of sound in distilled, degassed water are summarized in Fig. 4. To facilitate comparison, two sets of curves have been entered above the identical abscissa. The upper set of two curves refers to the ordinate at the extreme left and serves to compare the velocities of sound at 30°C and 50°C; the intercept at zero applied pressure has been normalized to Willard's values of 1509_6 m/sec for 30°C, 1543 m/sec for 50°C.

The lower set of two curves presents the experimentally more direct quantity, velocity (u) at given pressures divided by velocity (u_{atmos}) at the atmospheric pressure and the same temperature. The higher line of the two (empty circles) is for 30°C, the lower (× in circles) for 50°C. In either case the deviation of any one experimental point from a smooth curve is at most 3 pro mille.

It may seem surprising that these two curves overlap and are straight to about 1800 kg/cm², but this behavior is expected from the theoretical values of the velocities; the latter are entered on the same graph (full circles for 30°C, + in circle for 50°C). The deviations of the theoretical points are of the order of 1 percent. A discussion of these theoretical values is given in the next section.

The points marked $B1$ and $B2$ correspond to extrapolations to 1000 kg/cm² of Biquard's data[18] on the velocity of sound to about 600 kg/cm²; $B1$ is for 16.3 ± 0.5°C, $B2$ for 9.5°C. Examination of Biquard's original paper reveals that the position of $B1$ is fairly uncertain owing to widely scattered data at low pressures. Theoretically, one would expect not only $B2$ but also $B1$ to fall close to the curves shown here.

Another result derived directly from experiment is a curve of the temperature coefficient of velocity at various pressures. For instance, from Fig. 4 we may immediately plot Fig. 5, $1/u(\partial u/\partial T)_{40°C}$. The curve runs as smoothly as may be expected on the basis of the uncertainty in the values of the individual factors of this coefficient. A notable feature of the curve is the crossing through zero and into negative values at about 5300 kg/cm² applied pressure.* It will be recalled that all "normal" liquids have a negative temperature coefficient of sound velocity; by this test, as by many others, water too is "normal" beyond a critical pressure range for the stated temperatures.

Besides high pressures, high temperatures also reduce the anomalies of water. As is well known, the temperature coefficient of sound velocity does change from positive to negative at about 74°C at atmospheric pressure. In the former case, as in this one, the thermodynamic explanation is that $\partial^2\rho/\partial T^2$ is zero and $\partial\gamma/\partial T$ very small in the critical range, whence $\partial u/\partial T$ must vanish.†

For other liquids than water, analogous data may be obtained provided the attenuation is not so large as to prohibit the use of a sufficiently large set of echoes. For example, the curves for toluene and ethyl ether, more highly attenuating liquids, revealed a maximum deviation of 3 in 1000 at a single point each.

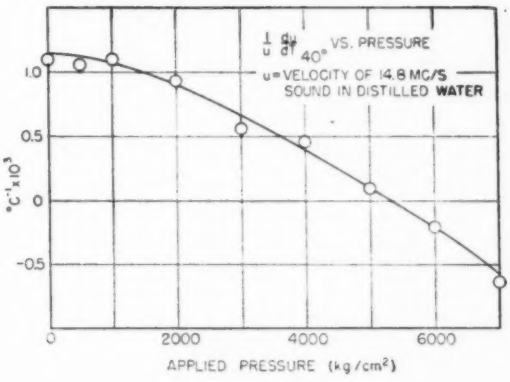

FIG. 5.

[17] G. W. Willard, J. Acoust. Soc. Am. **19**, 235 (1947).

[18] See reference 12, page 3.

* The point at 7000 kg/cm² in Fig. 5 is derived from extrapolation of the curves in Fig. 4.

† The engineering implications of this fact for delay line design are interesting and perhaps not entirely impractical: A delay line of water at about 40°C sealed at about 5300 kg/cm² pressure (and at corresponding pressures for other temperatures), should not require elaborate thermostating, will not suffer from wave front distortion due to temperature gradients across the line, shows no dispersion, and has effectively no attenuation. For a lower ambient temperature all these advantages can be obtained at a somewhat higher internal pressure. A better match between crystal and liquid might be achieved by affixing a suitable quarter-wave plate.

TABLE I.

Applied pressure kg/cm²	$(\partial v/\partial p)_T$ (cm³/dyne/cm⁸) ×10¹⁸ 30°C	50°C	v_s cm³/g 30°C	50°C	γ_{theor} ±0.02 30°C	50°C	$(u/u_{atmos})_{theor}$ 30°C	50°C	u_{exp}[a] (cm/sec) ×10⁻⁵ 30°C	50°C	γ[b] 30°C	50°C	ϵ[c] % 30°C	% 50°C
0	451(±1)	447(±1)	1.0041	1.0118	1.01	1.04	(1.00)	(1.00)	1.509_6	1.543	1.019	1.039	+1	−0.1
500	381_1	378_6	0.9837	0.9916	1.02	1.05	1.07	1.07	1.588	1.623	0.993	1.015	−2.6	−3.4
1000	336_7	335_7	0.9663	0.9743	1.03	1.05	1.12_5	1.12	1.667	1.703_5	1.002	1.026	−2.8	−2.3
2000	269_4	269_9	0.9364	0.9445	1.04	1.06	1.22_5	1.21	1.822	1.856	1.020	1.042	−1.9	−1.7
3000	229_6	227_6	0.9105	0.9205	1.07	1.05	1.32	1.28	1.968	1.989_5	1.073	1.063	+0.3	+1.3
4000	194_6	195_9	0.8897	0.8996	1.06	1.08	1.38	1.37	2.100	2.118	1.084	1.086	+2.2	+0.6
5000	169_4	168_4	0.8719	0.8818	1.07	1.09	1.46	1.45	2.222	2.227	1.101	1.074	+2.9	−1.5
6000	149_4	149_3	0.8654	0.8662	1.07	1.10	1.54	1.52	2.344	2.334	1.096	1.084	+2.4	−1.5

[a] u_{exp} with respect to Willard's experimental standard values at 1 atmos (u_{atmos}) of 1509_8 m/sec at 30°C, 1543 m/sec at 50°C.
[b] Calculated from u_{exp} in conjunction with Bridgman's data for $\partial v/\partial p$ and v_s, and Willard's for u_{atmos}.
[c] ϵ = correction to be applied to γ_{theor}.

Evaluation

The uses to which this type of experimental information can be put are fairly direct. From

$$u^2=\left(\frac{\partial p}{\partial \rho}\right)_\phi, \quad \gamma=-\left(\frac{\partial v}{\partial p}\right)_T\cdot\left(\frac{u}{v_s}\right)^2.$$

The data for p, v, and T for water were determined by Bridgman in 1912 to five significant figures (though the published data are to four figures only).[19] These should allow calculation of the compressibilities to at least three figures; and therefore the values of γ will be determined to a few parts in 1000 if the above equation is used together with these new velocity data.

Actually, the original p-v-T surface for water has since been modified a little from time to time. The *Handbook of Physical Constants*[20] shows an average deviation among different determinations of v_s at 25 degrees of about 3 in 10,000 to 3500 atmospheres, rising to about 5 in 1000 at higher pressures; the original values of compressibilities are correspondingly uncertain. Another example would be the newer values at certain temperatures for the specific volume of water.[21] At 6000 atmospheres and 50°C, the value differs by about 2 in 1000 from the 1912 results. The difference between the new and the old compressibilities is somewhat higher and should affect the theoretical velocity to a few tenths percent.

Nevertheless, it is reasonable to take Bridgman's more complete 1912 data as a reference for the calculation of γ. Future corrections of v_s and $(\partial v/\partial p)_T$, when established with certainty, can then easily be applied to the new values for γ. A search now for greater accuracy in these constants would probably be premature. As Bridgman has stated, "A great deal more work would be necessary before the p-T-v surface of water is known with an accuracy corresponding to the accuracy of our knowledge of volume as a function of temperature at atmospheric pressure."

The values of γ derived from these experiments, and pertinent data leading to these values, are tabulated in Table I. Specific volumes, compressibilities and specific heats are derived from reference 19. The values of $(u/u_{atmos})_{theor}$ are calculated from these statically determined values and were plotted in Fig. 4. They may be compared with $(u/u_{atmos})_{exp}$ from these experiments. In the determination of u_{exp}, the correction for the change in length of sonic path with pressure owing to shrinkage of the steel spacers amounts to less than 4 in 1000 at our highest pressures, wherefore the compressibility of iron[22] was considered accurate enough for our purposes. Twice the linear compression $\Delta l/l_0$ gives directly the fractional decrease of u/u_{atmos} needed for the correction at any pressure and temperature.

Since our equipment had not been designed for absolute velocity measurements, it was logical to calculate first, instead of u_{exp} itself, the ratio $(u/u_{atmos})_{exp}$

TABLE II. Velocity in water, in cm/sec (×10⁻⁵).

	30°C	50°C	Comments
Schreuer[a], Seifen[b]	1.509_7		Calculated from 25°C data and $\partial u/\partial T$ for the range 25°–30°C (=2.5 m/sec)
Freyer[c]	1.510_8		
TRE-Report (cited in d)	1.510	1.544_5	30°C value extrapolated; to ±1 m/sec
Rosenberg[d]	1.500	1.534	Temp. to ±1°C Vel. to ±0.5 percent
Hubbard-Loomis[e]	1.509_9		
Willard[f], Randall[g]	1.509_6	1.543	To ±1 m/sec
Singh[h]		(1.545)	At 50.4°C
Jones-Gale[i]		1544.7	Extrapolated
McMillan-Lagemann[j]	1509.5		Extrapolated from 25°C data as for Schreuer and Seifen
Weissler-del Grosso[k]	1509.9		Airsaturated water
	1510.9		Degassed water

[a] See reference 13.
[b] N. Seifen, Z. Physik **108**, 681 (1938).
[c] E. B. Freyer, J. Am. Chem. Soc. **53**, 1313 (1931).
[d] P. Rosenberg, Radiation Laboratory (M.I.T.) Report No. **56** (1946).
[e] See reference 7.
[f] See reference 17.
[g] C. R. Randall, Bur. Standards J. Research **8**, 79 (1932).
[h] B. Kanwal Singh, Nature **156**, 569 (1945).
[i] P. L. F. Jones and A. J. Gale, Nature **157**, 341 (1946).
[j] D. R. McMillan, Jr., and R. T. Lagemann, J. Acoust. Soc. Am. **19**, 959 (1947).
[k] A. Weissler and V. A. del Grosso, J. Acoust. Soc. Am. **23**, 221 (1951).

[19] P. W. Bridgman, Proc. Am. Acad. Arts Sci. **48**, 309 (1912).
[20] *Handbook of Physical Constants* (Geol. Soc. Amer., 1942).
[21] P. W. Bridgman, J. Chem. Phys. **3**, 597 (1935).
[22] Taken from P. W. Bridgman's *The Physics of High Pressures* (The Macmillan Company, New York, 1931), p. 160.

at increasing pressures. The values of u_{atmos} at the various temperatures, needed for the determination of corresponding absolute values, could then be taken from independent absolute measurements.

Various published values of ultrasonic velocities at these sample temperatures (30° and 50°C) and atmospheric pressure are given in Table II. They are seen to be in fair agreement.

Of these, Willard's data have been chosen to serve as standard values of u_{atmos} at 30°C and 50°C, partly because they represent one continuous set of measurements over the whole temperature range. Any future adjustment of these values, like those of v_s and $(\partial v/\partial p)_T$, can be directly applied to new corrections of γ. Apart from those uncertainties, the final values of γ of water at pressures to 6000 kg/cm² are considered to be accurate to within 0.3 percent.

Since one of the claims of the multiple-echo method is its superiority in determining certain thermodynamic coefficients, we should compare this last result for γ with the usual derivation of γ from static experiments. It is well known that such an evaluation of specific heats requires a knowledge of the p-v-T surface accurate enough to give meaningful second derivatives of specific volumes with respect to temperature. Furthermore, the first function directly obtained is not C_p itself, but

$$\left(\frac{\partial C_p}{\partial p}\right)_T = -T\left(\frac{\partial^2 v}{\partial T^2}\right)_p.$$

The values of C_p at various pressures are obtained by integration, using independently determined results of C_p as a function of temperature at any one (say, atmospheric) pressure. As a second step toward finding γ, one may then turn to the relation

$$C_p - C_v = -T\frac{\left(\frac{\partial v}{\partial T}\right)_p^2}{\left(\frac{\partial v}{\partial p}\right)_T}.$$

The expected error in the value of C_p/C_v finally obtained may be ten times the error in γ as determined by sound velocity measurements.[23] In this light the old values of C_p and C_v derived from the 1912 paper[19] are very good, for they give ratios that deviate on the average only about 2 percent from these new results.

Other uses for sound velocity measurements offer themselves immediately. The adiabatic and isothermal compressibilities may be compared; or, from the last equations, C_p and C_v may be determined separately by

$$C_p = -T\frac{\left(\frac{\partial v}{\partial T}\right)^2}{\left(\frac{\partial v}{\partial p}\right)_T + \left(\frac{v_s}{u}\right)^2}.$$

In effect, the immediate availability from sound experiments of the adiabatic compressibility and of γ permits a series of cross-checks among coefficients derived from the p-v-T surface. It may be hoped that if *absolute* velocity data can be established to 0.1 percent or better (perhaps with a cartridge of new design), it will become possible to amend the published four-figure p-v-T values themselves.

If one wonders whether it is valid at all to compare statically and dynamically derived specific heat ratios, the answer is of course that no difference is expected if the sound frequency is sufficiently below a dispersive region. No evidence of dispersion has been found in water in this frequency region despite many different attempts throughout the past 20 years. There is evidence that no dispersion may be expected below about 10^{12} cps.[24]

In summary, we note that here, as in the more usual applications under normal conditions, velocity data yield thermodynamic coefficients far more precisely and directly than do static measurements alone. The remaining uncertainties rest chiefly in the statically derived p-v-T surfaces themselves; but any improvement there (particularly expansion to five significant figures) will, together with velocity data, result in improved thermodynamic coefficients like γ and $[(\partial v/\partial p)_\phi - (\partial v/\partial p)_T]$ of up to a whole significant figure more than may be hoped for without such velocity data. On the other hand, there is also still room for improvements on the equipment (mainly the cartridge) in order to achieve consistent absolute measurements of velocity.

ACKNOWLEDGMENTS

It is a pleasure to acknowledge gratefully the assistance received in the design and construction of the apparatus. Professor Bridgman's advice and interest, as well as the loan of his equipment and the help of his technical assistants, Mr. Abbot and Mr. Chase, were of course essential. I am also indebted to Professor F. V. Hunt for constructive suggestions, and to Dr. Pellam and Dr. Galt for generous help with technical details of instrumentation. Support for the project is being given jointly by the Harvard Foundation for Advanced Study and Research, and by the Office of Naval Research (Contract N5ori-76, Project Order X).

[23] Reference 19, p. 333: ". . . it must be remembered that the absolute compressibilities given here may be in error by as much as 1 percent at the higher pressures." And p. 335: "The agreement of the two best determinations [of $\partial v/\partial p$] at the higher pressures is about 5 percent for the lower temperature interval from 20° to 40°, 3 percent for the interval 40° to 60°, . . ."

[24] K. F. Herzfeld, J. Acoust. Soc. Am. **13**, 33 (1941).

JOURNAL OF APPLIED PHYSICS VOLUME 22, NUMBER 12 DECEMBER, 1951

The Propagation in a Compressible Fluid of Finite Oblique Disturbances with Energy Exchange and Change of State

FREDERICK W. ROSS
University of Detroit, Detroit, Michigan
(Received April 17, 1951)

Theory is presented for oblique shock waves involving (1) heat exchange, k_1, (2) transfer of part of the compressible fluid, k_2, to an incompressible state, and (3) change in specific heat ratios, k_3. By matching mass flow, momentum, and energy relations across an oblique finite disturbance it is shown that these additional conditions introduce new terms in the solution of the form $k_i u_1/(u_1-u_2)$. For k_i not zero a minimum shock angle is found which always exceeds the Mach angle by a definite increment. For air-flow at u_1/a^* of 1.5 with dew point $-20°$F this increment is calculated as 3.1 degrees. For expansion about a corner such flow differs from the Prandl-Meyer type and in supersonic nozzles, for example, oblique shock waves are predicted which can explain anomalous pressure losses, the presence of extraneous waves, and non-isentropic effects. Hodographs of the velocity solution include a triply infinite set of curves, one, the usual set, introduced by Mach number as parameter and the other two by k_i. The theory includes physically possible normal and oblique flows involving increase of supersonic velocities and subsonic velocities of which oblique flame fronts are indicated as one form. Applied to air condensations in hypersonic flows isentropic disturbances having appreciable angular flow shift and stagnation pressure losses are predicted.

INTRODUCTION

THE basic elements necessary for the theory of propagation of one-dimensional waves of finite amplitude in a compressible fluid were first set forth by Rankine in 1870[1] and subsequently have been developed into a basic theory for such disturbances. This theory, now generally referred to as the normal shock wave theory, as well as the more general theory of two-dimensional or oblique shock waves is well known. More recently, the sudden release of heat energy in compressible flow has been shown to induce finite disturbances in such flow, and the effects of such heat release on normal shock waves have been studied.[2,3] In many flow fields, for example those involving sudden condensation or combustion, the flow more generally includes two-dimensional or oblique disturbances as well. In addition, the energy or heat exchange is often induced by either a change in physical state or of chemical composition; and the accompanying heat exchange, by effecting the temperature change across the disturbance as well as the change in physical state or chemical composition, may also induce change in the ratio of specific heats of the fluid as well. These effects are studied by deriving a theory for oblique waves of finite amplitude which includes the conditions of (1) energy exchange, and (2) transfer of part of the mass to the incompressible state, and (3) finite change in specific heat ratios within the disturbance.

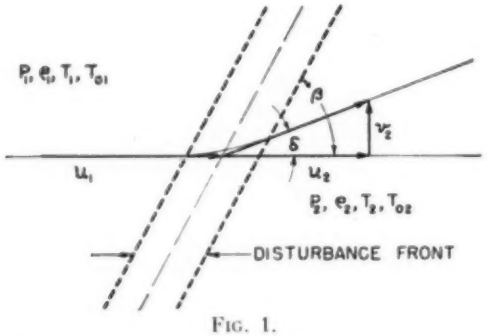

FIG. 1.

GENERAL CONSIDERATIONS

The following assumptions are made: (1) The radius of curvature of the disturbance front is sufficiently large so that the disturbance may be considered planar. (2) All appreciable effects of finite transition such as changes of pressure, density, and velocity, as well as all effects of energy exchange, change of state, and change of specific heat ratio, and the effects of viscosity, diffusion, and heat conductivity occur within the disturbance front. (3) No particular assumption of thickness of disturbance is made, it being assumed only that the finite disturbance front be distinguishable from the remaining portions of the field, and that changes in the flow induced by other conditions of flow be small compared to the changes within the disturbance. (4) All changes of direction of pertinent vectors may be considered as occurring at some plane within the disturbance parallel to the disturbance front (see Fig. 1). (5) For the regions on either side of the disturbance, it is assumed: (a) there are no viscous losses; (b) the flow is adiabatic; (c) the gas law, $PV=RT$, holds; and, (d) the velocity of sound, a, is given by $(dp/d\rho)^{\frac{1}{2}}$.

The conditions necessary to match end-point relations of mass flow, momentum, and energy on the two sides of the disturbance are derived.

DEFINITIONS

The subscript $(\ )_1$ designates quantities of uniform value on the initial or upstream side of the disturbance

[1] W. J. M. Rankine, Trans. Roy. Soc. (London) **clx 277**, 160 (1870).
[2] K. Oswatitsch "Condensation phenomena in supersonic nozzles." Z.A.M.M. **22**, 1–14 (No. 1, February, 1942).
[3] W. R. Hawthorne and H. Cohen, "Pressure losses and velocity changes due to heat release and mixing in frictionless, compressible flow," R.A.E. Report No. E-3997.

and the subscript ( )$_2$ those of uniform value on the final or downstream side. The final resultant velocity U_2, has two components u_2 and v_2, parallel and normal to initial velocity u_1, respectively, β is the angle between the initial velocity, u_1, and the disturbance front and δ is the angle of deflection of the flow. These quantities are indicated in Fig. 1.

Three nondimensional parameters are introduced. For the energy exchanged

$$k_1 = H/C_pT_{01} = JH \Big/ \frac{\gamma_1+1}{2(\gamma_1-1)}a_1^{*2},$$

where H is heat energy exchanged (it may be originally in any form but must manifest itself in the form of heat as considered here). C_p is the specific heat at constant pressure, γ is the ratio of specific heats, T_{01} is the initial temperature of the compressible fluid brought isentropically to rest, a^* is the critical speed of sound, and J is the mechanical equivalent of heat.

For the transfer of part of the mass to the incompressible state

$$k_2 = \rho_i/\rho_2,$$

where ρ_2 is the portion of the fluid density remaining compressible on the downstream side and ρ_i is the portion of the density transferred from the compressible to the incompressible state within the disturbance. The ratio of fluid transferred is

$$\rho_i/(\rho_2+\rho_i) = k_2/(1+k_2).$$

For the change in the ratio of specific heats

$$k_3 = \gamma_1 - \gamma_2.$$

EQUATIONS OF FLOW

If the disturbance is to be propagated permanently in form, the mass flow, momentum, and energy relations must be consistent across the disturbance. The equations are derived for unit area of the disturbance front.

For mass flow normal to the disturbance

$$\rho_1 u_1 \sin\beta = \rho_2(1+k_2)(u_2\sin\beta - v_2\cos\beta). \quad (1)$$

From the equation of motion in terms of the time rate of change of momentum normal to the disturbance

$$p_2 - p_1 = \rho_1 u_1^2 \sin^2\beta - \rho_2(1+k_2)(u_2\sin\beta - v_2\cos\beta)^2. \quad (2)$$

Equating the momentum components parallel to the front gives

$$\rho_1 u_1^2 \sin\beta\cos\beta = \rho_2(1+k_2)(u_2\sin\beta - v_2\cos)(u_2\cos\beta + v_2\sin\beta). \quad (3)$$

The energy equation per unit mass of fluid is taken as

kinetic energy + total heat = total energy.

On the upstream side the energy equation becomes

$$\frac{u_1^2}{2} + \frac{\gamma_1}{\gamma_1-1}\frac{p_1}{\rho_1} = JC_pT_{01} = \frac{\gamma_1+1}{2(\gamma_1-1)}a_1^{*2}, \quad (4)$$

where p_1 is the pressure, ρ_1 the density, and J the mechanical equivalent of heat.

On the downstream side it is assumed that the resultant total energy is the sum of the total energy of the portion of the fluid remaining compressible, plus the kinetic energy of the incompressible particles. It is assumed that these incompressible particles are distributed statistically throughout the compressible fluid on the downstream side and have the same velocity components as the compressible portions but do not contribute to the static pressure and have no potential energy in the sense that a compressible gas does. This assumption is discussed in the appendix. Hence, the energy equation on the downstream side may be written

$$\frac{\rho_2}{\rho_2+\rho_i}\left\{\tfrac{1}{2}(u_2^2+v_2^2) + \frac{\gamma_2}{\gamma_2-1}\frac{p_2}{\rho_2}\right\} + \frac{\rho_i}{\rho_2+\rho_i}\{\tfrac{1}{2}(u_2^2+v_2^2)\} = JC_pT_{01} + JH$$

or

$$\tfrac{1}{2}(u_2^2+v_2^2) + \frac{\gamma_2}{\gamma_2-1}\frac{p_2}{\rho_2(1+k_2)} = JC_pT_{01}(1+k_1) = \frac{\gamma_1+1}{2(\gamma_1-1)}a_1^{*2} + JH. \quad (5)$$

SOLUTION OF EQUATIONS

Equations (1) to (5) are sufficient for solving the problem. One such solution is considered here.

If u_1, p_1, ρ_1, and γ_1 are known there are four equations in five unknowns, β, u_2, v_2, ρ_2, and p_2 and three parameters k_1, k_2, and k_3. We shall solve first for v_2 in terms of u_2, k_1, k_2, and k_3.

From Eq. (3) using Eq. (1) we have

$$\tan\beta = (u_1-u_2)/v_2. \quad (6)$$

Also, from Fig. 1,

$$\tan\delta = v_2/u_2. \quad (7)$$

With the aid of Eqs. (1), (2), and (6)

$$p_2 = p_1 + \rho_1 u_1(u_1-u_2). \quad (8)$$

Using Eq. (8) and (1), and by elimination of β by Eq. (3) gives

$$\frac{p_2(u_1-u_2)}{\rho_2(1+k_2)[u_2(u_1-u_2)-v_2^2]} = \frac{p_1}{\rho_1 u_1} + (u_1-u_2). \quad (9)$$

Substitution of p_1/ρ_1 and $p_2/\rho_2(1+k_2)$ from the energy

equations (4) and (5) into Eq. (9) gives

$$v_2^2=(u_1-u_2)^2\frac{u_1u_2-a_1^{*2}-\dfrac{u_1}{(u_1-u_2)(\gamma_1+1)}\left[2JH(\gamma_1+1)+\dfrac{k_3}{\gamma_1-k_3}\left\{u_2^2-a_1^{*2}\left(\dfrac{\gamma_1+1}{\gamma_1-1}\right)-2JH\right\}\right]}{[2/(\gamma_1+1)]u_1^2-u_1u_2+a_1^{*2}+k_3[(u_1-u_2)u_1/(\gamma_1+1)(\gamma_1-k_3)]}. \tag{10}$$

In nondimensional form this becomes

$$\bar{v}_2^2=(\bar{u}_1-\bar{u}_2)^2\frac{\bar{u}_1\bar{u}_2-1-\dfrac{k_1\bar{u}_1}{\bar{u}_1-\bar{u}_2}-\dfrac{k_3\bar{u}_1}{\bar{u}_1-\bar{u}_2}\left\{\dfrac{\bar{u}_2^2-(1+k_1)(\gamma_1+1)/(\gamma_1-1)}{(\gamma_1-k_3)(\gamma_1+1)}\right\}}{\dfrac{2}{\gamma_1+1}\bar{u}_1^2-\bar{u}_1\bar{u}_2+1+k_3[\bar{u}_1(\bar{u}_1-\bar{u}_2)/(\gamma_1-k_3)(\gamma_1+1)]} \tag{11}$$

$$=(\bar{u}_1-\bar{u}_2)^2\frac{\bar{u}_1\bar{u}_2-1-t_1-t_2}{\dfrac{2}{\gamma_1+1}\bar{u}_1^2-\bar{u}_1\bar{u}_2+1+t_3}, \tag{11a}$$

where

$$\bar{u}_i=u_i/a_1^*,\quad \bar{v}_2=v_2/a_1^*,\quad t_1=k_1\bar{u}_1/(\bar{u}_1-\bar{u}_2),$$

$$t_2=k_3\bar{u}_1[\bar{u}_2^2-(\gamma_1+1)(1+k_1)/(\gamma_1-1)]/(\bar{u}_1-\bar{u}_2)(\gamma_1-k_3)(\gamma_1+1),$$

and

$$t_3=k_3\bar{u}_1(\bar{u}_1-\bar{u}_2)/(\gamma_1-k_3)(\gamma_1+1).$$

This is the desired solution $\bar{v}_2=f(\bar{u}_1,\ \bar{u}_2,\ \gamma_1,\ k_1,\ k_3)$. From Eq. (6)

$$\beta=\tan^{-1}\left\{\frac{\dfrac{2}{\gamma_1+1}\bar{u}_1^2-\bar{u}_1\bar{u}_2+1+t_3}{\bar{u}_1\bar{u}_2-1-t_1-t_2}\right\}^{\frac{1}{2}}. \tag{12}$$

δ can be calculated directly from Eqs. (7) and (11).

Using the relations

$$a_i^2=\gamma_i p_i/\rho_i \quad\text{and}\quad M_i=u_i/a_i \tag{13}$$

Eq. (4) gives

$$M_1=\left(\frac{\gamma_1+1}{2}\frac{1}{\bar{u}_1^2}-\frac{\gamma_1-1}{2}\right)^{-\frac{1}{2}}. \tag{14}$$

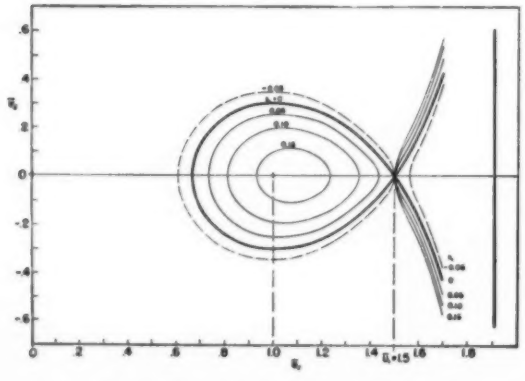

FIG. 2. Supersonic generalized shock polars.

Likewise from Eq. (5)

$$M_2=\left[(1+k_3)(\gamma_1-1-k_3)\times\left\{\frac{\gamma_1+1}{2(\gamma_1-1)}\cdot\frac{1+k_1}{\bar{u}_2^2+\bar{v}_2^2}-\frac{1}{2}\right\}\right]^{-\frac{1}{2}}. \tag{15}$$

Again using the relations (13) and substituting in Eq. (2) after rearrangement gives

$$\frac{p_2}{p_1}=\frac{1+\gamma_1M_1^2\sin\beta}{1+\dfrac{(\gamma_1-k_3)(1+k_2)M_2^2}{\bar{u}_2^2+\bar{v}_2^2}(\bar{u}_2\sin\beta-\bar{v}_2\cos\beta)^2} \tag{16}$$

which in view of Eqs. (11) and (15) determines the pressure ratio as a function of γ_1, u_1, u_2, k_1, k_2, and k_3.

From the isentropic relation

$$p_{0i}/p_i=[1+(\gamma_i-1)M_i/2]^{\gamma_i/(\gamma_i-1)}$$

applied separately to each side of the disturbance the ratio of stagnation pressures becomes

$$\frac{p_{02}}{p_{01}}=\frac{p_2}{p_1}\frac{[1+(\gamma_1-1-k_3)M_2^2/2]^{(\gamma_1-k_3)/(\gamma_1-1-k_3)}}{[1+(\gamma_1-1)M_1^2/2]^{\gamma_1/(\gamma_1-1)}}. \tag{17}$$

Using Eqs. (13)

$$\frac{\rho_2}{\rho_1}=\frac{p_2}{p_1}\left(\frac{M_2}{M_1}\right)^2\left(\frac{\bar{u}_1^2}{\bar{u}_2^2+\bar{v}_2^2}\right). \tag{18}$$

Equations (11), (12), (15), (16), (17), and (18) consist of a complete solution of Eqs. (1) to (5) without approximation and giving v_2, β, M_2, p_2, p_{02}, and ρ_2 respectively in terms of the initial conditions u_1, p_1, ρ_1, and a_1^* and the four parameters u_2, k_1, k_2, k_3. Any one of the quantities v_2, β, or δ, of course, may be used as parameter instead of u_2.

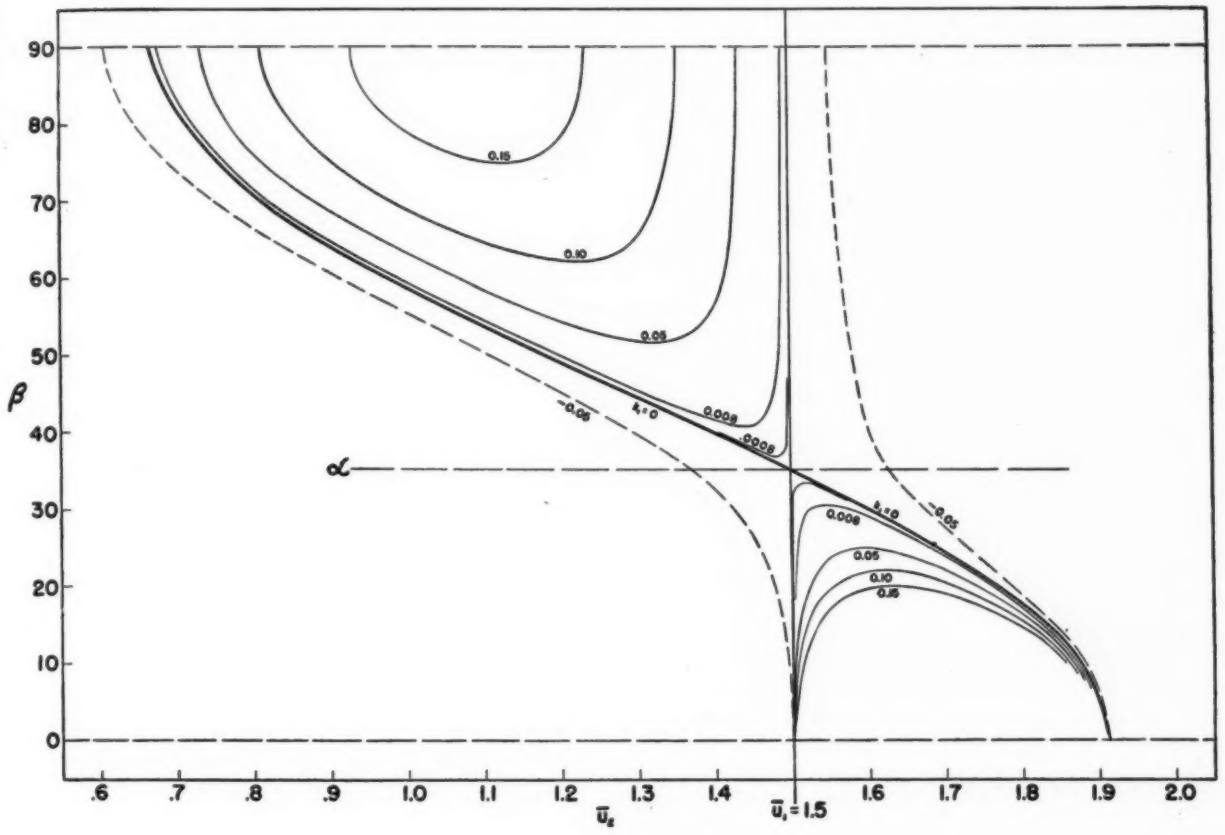

FIG. 3.

ENTROPY RELATIONS

The entropy on the initial side is given by

$$S_1=[R_1\gamma_1/(\gamma_1-1)]\log T_{01}-R_1\log p_{01}+S_{01}$$

and for the final side by

$$S_2=[R_2\gamma_2/(\gamma_2-1)]\log T_{02}-R_2\log p_{02}+S_{02}.$$

Since only changes in entropy are of interest we may choose the same reference $S_{01}=S_{02}$ for both sides of the disturbance. Hence, the change in entropy across the disturbance is

$$\begin{aligned}S_2-S_1&=[R_2\gamma_2/(\gamma_2-1)]\log T_{02}\\&\quad-[R_1\gamma_1/(\gamma_1-1)]\log T_{01}\\&\quad-R_2\log p_{02}+R_1\log p_{01}\\&=\log[\{T_{01}(1+k_1)\}^{[R_2(\gamma_1-k_3)]/[\gamma_1-1-k_3]}\\&\quad\cdot(T_{01})^{R_1\gamma_1/(\gamma_1-1)}\cdot(p_{01})^{R_1}\cdot(p_{02})^{-R_2}]\end{aligned}\tag{19}$$

where $C_pT_{02}=C_pT_{01}+H$.

For the special case where $k_3=0$, that is with $\gamma_1=\gamma_2$ then also $R_1=R_2$, and

$$\begin{aligned}(S_2-S_1)_{k_3=0}&=R\log(1+k_1)^{\gamma/(\gamma-1)}-R\log p_{02}/p_{01}\\&=R\log[(1+k_1)^{\gamma/(\gamma-1)}(p_{01}/p_{02})].\end{aligned}\tag{20}$$

DISCUSSION OF THE SOLUTION

It is noted that Eqs. (10) through (20) reduce to the usual equations for ordinary oblique shock waves when $k_1=k_2=k_3=0$. Likewise for $\beta=90°$ (or $\bar{v}_2=0$ with $\bar{u}_2\neq\bar{u}_1$), and $k_2=k_3=0$ but $k_1\neq0$ the equations reduce to the equations of normal shock waves with heat release.

The presence of the two terms t_1 and t_2 in Eq. (11a) for the velocity component, $\bar{v}_2$, and Eq. (12) for the wave front angle β, introduces important differences from the corresponding equations for ordinary oblique shock waves. The factor $1/(\bar{u}_1-\bar{u}_2)$ which appears in each of these terms becomes large as $\bar{u}_2$ approaches $\bar{u}_1$. Consequently $\bar{v}_2$ becomes zero for three distinct values of $\bar{u}_2$ rather than for three values two of which are coincident, as for ordinary oblique shock waves. These three values may be obtained by setting the numerator of Eq. (11a) to zero.

There is a discontinuity in the curve of $\bar{v}_2$ considered as a function of $\bar{u}_2$. The discontinuity consists of a "jump" between the two largest solutions, and $\bar{v}_2$ is imaginary between these two values. These features are to be noted on the typical curves given in Fig. 2.

For ordinary oblique shock waves, the wave front angle, β, when considered as a function of $\bar{u}_2$, decreases monotonically from 90° for $\bar{u}_2=1/\bar{u}_1$ to a mini-

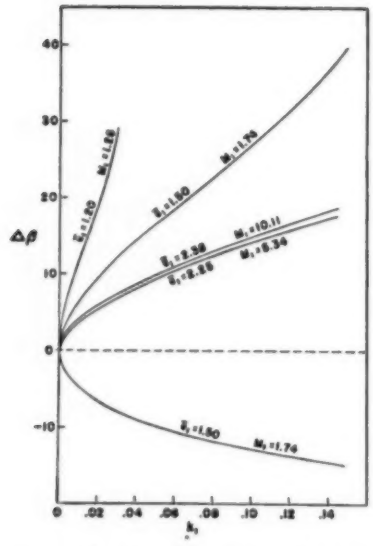

FIG. 4. Flow shift, $\Delta\beta$ *vs* heat exchange parameter, k_1.

mum value ($\beta \to \alpha$) called the Mach angle, $\alpha = \sin^{-1}(1/M_1)$ at $\bar{u}_2 = \bar{u}_1$. The mathematical solution for ordinary shock waves is continuous through $\bar{u}_1$ but has no physical significance because of entropy considerations. For the case where the sum of the additional terms containing k_1 and k_3 is negative, however, as $\bar{u}_2$ increases β decreases to a minimum, which is greater than α, and then increases again to 90°. For $\bar{u}_2 > \bar{u}_1$ β approaches a maximum value which is always less than α. For such circumstances then β is always a definite increment greater or less than the Mach angle.

Typical curves of β *vs* $\bar{u}_2$ are shown in Fig. 3. The difference between the minimum value of β and the corresponding Mach angle ($\Delta\beta = \beta - \alpha$) is shown in Fig. 4 as a function of typical values of k_1 and several values of initial Mach number, M_1. (k_3 has been assumed zero for these curves.)

The value of $\bar{u}_2$ at which the minimum (or maximum) possible β occurs is found by calculating from $d\beta/d\bar{u}_2$ using Eq. (12). This gives

$$(\bar{u}_2)_{\substack{\min \\ \max}\beta} = \frac{a-1-k_1}{a-1}\bar{u}_1 \pm [1/(a-1)] \times [(a-1-k_1)\bar{u}_1^2 - (a-1)\{\bar{u}_1^2(a-1) - k_1(\bar{u}_1^2+a)\}]^{\frac{1}{2}}$$

where

$$a = [\gamma/(\gamma-1)]\bar{u}_1^2 + 1.$$

The presence of the terms involving k_1, k_2, and k_3 in Eq. (17) for stagnation pressure and Eq. (19) or (20) for entropy change permits physically possible flows with $\bar{u}_2 > \bar{u}_1$, both in subsonic ($\bar{u}_1 < 1$) and supersonic ($\bar{u}_1 > 1$) flows. For ordinary oblique shock waves where $k_1 = k_2 = k_3 = 0$ for the entropy change to be positive or zero as noted from Eq. (20), $p_{01}/p_{02} \geq 1$. However, for $k_1 > 0$ because of the factor $1 + k_1$ in Eq. (20), p_{01}/p_{02} can be less than one and the entropy change across the disturbance can still be positive. Thus using Eq. (20) for $S_2 - S_1 \geq 0$

$$(1+k_1)^{\gamma/(\gamma-1)}(p_{01}/p_{02}) \geq 1$$

or $(p_{01}/p_{02}) \geq (1+k_1)^{\gamma/(\gamma-1)}$ is allowable.

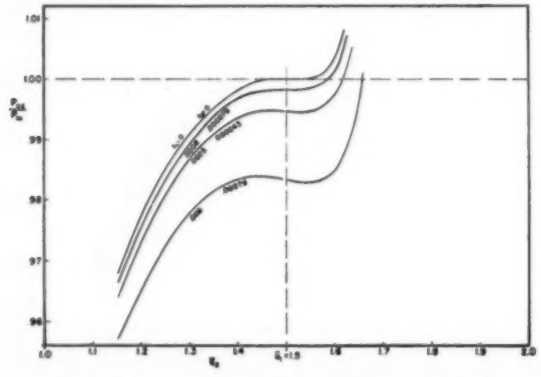

FIG. 5. Stagnation pressure ratio *vs* k_1 and $\bar{u}_2$.

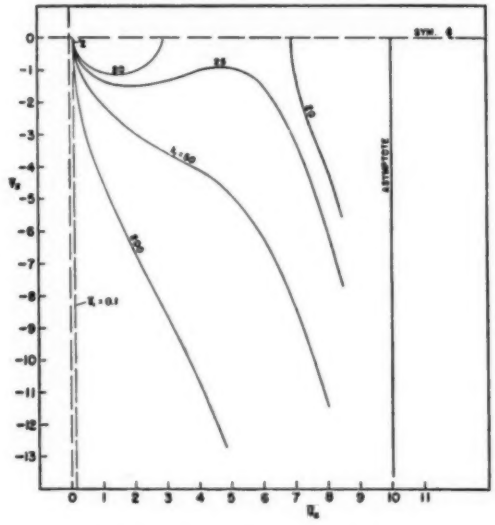

FIG. 6. Subsonic shock polars.

Typical curves of p_{02}/p_{01} as a function of $\bar{u}_2$ for various values of k_1 are given in Fig. 5.

The presence of the terms involving k_1 and k_3 makes it possible for $\bar{v}_2$ and β to have real values when $\bar{u}_1 < 1$ (or $M_1 < 1$). Thus it is seen that subsonic oblique shock waves are physically possible. A set of typical contours for subsonic shock waves is shown in Fig. 6.

The term t_3 in the denominator of Eq. (11a) (or numerator of Eq. (12)) introduces no important difference from that of the term t_1 beyond a slight distortion of the curves.

In Eqs. (14), (16), (17), and (18) for M_2, p_2, p_{02}, and ρ_2 respectively, the presence of the parameters k_1, k_2,

and k_3 introduces no important differences from the corresponding equations for ordinary shock waves except through the velocity component $\bar{v}_2$ given by Eq. (11).

It is noted that the parameter k_2 is absent as a direct factor in Eq. (11) (for the velocity) but that it does appear in the pressure and density relations. This is as expected from the nature of the assumption leading to Eq. (5) where it is assumed that the incompressible portion of the particles have the same velocity pattern as the portion of the fluid remaining compressible. Thus, only the pressure and density of the compressible fluid downstream would be effected by the transfer to the incompressible state, i.e., by the value of k_2.

GENERALIZED SHOCK WAVE POLARS

Equation (11) for the velocity may be represented graphically in the hodograph plane as the curve $\bar{v}_2=f(\bar{u}_2)$. By considering the parameters $\bar{u}_1$, k_1, and k_3 as constants, a different curve, of course is obtained for each set of values of the parameters. There being three parameters, each of which may have an infinite number of possible constant values, there exists the possibility of a triple infinity of such contours or curves. A number of such contours are shown in Figs. 2 and 6.

ORDINARY SHOCK POLARS

For k_1 and k_3 both zero, Eq. (11) reduces to the equation for ordinary oblique shock waves (the strophoid). For each value of the parameter $\bar{u}_1$ the curve known as the oblique shock wave polar is obtained. This polar is the loop of the strophoid. For values outside the loop, where $\bar{u}_2>\bar{u}_1$ a decrease in entropy across the shock wave would be required. As this is physically untenable such values of $\bar{u}_2$ are considered physically impossible. In addition, for ordinary shock waves, it is noted that the numerator of Eq. (11) becomes negative, and $\bar{v}_2$ and β become imaginary if $\bar{u}_1<1$. Likewise, the maximum value of $\bar{u}_1$ is limited (to 2.449 with $\gamma=1.405$) by Eq. (13). Within this range of values of $\bar{u}_1$ then the loop of the strophoid (where $\bar{u}_2<\bar{u}_1$) varies from a point for $\bar{u}_1=1$ ($M_1=1.0$) to a circle tangent to the asymptote of the strophoid for $\bar{u}_1$ maximum (where $M\rightarrow\infty$). The ordinary shock polar for $\bar{u}_1=1.5$ is shown by the heavy curve where $k_1=0$ in Fig. 2.

SHOCK POLARS WITH ENERGY EXCHANGE

For each ordinary shock polar (corresponding to a particular value of $\bar{u}_1$ with k_1 and k_3 both zero) and for each value of k_1 different from zero a modified shock polar is obtained. These modified polars are as shown in Fig. 2. They are no longer strophoids and a discontinuity is observed at values of $\bar{v}_2$ just less than $\bar{u}_1$ for $k_1>0$ and just greater than $\bar{u}_1$ for $k_1<0$. It is also observed that the curves with $k_1\neq0$ intersect the axis $\bar{v}_2=0$ normally rather than at the complement of the Mach angle.

TABLE I.

Dew point	k_1	k_2
−60°F	0.0002126	0.000,021
−40	0.000801	0.000,078
−20	0.002650	0.000,258
0	0.007910	0.000,770
+20	0.02210	0.002,150

SHOCK POLARS WITH CHANGE OF SPECIFIC HEAT RATIO

For $k_3\neq0$ (and $k_1=0$) the modifications to the ordinary shock polar are much the same as for $k_1\neq0$. The presence of $\bar{u}_2$ in the numerator of the k_3 term will introduce a slight distortion in the curve but otherwise the curve will have the same general characteristics as the curves for $k_1\neq0$.

For both $k_1\neq0$ and $k_3\neq0$ the effects are additive.

SUBSONIC SHOCK POLARS

Real values of the velocity component $\bar{v}_2$ are obtained as long as

$$\bar{u}_1\bar{u}_2-1-t_1-t_2\geq0.$$

Because of the factor $1/(\bar{u}_1-\bar{u}_2)$ in the terms t_1 and t_2 and the negative signs, if $\bar{u}_2>\bar{u}_1$ both $\bar{u}_1$ and $\bar{u}_2$ can be less than one and subsonic shock waves are possible. A typical set of subsonic shock polars is shown in Fig. 6 for $\bar{u}_1=0.1$ with $k_1>0$ and $k_3=0$. It is noted that the solution becomes imaginary over certain ranges of $\bar{u}_2$ for the smaller values of k_1. Values of k_1 and $\bar{u}_1$ of the order of those of interest in flame propagation studies fall within the range of values for which subsonic oblique shock waves can occur.

OBLIQUE CONDENSATION SHOCK PHENOMENA

From the work of Oswatitsch[2] and others, it has been shown that the rapid condensation of vapor induced by sudden expansion of unsaturated gases can induce shock waves in supersonic flow. For such cases k_1 (the heat released) is the latent heat of vaporization (and possibly of fusion) of a very rapid condensation process (of the order of 10^{-4} sec), k_2 is the portion of vapor condensed and k_3 is the change in the ratios of specific heats.

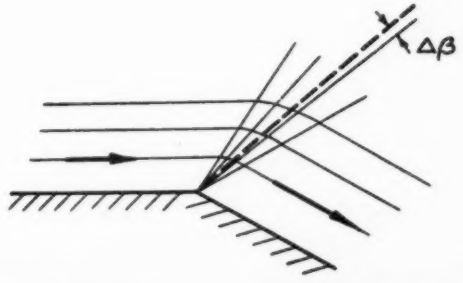

FIG. 7. Schematic illustrating flow shift induced by $\Delta\beta$.

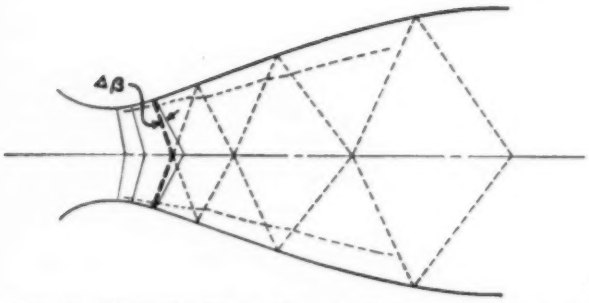

FIG. 8. Schematic illustrating (1) shock wave pattern induced by oblique condensation shock wave and (2) effect on boundary layer growth.

CONDENSATION OF WATER VAPOR

For expansion of moist air to supersonic speeds the parameters k_i are dependent upon the dew point of the air before the expansion. For expansion from atmospheric pressure and temperature, for example, (if it is assumed that all the water vapor condenses within the shock wave) then k_1 and k_2 are dependent upon dew point approximately as shown in Table I.[4] The effect of k_3 (which is less than 1 percent of the effect of k_1) on $\bar{v}_2$ is neglected.

These values of k_1 are approximately those shown in Figs. 2 to 5.

For flow fields where condensations occur, for example, in an expansion about a corner, the theory predicts an oblique condensation shock wave which will induce a shift in flow pattern because of the shift $\Delta\beta$. This is illustrated in Fig. 7. Likewise in a supersonic nozzle a shift induced by a condensation shock is also predicted. Such oblique condensation shocks form the forward leg of the x shaped shock pattern found under such circumstances (see reference 2). The downstream leg which would then be an ordinary shock wave, if all the condensation occurs in the forward leg, will be reflected at the walls and set up a criss-cross pattern of ordinary shock waves such as are often observed downstream in such cases. The shock waves are gradually dissipated, of course, as they pass down the nozzle, and the flow along the centerline of the nozzle, for example, is generally non-isentropic, (see Fig. 8).

The interaction of these condensation and ordinary shock waves with the boundary layer will induce shifts in the boundary layer thickness to satisfy the necessary shifts in the deflection of flow across the oblique shock waves, and thus, the condensation will accordingly induce "flat spots" in the boundary layer which will have an influence on the flow similar to that of irregularities in manufacture.

CONDENSATION OF AIR COMPONENTS

Application to the condensation of air components in a hypersonic expansion indicates important differences.

[4] I. D. Faro, "Condensation effects in supersonic blowdown tunnels," CF-1020, Applied Physics Lab./Johns Hopkins University (June 22, 1948).

TABLE II.

Percentage oxygen condensed	k_1	k_2	$(1+k_1)^{\gamma/(\gamma-1)}$ = maximum allowable P_{02}/P_{01}
5	0.005	0.011	1.017
10	0.01	0.023	1.035
20	0.02	0.046	1.07

The latent heat of condensation is much less, but larger portions of compressible fluid (air) can be condensed. Thus, values of the parameters k_1 and k_2 as shown in Table II are considerably different. Table II gives values for condensation of various percentages of oxygen expanded from 500°K.

From Eq. (20) the flow across the shock wave will be isentropic if $S_2-S_1=0$ or if $(1+k_1)^{\gamma/(\gamma-1)}(P_{01}/P_{02})=1$.

For $k_1>0$ this condition can be satisfied for a limited range of values of $\bar{u}_2>\bar{u}_1$ and for $k_1<0$ for $\bar{u}_2$ less than a certain limiting $\bar{u}_2$ which is greater than $\bar{u}_1$.

While such flows are isentropic allowable values of $\Delta\beta$ and consequently of the shift in flow pattern are appreciable and the values P_{02}/P_{01} can be somewhat different from 1.0. In keeping with the third assumption also, the wave or disturbance can be of considerable thickness and need not be considered an infinitesimally thin discontinuity. These predictions are generally in accordance with experimental findings for such flows.[5]

APPENDIX

In transferring from the compressible to the incompressible state, e.g., in cases involving condensation, on the upstream side there is an *average* total energy, E_t, associated with each of the vapor molecules to be condensed. E_t comprises both kinetic energy of molecular agitation (heat energy) E_k, and molecular potential energy, E_p. Hence

$$E_t=E_k+E_p.$$

Upon condensation a number of these molecules, say n, form a droplet. Immediately after formation the droplet has a total energy equal to the sum of the total energies of all n molecules which make up the droplet namely, nE_t. In the state of association in close proximity with other molecules within the droplet, however the resultant molecular potential energy of the molecules making up the droplet is less than the sum of the separate molecular energies prior to formation of the droplet. Hence

$$(nE_p)_2<(nE_p)_1.$$

Since, by the law of conservation of energy

$$(nE_t)_2=(nE_t)_1,$$

then

$$(nE_k)_2>(nE_k)_1,$$

and it is noted that the kinetic energy of agitation of

[5] S. G. Reed, Jr., Phys. Rev. **82**, 312(A) (1951).

the droplet is greater than the sum of the separate kinetic energies of the free vapor molecules.

This increased agitation energy, $(nE_k)_2-(nE_k)_1$ which is largely distributed statistically by collisions to the surrounding compressible gaseous molecules, is, of course, the heat energy which is exchanged. If m droplets of n molecules each are formed per unit volume then

$$m[(nE_k)_2-(nE_k)_1]=H.$$

The heat energy is thus exchanged in a statistical manner and it follows that the droplets and the gaseous molecules reacting statistically in this way must approach the same drift (or stream) velocity if the energy exchange from droplets to free gaseous molecules is to approach equilibrium. The average drift velocity times the time required for the exchange is the width of the transition region necessary for the exchange and is one of the factors determining the thickness of the wave front as discussed in assumption (3).

If other forces such as may be induced by gravity or by an electric or magnetic field act on the droplets an additional drift velocity component (downward for a gravity field) will be induced. By Stokes law the limiting value is proportional to $\rho r^2/\eta$, where ρ is the density, η is coefficient of viscosity, and r is the radius of the droplet.

In this analysis it is assumed either (1) that no such resultant forces are present or (2) that the droplets are sufficiently small in radius or that the region of consideration downstream of the wave front is sufficiently close to the wave front so that any additional velocity components induced by such extraneous forces are negligible by comparison.

JOURNAL OF APPLIED PHYSICS VOLUME 22, NUMBER 12 DECEMBER, 1951

Studies in Nonlinear Vibration Theory*

STANLEY FIFER
The Reeves Instrument Corporation, New York, New York
(Received May 21, 1951)

In his paper, the author determines the stability of periodic solutions of (1) the general forced Duffing equation without damping, $\ddot{x}+x+\epsilon f(x)=\epsilon E\cos\omega t$, $f(x)$ a polynomial, $\epsilon\ll 1$; (2) the forced Duffing equation with damping, $\ddot{x}+\epsilon r\dot{x}+\alpha x+\epsilon x^3=\epsilon E\cos(\omega t+\psi)$, $\epsilon\ll 1$; and (3) the general forced Van der Pol equation, $\ddot{x}-\epsilon f(\dot{x})+x=\epsilon E\cos(\omega t+\psi)$, $f(\dot{x})$ an odd polynomial, $\epsilon\ll 1$, by seeking conditions necessary to insure periodic or almost-periodic solutions of the corresponding variational equation. The former are obtained rigorously by means of an existence proof and the latter formally by perturbation series. A vertical tangent theorem is derived which states that the locus of the points of contact of the vertical tangents to the response curves is a stability boundary, since it coincides, in the first approximation, with the locus of periodic solutions of the variational equation. These techniques are illustrated by considering the forced vibrations of a triode oscillator with a fifth-order tube characteristic, this being a particular case of (3), where we set $f(\dot{x})=\dot{x}-\frac{1}{3}\dot{x}^3+\lambda\dot{x}^5$.

1. INTRODUCTION

THE Van der Pol and Duffing equations are basic in the field of nonlinear vibrations. Both are of the second order; the first contains a nonlinear damping term and the second a nonlinear spring term. In his paper, the author treats three forms of these equations:

1. the general forced Duffing equation without damping,

$$\ddot{x}+x+\epsilon f(x)=\epsilon E\cos\omega t,\ f(x)\text{ a polynomial},\ \epsilon\ll 1; \quad (1.1)$$

2. the forced Duffing equation with damping,

$$\ddot{x}+\epsilon r\dot{x}+\alpha x+\epsilon x^3=\epsilon E\cos(\omega t+\psi),\quad \epsilon\ll 1; \quad (1.2)$$

3. the general forced Van der Pol equation,

$$\ddot{x}-\epsilon f(\dot{x})+x=\epsilon E\cos(\omega t+\psi),\quad f(\dot{x})\text{ an odd polynomial},\ \epsilon\ll 1. \quad (1.3)$$

Periodic solutions of each of these equations with frequency ω equal to that of the driving force are known to exist.[1] Several methods have been employed[2–6] to determine the stability of periodic solutions for some special cases of these equations. We use the following definition of stability:[3]

Let $x_\epsilon(t)$ be a periodic solution of the particular differential equation. Then if we insert $x_\epsilon(t)+\delta(t)$ for $x_\epsilon(t)$ in the equation, and neglect powers of $\delta(t)$ above the first, we obtain a linear "variational" equation for $\delta(t)$. The periodic solution $x_\epsilon(t)$ is said to be stable or unstable according as all solutions $\delta(t)$ of the variational equation are bounded or not.

* Submitted in partial fulfillment of the requirements for the degree of Doctor of Philosophy at New York University.

[1] K. O. Friedrichs, *Justification of the perturbation method*, lectures delivered at Brown University, December 5, 1942 to January 23, 1943.
[2] A. Andronow and A. Witt, Arch. Elektrotech. **24**, 99–110 (1930).
[3] J. J. Stoker, *Nonlinear Vibrations in Mechanical and Electrical Systems* (Interscience Publishers, Inc., New York, 1950).
[4] B. Van der Pol, Phil. Mag. [7] **3**, 65–80 (1927).
[5] B. Van der Pol and M. J. O. Strutt, Phil. Mag. [7] **5**, 18–38 (1928).
[6] B. Van der Pol, Proc. Inst. Radio Engrs. **22**, 1051–1086 (1934).

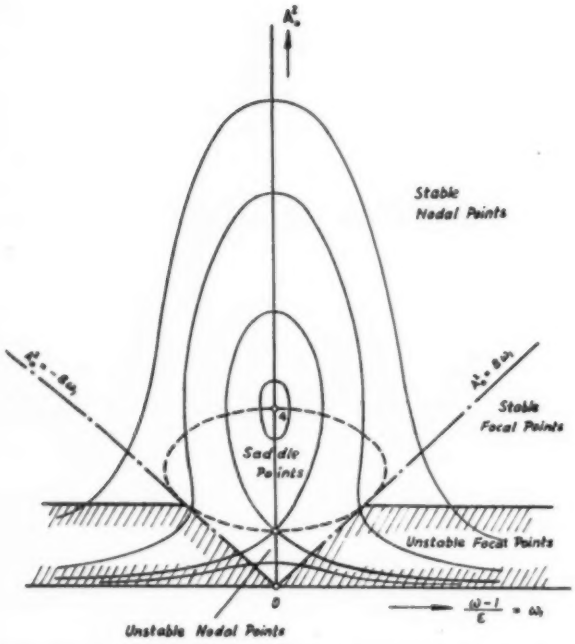

FIG. 1. Response curves and stability boundaries for Van der Pol equation with third-order characteristic.

The variational equation is in general a Hill equation. If we seek stability criteria for the periodic solutions $x_\epsilon(t)$, then, following the definition, the crux of the matter is to determine those solutions $\delta(t)$ of the variational equation which separate the stable from the unstable solutions of this equation. These solutions may be periodic or almost-periodic, for in both of these cases $\delta(t)$ neither approaches infinity nor does it damp out with increasing t, and hence is the type we seek. To sum up, the conditions imposed on the amplitude and frequency of the periodic solution of the given nonlinear equation to insure periodic or almost-periodic solutions of its variational equation are precisely the conditions which yield stability loci for the given equation. While periodic solutions of the variational equation are determined for all three equations (1.1–1.3), only in the case of Eq. (1.3) are almost-periodic solutions found.

We consider, first, periodic solutions of the variational equation. An existence proof which we derive for these solutions furnishes a general, rigorous, and comparatively simple means, in contrast to present methods, for obtaining stability criteria for the periodic solutions of Eqs. (1.1)–(1.3). (Although we have not carried it out, it seems likely that this method applies to Eq. (1.2) with a general damping term $\epsilon f(\dot{x})$, where $f(\dot{x})$ is an odd polynomial.) This method also demonstrates the validity of the following vertical tangent theorem:

Consider the response curves to first order in ϵ of the given nonlinear differential equation in the amplitude-frequency plane, with the amplitude of the driving force as parameter. The locus of the points of contact of the vertical tangents to these curves is a stability boundary, since it coincides, in the first approximation, with the locus of periodic solutions of the variational equation.

As far as we know, this has been proved only for some special cases of Eqs. (1.1) and (1.3).[3] As a means of obtaining stability boundaries, this theorem, once established, enables us to deal directly with the given nonlinear equation and eliminates the need for the variational equation.

In the case of the general Van der Pol equation (1.3), the results of Andronow and Witt[2,7] for the standard Van der Pol equation with a third-order characteristic lead us to seek almost-periodic solutions of the variational equation, as well as periodic ones, in our search for stability boundaries. The approach is a purely formal one—by perturbation series—since an attempt to prove the convergence of this series is confronted with the "difficulty of the small divisors" pointed out by Poincaré.[3]

As an interesting example of these techniques, we consider here the forced vibrations of a triode oscillator with a fifth-order tube characteristic, this being a particular case of the general Van der Pol equation (1.3), where we set

$$f(\dot{x})=\dot{x}-\tfrac{1}{3}\dot{x}^3+\lambda\dot{x}^5. \tag{1.4}$$

If we set λ equal to zero, we have the standard Van der Pol equation

$$\ddot{x}-\epsilon(\dot{x}-\dot{x}^3/3)+x=\epsilon E\cos(\omega t+\psi), \tag{1.5}$$

for which the possible amplitudes to lowest order in ϵ of the free periodic vibration are given by $A^2=0$ and $A^2=4$, where A is the initial displacement. (The response curves for Eq. (1.5) are shown in Fig. 1.) The equilibrium state is unstable, while $A^2=4$ yields a stable oscillation. It has been experimentally observed, and demonstrated by Appleton and Van der Pol,[8,9] and Eckweiler,[10] that three possible amplitudes may exist for the free periodic vibration of a triode oscillator if the nonlinear tube characteristic defining the anode current as a function of the anode voltage is approximated by a fifth-order polynomial rather than by one of the third order. If $f(\dot{x})$ is taken as in Eq. (1.4), the equilibrium state ($A^2=0$) is unstable, while the other two amplitudes, in order of increasing amplitude, are stable and unstable, respectively. If $f(\dot{x})$ is replaced by $-f(\dot{x})$, then there are two stable amplitudes separated by an unstable one. In this case, if a sufficiently large initial condition is imposed on the system, a stable amplitude $A^2\neq 0$ will be approached, while if the disturbance is small, the motions will damp out; i.e., they will approach the equilibrium state $A^2=0$. Although this is the

[7] N. Minorsky, *Introduction to Nonlinear Mechanics* (Edwards Brothers, Inc., Ann Arbor, Michigan, 1947).

[8] E. V. Appleton and B. Van der Pol, Phil. Mag. [6] **45**, 177–193 (1923).

[9] B. Van der Pol, Radio Rev. **1**, 701–710, 754–762 (1920).

[10] H. J. Eckweiler, "Non-linear differential equations of the Van der Pol type with a variety of periodic solutions," *Studies in Non-Linear Vibration Theory* (Institute for Mathematics and Mechanics, New York University, New York, 1946).

case considered by the authors cited above, we take the positive sign for the damping $f(\dot{x})$ in what follows, so that for $\lambda=0$ the equation reduces to the standard Van der Pol equation (1.5). Once we have divided the response plane into various types of stability regions with $f(\dot{x})$ as the damping term, it will be clear that the description is similar for $-f(\dot{x})$, except that the stability characteristics of several of the regions are reversed.

2. STABILITY BOUNDARIES CORRESPONDING TO PERIODIC SOLUTIONS OF THE VARIATIONAL EQUATION

We consider the Van der Pol equation with a fifth-order tube characteristic and a periodic excitation of small amplitude,

$$\ddot{x}+x=\epsilon f(\dot{x}, \omega, \psi), \quad \epsilon \ll 1, \tag{2.1}$$

where

$$f(\dot{x}, \omega, \psi)=(\dot{x}-\dot{x}^3/3+\lambda\dot{x}^5)+E\cos(\omega t+\psi). \tag{2.2}$$

Since we seek periodic solutions, we may impose the initial conditions

$$\begin{aligned} x(0)&=A, \\ \dot{x}(0)&=0, \end{aligned} \tag{2.3}$$

by proper choice of the phase ψ. (The reader is referred to this author's dissertation for a more complete treatment of the following type of derivation.)

It has been shown[1] that functions $\psi(A, \epsilon)$ and $\omega(A, \epsilon)$ can be found such that for A arbitrary, within a range, and for ϵ sufficiently small, the solution

$$x_\epsilon(t)=x(t; A, \epsilon)=x(t; \psi[A, \epsilon], \omega[A, \epsilon]), \tag{2.4}$$

after the insertion of (2.2) in (2.1), is then periodic with period

$$T=2\pi/\omega(A, \epsilon). \tag{2.5}$$

We shall prove that the variational equation "at" the periodic solution

$$x_\epsilon(t)=x(t; A, \epsilon)$$

possesses periodic solutions with the same period as those of the Van der Pol equation, provided that A is now determined as a definite function of ϵ, and provided that E lies in a specific range.

This may be interpreted geometrically. If we refer to Fig. 2 showing the response curves for the Van der Pol equation (2.1), for $\lambda=0.019$ and for several values of E, then we shall show that E is restricted to the range for which these response curves have vertical tangents. This follows from the vertical tangent theorem which we shall prove, namely, that the locus of the points of contact of the vertical tangents to the response curves coincides, in the first approximation, with the locus of periodic solutions of the variational equation. (For example, if we consider a response curve which does not have a vertical tangent, then no point on this curve can yield a set of values for A and E for which the variational equation possesses a periodic solution.)

Upon inserting the function $x_\epsilon+\delta$ for x in Eq. (2.1) and neglecting powers of δ above the first, we obtain the linear variational equation

$$\ddot{\delta}+\delta=\epsilon f_x\delta=\epsilon g(\dot{x}_\epsilon, \dot{\delta}), \tag{2.6}$$

where

$$g(\dot{x}_\epsilon, \dot{\delta})=(1-\dot{x}_\epsilon^2+5\lambda\dot{x}_\epsilon^4)\dot{\delta}. \tag{2.7}$$

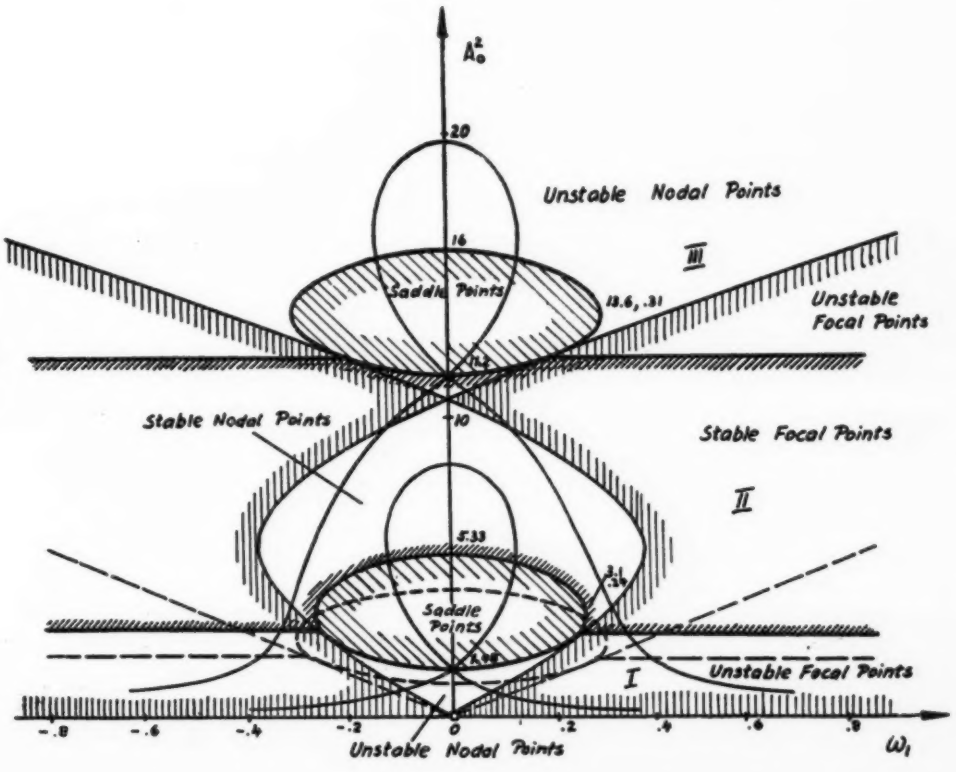

FIG. 2. Response curves and stability boundaries for Van der Pol equation with fifth-order characteristic ($\lambda=0.019$).

We impose the initial conditions

$$\delta(0)=B,\qquad \dot{\delta}(0)=C. \tag{2.8}$$

Equation (2.6) with the initial conditions (2.8) possesses a unique solution $\delta(t; A, B, C, \epsilon)$ which is analytic in t, A, B, C, and ϵ. This equation will not in general have a periodic solution for δ. We therefore seek functions $A(\epsilon)$, $B(\epsilon)$, and $C(\epsilon)$ such that, for

$$x_\epsilon(t)=x(t; A[\epsilon], \epsilon),$$

there exists a solution $\delta(t; A[\epsilon], B[\epsilon], C[\epsilon], \epsilon)$ which is periodic with period $T=2\pi/\omega(A[\epsilon], \epsilon)$. From the double infinity of values for $\psi(A, \epsilon)$ and $\omega(A, \epsilon)$ which insure the periodicity of x_ϵ for the Van der Pol equation, we thus seek a single infinity of values $\psi(A[\epsilon], \epsilon)$ and $\omega(A[\epsilon], \epsilon)$ which simultaneously insure the periodicity of δ.

Since Eq. (2.6) remains unaltered if we replace t by $t+2\pi$, the periodicity conditions for δ are

$$\delta(T[A, \epsilon]; A, B, C, \epsilon)=\delta(0; A, B, C, \epsilon)=B, \tag{2.9}$$

$$\dot{\delta}(T[A, \epsilon]; A, B, C, \epsilon)=\dot{\delta}(0; A, B, C, \epsilon)=C. \tag{2.10}$$

Since T has been determined through $x_\epsilon(t)$ as a function of A and ϵ, these are two equations for three unknowns A, B, and C, one of which may be prescribed arbitrarily. We prescribe the initial velocity C and then determine $A(C, \epsilon)$ and $B(C, \epsilon)$ such that the two periodicity conditions (2.9)–(2.10) are satisfied. We could equally well have taken the initial displacement B as arbitrary in place of C, which could then be determined.

Periodicity is insured if we can solve Eqs. (2.9)–(2.10) for A and B as functions of C and ϵ. A periodic solution of the variational equation exists for $\epsilon=0$, namely, $\delta=B\cos t+C\sin t$. It is natural to use the implicit function theorem to solve (2.9)–(2.10) in the neighborhood of $\epsilon=0$. The theorem, however, cannot be applied directly for a neighborhood of $\epsilon=0$, since for $\epsilon=0$, $T=2\pi$, and the relations (2.9)–(2.10) are satisfied identically in B and C. To overcome this difficulty, we form the expressions

$$P(A, B, C, \epsilon)=\epsilon^{-1}(B-\delta(T[A, \epsilon]; A, B, C, \epsilon)), \tag{2.11}$$

$$Q(A, B, C, \epsilon)=\epsilon^{-1}(C-\dot{\delta}(T[A, \epsilon]; A, B, C, \epsilon)). \tag{2.12}$$

The periodicity conditions are

$$P=0, \tag{2.13}$$

$$Q=0. \tag{2.14}$$

To prove that periodic solutions of the variational equation exist in the neighborhood of $\epsilon=0$ by means of the implicit function theorem, reduces to proving that we can find solutions A_0, B_0 of the equations $P_0=0$, $Q_0=0$, obtained by taking ϵ equal to zero, such that the jacobian

$$J_0=\partial(P_0, Q_0)/\partial(A_0, B_0)\neq 0. \tag{2.15}$$

We replace the differential equation (2.6) and the initial conditions (2.8) by the integral equations

$$\delta(t)=B\cos t+C\sin t+\epsilon\int_0^t g(\dot{x}_\epsilon, \dot{\delta})\sin(t-\tau)d\tau, \tag{2.16}$$

$$\dot{\delta}(t)=-B\sin t+C\cos t+\epsilon\int_0^t g(\dot{x}_\epsilon, \dot{\delta})\cos(t-\tau)d\tau. \tag{2.17}$$

The relations for P and Q become

$$P=\epsilon^{-1}\Big(B[1-\cos T]-C\sin T-\epsilon\int_0^T g(\dot{x}_\epsilon, \dot{\delta})\sin(T-\tau)d\tau\Big), \tag{2.18}$$

$$Q=\epsilon^{-1}\Big(B\sin T+C[1-\cos T]-\epsilon\int_0^T g(\dot{x}_\epsilon, \dot{\delta})\cos(T-\tau)d\tau\Big). \tag{2.19}$$

For ϵ equal to zero, we have

$$T=2\pi, \tag{2.20}$$

$$x_0=A_0\cos t, \tag{2.21}$$

$$\dot{x}_0=-A_0\sin t, \tag{2.22}$$

$$\delta_0=B_0\cos t+C\sin t, \tag{2.23}$$

$$\dot{\delta}_0=-B_0\sin t+C\cos t. \tag{2.24}$$

At this point, we introduce the variable η, where η is given by the relation

$$T(A, \epsilon)=2\pi/\omega(A, \epsilon)=2\pi+\epsilon\eta(A, \epsilon), \tag{2.25}$$

so that the terms $\epsilon^{-1}(1-\cos T)$ and $\epsilon^{-1}\sin T$ in the expressions for P and Q (2.18)–(2.19) approach definite limits as ϵ approaches zero. The function $\eta(A, \epsilon)$ defines the response curves for the Van der Pol equation (2.1) in the $\eta-A$ plane. For $\epsilon=0$, we have

$$\eta_0=\eta(A_0, 0), \tag{2.26}$$

which is the first-order approximation to the response curves, and is given by

$$\eta_0^2=(\pi^2/A_0^2)(E^2-A_0^2[1-\tfrac{1}{4}A_0^2+\tfrac{5}{8}\lambda A_0^4]^2). \tag{2.27}$$

This response relationship may be derived by standard perturbation techniques applied to Eq. (2.1). For $\epsilon=0$, the periodicity relations become

$$P_0=-C\eta_0-\pi B_0(1-\tfrac{3}{4}A_0^2+25\lambda A_0^4/8)=0, \tag{2.28}$$

$$Q_0=B_0\eta_0-\pi C(1-\tfrac{1}{4}A_0^2+5\lambda A_0^4/8)=0. \tag{2.29}$$

They are satisfied if A_0^2 is such that

$$\eta_0^2=-\pi^2(1-\tfrac{1}{4}A_0^2+5\lambda A_0^4/8)\times(1-\tfrac{3}{4}A_0^2+25\lambda A_0^4/8) \tag{2.30}$$

and if B_0 is chosen so that Eq. (2.29) is satisfied, which is possible if

$$25\lambda A_0^4-6A_0^2+8\neq 0. \tag{2.31}$$

Equation (2.30) is precisely the stability boundary in the $\eta_0-A_0^2$ plane which we seek. As will be seen later, this boundary is in general a pair of ovals symmetrically disposed with respect to the η_0-axis. The upper vertices of these ovals correspond to free vibrations and the lower ones to forced vibrations.

Thus, periodic solutions of the variational equation exist, for values of η_0 and A_0^2 which satisfy Eq. (2.30), except for those values for which condition (2.31) is violated or for which the jacobian $J_0=\partial(P_0, Q_0)/\partial(A_0, B_0)=0$ (2.15). Condition (2.31) is violated at the lower vertices of the ovals represented by (2.30); J_0 vanishes here as well as at the points where the ovals have vertical tangents. If we exclude values of η_0 and A_0^2 corresponding to these points, then the existence of periodic solutions of Eq. (2.6) is insured.

We can express the response relationships (2.27) for the Van der Pol equation and the stability locus (2.30) in terms of the frequency and amplitude. From the relationships

$$\omega=1+\epsilon\omega_1+\cdots, \tag{2.32}$$

$$T=2\pi/\omega=2\pi(1-\epsilon\omega_1+\cdots)=2\pi+\epsilon\eta_0+\cdots, \tag{2.33}$$

we have

$$\eta_0=-2\pi\omega_1. \tag{2.34}$$

Equation (2.21) becomes

$$4\omega_1^2=(E^2/A_0^2)-(1-\tfrac{1}{4}A_0^2+5\lambda A_0^4/8)^2 \tag{2.35}$$

and Eq. (2.30) becomes

$$4\omega_1^2=-(1-\tfrac{1}{4}A_0^2+5\lambda A_0^4/8)\times(1-\tfrac{3}{4}A_0^2+25\lambda A_0^4/8). \tag{2.36}$$

To demonstrate that the locus of periodic solutions of the variational equation coincides in the first approximation with the locus of the points of contact of the vertical tangents to the response curves, we differentiate Eq. (2.35) with respect to A_0 and set $\omega_1'=0$. The result is

$$8\omega_1\omega_1'=(-E^2/A_0^4)-2(1-\tfrac{1}{4}A_0^2+5\lambda A_0^4/8)\times(-\tfrac{1}{4}+5\lambda A_0^2/4)=0. \tag{2.37}$$

Inserting the value of E^2 from (2.35),

$$E^2=4A_0^2\omega_1^2+A_0^2(1-\tfrac{1}{4}A_0^2+5\lambda A_0^4/8)^2, \tag{2.38}$$

we obtain

$$4\omega_1^2=-(1-\tfrac{1}{4}A_0^2+5\lambda A_0^4/8)(1-\tfrac{3}{4}A_0^2+25\lambda A_0^4/8)$$

which is the stability boundary derived before, Eq. (2.36). This proves, for the present case, the vertical tangent theorem.†

† The theorem has been proved similarly for Eqs. (1.1)–(1.3) in this author's dissertation.

3. STABILITY BOUNDARIES CORRESPONDING TO ALMOST PERIODIC SOLUTIONS OF THE VARIATIONAL EQUATION

Every point in the response plane for Eq. (2.1) yields an amplitude and frequency of a possible harmonic oscillation of this equation for a given amplitude of the excitation. In Sec. 2 we obtained a stability boundary for these periodic solutions by deriving a condition necessary to insure the existence of periodic solutions of the variational equation of (2.1). In this section, we shall seek a condition necessary to insure almost-periodic solutions of the variational equation, i.e., solutions containing frequencies whose ratios are, in general, incommensurable. Almost-periodic solutions neither grow large nor decay with increasing t and hence may separate unstable from stable solutions, according to the definition of stability given in Sec. 1.

The approach is a purely formal one and is carried out by means of perturbation series. Before we proceed, we shall explain why it is reasonable to look for almost-periodic solutions $\delta(t)$. Andronow and Witt[2] apply the Poincaré theory of singularities to divide the response plane for the standard Van der Pol equation into regions of stable and unstable focal and nodal points, and unstable saddle points, as shown in Fig. 1. (We carry out such a classification for Eq. (2.1) in Sec. 4.) If a point is an unstable focal point, for example, it means that the corresponding periodic solution is unstable, since any slight disturbance would result in a solution which departs with increasing t from the periodic one. Andronow and Witt have shown and it has been observed experimentally that, if an unstable focal point lies sufficiently far from the line $\omega_1=0$, the amplitude of the oscillation may itself approach a stable limit cycle. The resulting oscillation is then a stable combination oscillation which is, in general, almost-periodic and is characterized by phase and amplitude modulation. These observations lead us to seek almost-periodic solutions of the variational equation; in Sec. 4 we shall verify that the stability boundary obtained in this way separates unstable from stable focal points (see Fig. 1).

Since this phenomenon occurs in the response plane for a region not in the immediate neighborhood of $\omega=1$, the linear free periodic vibration, we consider the Van der Pol equation in the form

$$\ddot{x}+x-\epsilon(\dot{x}-\dot{x}^3/3+\lambda\dot{x}^5)=E\cos(\omega t+\psi), \tag{3.1}$$

$$x(0)=A_0,\qquad \dot{x}(0)=0. \tag{3.2}$$

The fact that we do not take the driving force small, as in our previous treatment, means that we seek solutions of the Van der Pol equation in the neighborhood of the linear forced, rather than free, periodic vibration.

First, a periodic solution $x_\epsilon(t)$ of Eq. (3.1) is desired with the same frequency as that of the driving force. A proof that periodic solutions of Eq. (3.1) exist, and a

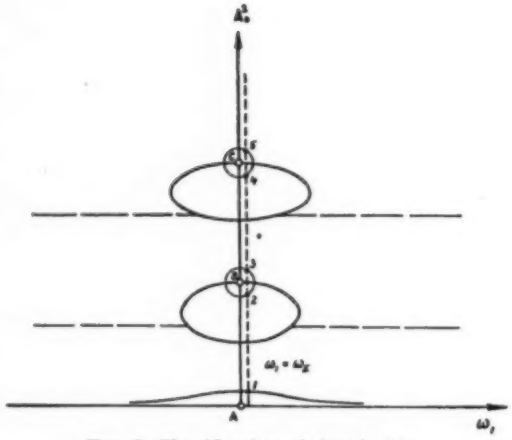

FIG. 3. Classification of singularities.

justification for this method are given in this author's dissertation.

We make the substitution $\omega t=\theta$ in Eq. (3.1). The result is

$$\omega^2x''+x-\epsilon(\omega x'-\tfrac{1}{3}\omega^3x'^3+\lambda\omega^5x'^5)=E\cos(\theta+\psi), \quad (3.3)$$

the prime denoting differentiation with respect to θ. We develop x_ϵ and ω with respect to ϵ:

$$x_\epsilon=x_0+\epsilon x_1+\cdots, \quad (3.4)$$

$$\omega=\omega_0+\epsilon\omega_1+\cdots. \quad (3.5)$$

We impose the conditions

$$\begin{aligned}&\text{(a)} && x_i(\theta+2\pi)=x_i(\theta), && i=0,\,1,\,2,\,\cdots;\\ &\text{(b)} && x_0(0)=A_0,\quad x_i(0)=0, && i=1,\,2,\,\cdots;\\ &\text{(c)} && \dot{x}_i(0)=0, && i=0,\,1,\,2,\,\cdots.\end{aligned} \quad (3.6)$$

We insert the series for x_ϵ (3.4) and ω (3.5) in Eq. (3.3) and set the coefficient of ϵ^0 equal to zero. The result is

$$\omega_0^2x''+x=E\cos(\theta+\psi). \quad (3.7)$$

Imposing the conditions (3.6) yields

$$x_0=A_0\cos\theta=A_0\cos\omega t,\quad A_0=E/(1-\omega_0^2),\quad \omega_0\neq1. \quad (3.8)$$

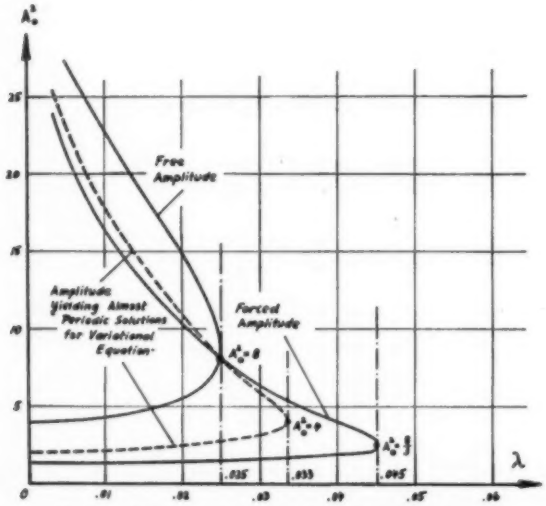

FIG. 4. Cross section of stability boundaries in $A_0^2\lambda$-plane for $\omega_1=0$.

Having obtained the zero-order approximation for the periodic solutions of (3.1), we employ the variational equation to determine the stability of these solutions. The variational equation for (3.1) is

$$\frac{d^2\delta}{dt^2}+\delta-\epsilon(1-\dot{x}_\epsilon^2+5\lambda\dot{x}_\epsilon^4)\frac{d\delta}{dt}=0. \quad (3.9)$$

We develop δ in a power series in ϵ,

$$\delta=\delta_0+\epsilon\delta_1+\cdots, \quad (3.10)$$

and require that the δ_i satisfy the conditions

$$\begin{aligned}&\text{(d)} && \delta_0(0)=B,\quad \delta_i(0)=0, && i=1,\,2,\,\cdots;\\ &\text{(e)} && \dot{\delta}_0(0)=C,\quad \dot{\delta}_i(0)=0, && i=1,\,2,\,\cdots.\end{aligned} \quad (3.11)$$

We have not imposed a periodicity condition on δ, since

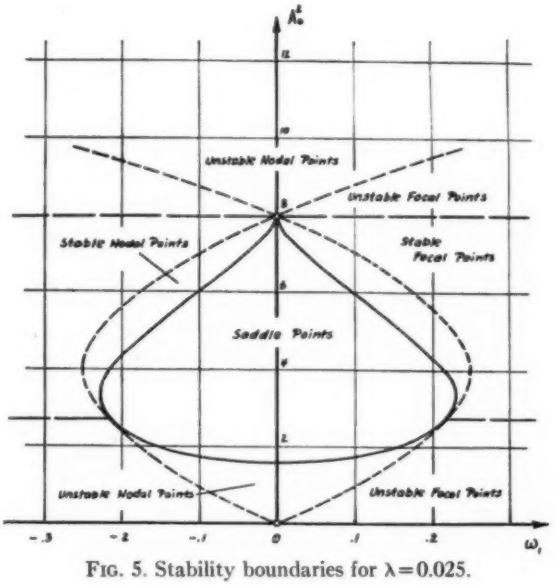

FIG. 5. Stability boundaries for $\lambda=0.025$.

we seek almost-periodic functions. We still insist, however, that the δ_i remain bounded for all t.

We insert the power series for x_ϵ and δ in Eq. (3.9) and equate the coefficients of successive powers of ϵ to zero The term of zero order in ϵ yields, subject to conditions (3.11),

$$\delta_0=B\cos t+C\sin t. \quad (3.12)$$

The term of first order in ϵ is

$$\frac{d^2\delta_1}{dt^2}+\delta_1=(1-\dot{x}_0^2+5\lambda\dot{x}_0^4)\frac{d\delta_0}{dt}. \quad (3.13)$$

For boundedness, the coefficients of the terms $\sin t$ and $\cos t$ occurring on the right-hand side of Eq. (3.13), after the insertion of the expressions for x_0 (3.8) and δ_0 (3.12), must be set equal to zero. This leads to the condition

$$15\lambda\omega^4A_0^4-4\omega^2A_0^2+8=0. \quad (3.14)$$

Although we have excluded the value $\omega=1$ in the derivation, we now set $\omega^2=1$, and $\omega^4=1$ in the above

locus, so that we can investigate its behavior in the neighborhood of the stability boundary obtained before (2.36). The result is

$$15\lambda A_0^4-4A_0^2+8=0. \tag{3.15}$$

This expression yields, in general, two values for A_0^2 for a given value of λ. The almost-periodic solutions for the variational equation therefore fall along two straight lines.

If we solve Eq. (3.13) for δ_1, we obtain terms with period $2\pi/(2\omega\pm1)$ and $2\pi/(4\omega\pm1)$. Since δ_0 is of period 2π and since ω is close to, but not equal to, unity, it follows that δ is, in general, an almost-periodic function.

4. CLASSIFICATION OF STABILITY REGIONS

Before we consider the general dependence of the stability boundaries which we have derived

$$4\omega_1^2=-(1-\tfrac{1}{4}A_0^2+5\lambda A_0^4/8)\times(1-\tfrac{3}{4}A_0^2+25\lambda A_0^4/8), \tag{2.36}$$

$$15\lambda A_0^4-4A_0^2+8=0, \tag{3.15}$$

on δ, we take the particular case of $\lambda=0.019$. This case is of interest, since it yields all of the possible stability regions. The stability boundaries together with the response curves are shown in Fig. 2. (The boundaries for the standard Van der Pol equation, $\lambda=0$, are shown in the same figure by dashed lines.) Since the point, $A_0^2=0$, $\omega_1=0$, is unstable, Region I is unstable, while II is stable and III is unstable.

The interior of the ovals is unstable, as may be demonstrated by the following argument. Consider Fig. 3. The three points A, B, and C are three possible amplitudes for the free vibration. For small E, the response curves are closed in the neighborhood of B and C, and open near A, as shown. Consider a line $\omega_1=\omega_E$ such that it intersects two closed curves corresponding to the same E, and each of these twice. Let us assume that the intersection point 2 lies in a stable region. This implies that for the fixed E and ω_1 that we have chosen there are two limit cycles in the phase plane corresponding to the points 2 and 3, both stable, without any intervening unstable limit cycle. Since two adjoining closed integral curves cannot both be stable,[11] this leads to a contradiction. Therefore, the interior of the oval is unstable; the same reasoning applies to the interior of the other oval. This completes the classification of the response plane into stable and unstable regions.

We now consider the stability relations (2.36) and (3.15) more generally. For $\omega_1=0$, the roots of the two factors on the right-hand side of Eq. (2.36) yield the vertices of the two ovals. The roots of the first factor,

$$A_0^2=1\pm(1-40\lambda)^{\frac{1}{2}}/5\lambda, \tag{4.1}$$

yield the amplitudes of the free vibration (in addition to $A_0^2=0$), while the roots of the second,

$$A_0^2=3\pm(9-200\lambda)^{\frac{1}{2}}/25\lambda, \tag{4.2}$$

correspond to forced vibrations.

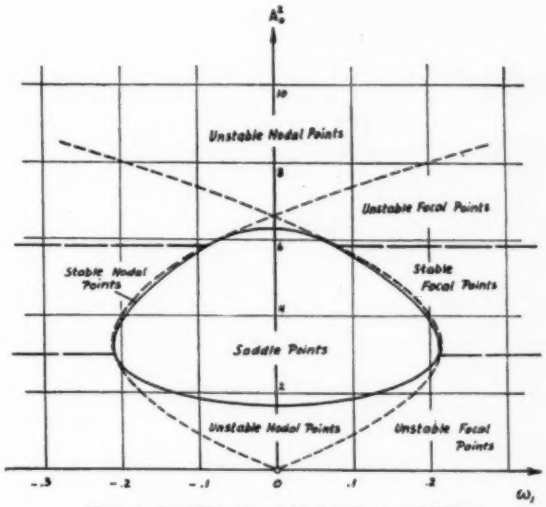

FIG. 6. Stability boundaries for $\lambda=0.030$.

These functions are plotted in Fig. 4. As λ approaches zero, one of the free vertices and one of the forced vertices, corresponding to the upper oval, recede to infinity, while the other two approach $A_0^2=4$ and $A_0^2=8/3$, the vertices of the Van der Pol ellipse. When λ exceeds 0.025, the nonzero free vibration no longer exists and only one oval remains. Closed curves still exist, however, in the response plane, enclosing the upper vertex which is the amplitude for $E=E_r\neq0$, say. For $E<E_r$, only open curves exist, in the neighborhood of $A_0^2=0$. At $\lambda=0.045$, the oval disappears and open response curves alone remain.

Equation (3.15), the other stability locus, may be written as

$$A_0^2=(2/15\lambda)[1+(1-30\lambda)^{\frac{1}{2}}]. \tag{4.3}$$

This relation is also plotted in Fig. 4. As λ approaches zero, one value of A_0^2 approaches infinity, while the

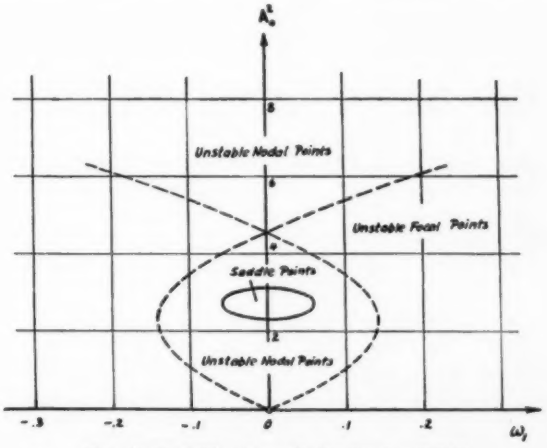

FIG. 7. Stability boundaries for $\lambda=0.044$.

[11] N. Levinson and O. K. Smith, Duke Math. J. 2, 382–403 (1942).

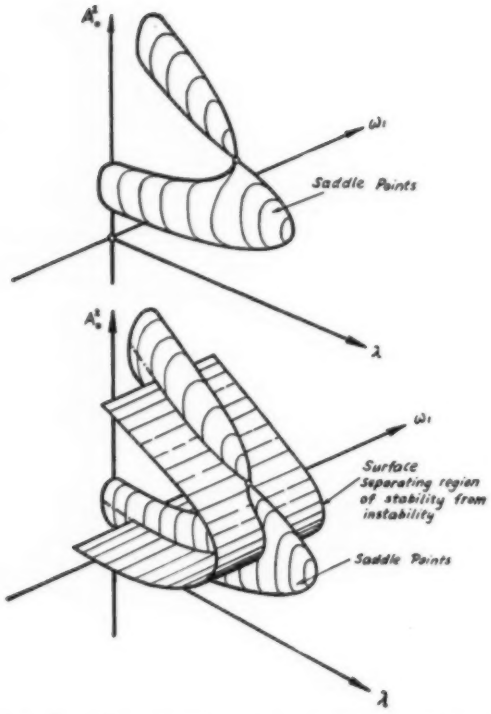

FIG. 8. Stability boundaries in $A_0^2\omega_1\lambda$-space, exterior view.

other approaches $A_0^2=4$, the Van der Pol locus. At $\lambda=0.033$, the two lines merge and the stable region between them disappears. All periodic solutions for $\lambda \gtrsim 0.033$ are unstable.

These stability loci are plotted in Figs. 5 to 7 for values of λ equal to 0.025, 0.030, and 0.044, respectively (in addition to $\lambda=0.019$, shown in Fig. 2) to illustrate the transformations in the stability loci with the variation in λ. At the value $\lambda=0.025$, the two ovals merge into one with a cusp at $A_0^2=8$. This is a triple point,

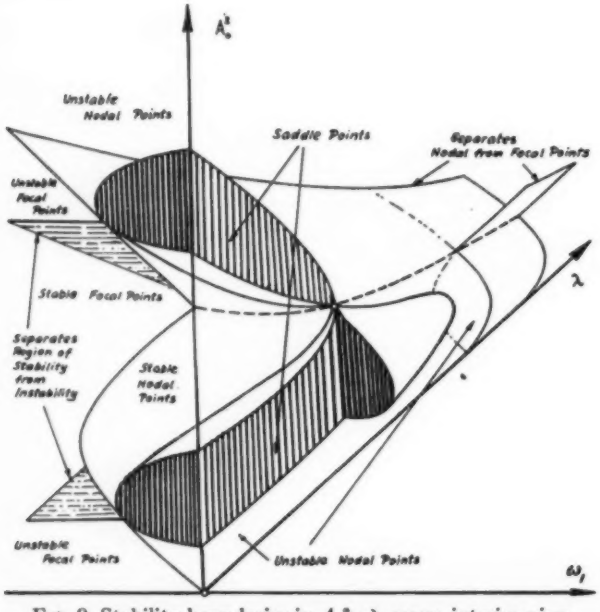

FIG. 9. Stability boundaries in $A_0^2\omega_1\lambda$-space, interior view.

since for $\lambda=0.025$ the upper oval shrinks to this point, which is also a vertex of the lower oval.

Several three-dimensional views of the stability regions in $A_0^2\omega_1\lambda$-space are shown in Figs. 8 and 9.

As explained in Sec. 3, the Poincaré theory may be applied to refine the classification of the response plane into stable and unstable regions, by dividing the stable regions into focal and nodal points and the unstable regions into focal, nodal, and saddle points. This classification is carried out in this author's dissertation where it is shown that

(a) the locus of almost-periodic solutions of the variational equation

$$15\lambda A_0^4-4A_0^2+8=0 \tag{3.15}$$

separates unstable from stable focal points;

(b) the locus of periodic solutions of the variational equation

$$4\omega_1^2=-(1-\tfrac{3}{4}A_0^2+25\lambda A_0^4/8)\times(1-\tfrac{1}{4}A_0^2+5\lambda A_0^4/8) \tag{2.36}$$

separates unstable saddle points from stable and unstable nodal points;

(c) a third locus,

$$\begin{aligned} A_0^2(1-5\lambda A_0^2)+8\omega_1=0,\\ A_0^2(1-5\lambda A_0^2)-8\omega_1=0, \end{aligned} \tag{4.4}$$

separates focal from nodal points.

The parabolas given by the third locus do not constitute genuine stability boundaries, since they subdivide regions which are stable or unstable. The curves are shown in Fig. 1 and in Figs. 5 to 7. The vertices of the parabolas are given by

$$\omega_1=\pm 1/160\lambda, \quad A_0^2=1/10\lambda. \tag{4.5}$$

As λ approaches zero, these parabolas degenerate into the two straight lines

$$A_0^2=\pm 8\omega_1, \tag{4.6}$$

which characterize the standard Van der Pol equation (1.5) and which are shown by dashed lines in Fig. 1.

In general, the two parabolas cross at $A_0^2=0$ and pass through the points of contact of the ovals (corresponding to periodic solutions of the variational equation) and the straight lines (corresponding to almost-periodic solutions of the variational equation). For $\lambda>0.045$ only the parabolas remain. Therefore, for large but finite λ, the $A_0^2-\omega_1$ plane is divided into unstable focal and nodal points. As λ becomes infinite, the two parabolas approach the line $A_0^2=0$, with the response plane covered almost entirely by unstable focal points.

ACKNOWLEDGMENT

The author wishes to thank Professors K. O. Friedrichs and J. J. Stoker for their helpful guidance and valuable criticisms.

JOURNAL OF APPLIED PHYSICS VOLUME 22, NUMBER 12 DECEMBER, 1951

A Critical Study of the Circuit Concept

JESSE GERALD CHANEY*
United States Naval Postgraduate School, Annapolis, Maryland†
(Received May 23, 1951)

From Maxwell's equations, an expression for the complex power associated with a wire circuit is formulated and broken into a complex input power and a complex power into the external fields associated with the circuit, the latter including the radiated power. From these powers, the internal and external impedances of the circuit are obtained such that the current is not required to be everywhere in time phase within the circuit. This concept is extended to coupled circuits, bringing out some of the relations between some conventional methods for obtaining the driving point impedance of antenna arrays. The theory does not require the current distributions to be postulated, but in practical applications such a postulate becomes necessary unless the solution is obtained by a method such as the integral equation method. The resulting circuitry may readily be reduced to that for lumped elements. A more critical study of the impedance formulas is given in the appendix, based upon the reciprocity theorem which is derived therein.

THE CIRCUIT COMPLEX POWER

CONSIDER a circuit formed by a wire of radius a containing a slice between positions b and c (Fig. 1). Positions d and e may or may not coincide. The steady-state form of Maxwell's equations, along with Ohm's law, are postulated within and exterior to the wire, that is,

$$\begin{aligned} &\nabla\cdot\bar{H}=0, \quad \nabla\cdot\bar{E}=\rho/\epsilon,\\ &\nabla\times\bar{H}=\bar{\imath}+j\omega\epsilon\bar{E},\\ &\nabla\times\bar{E}=-j\omega\mu\bar{H},\\ &\bar{\imath}=\sigma\bar{E}. \end{aligned} \tag{1}$$

The solutions for $\bar{E}$ and $\bar{H}$ are given in terms of the retarded vector potential $\bar{A}$, with

$$\bar{A}=\frac{1}{4\pi}\int_V \bar{\imath}e(r_{21})dV,\ r_{21}=|\bar{r}_1-\bar{r}_2|,\ e(r_{21})=e^{-jkr_{21}}/r_{21}, \tag{2}$$

being a solution of

$$[\nabla^2+k^2]\bar{A}=-\bar{\imath}, \quad k=\omega(\mu\epsilon)^{\frac{1}{2}}=2\pi/\lambda. \tag{3}$$

Thus, since

$$\begin{aligned} &\mu_0=4\pi(10^{-7}) \text{ henries/meter},\\ &\epsilon_0=1/36\pi(10^{-9}) \text{ farads/meter},\\ &\eta_0=(\mu_0/\epsilon_0)^{\frac{1}{2}}=120\pi \text{ ohms}, \end{aligned}$$

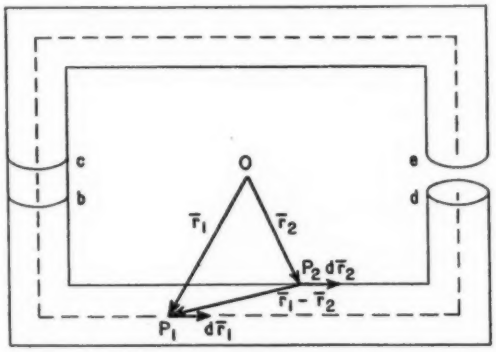

FIG. 1. Open or closed wire circuit.

for unity relative permeability and dielectric constants, defining the operator *deltil* by

$$\diamondsuit[\ ]=[\nabla(\nabla\cdot\ )+k^2][\ ],$$

$\bar{E}$ and $\bar{H}$ are given by

$$\begin{aligned} &\bar{H}=\nabla\times\bar{A},\\ &\bar{E}=\frac{1}{j\omega\epsilon_0}\nabla(\nabla\cdot\bar{A})-j\omega\mu_0\bar{A}=\frac{\eta_0}{jk}\diamondsuit\bar{A}. \end{aligned} \tag{4}$$

Now, denoting the complex conjugate by the superscript *,

$$\frac{1}{2}\int_V \bar{E}\cdot\bar{\imath}^*dV=\frac{1}{2\sigma}\int|\imath|^2dV=W_{Av}, \tag{5}$$

in which V is the volume of the wire and W_{Av} is the time average power loss within the wire. Since

$$\bar{\imath}^*=\nabla\times\bar{H}^*+j\omega\epsilon\bar{E}^*$$

and

$$\nabla\cdot(\bar{E}\times\bar{H}^*)=\bar{H}^*\cdot\nabla\times\bar{E}-\bar{E}\cdot\nabla\times\bar{H}^*,$$

substitution into (5) yields

$$\begin{aligned} \frac{1}{2}\int_V \bar{E}\cdot\bar{\imath}^*dV&=\frac{1}{2}\int_V[j\omega\epsilon|\bar{E}|^2+\bar{E}\cdot\nabla\times\bar{H}^*]dV\\ &=\frac{1}{2}\int_V[j\omega\epsilon|\bar{E}|^2-j\omega\mu|\bar{H}|^2]dV-\frac{1}{2}\int_S\bar{E}\times\bar{H}^*\cdot d\bar{S}, \end{aligned}$$

or

$$W_{Av}=j\omega[|U_E|-|U_H|]-\int_S\bar{P}\cdot d\bar{S}, \tag{6}$$

where $|U_E|$ and $|U_H|$ are the peak energies stored in the electric and magnetic fields within the wire, respectively, and $\bar{P}$ is the complex Poynting vector. Hence,

$$W_{Av}=-Re\int_S\bar{P}\cdot d\bar{S}$$

* Professor of Electronics.
† Recently moved to Monterey, California.

and

$$j\omega[|U_H|-|U_E|]=Im\int_S \bar{P}\cdot d\bar{S}. \quad (7)$$

Thus, by writing

$$\bar{P}=\bar{P}_0+\bar{P}_r,$$

the resultant field $\bar{E}$ may be broken into two components

$$\bar{E}=\bar{E}_0+\bar{E}_i,$$

such that

$$\frac{1}{2}\int_V \bar{E}_0\cdot\bar{\imath}^*dV=-\int_S \bar{P}_0\cdot d\bar{S}=\tilde{W}_0 \quad (8)$$

and

$$-\frac{1}{2}\int_V \bar{E}_i\cdot\bar{\imath}^*dV=j\omega[|U_H|-|U_E|]+\int_S \bar{P}_r\cdot d\bar{S} \quad (9)$$

$$=j\omega[|U_H|-|U_E|]+\tilde{W}_r$$

with $\tilde{W}_0$ being the complex power input to the wire and with $\tilde{W}_r$ being the complex power into the external fields associated with the circuit. The time average power radiated from the circuit is given by $Re[\tilde{W}_r]$. In other words, $\bar{E}_0$ becomes the applied field, or that

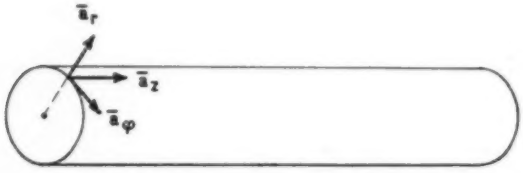

FIG. 2. Unit length volume of wire with vector directions.

component of $\bar{E}$ originating outside the wire which is required for maintaining

$$|U_H|-|U_E|=\text{constant},$$

as required for a steady-state condition, and $\bar{E}_i$ becomes the induced field, or the component of $\bar{E}$ which arises from the currents and charges within and on the wire itself. The induced field is given by

$$\bar{E}_i=\frac{\eta_0}{jk}\diamondsuit\bar{A}, \quad \bar{A}=\frac{1}{4\pi}\int_V \tilde{\imath}e(r_{21})dV, \quad (10)$$

where V is the volume of the wire itself, whereas $\bar{E}_0$ may or may not be given by a similar expression. For example, if the applied field arises from another circuit within the neighborhood, $\bar{E}_0$ will be given by a vector potential integrated over the volume of that circuit. But in this case, due to the interaction of the circuits, $\bar{E}_0$ also will be a function of the current in the given circuit. However, here it will be postulated that $\bar{E}_0$ is supplied by a slice generator inserted between terminals b and c such that if

$$\begin{aligned}\tilde{\imath}&=\tilde{\imath}_0 f(P) \quad \text{for} \quad b\leq P\leq c,\\ \tilde{\imath}&=\tilde{\imath}_0 \quad \text{for} \quad c\leq P\leq b,\end{aligned}$$

then

$$\frac{1}{2}\int \bar{E}_0\cdot\bar{\imath}^*dV=-\frac{1}{2}\int_{V'} \bar{E}_0\cdot\tilde{\imath}_0^*dV', \quad (11)$$

with V' being the volume of the slice and with P being a position within the circuit.

If the applied voltage V_0 is defined as

$$V_0=-\int_c^b \bar{E}_0\cdot d\bar{r}=\phi_b-\phi_c, \quad \phi=-\frac{1}{j\omega\epsilon}\nabla\cdot\bar{A}, \quad (12)$$

then

$$\tilde{W}_0=\frac{1}{2}\int_V \bar{E}_0\cdot\bar{\imath}^*dV=-\frac{1}{2}\int_{V'} \bar{E}_0\cdot\tilde{\imath}_0^*dV'$$

$$=-\frac{1}{2}\int_c^b \bar{E}_0\cdot\left(\int_S \tilde{\imath}_0^*\cdot d\bar{S}\right)\cdot d\bar{r},$$

or the complex power input becomes

$$\tilde{W}_0=\tfrac{1}{2}V_0I_0^*, \quad I_0=\int_S \tilde{\imath}_0\cdot d\bar{S}, \quad (13)$$

it being tacitly assumed that $\bar{E}_0$ is cross-sectionally constant within the slice generator.

Thus, the input impedance becomes

$$Z_0=2\tilde{W}_0/|I_0|^2=V_0/I_0. \quad (14)$$

But from (8) and (10),

$$\tilde{W}_0=\frac{1}{2}\int_V \bar{E}\cdot\bar{\imath}^*dV-\frac{1}{2}\int_V \bar{E}_i\cdot\bar{\imath}^*dV$$

$$=\frac{1}{2}\int_V\left[\bar{E}\cdot\bar{\imath}^*+j\frac{\eta_0}{k}\diamondsuit\bar{A}\cdot\bar{\imath}^*\right]dV. \quad (15)$$

THE INTERNAL IMPEDANCE

Now the complex power input density $\tilde{W}_{01}$ per unit length at each position on the circuit where $\tilde{\imath}\neq 0$, required to overcome the ohmic loss and to supply the reactive power due to the current through a cross section at that position, may be found by postulating the current and fields to extend one meter axially constant, with no retardation, within a right circular cylinder of radius a, and with a direction $\bar{a}_z$ equivalent to that of the wire at such a position, integrating over this volume and dividing by one meter of length. Since (Fig. 2)

$$dV=rd\phi dr(1)=dS',$$
$$d\bar{S}=\bar{a}_r dl(1)=\bar{a}_r a d\phi,$$

over the unit length volume, from (8) and (9),

$$\tilde{W}_{01}=\frac{1}{2}\int_V \bar{E}_0\cdot\bar{\imath}^*dV=-\int_S \bar{P}\cdot d\bar{S}+\int_S \bar{P}_r\cdot d\bar{S}$$

$$=\frac{1}{2}\int_S \bar{E}\times\bar{H}^*\cdot d\bar{S}+\tilde{W}_{r1},$$

$$\tilde{W}_{01}-\tilde{W}_{r1}=-\frac{1}{2}\int_S E_{za}H_{\phi a}^*\bar{a}_z\times\bar{a}_\phi\cdot\bar{a}_r dS$$

$$=\tfrac{1}{2}E_{za}\int_0^{2\pi} H_{\phi a}^* a d\phi,$$

or since

$$\tilde{W}_{r1}=j\omega[|U_{E1}|-|U_{H1}|]-\frac{1}{2}\int_{S'}\bar{E}_i\cdot\bar{\imath}^*dS'\approx 0,$$

$$\tilde{W}_{01}=\tfrac{1}{2}E_{za}(2\pi aH_{\phi a}^*). \tag{16}$$

But since S' is the cross-sectional surface,

$$2\pi aH_{\phi a}^*=\oint\bar{H}_a^*\cdot d\bar{l}=\int_{S'}\nabla\times\bar{H}^*\cdot d\bar{S}'$$

$$=\int_{S'}\left[1-\frac{j\omega\epsilon}{\sigma}\right]\bar{\imath}^*\cdot d\bar{S}'\approx I_z, \tag{17}$$

and hence if the internal impedance per unit length of wire is defined as

$$Z_i=E_{za}/I_z, \tag{18}$$

substitution of (17) and (18) into (16) yields

$$\tilde{W}_{01}=\tfrac{1}{2}Z_i|I_z|^2. \tag{19}$$

To find I_z, first form the wave equations within the unit volume from (1), replacing $\bar{E}$ by $(1/\sigma)\bar{\imath}$, that is, write

$$\nabla\times\bar{\imath}=-j\omega\mu\sigma\bar{H}$$

$$\nabla\times\bar{H}=\left(1+\frac{j\omega\epsilon}{\sigma}\right)\bar{\imath}\approx\bar{\imath}. \tag{20}$$

Then, since $\nabla\cdot\bar{\imath}=0$ through this volume,

$$-\nabla\times\nabla\times\bar{\imath}=\nabla^2\bar{\imath}=j\omega\mu\sigma\bar{\imath},$$

or assuming the current is symmetrically distributed in azimuth,

$$\frac{d^2\imath_z}{dr^2}+\frac{1}{r}\frac{d\imath_z}{dr}-j\omega\mu\sigma\imath_z=0. \tag{21}$$

The solution of (21) in terms of the Bessel functions for an imaginary argument is

$$\imath_z=\imath_{za}\frac{I_0[j^{\frac{1}{2}}(\sqrt{2}/\delta)r]}{I_0[j^{\frac{1}{2}}(\sqrt{2}/\delta)a]},\quad \delta=\frac{1}{(\pi f\mu\sigma)^{\frac{1}{2}}}. \tag{22}$$

Integrating over a cross section for I_z,

$$I_z=-j\frac{2\pi a\delta\imath_{za}}{\sqrt{2}}\frac{\mathrm{Ber}'(\sqrt{2}a/\delta)+j\,\mathrm{Bei}'(\sqrt{2}a/\delta)}{\mathrm{Ber}(\sqrt{2}a/\delta)+j\,\mathrm{Bei}(\sqrt{2}a/\delta)}. \tag{23}$$

Hence,

$$Z_i=\frac{\imath_{za}}{\sigma I_z}=j\frac{\sqrt{2}R_s}{2\pi a}\frac{\mathrm{Ber}(\sqrt{2}a/\delta)+j\,\mathrm{Bei}(\sqrt{2}a/\delta)}{\mathrm{Ber}'(\sqrt{2}a/\delta)+j\,\mathrm{Bei}'(\sqrt{2}a/\delta)}, \tag{24}$$

with

$$R_s=\frac{1}{\sigma\delta}=(\pi f\mu/\sigma)^{\frac{1}{2}}.$$

At high frequencies,

$$Z_i=R_s/2\pi a(1+j), \tag{25}$$

and at very low frequencies,

$$Z_i=(1/\pi a^2\sigma)+j15k. \tag{26}$$

THE INPUT IMPEDANCE

Returning to (15), since the current has been postulated continuous through the slice generator of negligible thickness, by writing

$$\bar{I}\cdot d\bar{r}=I_0f(P)dl,$$

substitution from (19) yields

$$\tilde{W}_0=\tfrac{1}{2}Z_i|I_0|^2\int_e^d|f(P)|^2dl+j\frac{60\pi}{k}\int_V\diamondsuit\bar{A}\cdot\bar{\imath}^*dV, \tag{27}$$

with $\bar{A}$ given by the integration of the retarded current over the volume of the wire with the exception of the cross section included in the element $\bar{\imath}^*dV$.

Now write,

$$\int_V\diamondsuit\bar{A}\cdot\bar{\imath}^*dV=\int_{V1}\left[\int_{V2}\frac{\bar{\imath}_2e(r_{21})}{4\pi}dV_2\right]\cdot\bar{\imath}_1^*dV_1,$$
$$V_1=V_2=V, \tag{28}$$

in which the subscripts are introduced for distinguishing between the operations to be carried out at two different positions along the wire.

Furthermore, write

$$\begin{aligned}\bar{\imath}_2dV_2&=\imath_2dS_2d\bar{r}_2=(\bar{\imath}_2\cdot d\bar{S}_2)d\bar{r}_2,\\ \bar{\imath}_1dV_1&=\imath_1dS_1d\bar{r}_1=(\bar{\imath}_1\cdot d\bar{S}_1)d\bar{r}_1.\end{aligned} \tag{29}$$

But $d\bar{r}_1$ and $d\bar{r}_2$ also should actually be integrated cross sectionally along with $\bar{\imath}_1$ and $\bar{\imath}_2$. However, if $ka\ll 1$, they may be assumed essentially independent of their radial positions. Nevertheless, the question arises as to where their radial positions should be chosen. Choosing both positions along the same path is equivalent to postulating an infinitely thin wire and yields an infinite reactance. The conventional choice assumes one path along the axis and the other along the surface of the wire. If this is done, since $\bar{\imath}_2$ is a function of position two whereas the differentiations required by the operator $\diamondsuit_1$ are to be performed at position one,

$$\int_V\diamondsuit\bar{A}\cdot\bar{\imath}^*dV$$
$$=\frac{1}{4\pi}\oint_1\oint_2\left(\int_{S_2}\bar{\imath}_2\cdot d\bar{S}_2\right)$$
$$\times\left(\int_{S_1}\bar{\imath}_1^*\cdot d\bar{S}_1\right)\diamondsuit_1[e(r_{21})d\bar{r}_2]\cdot d\bar{r}_1$$
$$=\frac{|I_0|^2}{4\pi}\oint_1\oint f(P_2)f(P_1)^*\diamondsuit_1[e(r_{21})d\bar{r}_2]\cdot d\bar{r}_1. \tag{30}$$

By selecting $d\bar{r}_1$ along the axis of the wire with $d\bar{r}_2$ along the inner periphery, substitution from (30) into

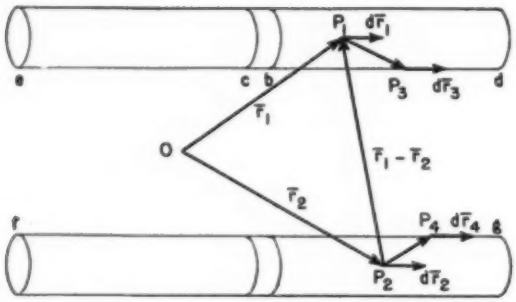

FIG. 3. Two indirectly coupled circuits.

(27) yields

$$\bar{W}_{12}=\tfrac{1}{2}Z_i|I_0|^2\oint_e^d|f(P)|^2dl+j\frac{15}{k}|I_0|^2 \times\oint_e^d\oint_e^d f(P_2)f(P_1)^*\diamondsuit_1[e(r_{21})d\bar{r}_2]\cdot d\bar{r}_1, \quad (31)$$

from which it is possible to write an input impedance. However, if the path selections were reversed, the expression for the complex power would become

$$\bar{W}_{21}=\tfrac{1}{2}Z_i|I_0|^2\oint_e^d|f(P)|^2dl+j\frac{15}{k}|I_0|^2 \times\oint_e^d\oint_e^d f(P_1)f(P_2)^*\diamondsuit_2[e(r_{12})d\bar{r}_1]\cdot d\bar{r}_2. \quad (32)$$

It may be demonstrated that,[1]

$$\diamondsuit_1[e(r_{21})d\bar{r}_2]\cdot d\bar{r}_1=\diamondsuit_2[e(r_{12})d\bar{r}_1]\cdot d\bar{r}_2, \quad (33)$$

which is the reciprocity theorem for the electromotive force and a current moment. Hence, it becomes apparent that unless the current distribution function becomes real, the two different selections seemingly yield different expressions for the complex power. To remove this seemingly paradoxical result, the final form for the complex power will be taken as the arithmetic mean of the powers for the two different choices. That is,

$$\bar{W}=\tfrac{1}{2}(\bar{W}_{12}+\bar{W}_{21}), \quad (34)$$

or if f_m is the spatial root-mean-square current distribution and l is the length of the circuit, it follows from (14), (33), and (34), that since

$$\tfrac{1}{2}[f(P_1)f(P_2)^*+f(P_2)f(P_1)^*] =Re[f(P_1)f(P_2)^*]=Re[f(P_2)f(P_1)^*], \quad (35)$$

then

$$Z_0=lZ_if_m^2+j\frac{30}{k}\oint_e^d\oint_e^d Re[f(P_1)^*f(P_2)] \times\diamondsuit_1[e(r_{21})d\bar{r}_2]\cdot d\bar{r}_1. \quad (36)$$

COUPLED CIRCUITS

For two indirectly coupled circuits, such as for two open wire antennas (Fig. 3), the field applied to circuit one now consists of that applied from the slice generator plus that supplied from the currents and charges in circuit two. In other words, the resultant field $\bar{E}_1$ becomes

$$\bar{E}_1=\bar{E}_{01}+\bar{E}_{12}+\bar{E}_{i_1}, \quad (37)$$

with

$$\bar{E}_{12}=\frac{\eta_0}{jk}\diamondsuit_1\bar{A}_{12}, \quad \bar{A}_{12}=\int_{V_2}\frac{\bar{\imath}_2e(r_{21})}{4\pi}dV_2. \quad (38)$$

Similarly,

$$\bar{E}_2=\bar{E}_{02}+\bar{E}_{21}+\bar{E}_{i_2}, \quad (39)$$

with

$$\bar{E}_{21}=\frac{\eta_0}{jk}\diamondsuit_2\bar{A}_{21}, \quad \bar{A}_{21}=\int_{V_1}\frac{\bar{\imath}_1e(r_{12})}{4\pi}dV_1. \quad (40)$$

Letting $\bar{W}_1$ and $\bar{W}_2$ represent the complex powers of circuits one and two, respectively, and using the additional subscripts three and four, respectively, for indicating the order of path selections within the individual circuits,

$$\bar{W}_{13}=\tfrac{1}{2}Z_{i_1}l_1f_{1m}^2|I_{01}|^2 +j\frac{15}{k}|I_{01}|^2\oint_1\oint f_1(P_1)^*f_1(P_3) \times\diamondsuit_1[e(r_{31})d\bar{r}_3]\cdot d\bar{r}_1+j\frac{15}{k}(I_{01}{}^*I_{02}) \times\oint_1\oint_2 f_1(P_1)^*f_2(P_2)\diamondsuit_1[e(r_{21})d\bar{r}_2]\cdot d\bar{r}_1, \quad (41)$$

$$\bar{W}_{24}=\tfrac{1}{2}Z_{i_2}l_2f_{2m}^2|I_{02}|^2 +j\frac{15}{k}|I_{02}|^2\oint_2\oint_4 f_2(P_2)^*f_2(P_4) \times\diamondsuit_2[e(r_{42})d\bar{r}_4]\cdot d\bar{r}_2+j\frac{15}{k}(I_{01}I_{02}{}^*) \times\oint_2\oint_1 f_2(P_2)^*f_1(P_1)\diamondsuit_2[e(r_{12})d\bar{r}_1]\cdot d\bar{r}_2. \quad (42)$$

Multiplying (41) by $2/I_{01}{}^*$ and (42) by $2/I_{02}{}^*$, a pair of mesh equations is obtained as follows:

$$I_{01}\left[Z_{i_1}l_1f_{1m}^2+j\frac{30}{k}\oint_1\oint_3 f_1(P_1)^*f_1(P_3) \times\diamondsuit_1[e(r_{31})d\bar{r}_3]\cdot d\bar{r}_1\right]+I_{02}\left[j\frac{30}{k}\oint_1\oint_2 f_1(P_1)^*f_2(P_2) \times\diamondsuit_1[e(r_{21})d\bar{r}_2]\cdot d\bar{r}_1\right]=V_{01} \quad (43)$$

$$I_{01}\left[j\frac{30}{k}\oint_1\oint_2 f_1(P_1)f_2(P_2)^*\diamondsuit_2[e(r_{12})d\bar{r}_1]\cdot d\bar{r}_2\right] +I_{02}\left[Z_{i_2}l_2f_{2m}^2+j\frac{30}{k}\oint_2\oint_4 f_2(P_2)^*f_2(P_4) \times\diamondsuit_2[e(r_{42})d\bar{r}_4]\cdot d\bar{r}_1\right]=V_{02} \quad (44)$$

[1] J. G. Chaney, "On the generalized circuit theory as applied to antennas and radiating lines," U. S. Naval Postgraduate School, Research Paper No. 1 (March, 1951).

or

$$I_{01}Z_{13}+I_{02}Z_{12}'=V_{01} \qquad (45)$$
$$I_{01}Z_{21}'+I_{02}Z_{24}=V_{02}.$$

Again, inspection reveals that the self impedances are a function of the path selections and that the mutual impedances are asymmetric in the subscripts. But the reciprocity theorem[2] requires that

$$Z_{21}=Z_{12}.$$

In other words, the two current distribution functions are not mutually independent. Hence, the final forms of the equations again will be taken as the arithmetic means of the equations formed by the different orders of path selections, along with the interchanging of Z_{21}' and Z_{12}' in one set. Thus,

$$I_{01}\tfrac{1}{2}(Z_{13}+Z_{31})+I_{02}\tfrac{1}{2}(Z_{12}'+Z_{21}')=V_{01}, \qquad (46)$$
$$I_{01}\tfrac{1}{2}(Z_{21}'+Z_{12}')+I_{02}\tfrac{1}{2}(Z_{24}+Z_{42})=V_{02},$$

or

$$I_{01}Z_{11}+I_{02}Z_{12}=V_{01}, \qquad (47)$$
$$I_{01}Z_{21}+I_{02}Z_{22}=V_{02},$$

with

$$Z_{11}=Z_{i1}l_1f_{1m}^2+j\frac{30}{k}\oint_1\oint_3 Re[f_1(P_1)^*f_1(P_3)]\times\diamondsuit_1[e(r_{31})d\bar{r}_3]\cdot d\bar{r}_1,$$

$$Z_{22}=Z_{i2}l_2f_{2m}^2+j\frac{30}{k}\oint_2\oint_4 Re[f_2(P_2)^*f_2(P_4)]\times\diamondsuit_2[e(r_{42})d\bar{r}_4]\cdot d\bar{r}_2,$$

$$Z_{12}=Z_{21}=j\frac{30}{k}\oint_1\oint_2 Re[f_1(P_1)^*f_2(P_2)]\times\diamondsuit_1[e(r_{21})d\bar{r}_2]\cdot d\bar{r}_1. \qquad (48)$$

The circuit equations already formulated hold for any frequency provided the radius is small in comparison with the circuit length and provided $ka\ll 1$, and also, provided the circuit is within an isotropic medium and due cognizance is taken of the values of μ and ϵ, the latter having been taken above for free space. However, it is suggested that in cases where proximity effect should be considered, the actual path should be replaced by the centroidal current path. This would be equivalent to changing the radius of the wire, or in the mutual case, to slightly changing the spacing of the wires.

LUMPED ELEMENTS

If the current fails to vanish at the ends of a wire, Z_0 in (36) contains a transfer capacitative reactance, which may be illustrated by postulating

$$f(P)=1, \quad e<P<d$$
$$f(P)=0, \quad d<P<e \qquad (49)$$
$$|\epsilon^{-jkr_{12}}|\approx 1.$$

[2] A. G. Clavier, Proc. Inst. Radio Engrs. **38**, 1, 69 (1950).

Thus

$$j\frac{30}{k}\oint_e^d\oint_e^d \diamondsuit_1[e(r_{21})d\bar{r}_2]\cdot d\bar{r}_1 \approx -\frac{1}{j\omega\epsilon_0 4\pi}\oint_e^d\oint_e^d \nabla_1\left(\nabla_1\cdot\frac{d\bar{r}_2}{r_{21}}\right)\cdot d\bar{r}_1 + j\omega\mu_0\oint_e^d\oint_e^d\frac{d\bar{r}_2\cdot d\bar{r}_1}{4\pi r_{21}}. \qquad (50)$$

Since

$$\nabla_1\cdot\frac{d\bar{r}_2}{r_{21}}=\left(\nabla_1\frac{1}{r_{21}}\right)\cdot d\bar{r}_2+\frac{1}{r_{21}}\nabla_1\cdot d\bar{r}_2=-\left(\nabla_2\frac{1}{r_{21}}\right)\cdot d\bar{r}_2,$$

and since Neumann's formula appears within the last term,

$$j\frac{30}{k}\oint_e^d\oint_e^d\diamondsuit_1\left(\frac{d\bar{r}_2}{r_{21}}\right)\cdot d\bar{r}_1 = \frac{1}{j\omega\epsilon_0 4\pi}\oint_e^d\nabla_1\left(\frac{1}{r_{d1}}-\frac{1}{r_{e1}}\right)\cdot d\bar{r}_1+j\omega L$$
$$=\frac{1}{j\omega\epsilon_0 4\pi}\left(\frac{1}{r_{dd}}-\frac{1}{r_{de}}-\frac{1}{r_{ed}}+\frac{1}{r_{ee}}\right)+j\omega L$$
$$=\frac{2}{j\omega}\left[\frac{1}{4\pi\epsilon_0}\left(\frac{1}{a}-\frac{1}{r_{de}}\right)\right]+j\omega L \qquad (51)$$
$$=\frac{2}{j\omega C}+j\omega L, \qquad (52)$$

where

$$\frac{1}{C}=\frac{1}{4\pi\epsilon_0}\left(\frac{1}{a}-\frac{1}{r_{de}}\right)$$

is the elastance of a spherical capacitor having an inner radius equivalent to the radius of the wire, and an outer radius equivalent to the distance between the ends of the wire. Two such capacitors appear in series since the integration passes twice around the circuit (Fig. 4).

If the circuit includes lumped elements, or concentrated R, L, and C, then R and L will appear merely by choosing the proper values of σ and μ over the resistor and inductor, respectively. However, due to the presence of the capacitor, the peak energy stored within the internal electric field of the circuit now exceeds that stored within the electric field contained within the wire itself. But the expressions for the complete power $\tilde{W}$ implies that all the energy of the electric field within the circuit itself must be within the wire. Hence, the reactive power of the capacitor must be subtracted from $\tilde{W}_0$. Thus, if V' now represents the volume within the capacitor, $\tilde{W}_0$ must contain the additional term $-j\omega(\epsilon/2)\int_{V'}|E|^2dV'$. For example, for a capacitor formed by two parallel plates of area S

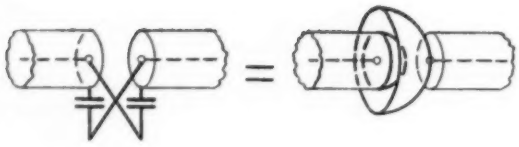

FIG. 4. Equivalent end capacitor.

and separated a distance s, inserted between terminals d and e,

$$-\frac{j\omega\epsilon}{2}\int_{V'}\bar{E}\cdot\bar{E}dV'=-\frac{j\omega\epsilon S|V_c|^2}{2s}=-\tfrac{1}{2}j\omega C|V_c|^2$$

$$=-\frac{1}{2}\frac{(j\omega CV_c)(-j\omega CV_c^*)}{j\omega C}=\frac{1}{2}\frac{[I_0f(d)][I_0^*f(e)^*]}{j\omega C}$$

$$=\frac{|I_0|^2}{2j\omega C}|f_c|^2, \quad (53)$$

in which

$$C=S\epsilon/s, \quad f_c=f(d)=f(e).$$

Since the current has been postulated continuous through both the generator and the capacitor, if the axial dimensions of the resistor and the capacitor are excluded from l, the input impedance Z_0 becomes

$$Z_0=R|f_r|^2+\frac{|f_c|^2}{j\omega C}+lZ_i f_m^2$$

$$+j\frac{30}{k}\oint_1\oint_2 Re[f(P_1)^*f(P_2)]\diamondsuit_1[e(r_{21})d\bar{r}_2]\cdot d\bar{r}_1, \quad (54)$$

with $j\omega L$ for the inductor given by the integration of the last term over that portion of the circuit forming the inductor. Thus, for a circuit having $f(P)=1$ and $|kr_{21}|\ll 1$, Z_0 reduces to

$$Z_0=R+j\left(\omega L-\frac{1}{\omega C}\right)+lZ_i, \quad (55)$$

with

$$L=\mu\oint_1\oint_2\frac{d\bar{r}_1\cdot d\bar{r}_2}{4\pi r_{12}}.$$

It becomes apparent that antenna circuits may be thought of in the same manner as low frequency lumped network circuits. Of course, in practice, the impedance formulas will require an *a priori* assumption of current distributions, which is sufficient for many engineering purposes, but not too accurate for certain broad band types of antennas. This method of finding the driving point impedance of an antenna array when postulating sinusoidal currents in open wire antennas is commonly referred to as the Carter circuit method.[3]

[3] P. S. Carter, Proc. Inst. Radio Engrs. **20**, 1004 (1932).

OTHER CONVENTIONAL METHODS

It is quite interesting to note how some of the more conventional methods for finding antenna impedances and radiation resistances appear from the original formulation of the complex power expressions.

Suppose the antenna is well constructed so that the internal impedance is negligible with respect to the radiation or intrinsic impedance. Then, from (15),

$$\frac{1}{2}\int_V\bar{E}_0\cdot\bar{\imath}^*dV=-\frac{1}{2}\int_V\bar{E}_i\cdot\bar{\imath}^*dV, \quad (56)$$

or from (13) and (14), this is frequently written

$$Z_0=-\frac{1}{|I_0|^2}\int\bar{E}_i\cdot\bar{\imath}^*dV$$

$$=-\frac{1}{|I_0|^2}\oint\bar{E}_i\cdot\bar{I}^*dl. \quad (57)$$

Upon substituting from (10), this becomes the conventional method of taking the self impedance as the mutual impedance between the axis and an element on the surface, or if the paths are both chosen along the axis, it becomes the induced emf method for finding the radiation resistance R_r as

$$R_r=Re\left[\frac{1}{|I_0|^2}\oint\oint\frac{j\eta_0}{k}\diamondsuit\bar{A}\cdot\bar{I}^*d\bar{l}^2\right]. \quad (58)$$

Also, since within the wire,

$$\nabla\times\bar{H}^*\approx\bar{\imath}^*, \quad (59)$$

$$R_r=-Re\left[\frac{1}{|I_0|^2}\int_V\bar{E}_i\cdot\nabla\times\bar{H}^*dV\right]$$

$$=\frac{1}{|I_0|^2}Re\left[\int_V\nabla\cdot(\bar{E}\times\bar{H}^*)dV\right]$$

$$=\frac{1}{|I_0|^2}Re\left[\int_S\bar{E}_i\times\bar{H}^*\cdot d\bar{S}\right], \quad (60)$$

which is the Poynting vector method for finding the radiation resistance.

Another interesting concept following from $Z_i\approx 0$ and the resulting equation,

$$\bar{E}=\bar{E}_0+\bar{E}_i=0,$$

is that the Poynting vector integration over the surface of the wire vanishes; that is, the power flow into the wire balances the power flow outward through the surface of the wire. But from (8), (9), and (56),

$$\int_{S'}\bar{P}_0\cdot d\bar{S}'=\int_S\bar{P}_i\cdot d\bar{S}, \quad (61)$$

with S' being the surface enclosing the gap and with S being the surface enclosing the wire. Hence, it is frequently concluded that the radiation from an antenna actually occurs at the gap.

Also, there is no conflict between the integral equation method for finding the driving point impedance of an antenna array and the circuit concept considered herein. For, consider the complex power density as given in (27) with the last term again taken as in (57). In other words, now let $\bar{W}_{01}$ be the total power density per unit length with $\int_{S'}\bar{E}_i\cdot\bar{i}^*dS'$ replaced by $\bar{E}_i\cdot\bar{I}^*$, that is,

$$\bar{W}_{01}=\tfrac{1}{2}Z_i|I|^2-\tfrac{1}{2}\bar{E}_i\cdot\bar{I}^*. \tag{62}$$

Integration along the wire with the current constant through the infinitely thin slice yields

$$\bar{W}_{01}=\frac{1}{2}\oint_e^b(Z_i\bar{I}-\bar{E}_i)\cdot\bar{I}^*dl,$$

or

$$-\frac{1}{2}\oint_e^b\bar{E}_0I_0^*\cdot d\bar{r}=\frac{1}{2}\oint_e^d(Z_i\bar{I}-\bar{E}_i)\cdot\bar{I}^*dl. \tag{63}$$

Then, since the right member includes the slice, the expression $Z_i\bar{I}-\bar{E}_i$ may be assumed to vanish along the wire with a discontinuity in the scalar potential of $\phi_b-\phi_e$ existing at the gap. This, for a straight cylindrical antenna, yields the following differential equation in the vector potential $\bar{A}$,

$$(\partial^2A_z/\partial z^2)+k^2A_z=j\omega\epsilon_0Z_iI_z, \tag{64}$$

which is the equation usually obtained in the integral equation method by matching the external field to the internal field at the surface of the wire.[4]

By the integral equation method for finding the driving point impedance, an *a priori* current distribution is not postulated, and the mutual impedance of two antennas otherwise unaltered varies within the presence of other antennas. This variation in the mutual impedance also theoretically occurs in the Carter circuit method, for the current distribution functions are not assumed independent and the mutual impedances are subjected to the reciprocity theorem. However, in numerical applications using the circuit method, the current distribution is postulated *a priori*, which causes the mutual impedances to remain unaltered within the presence of other antennas. This approximation usually is sufficiently accurate for multiple arrays to more than offset the increased difficulty and approximations encountered in the integral equation method of determining the solution.

However, the theoretical circuit equations developed herein hold true even if the exact current distributions are first determined by some method such as the integral equation method, thus relating the integral equation concept to the more conventional circuit concept.

[4] R. King and C. W. Harrison, Jr., Proc. Inst. Radio Engrs. **31**, 10, 548 (1943).

APPENDIX

Let $\bar{r}_{21}$ be the radius vector from a point P_2 to another distinct point P_1 within a three-dimensional space, and let $\psi(r_{21})$ be a function twice differentiable, then Chaney's identity may be stated,[1]

$$\bar{a}_1\cdot\nabla_1[\nabla_1\cdot\psi(r_{21})\bar{a}_2]=\bar{a}_2\cdot\nabla_2[\nabla_2\cdot\psi(r_{12})\bar{a}_1], \tag{65}$$

where $\bar{a}_1$ and $\bar{a}_2$ are any two unit vectors at points P_1 and P_2, respectively, where the subscripts on the vector operators indicate the points at which the differentiations occur, and where

$$\bar{r}_{12}=-\bar{r}_{21},\quad r_{21}=|\bar{r}_{21}|.$$

From (65), it immediately follows that

$$\frac{\eta_0}{j4\pi k}I_{02}f_2(P_2)\diamond_1[e(r_{21})d\bar{r}_2]\cdot d\bar{r}_1=\frac{\eta_0}{j4\pi k}I_{02}f_2(P_2)\diamond_2[e(r_{12})d\bar{r}_1]\cdot d\bar{r}_2, \tag{66}$$

where $I_{02}f_2(P_2)$ is the current at P_2, where

$$e(r_{12})=e^{-jkr_{21}}/r_{21},$$

and where

$$\diamond=\nabla[\nabla\cdot+k^2],\quad k=2\pi/\lambda.$$

The left member of (66) gives the emf acting within a circuit element at P_1 due to a current moment at P_2, and the right member gives the emf acting within a circuit element at P_2 due to the removal of the current moment from P_2 to P_1. Hence, Eq. (66) is an analytic statement of the reciprocity theorem.

Also, from (66),

$$\oint_2\frac{30}{jk}I_{02}f_2(P_2)\diamond_1[e(r_{21})d\bar{r}_2]\cdot d\bar{r}_1=\oint_2\frac{30}{jk}I_{02}f_2(P_2)\diamond_2[e(r_{12})d\bar{r}_1]\cdot d\bar{r}_2. \tag{67}$$

The left member of (67) gives the resultant emf at P_1 due to all the current in circuit *two* and the right member gives the total emf that would act around circuit *two* if each current moment of *two* were at P_1.

From (67),

$$j\frac{15I_{01}^*I_{02}}{k}\oint_1\oint_2f_1(P_1)^*f_2(P_2)\diamond_1[e(r_{21})d\bar{r}_2]\cdot d\bar{r}_1=j\frac{15I_{01}^*I_{02}}{k}\oint_1\oint_2f_1(P_1)^*f_2(P_2)\diamond_2[e(r_{21})d\bar{r}_1]\cdot d\bar{r}_2. \tag{68}$$

Now, the left member of (68) gives the additional complex power which must be supplied by the generator of circuit *one* because of the presence of circuit *two*, provided the current in one is maintained the same as it was before circuit *two* was moved into place. However, this is physically impossible because the current distribution in *one* is actually altered by the presence of circuit *two*. The right member of (68) gives the complex power resulting from considering each current element of *two* removed to each point of *one* and finding the emf around *two* corresponding to each position of *one*, and then assuming this emf is acting at the corresponding point in *one*. In short, the right member transforms circuit *two* into circuit *one*.

A reversal of the order of the above integration yields,

$$j\frac{15I_{01}I_{02}^*}{k}\oint_1\oint_2f_1(P_1)f_2(P_2)^*\diamond_2[e(r_{12})d\bar{r}_1]\cdot d\bar{r}_2=j\frac{15I_{01}I_{02}^*}{k}\oint_1\oint_2f_1(P_1)f_2(P_2)^*\diamond_1[e(r_{12})d\bar{r}_2]\cdot d\bar{r}_1. \tag{69}$$

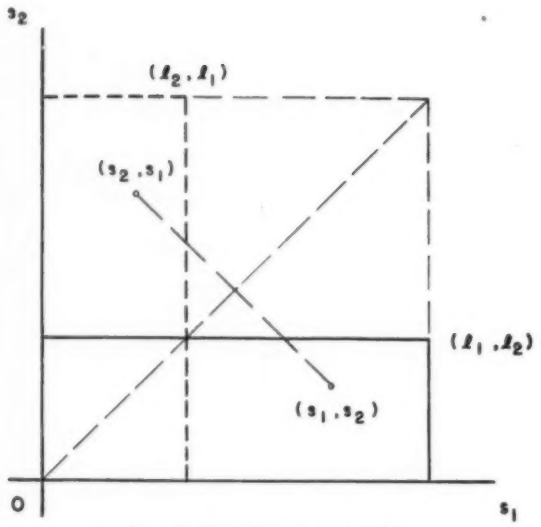

FIG. 5. Curvilinear rectangles.

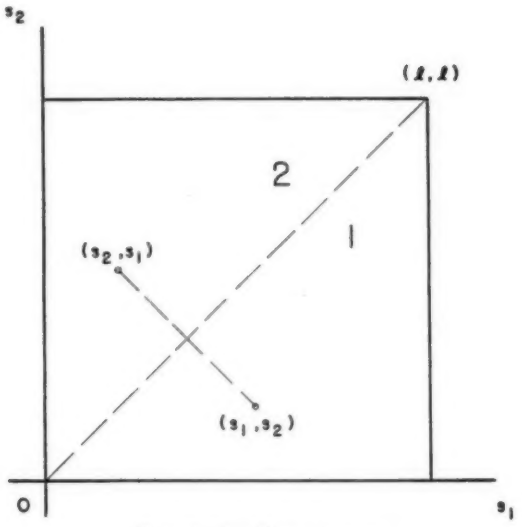

FIG. 6. Curvilinear square.

Thus, from (68) and (69), each generator sees its own circuit plus the other circuit transformed into its own circuit. Indeed, it might be stated that it is this transformation which causes the current distributions to alter in such a manner as to bring about an equality of the two mutual impedances.

Now consider the applied voltage to exist only in circuit *two* at position P_{02}. The voltage at a point P_{01} is given by the negative left member of (67). If the circuit element at P_{01} is replaced by the applied voltage V_2, as far as the circuits are concerned, this is equivalent to interchanging the emf in the elements of P_{01} and P_{02}. Hence, from (66), the current at P_{02} becomes the same as the current that formerly existed at P_{01}. Thus, one obtains the system of equations,

$$\begin{aligned} &I_{01}Z_{11}+I_{02}Z_{12} &&=0\\ &I_{01}Z_{21}+I_{02}Z_{22} &&-V_2=0\\ &I_{01}Z_{12} &&+I_{01}'Z_{11}-V_2=0\\ &I_{01}Z_{22} &&+I_{01}'Z_{21} \quad =0 \end{aligned} \tag{70}$$

for which a necessary and sufficient condition for their having a solution is that[2] $Z_{12}=Z_{21}$.

The equality of Z_{12} and Z_{21} requires that

$$\oint_1\oint_2 f_1(P_1)^*f_2(P_2)\diamond_1[e(r_{21})d\bar{r}_2]\cdot d\bar{r}_1 = \oint_1\oint_2 f_1(P_1)f_2(P_2)^*\diamond_2[e(r_{12})d\bar{r}_1]\cdot d\bar{r}_2. \tag{71}$$

In terms of arc lengths, by letting

$$d\bar{r}_1=d\bar{s}_1,\quad d\bar{r}_2=d\bar{s}_2,\quad \bar{a}_1\cdot\bar{a}_2=\cos[\theta(s_1,s_2)],$$
$$e(r_{12})=g(s_1,s_2)=g(s_2,s_1)=e(r_{21}),$$

Eq. (71) may be written as

$$\int_0^{l_1}\int_0^{l_2} f_1(s_1)^*f_2(s_2)\left[\frac{-\partial^2}{\partial s_1\partial s_2}+k^2\cos\theta\right]g(s_2,s_1)ds_1ds_2, = \int_0^{l_2}\int_0^{l_1} f_1(s_1)f_2(s_2)^*\left[\frac{-\partial^2}{\partial s_2\partial s_1}+k^2\cos\theta\right]g(s_1,s_2)ds_1ds_2, \tag{72}$$

which may be interpreted as integrations over curvilinear rectangles (Fig. 5). Since

$$f_1(s_1)f_2(s_2)^*=[f_1(s_1)^*f_2(s_2)]^*$$

and

$$\left[\frac{-\partial^2}{\partial s_1\partial s_2}+k^2\cos\theta\right]g(s_2,s_1)=\left[\frac{-\partial^2}{\partial s_2\partial s_1}+k^2\cos\theta\right]g(s_2,s_1),$$

it follows that the current distribution functions must be such that

$$\int_0^{l_1}\int_0^{l_2} f_1(s_1)^*f_2(s_2)\left[\frac{-\partial^2}{\partial s_1\partial s_2}+k^2\cos\theta\right]g(s_2,s_1)ds_2ds_1 = \int_0^{l_1}\int_0^{l_2} Re[f_1(s_1)^*f_2(s_2)]\left[\frac{-\partial^2}{\partial s_1\partial s_2}+k^2\cos\theta\right]g(s_1,s_2)ds_1ds_2. \tag{73}$$

The retention of only the real part of the product current functions in (36) may similarly be justified. Here, the functional forms are the same. Letting

$$f(s_1)^*f(s_2)=u(s_1,s_2)+jv(s_1,s_2),$$

the integral of (31) may be written

$$A=\oint_s\oint_s f(P_1)^*f(P_2)\diamond_1[e(r_{21})d\bar{r}_2]\cdot d\bar{r}_1 = \int_0^l\int_0^l f(s_1)^*f(s_2)\left[\frac{-\partial^2}{\partial s_1\partial s_2}+k^2\cos\theta\right]g(s_1,s_2)ds_2ds_1$$

or

$$A=\left(\int_{S_1}+\int_{S_2}\right)[u(s_1,s_2)+jv(s_1,s_2)] \times\left[\frac{-\partial^2}{\partial s_1\partial s_2}+k^2\cos\theta\right]g(s_1,s_2)ds_2ds_1, \tag{74}$$

where S_1 is the surface below the diagonal of the curvilinear square and S_2 is the surface above the diagonal (Fig. 6).

Integrating simultaneously over positions symmetric with respect to the diagonal and considering

$$f(s_2)^*f(s_1)=u(s_1,s_2)-jv(s_1,s_2),$$

$$A=2\int_{S_1}u(s_1,s_2)\left[\frac{-\partial^2}{\partial s_1\partial s_2}+k^2\cos\theta\right]g(s_1,s_2)ds_2ds_1 = \oint_s\oint_s Re[f(P_1)^*f(P_2)]\diamond_1[e(r_{21})d\bar{r}_2]\cdot d\bar{r}_1. \tag{75}$$

JOURNAL OF APPLIED PHYSICS VOLUME 22, NUMBER 12 DECEMBER, 1951

Free Convection Heat Transfer from Electrically Heated Wires

ERICH A. FARBER
University of Wisconsin, Madison, Wisconsin
(Received June 4, 1951)

In this paper the author discusses the heat transfer by free convection from electrically heated wires (copper and iron) to distilled water between freezing and boiling, to water boiling at atmospheric conditions and to air at room temperature. The wire surface temperatures needed for the heat transfer determination are calculated from the theoretical temperature distribution in the wire. The experimental results show maximum heat transfer rates of about 2,200,000 Btu/hr, ft² near freezing and 450,000 Btu/hr, ft² near boiling. For boiling water, as the temperature difference between the wire surface and water is increased, the heat transfer coefficient first increases reaching a maximum, then decreases reaching a minimum and increases again (because of radiation) until the wire fails by melting. For copper the maximum film coefficient of 9100 Btu/hr, ft², °F is observed at 49 degrees temperature difference and the minimum of 136 Btu/hr, ft², °F at a temperature difference of 690 degrees F. Corresponding values for iron are 12,300 Btu/hr, ft², °F at a 33 degree temperature difference and 142 Btu/hr, ft², °F at a 620 degree difference. When air at room temperature surrounds the wire the heat transfer coefficient for copper with an oxide film varies from 0 to 30 and for iron from 0 to 26 Btu/hr, ft², °F as the surface temperature of the wires is raised until failure occurs.

I. INTRODUCTION

THIS paper dealing with the heat transfer and the heat transfer coefficients of electrically heated wires with only free convection currents present in the heat absorbing medium automatically falls into three parts. A. Heat transfer to liquids between their freezing and boiling points. B. Heat transfer to boiling liquids, changing them into vapors. C. Heat transfer to vapors and gases. For the absorbing media distilled water and atmospheric air are used. The wire materials for which results are reported here are copper and iron in as pure a form as can be obtained commercially. The results presented in graphical form refer to horizontal, commercially smooth wires. The surfaces are perfectly clean in parts A and B of this investigation, but have an oxide film in part C. Questions, arising from work with heating and heat dissipating equipment, as well as boiler tubes under various operating conditions, instigated this investigation.

II. PROCEDURE

The equations used to obtain the results are derived by combining the fundamental laws of electrical heat generation and heat transfer including the theoretical temperature distribution in the wires. After simplifying the mathematical expressions and streamlining the procedure, seven steps remain to be followed.

1. The measuring of the wire diameter (D), the length of the test element (L), the voltage drop across the test element (E), the current through the test element (I), and the bulk temperature of the fluid surrounding the wire (T_f).

2. From the data taken above the mean electrical resistivity ($\bar{e}$) of the wire can be calculated

$$\bar{e}=\pi D^2E/4LI. \tag{1}$$

3. Entering a graph of electrical resistivity *versus* temperature (of the material used) with this value of ($\bar{e}$) the average temperature of the wire ($\bar{T}$) is determined.

4. A value for the average coefficient of thermal conductivity ($\bar{k}$) can now be found with ($\bar{T}$) from a graph of thermal conductivity *versus* temperature.

5. The mean field temperature ($\bar{\theta}$) of the wire is calculated by

$$\bar{\theta}=JEI/4\pi\bar{k}L \tag{2}$$

where J is a conversion factor.

6. Having calculated the mean field temperature, the surface temperature of the wire (T_s) can be found

$$T_s=\bar{T}-\bar{\theta}. \tag{3}$$

7. With the results of steps 1 to 6 available, either the heat transfer coefficients for free convection (h), or the free convection heat transfer rate (q) can be calculated.

$$h=\frac{JEI}{\pi DL(T_s-T_f)} \tag{4}$$

$$q=h(T_s-T_f)=JEI/\pi DL. \tag{5}$$

III. DISCUSSION AND EVALUATION OF THE RESULTS

General

Difficulty is experienced in obtaining from literature resistivity-temperature curves applicable to the wires used here, since different wire compositions and im-

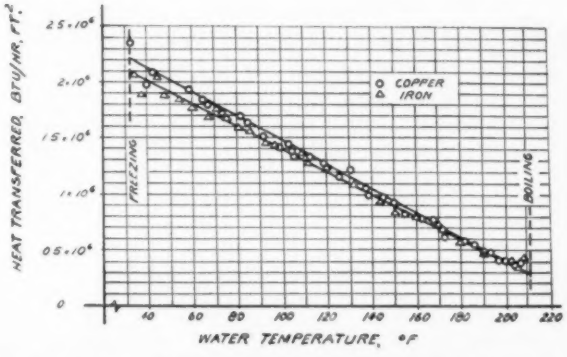

FIG. 1. Maximum heat transfer rates for copper and iron wires.

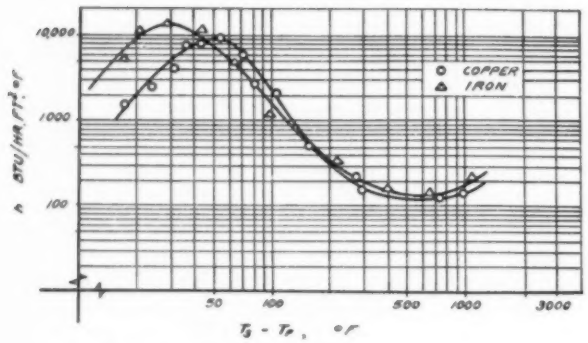

FIG. 2. Heat transfer coefficients to boiling water.

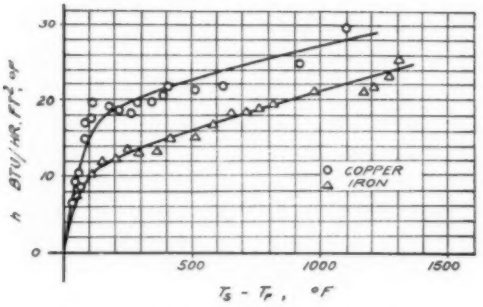

FIG. 3. Heat transfer coefficients to air.

purities affect the resistivity considerably. Therefore the resistivity-temperature curves for the wires used in these experiments are determined in our laboratory. The data for the thermal conductivity found in the literature proved to be satisfactory. Some of the calculated values for surface temperatures have been checked experimentally (a very difficult measurement) and the agreement is good.

Part A

Figure 1 shows graphically the maximum rates of heat transfer possible when the water is between freezing and boiling. More heat (about 5 times as much) can be transferred at lower water temperatures and heat transfer rates of better than 2,200,000 Btu/hr, ft² can be reached. When the water is boiling the maximum is about 450,000 Btu/hr, ft². The results between these limiting values indicate an almost linear decline in the maximum heat transfer rates with increase of the water temperature. The iron seems to have a somewhat lower, upper limit of heat transfer than copper.

Part B

Figure 2 presents the heat transfer coefficients for the copper and iron wires to boiling water. The amount of heat transferred depends, as can be seen, greatly upon the temperature difference between the wire surface and the water. With increasing temperature difference the coefficients of heat transfer first increases reaching a maximum, then decreases to a minimum and finally increases again until the temperature becomes high enough to melt the wire. The physical appearance of the heat transfer process changes considerably along this curve. It starts with slightly superheated liquid streaming upward, then with some bubble formation which increases until a steam film or jacket is formed around the wire. In this jacket the wire begins to glow for high enough temperatures and fails when the melting point is reached. The maximum heat transfer coefficients of 9100 for copper and 12,300 Btu/hr, ft², °F for iron are reached at temperature differences of 49 and 33 Farenheit degrees respectively. The minimum coefficients of 136 for copper and 142 Btu/hr, ft², °F for iron occur at respective temperature differences of 690 and 620 Farenheit degrees.

Part C

The heat transfer coefficients from copper and iron to atmospheric air are the easiest to determine, but the most difficult ones to standardize due to oxidation of the iron and copper. Under many conditions however wires must transfer heat to atmospheric air directly and oxidation occurs. These experiments therefore are similar to actual problems. With clean wires the oxidation occurs rather rapidly at first and at a rate hardly noticeable later. For this reason the wires used in these tests are held at a particular temperature until no further change in the oxide film can be detected, then the data is taken. Copper forms a heavier oxide film than iron for corresponding temperatures. The heat transfer coefficients for copper vary from 0 to 30 and for iron from 0 to 26 Btu/hr, ft², °F. These results are shown graphically in Fig. 3.

ACKNOWLEDGMENTS

The author wishes to acknowledge the support obtained from the Engineering Experiment Station, and the help of a number of his students, especially Mr. Ruesch and Mr. Zelinske, who have done some of the experimental work.

A Finite Difference Treatment of a Helium Cryostat Design Problem

WARREN E. HENRY
Naval Research Laboratory, Washington, D. C.

(Received May 28, 1951)

A mathematical expression is derived for computing dimensions of a liquid helium cryostat of specified performance characteristics. Use is made of a finite difference summation scheme applied to a simple thermomechanical model, using T as the independent variable, for a liquid evaporating in a container with good exchange to the walls. The scheme thus takes into account the heat capacity of the gas between the boiling point and the upper cryostat temperature. The results obtained are compatible with the actual performance of cryostats in operation.

IN the design of metal cryostats for liquid helium, one considers the sources of heat input: namely, (1) radiation from the top and the radiation shield, (2) gaseous conduction and convection, and (3) conduction down the walls of the dewar. By well-known methods, leaks contributed by radiation[1] and by the gas[2] are calculated. These contributions can be neglected or reduced by careful design to an unimportant minimum. The wall conduction problem will be treated here, using a thermomechanical model and a finite difference mathematical scheme.

Since the upper and lower temperatures of the thin inner wall of a contemplated Dewar can be fixed, a straightforward attack on the problem of the determination of dimensions is made possible by the above-mentioned model. Application of a finite difference method to this model and the evaluation of a finite series yields the depth of a dewar for a given evaporation rate. Even a rough calculation with simplifying approximations gives a reasonable upper bound to the Dewar depth. Evaporation rates of liquid helium in Dewars designed here[3] and elsewhere[4] are compatible with this analysis.

A simple model, in which monotone decreasing heat flow takes place, taking into account the heat required to raise the temperature of the helium gas as well as the heat required to evaporate it at the boiling point is shown in Fig. 1. The Dewar model is really a double model in which the z-axis is temperature in one model and depth in the other. The depth does not necessarily vary linearly with temperature, but the temperature is single-valued in X. The models are thus topological equivalents. The horizontal arrows represent heat flow, $\dot{Q}$ (the assumption of nearly radial flow is justified[5] on the basis of the small Reynolds number of the flow system), and the vertical arrows represent mass flow, $\dot{M}$, which is the rate at which liquid helium is lost from the cryostat. The cells, R_i, are all cylinders of equal volume in the mixed space. The quantity of heat, $\dot{Q}_i$, coming from the walls, pushes the mass, $\dot{M}$, up into the next cell. Now if we take an arbitrary temperature interval, ΔT_n, as the temperature difference between adjacent cells, with

$$\Delta T_n = T_n - T_{n+1} = \text{constant}, \tag{1}$$

the corresponding coordinate space intervals are X_0 for the top cell, X_1 for the next, and so on, where the X_n's are not in general equal. The length of the thin inner wall of the Dewar is

$$l = \sum_{n=0}^{N} X_n. \tag{2}$$

Along X_n heat is being conducted at the rate $\dot{H}_n$. Since each cell has the mass, $\dot{M}$, passing through it each second, and since the heat needed to put the mass into the next cell is the heat required to change the temperature of the mass, $\dot{M}$, by ΔT_n,

$$\dot{Q}_n = \dot{M} C_p \Delta T_n, \tag{3}$$

where C_p is the heat capacity of the gas. An inspection of Fig. 1 gives the recursion formula for heat flowing down the walls in any cell, R_{n+1}, as

$$\dot{H}_{n+1} = \dot{H}_n - \dot{Q}_n, \tag{4}$$

where $\dot{Q}_n$ is given by Eq. (3). The total heat flowing

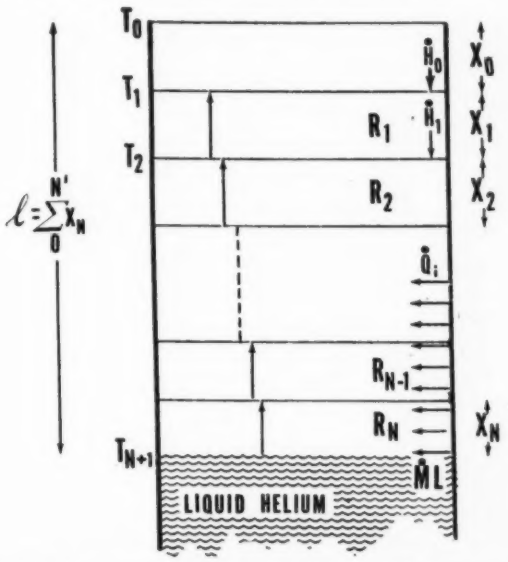

FIG. 1. A thermomechanical model of a liquid helium container for analyzing a heat flow problem with good exchange. The independent variable is T. The direction of heat flow from the walls to the gas is nearly horizontal and the mass flow is vertical.

[1] R. T. Birge, Revs. Modern Phys. **13**, 233 (1941); W. H. McAdams, *Heat Transmission*, 2nd Edition (McGraw-Hill Book Company, Inc., New York, 1942), p. 49.
[2] See reference 1, p. 240.
[3] W. E. Henry and R. L. Dolecek, Rev. Sci. Instr. **21**, 496 (1950).
[4] A. Wexler and H. S. Jacket, Rev. Sci. Instr. **22**, 282 (1951).
[5] S. D. Poisson, *Theorie Mathematique de la Chaleur* (Bachelier, Paris, 1935), p. 188; Drew, Hottel, and McAdams, Trans. Am. Inst. Chem. Eng. **32**, 271 (1936).

into the Dewar is the sum of the heat required to evaporate the liquid helium plus the heat required to raise the temperature from the boiling point of helium to the temperature of boiling nitrogen, or

$$\dot{H}_0=\dot{M}L+\sum_{n=0}^{N}\dot{M}C_p\Delta T_0=\dot{M}[C_p(T_0-T_N)+L]=\frac{\kappa_0 A\Delta T_0}{X_0}, \quad (5)$$

where κ_0 is the thermal conductivity of the wall material in the top cell, A is the cross-sectional area of the thin-walled cylinder, and L is the heat of vaporization of the liquid at the boiling point. From (5) one may compute X_0, the depth of the first cell. The use of $C_p(T_n)$ as a constant throughout the temperature range is justified[6] and simplifies the treatment. One may now derive a recursion formula for the X's on the basis of Eq. (4). From this, the formula for the entire depth may be obtained.

$$l=\sum_{n=0}^{N}X_n=X_0\sum_{n=0}^{N}\frac{\kappa_n}{\kappa_0}\frac{N(1+\alpha)}{N(1+\alpha)-n}, \quad (6)$$

where $N+1$ is the total number of cells, κ_n is the thermal conductivity at T_n and α is the ratio between the heat of vaporization of the liquid at the boiling point and the heat capacity of the gas for the temperature range. For the case under consideration, *viz.*, liquid helium boiling at 4.23°K and being raised to the temperature of liquid nitrogen, $\alpha=0.064$. Equation (6) may be evaluated as closely as one chooses. However, one may use various simplifying approximations to arrive at a solution. Two of these approximations will be considered here.

The first approximation involves the assumption of a constant thermal conductivity equal to the maximum conductivity[7] in the range, which reduces the ratio of thermal conductivities to unity. The remaining finite sum,

$$\sum_{0}^{N}\frac{N(1+\alpha)}{N(1+\alpha)-n},$$

can now be quickly estimated by using a $1/n$ table and an adding machine, or by means of a Leibniz[8] type summation. This first approximation leads to a calculated value of the depth which, for a given evaporation rate assumed, is an upper bound, i.e., the performance of the dewar will be as good as or better than calculated.

The other approximation involves the assumption that the coefficient of X_0 in Eq. (6) is a constant. Actually, an examination of the pertinent case, namely that of helium as the evaporating liquid and an alloy as the Dewar wall material, shows that the assumption of constancy or an easily calculable average of this coefficient is justified. It will now be shown that

$$N(1+\alpha)/N(1+\alpha)-n$$

multiplied by the varying part of κ_n/κ_0 is a constant, or, at worst, is a slowly varying function which may be easily averaged.

Although pure metals exhibit a maximum in the thermal conductivity, as borne out experimentally by work such as that by Andrews, Spohr, and Webber,[7] alloys such as stainless steel which we have used for some time in Dewar design[3] behave more agreeably from this standpoint. The electronic contribution to the thermal conductivity (which is the major contribution for most metals), is given, according to A. H. Wilson,[9] by the formula,

$$1/\kappa=1/AT+1/\kappa, \quad (7)$$

where

$$A=1/3\rho_0(\pi k/e)^2=\text{constant},$$

where ρ_0 is the residual electrical resistivity, and k and e have their usual significance. The first term on the right in Eq. (7) gives the effect of impurity scattering and the second, lattice scattering. Then, for a sufficiently high impurity concentration, the impurity term may become dominant and give a linear dependence of the thermal conductivity of an alloy on temperature. Recently, in keeping with the Wilson prediction, Zimmermann[10] has experimentally confirmed this linear dependence on temperature for stainless steel. The linear law is then compatible with a characterization of our κ_n/κ_0 as

$$\frac{\kappa_n}{\kappa_0}\cong\frac{N(1+\beta)-n}{N(1+\beta)}\cong\frac{N(1+\alpha)-n}{\text{constant}}, \quad (8)$$

where $\beta=4.23°/77.4°=0.055$, and comes about as a result of having the nth cell at 4.23°K instead of at 0°K. Substituting (8) into (6), we get

$$l=X_0\frac{(\alpha+1)}{(\beta+1)}\sum_{n=0}^{N}\frac{N(1+\beta)-n}{N(1+\alpha)-n}. \quad (6a)$$

Taking the midpoint of the extreme values of the slowly varying summand in (6a), we obtain for large values of N a simple formula:

$$l=X_0(0.93N)=\frac{0.93\kappa_0 A(T_0-T_N)}{\dot{M}[C_p(T_0-T_N)+L]} \quad (9)$$

for the dewar depth. X_0 is obtained from Eq. (5) and $\dot{M}$ is the liquid helium loss rate for the cryostat to be designed.

The author expresses thanks to Dr. R. T. Webber, Mr. M. F. M. Osborne, and Dr. A. H. Ryan, of the Naval Research Laboratory, for critical perusal of this paper.

[6] W. H. Keesom, *Helium* (Elsevier, Amsterdam, 1942), p. 96.
[7] R. T. Webber, Private Communication, 1949; Andrews, Spohr, and Webber, Phys. Rev. **78**, 313 (1950).
[8] E. T. Whittaker and G. N. Watson, *Modern Analysis* (MacMillan, New York, 1947), p. 15; J. M. Childs, *Early Mathematical Manuscripts of Leibniz* (Open Court Publishing Company, Chicago, 1920).
[9] A. H. Wilson, Proc. Cambridge Phil. Soc. **33**, 371 (1937).
[10] J. E. Zimmermann, Phys. Rev. **83**, 192 (1951).

JOURNAL OF APPLIED PHYSICS VOLUME 22, NUMBER 12 DECEMBER, 1951

Electron Microscopic Replica Studies of Porosity in Fused Iron Catalysts

J. T. McCartney
Coal Constitution and Miscellaneous Analysis Section, Bureau of Mines, Pittsburgh, Pennsylvania

AND

R. B. Anderson
Research and Development Branch, Office of Synthetic Liquid Fuels, Bureau of Mines, Bruceton, Pennsylvania

(Received June 8, 1951)

The preparation of various replicas of a fused iron catalyst is described. Micrographs of these replicas show comparable fine structures that are attributed to the pores developed in the catalyst upon reduction. Dimensions of these fine structures compare reasonably well with pore diameters calculated from pore volume-surface area determinations.

I. INTRODUCTION

THIS paper reports an electron microscopic study of a typical fused-iron (Fe_3O_4-MgO-K_2O) synthetic-ammonia catalyst. The raw catalyst consists of a solid solution of magnetite and the structural promotors and possesses virtually no porosity or internal surface area. Upon reduction in hydrogen, the external volume of the particle remains unchanged, and the volume change in the transformation from magnetite to α-iron results in the formation of a fine pore structure with high surface area. For catalyst D3006, the average diameters of these pores, estimated from pore volumes and surface areas, were 370 and 800A for reduction at 450° and 550°C, respectively.[1] The present paper describes the preparation and interpretation of electron micrographs of replicas stripped from reduced catalyst D3006. The sizes of the pores observed by the replica methods are of the same magnitude as those estimated from pore volumes and surface areas.

II. EXPERIMENTAL PROCEDURE

Catalyst D3006 was prepared by the electrical fusion method. 2- to 4-mesh pieces of the catalyst were polished on one surface by ordinary methods, concluding with a final buffing on soft cloth with wet cerium oxide. The samples were then reduced in dry hydrogen at hourly space velocities of 2500 and at temperatures of 450° or 550°C in a metal block reactor.[2] The reduced catalyst was cooled in hydrogen and then transferred, without exposure to air, into a jar of toluene. A more complete description of this catalyst and the method of reduction has been given in references 1 and 2.

The catalyst pieces were taken from the toluene only a few minutes before replica preparation to allow the excess toluene to evaporate. In preparing a Formvar replica, the polished surface was dipped in a 0.5 percent solution of Formvar in ethylene dichloride. After drying, a 10 percent solution of nitrocellulose in butyl acetate was spread over the surface. When this had dried, the double film was loosened at one edge with a razor blade and then peeled from the surface. When metal shadowing was desired, the film was placed in a vacuum chamber, Formvar side up, and chromium was evaporated onto it from a tungsten filament at an angle of about 10° with the film surface.[3] 200-mesh specimen screens were then fastened to the Formvar side of the double film by dipping a small segment of the screen in rubber cement and fastening to equivalent-size pieces of the replica. These were placed, film side up, on a small tray, the corners of the film were cemented to the tray, and it was immersed in amyl acetate, a solvent for the nitrocellulose. After about an hour, the tray was placed in a second bath of amyl acetate. Upon removal and drying, the specimens were ready for observation in the electron microscope.

In preparing the silica replicas, the 10-percent solution of nitrocellulose was spread on the catalyst surface and the film peeled after drying. These films were placed in the vacuum chamber, and silica was evaporated onto them at right angles to the surface.[4] Some of these were also subsequently shadowed with chromium, as described above. The nitrocellulose was dissolved as in the first procedure. These silica films are positive replicas, whereas the Formvar replicas are negatives.

III. DESCRIPTION AND DISCUSSION OF MICROGRAPHS

Formvar and silica replicas of polished surfaces of the unreduced catalyst showed no fine structure of any kind. Figures 1 to 5 show electron micrographs of the various replicas of the reduced catalyst. Figure 1 is an unshadowed Formvar replica; Fig. 2, a shadowed Formvar replica; Fig. 3, an unshadowed silica replica; Fig. 4, a silica film that has broken and folded over; and Fig. 5, a shadowed silica replica. It is apparent that the same type of microstructure is reproduced in each of these replicas, and it is assumed that this structure represents pores that have been developed in the catalyst by the reduction process. Figure 6 illustrates a reasonable interpretation of the manner in which this

[1] Hall, Tarn, and Anderson, J. Am. Chem. Soc. (to be published).
[2] Anderson, Shultz, Seligman, Hall, and Storch, J. Am. Chem. Soc. **72**, 3502 (1950).
[3] R. C. Williams and R. W. G. Wyckoff, J. Appl. Phys. **17**, 23 (1946).
[4] C. H. Gerould, J. Appl. Phys. **18**, 333 (1947).

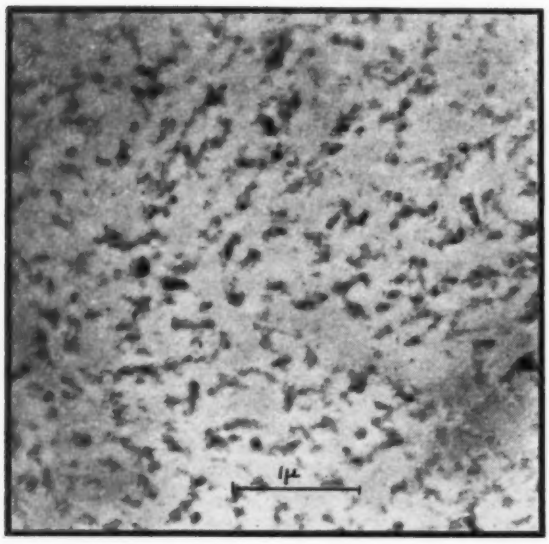

FIG. 1.

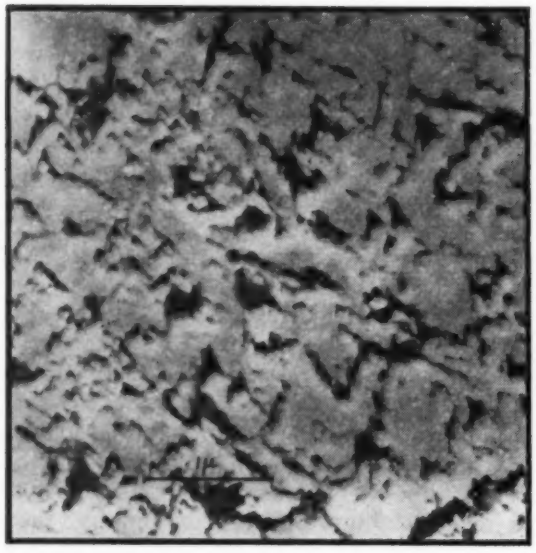

FIG. 2.

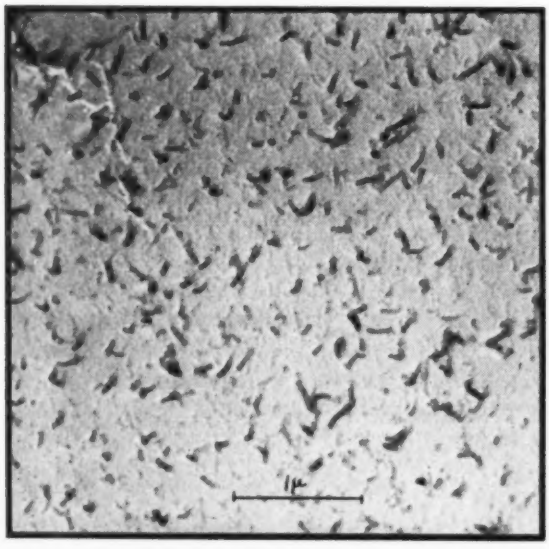

FIG. 3.

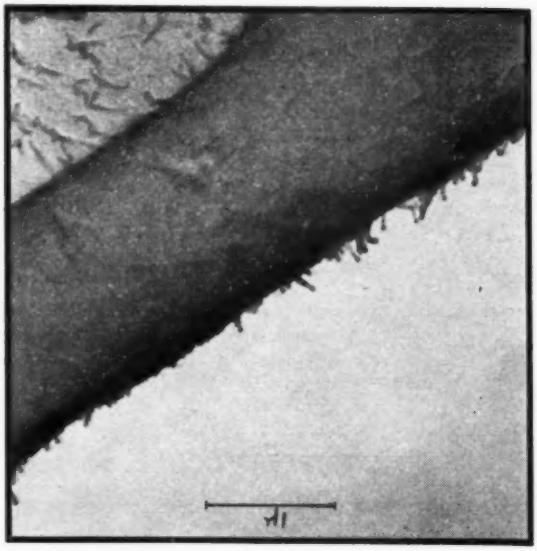

FIG. 4.

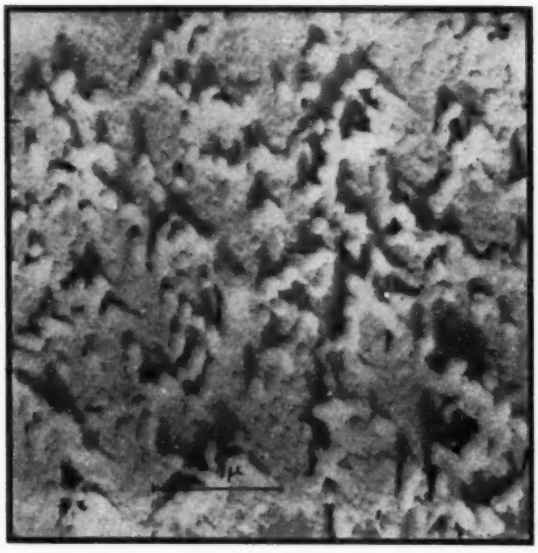

FIG. 5.

FIGS. 1–5. Electron micrographs of various replicas of reduced fused iron catalyst. FIG. 1. Unshadowed Formvar. FIG. 2. Shadowed Formvar. FIG. 3. Unshadowed silica. FIG. 4. A folded silica replica. FIG. 5. Shadowed silica.

pore structure is reproduced in the replicas. It is believed that the Formvar and nitrocellulose solutions penetrate the pores and that the surfaces in contact with the catalyst contain marked projections at points where such penetration has occurred. There is some difference of opinion as to the contour of the reverse surface of these films,[5–7] but it is believed that they approach flatness, but with moderate concavities oppo-

[5] V. J. Schaefer and D. Harker, J. Appl. Phys. **13**, 427 (1942).
[6] R. D. Heidenreich and L. A. Matheson, J. Appl. Phys. **15**, 423 (1944).
[7] Deacon, Ellis, Cross, and Sennett, J. Appl. Phys. **19**, 704 (1948).

site the projections. The shadowed Formvar replica (Fig. 2) markedly shows these projections and aids in the interpretation of the unshadowed Formvar replica (Fig. 1).

When silica is deposited normally on the negative nitrocellulose replica, it might be expected that a replica of nearly uniform thickness would be formed. However, it is believed that the condensing silica molecules exhibit considerable mobility over the surface on which they condense,[8] and it has been suggested that the silica tends to accumulate along sharp changes in elevation. Such migration and accumulation of silica on the projections of the nitrocellulose replica may account for the detail seen in the silica replicas of Figs. 3–5. The projections appear to be very uniform in width and exaggerated in height. This could be the result of extensive accumulation of silica on the tips of the projections of the replica.

The spots on the Formvar replica of Fig. 1 average about 500 to 600A in their smallest dimension. The silica projections of Figs. 3 and 4 average about 400 to 500A in width. The latter figure may not represent the actual pore diameters if the concept of exaggerated accumulation of silica is valid. However, both of these figures compare reasonably well with the pore diameters of 370 to 800A, as estimated from surface area-pore volume data, assuming long cylindrical pores.[9] No definite differences were observed in the dimensions of the replica structures from samples reduced at the different temperatures 450° and 550°C.

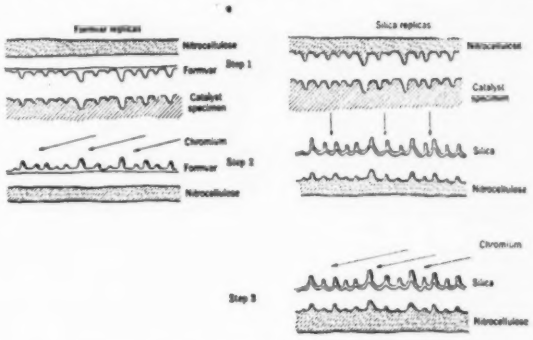

FIG. 6. Diagrammatic interpretation of the mode of formation of Formvar and silica replicas of a porous catalyst surface.

[8] R. D. Heidenreich, J. Appl. Phys. 14, 312 (1943).

[9] It should be emphasized that in this method the pore volume to surface area ratio is determined, and the estimation of an average pore diameter involves an assumption of the type of pore system. For example, for a pore of cylindrical or square cross section, $\bar{d}=4V/A$, where $\bar{d}$ is the average pore diameter or length of a side of the square, V the pore volume, and A the surface area. If one side of the square pore is increased indefinitely, the equation becomes $\bar{d}=2V/A$, where $\bar{d}$ is the separation between two parallel plates. These examples illustrate the fact that the smaller dimension of a pore opening is the most significant in determining its pore volume-area ratio.

A Method of Growing Single Crystals of Lead Telluride and Lead Selenide

W. D. LAWSON
Telecommunications Research Establishment, Malvern (Ministry of Supply), England
(Received May 31, 1951)

Single crystals of lead telluride measuring up to 1¼-cm diameter and 6 cm long have been grown in sealed silica crucibles by the Bridgman-Stockbarger method of lowering a melt slowly through a freezing level. The crystals have been grown for the purpose of testing the semiconducting and allied properties of lead telluride in that form. Extreme purity of the materials and cleanliness of the crucible have been found essential for successful growth. X-ray tests have shown that the specimens are single crystals. The purest crystal grown so far had a conductivity corresponding to an electron concentration of 5×10^{14} per cc. Attempts to introduce excess of one of the constituents—lead or tellurium into the crystal lattice during growth have not so far been successful.

1. INTRODUCTION

IT is necessary, in order to understand the fundamental electronic behavior of semiconductors like PbTe, to make measurements over a wide range of temperature of such electrical properties as conductivity and Hall constant. It is possible to make the measurements, as indeed has often been done, on evaporated layers, compressed powder slabs, or polycrystalline ingots, but the values of conductivity so obtained are bound to be affected to some extent, particularly at lower temperatures, by the intergranular boundaries present in such specimens. The best way of overcoming this difficulty is by making measurements on specimens which have no such boundaries, i.e., on single crystals, and it is for this purpose that the crystals have been grown.

A crystal size of 4 cm, by 1 cm, by 1 mm was initially required for the electrical experiments so this size was set as the target to be achieved in growing the crystals.

2. METHOD OF GROWING THE CRYSTALS

A study of the various ways of growing single crystals—by evaporation, from solution, etc., led to the conclusion that the method of growing from a melt offered most hope of yielding crystals of the size required. Even after this decision had been made there was still a considerable choice of experimental technique of growing crystals from a melt. After some initial experiments the double-furnace method, which has been used with considerable success in recent years by Stockbarger[1] and others[2] for growing crystals of optical materials, was selected because it gives best control of the growing conditions and is therefore most likely to give consistent results. In this method the material is melted in an upper furnace, in a crucible with a conical bottom, and lowered slowly into a lower furnace whose temperature is below the melting point. At some intermediate level there exists a freezing plane at which the molten material solidifies, and if conditions are right a single crystal grows.

FIG. 1. Silica crucible.

Stockbarger puts the main essentials for successful growth of pure single crystals in this way as follows: (i) Dropping rate and temperature gradient such that isothermals around the freezing level are horizontal. This condition ensures that cooling is from the bottom and not from the sides, and prevents random crystal growth inward from the sides.

(ii) Sharp temperature gradient around the freezing level. This produces a high flow of heat through the freezing surface and enhances rejection of impurities by vigorous bombardment of the freezing level.

3. SPECIAL PROBLEMS WITH LEAD TELLURIDE

The melting point of PbTe is 904°C so the temperatures within the top and bottom furnaces should be in the region of 950°C and 850°C, respectively. The difficulties associated with heating PbTe to 950° are as follows:

(i) PbTe cannot be heated in air as it oxidizes readily. It must therefore be heated in an inert atmosphere or in vacuo.

(ii) At 950°C the vapor pressure of lead telluride is fairly high (several cm Hg) so there is considerable loss of material if it is heated at that temperature for any length of time in an open crucible. There is also a certain amount of dissociation into free lead and tellurium, and since, at 950°C, the vapor pressure of

[1] D. C. Stockbarger, Rev. Sci. Instr. **7**, 133, 1936.
[2] Tuttle and Egli, J. Chem. Phys. **14**, 571, 1946.

tellurium is considerably higher—the order of 100 times —than that of lead, the material left after free evaporation from an open crucible will have a stoichiometric excess of lead. Thus if it is required to retain the initial proportions of Pb and Te the crystal must be grown in a sealed crucible.

(iii) At 950°C lead telluride and the dissociated elements are fairly active chemically so the crucible material has to be chosen with some care. Fused silica does not react with lead telluride in the absence of oxygen, so the crystals have been grown in sealed crucibles of this material.

4. PREPARATION OF THE MATERIALS

It is well known that extreme purity of the materials is essential both for growing good single crystals and for obtaining reliable results from the electrical experiments. It is thus essential firstly to start with high grade materials of guaranteed purity and secondly to take all necessary precautions to prevent contamination during handling and growth. The ordinary commercial grades of chemically pure material do not achieve anything like the standard of purity required but spectrographically standardized grades of both lead and tellurium with a total impurity content better than 1 in 10^5 have been obtained and used as the starting material. It is necessary to remove the oxide coat with which these are covered when received. This can be done with lead by heating it to 700°C in an alumina boat in a stream of hydrogen. Tellurium cannot be treated this way as there is a tendency for hydrogen telluride to be formed, so the oxide is separated by distillation in a pyrex glass tube at a residual pressure of 10^{-6} mm Hg. Before distilling the tellurium the tube and pumping system are flushed several times with argon.

A crucible of the shape shown in Fig. 1 is formed from clear fused silica tube of about 1-cm bore. The shape of the cone at the bottom has not been found to be critical in any way. The transparent variety of silica is used in preference to the translucent variety as there is some danger of contamination from the latter by the emission, at high temperature, of gas from the small bubbles which are the cause of its translucency. The crucible is cleaned before use by boiling with nitric and chromic acids and flushing several times and then boiling with distilled water. It is then connected to a vacuum system, pumped out, and outgased at about 600°C.

The lead and tellurium, in the required proportions, are then put in, and the crucible sealed back on to the pumping system. It is left on the system at a pressure of 10^{-6} mm Hg for about two days before it is sealed off at the constriction. This long period of pumping out is necessary to ensure that as much occluded air as possible is removed from the mixture. It is not possible to heat the mixture above about 100°C to help in expelling this air as further heating merely assists the formation of an oxide and causes evaporation of tellurium.

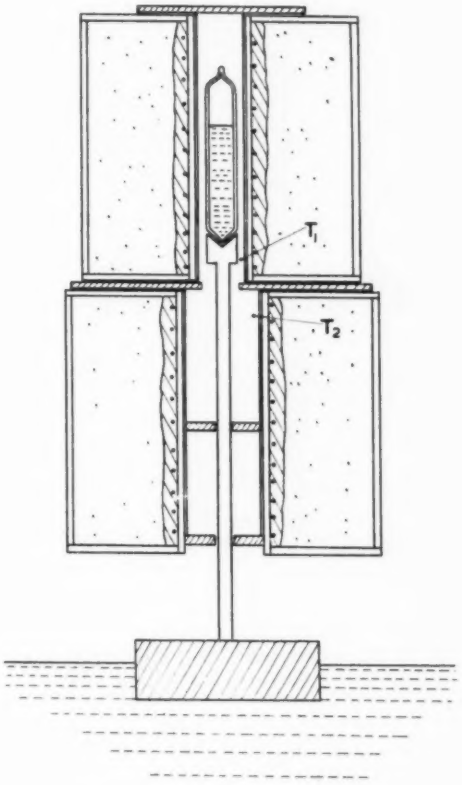

FIG. 2. Crystal growing apparatus.

Combination of the lead and tellurium is effected at this stage, after sealing off, by heating the crucible and contents in a Bunsen flame. The reaction is exothermic and a flash of redness along the mixture indicates the formation of lead telluride.

5. GROWTH OF CRYSTAL

The crucible is then transferred to the crystal growing apparatus which is illustrated in Fig. 2. The two furnaces are made as separate units and mounted vertically one on top of the other as shown, on a stand above a trough of water. The crucible is cemented to the nickel supporting rod which rests on a float on the water, and the level of the water is adjusted until the crucible is entirely within the top furnace. The crucible can be lowered at the appropriate time by letting water run out of the tank. The furnace tubes are lined with nickel tubes which serve the double purpose of eliminating temperature gradients within the separate furnaces and protecting the refractory furnace tubes in the event of explosions. Any gaps at the furnace junction and top cap are sealed with alumina cement to exclude draughts.

The furnaces are then switched on and the power supply increased gradually until the upper and lower temperatures of 950°C and 850°C, respectively, are

reached. The temperatures are measured bychromel-alumel thermocouples T_1 and T_2 placed one inch on either side of the insulating baffle. The power supply is controlled by Sunvic Energy Regulators which give enough control to keep the temperature well within 10°C of the nominal values. This degree of stabilization is adequate for the lowering rates used, particularly in view of the high thermal inertia of the furnaces.

The apparatus is left in this condition, with the contents of the crucible molten, for about 12 hours. This prolonged melting is necessary for the following reasons: first, it insures that the lead telluride is completely molten so that no small seeds of solid material remain; second, it allows thorough mixing and reaction of the elements so that the composition of the compound is uniform throughout the melt, and finally it permits diffusion of insoluble impurities to either top or bottom of the melt leaving the middle relatively purer. The crucible is then lowered at any desired rate by siphoning water out of the trough through a glass tube fitted with a stopcock. This gives control of the lowering speed between 2 mm/hr and 2 cm/hr as desired. The lowering method has the great advantages of simplicity and almost complete freedom from breakdown of any kind, provided the stopcock is thoroughly clean. The lowering speed diminishes very slowly as the water level falls but this has not been found to be any disadvantage and could, if necessary, be almost completely eliminated by using a long siphon tube so that the head of water remains practically constant. It has been found necessary, with the above temperature difference, to use a lowering speed less than 1 cm/hr to insure single crystal growth.

When the crucible is lowered completely into the bottom furnace it is cooled to room temperature over a period of about 24 hours. More rapid cooling sets up strains in the crystal which leave it weak and fragile so that it breaks up very easily.

Usually, if no oxide of either element is present, the crystal slips easily and cleanly out of the crucible. If however one or more of the oxides of lead or tellurium are present, either through inadequate pumping out, or incomplete deoxidizing, these react with silica to form a kind of glass which glues the crystal very effectively to the crucible. When this happens it is almost impossible to extract the crystal whole and sometimes shattering of the crucible during cooling is caused by differential contraction.

6. EXPERIMENTAL RESULTS

Single crystals measuring up to $1\frac{1}{4}$ cm diameter by 6 cm long have been grown using this technique and there is no apparent reason why larger ones could not be grown if required. The crystals, which have a face-centered cubic NaCl type structure, are opaque and have a metallic, almost silvery, appearance. They are brittle and cleave quite readily parallel to (100) planes when tapped with a razor blade. Cleavage in other planes is difficult, though not impossible, to produce.

The purest crystal so far grown had an electrical conductivity corresponding to an electron concentration of 5×10^{14} per cc and has been shown to be an intrinsic semiconductor down to 200°K. The conductivity and Hall constant measurements which lead to this conclusion are being published elsewhere.

Tests in an x-ray goniometer have indicated as follows that the specimens are in fact single crystals. Rectangular slabs with faces parallel to (100) crystal planes were cleaved from the ingots and the angles between their faces measured. It was found that, within the accuracy of the measurement, opposite faces were parallel to each other and perpendicular to adjacent faces. The individual faces were also examined, section by section, with a narrow x-ray beam 0.4 mm wide, and found to be plane. Owing to the very high absorption of x-rays in lead telluride (absorption coefficient $\doteqdot 250$ for the x-rays used) it is only the surface layers which are being examined and not the bulk crystal, but the evidence is nevertheless fairly conclusive that the slabs are single crystals.

Specimens have also been tested by x-rays for traces of free lead or tellurium but none have been found.*

In order to test the effect of an excess of one of the constituents lead or tellurium on semiconducting properties, an attempt was made to grow a number of crystals ranging in composition from 2 percent excess Pb to 2 percent excess Te. The appropriate excess was introduced into the initial mixture and the crystal growing experiment carried out in the usual way. Examination of the resulting crystal revealed however that the excess had not been absorbed by the crystal lattice but had been forced to the top during the growing process, and the crystal underneath retained an approximately stoichiometric composition. This was most noticeable when a large excess of lead had been added, as the top of the resulting crystal was then tough and could not be cleaved and was obviously almost entirely composed of lead. Varying the growing conditions has not so far made any appreciable difference to this result.

Experiments are continuing in an endeavor to produce purer crystals and to introduce excess of the individual constituents into the crystal lattice.

7. LEAD SELENIDE

A single crystal of lead selenide has been grown recently in the same way, in a silica crucible. The melting point of this compound is 1065° so furnace temperatures of 1110°C and 1010°C were used in conjunction with a lowering rate of nearly 1 cm/sec. The selenide has a crystal structure and cleavage properties similar to the telluride, but is darker and

* This test was carried out by K. Lark-Horovitz of Purdue University.

less silvery in appearance. Its electrical properties are being measured.

ACKNOWLEDGMENTS

The author wishes to thank Mr. G. E. Bacon of A.E.R.E., Harwell, Berkshire, for carrying out x-ray measurements to determine the form of the crystals. The work described in this paper was carried out at the Telecommunications Research Establishment, Malvern, England, as part of the research program of the British Ministry of Supply, and is published by permission of the Chief Scientist, British Ministry of Supply. British Crown Copyright reserved. Reproduced by permission of the Controller of H.B.M. Stationery Office, England.

JOURNAL OF APPLIED PHYSICS VOLUME 22, NUMBER 12 DECEMBER, 1951

General Theory of Electromagnetic Horns*

A. F. STEVENSON
Department of Mathematics, Faculty of Science, Farouk I University, Alexandria, Egypt†
(Received June 8, 1951)

Exact equations for the propagation of electromagnetic waves in a perfectly conducting horn of arbitrary shape are given. They take the form of an infinite set of simultaneous ordinary linear differential equations, and can be interpreted as the equations of propagation of a system of coupled E- and H-waves. If the coupling is neglected, we need only consider a single differential equation for each E- and H-wave, which can be solved approximately by the W.K.B. method. This approximate solution brings out the distinction between "transmission regions" and "attenuation regions" of the horn, as found by Barrow and Chu for the sectoral horn.

It is shown that the error due to neglect of coupling is, in general, of the order of the square of the flare angle as far as the variation of the field along the horn is concerned, but is of the first order in the flare angle as regards the variation of the field over the cross section. The coupling cannot, however, be neglected between modes of propagation which have the same cut-off frequency for all cross sections. The propagation characteristics of several special shapes of horn are discussed in detail.

1. INTRODUCTION

THE theory of the propagation of electromagnetic waves in a perfectly conducting sectoral horn has been given by Barrow and Chu.[1] Exact solutions for a conical horn are also available.[2] But no attempt appears to have been made to give a general theory applicable to horns of any shape.[3] It is the purpose of this paper to give such a general theory.

In Sec. 2, exact equations for the propagation of electromagnetic waves of a single frequency in a perfectly conducting horn of arbitrary shape are given—a "horn" being defined as a surface such that any plane perpendicular to a given line meets this surface in a single closed curve. The equations take the form of an infinite set of simultaneous ordinary linear differential equations in an infinite number of unknowns, the coefficients occuring in the equations being known when the eigenfunctions and eigenvalues which occur in waveguide theory are known for all sections of the horn. These differential equations can be regarded as giving rise to a system of coupled E- and H-waves.

In Sec. 3, the case of horns of small flare is considered, the coupling between different modes of propagation being neglected, so that we have to deal with a single ordinary differential equation. An approximate explicit solution of this equation can be given for what is here termed the "normal case." This approximate solution brings out the distinction between "transmission regions" and "attenuation regions" of the horn, as found by Barrow and Chu[1] for the sectoral horn, and approximate expressions for the phase velocity (in the transmission region) and the attenuation constant are given.

In Sec. 4, the validity of the neglect of coupling is investigated. It is shown that, as far as the variation of the field components along the horn is concerned, the error committed by neglecting coupling is of the second order in the flare angle, provided that the modes concerned do not have the same cut-off frequency for all cross sections; but that the error is of the first order in the flare angle as regards the variation of the field over a cross section. The coupling cannot be neglected between modes having the same cut-off frequency.

In Sec. 5 expressions for the field components correct to the first order in the flare angle are given for the normal case, and the problem of calculating the field *outside* the horn is discussed briefly. In Sec. 6 various special horns are considered in detail, and some general

* A preliminary account of this paper was given at the American Mathematical Society's Symposium on Electromagnetic Theory held at Cambridge, Massachusetts, in July, 1948.

† Now at Bishop's University, Lennoxville, Quebec, Canada.

[1] W. L. Barrow and L. J. Chu, Proc. Inst. Radio Engrs. **27**, 51 (1939).

[2] See, for instance, S. A. Schelkunoff, *Electromagnetic Waves* (D. Van Nostrand Company, Inc., New York, 1943), pp. 399–404.

[3] The case of horns of small flare is referred to briefly by Schelkunoff (pp. 405, 406 of reference 2). The equations there suggested, however, do not appear to be correct, even as approximate equations for what is termed the "normal case" in this paper (the terms involving U_{nn}, X_{nn} in our Eqs. (3.1), (3.2) appear to be omitted).

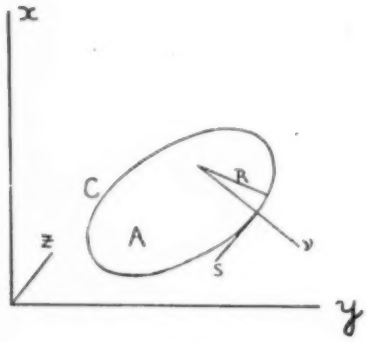

FIG. 1(a). Cross section of the horn.

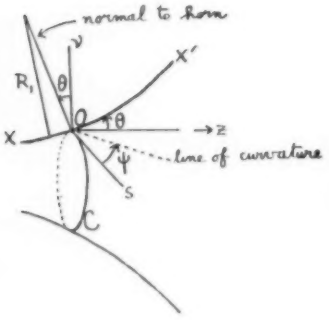

FIG. 1(b). General view of horn. The curve XX' is the normal section of the horn at 0 which is parallel to the z-axis.

results relating to horns of rectangular and circular sections are established.

For a complete discussion of the radiation properties of a horn, the field pattern outside the horn is, of course, of considerable importance. This is not considered in any detail in this paper, being only touched on in Sec. 5. A theory of wave propagation inside the horn must, however, precede any such investigation, and with the general formulas given in this paper the calculation of the field outside the horn can be undertaken by the usual approximate methods.

2. EXACT EQUATIONS FOR A PERFECTLY CONDUCTING HORN

We shall understand by a "horn" any surface such that any plane perpendicular to the z-axis (the direction of the horn) cuts this surface in a single closed curve, the cross section of the horn. We denote (Fig. 1) the interior of any cross section by A and its boundary by C (A and C vary, of course, with z). We denote the direction of the outward normal and the tangent to C by ν, s, respectively, the direction of s being such that a right-handed rotation from ν to s carries us in the direction of the z axis (we use right-handed axes).

To specify the geometry of the horn, we require for our purpose four quantities θ, ψ, R, R_1 defined as follows (Fig. 1):

θ = angle between the normal ν to C and the normal to the horn, θ being positive if a right-handed rotation from the direction ν to the direction of the normal to the horn carries us in the direction s. We define the direction of the normal to the horn by requiring $|\theta| < \pi/2$ (alternatively, θ is the angle between the z-axis and the tangent to the normal section of the horn which is parallel to the z-axis). We may term θ the "flare angle" of the horn; as defined, it is positive if the horn flares outwards as we go along the z-axis.

ψ = angle between a line of curvature of the horn and the direction s, ($|\psi| \leqslant \pi/4$), ψ being positive if a right-handed rotation from the direction s to the line of curvature carries us in the direction of the normal to the horn.

R = radius of curvature of C, reckoned positive if C is concave inwards.

R_1 = radius of curvature of the normal section of the horn which is parallel to the z-axis, reckoned positive if this section is concave to the normal to the horn.

Of these four quantities, the most important is the flare angle θ. Indeed it is the only one which usually arises, but we require all four quantities for the exact equations in the general case. We shall be concerned primarily with horns for which θ, ψ, R/R_1 are small, but we make no approximations in developing the general equations.

We confine ourselves to a steady state with a time factor $e^{-i\omega t}$ and write $k=\omega/c=2\pi/\lambda$ (Gaussian units being employed). The problem then is to solve the maxwell equations,

$$\text{curl}\mathbf{E}=ik\mathbf{H}, \quad \text{curl}\mathbf{H}=-ik\mathbf{E}, \tag{2.1}$$

subject to the boundary conditions:

$$\text{components of } \mathbf{E} \text{ tangential to horn}=0. \tag{2.2}$$

From these boundary conditions it follows that, on C:

$$E_s=0, \quad E_z+\tan\theta E_\nu=0, \quad H_\nu=\tan\theta H_z. \tag{2.3}$$

Instead of using all the components of $\mathbf{E}$ and $\mathbf{H}$ directly, we shall use the six functions E_z, H_z, F, G, P, Q, where

$$E_x=\frac{\partial F}{\partial x}+\frac{\partial G}{\partial y}, \quad E_y=\frac{\partial F}{\partial y}-\frac{\partial G}{\partial x}, \tag{2.4}$$

$$H_x=\frac{\partial P}{\partial x}+\frac{\partial Q}{\partial y}, \quad H_y=\frac{\partial P}{\partial y}-\frac{\partial Q}{\partial x}. \tag{2.5}$$

Regarding E_z, E_y as given, we can always define two functions F, G by means of (2.4), and impose the boundary condition

$$F=0 \text{ on } C. \tag{2.6}$$

F, G are then uniquely determined to within an additive function of z to G, which is of no importance.[4]

Similarly, (2.5) determined P, Q uniquely, apart from an additive function of z to P, if we impose the boundary condition

$$Q=0 \text{ on } C. \tag{2.7}$$

We note that, from (2.4)–(2.7) follow (on C):

$$E_\nu=\frac{\partial F}{\partial \nu}+\frac{\partial G}{\partial s}, \quad E_s=-\frac{\partial G}{\partial \nu}, \tag{2.8}$$

$$H_\nu=\frac{\partial P}{\partial \nu}, \quad H_s=\frac{\partial P}{\partial s}-\frac{\partial Q}{\partial \nu}. \tag{2.9}$$

[4] For, if we first determine (uniquely) a function $F(x, y, z)$ by means of the equation $\partial^2F/\partial x^2+\partial^2F/\partial y^2=\partial E_x/\partial x+\partial E_y/\partial y$ with the boundary condition (2.6), then (2.4) give two equations to determine $G(x, y, z)$ which are compatible, and which determine G to within an additive function of z.

From (2.1), (2.4), (2.5) it is now easily shown that our six functions E_z, H_z, F, G, P, Q satisfy the following differential equations:

$$\left(\nabla^2+\frac{\partial^2}{\partial z^2}+k^2\right)E_z=0, \tag{2.10}$$

$$\left(\nabla^2+\frac{\partial^2}{\partial z^2}+k^2\right)H_z=0, \tag{2.11}$$

$$\nabla^2F=-\frac{\partial E_z}{\partial z}, \tag{2.12}$$

$$\nabla^2G=-ikH_z, \tag{2.13}$$

$$\nabla^2P=-\frac{\partial H_z}{\partial z}, \tag{2.14}$$

$$\nabla^2Q=ikE_z, \tag{2.15}$$

where (here and throughout the paper) ∇^2 denotes the *two*-dimensional laplacian operator:

$$\nabla^2=\frac{\partial^2}{\partial x^2}+\frac{\partial^2}{\partial y^2}.$$

As boundary conditions, we have the following, to be satisfied on C:

$$E_z=-\tan\theta H_\nu, \tag{2.16}$$

$$\partial P/\partial\nu=\tan\theta H_z, \tag{2.17}$$

$$F=0, \tag{2.18}$$

$$Q=0, \tag{2.19}$$

$$\partial G/\partial\nu=0, \tag{2.20}$$

$$\frac{\partial H_z}{\partial\nu}=pH_s+qH_z+\tfrac{1}{2}\tan2\theta\left(\frac{\partial H_s}{\partial s}+2\frac{\partial H_z}{\partial z}\right), \tag{2.21}$$

where[5]

$$p=-\tfrac{1}{2}\left(\frac{\cos\theta}{R}+\frac{1}{R_1}\right)\sec2\theta\tan2\psi,$$
$$q=\left(\frac{\sin^2\theta}{R}+\frac{\sec\theta}{R_1}\right)\sec2\theta, \tag{2.22}$$

and $\partial H_s/\partial s$ means $\partial H_s(s,z)/\partial s$. The first five of these boundary conditions follow from (2.3), (2.6)–(2.9); the last, (2.21), is proved in Appendix I. It may be shown that the differential Eqs. (2.10)–(2.15), together with the boundary conditions (2.16)–(2.21), are completely equivalent to the maxwell Eqs. (2.1) with the boundary conditions (2.2).

[5] The definitions (2.22) become meaningless if θ or ψ is $\pm\pi/4$. If $|\psi|=\pi/4$, p may still be defined (see Appendix I); if $|\theta|=\pi/4$, the method is not applicable.

We now introduce the eigenfunctions and eigenvalues used in the theory of wave guides. Let the normalized and orthogonal eigenfunctions u_n, with corresponding eigenvalues α_n ($n=1, 2, \cdots$), be defined by

$$(\nabla^2+\alpha_n{}^2)u_n=0 \text{ in } A, \tag{2.23}$$

$$u_n=0 \text{ on } C, \tag{2.24}$$

$$\int_A u_nu_m dS=\delta_{nm}, \tag{2.25}$$

where δ_{nm} is the usual Kronecker delta ($\delta_{nm}=0$ if $n\neq m$, $\delta_{nn}=1$). Also let the eigenfunctions v_n, with corresponding eigenvalues β_n, be defined by

$$(\nabla^2+\beta_n{}^2)v_n=0 \text{ in } A, \tag{2.23a}$$

$$\partial v_n/\partial\nu=0 \text{ on } C, \tag{2.24a}$$

$$\int_A v_nv_m dS=\delta_{nm}. \tag{2.25a}$$

The u_n, α_n are required for E-waves in wave guides, and the v_n, β_n for H-waves; α_n, β_n are of course, functions of z, and u_n, v_n functions of x, y and z in the case of the horn. We suppose that these eigenfunctions and eigenvalues are known.

We now assume the following expansions for the six functions E_z, $\cdots$, Q:

$$E_z=\sum_n e_n(z)u_n, \tag{2.26}$$

$$H_z=\sum_n h_n(z)v_n, \tag{2.27}$$

$$F=\sum_n f_n(z)u_n, \tag{2.28}$$

$$G=\sum_n g_n(z)v_n, \tag{2.29}$$

$$P=\sum_n p_n(z)v_n, \tag{2.30}$$

$$Q=\sum_n q_n(z)u_n. \tag{2.31}$$

Taking account of the boundary conditions (2.16)–(2.21), we may assume that these expansions hold within *and on* C, except for (2.26) which only holds within C. Since F, Q satisfy the same boundary conditions as the u_n, and G satisfies the same boundary conditions as the v_n, we may assume that (2.28), (2.29), (2.31) may be differentiated term by term with respect to x or y, but we shall not assume that the other equations may be so differentiated. We shall, however, assume that certain series of functions of z may be differentiated term by term.

The procedure for solving Eqs. (2.10)–(2.15) is now as follows: we multiply Eqs. (2.10), (2.12), (2.15) by u_n, the remaining equations by v_n, integrate over the area A and use the boundary conditions (2.16)–(2.21) to obtain a set of differential equations for the coefficients

$e_n, \cdots, q_n$ occurring in (2.26)–(2.31). As an example, we take Eq. (2.11), which is the most complicated to deal with. Carrying out the procedure indicated, we obtain

$$\int_A v_n \nabla^2 H_z dS + \int_A v_n \frac{\partial^2 H_z}{\partial z^2} dS + k^2 h_n = 0. \quad (2.32)$$

By Green's theorem, using the properties of the v_n and the boundary condition (2.21), we have

$$\begin{aligned}\int_A & v_n \nabla^2 H_z dS \\ &= \int_A H_z \nabla^2 v_n dS + \int_C \left(v_n \frac{\partial H_z}{\partial \nu} - H_z \frac{\partial v_n}{\partial \nu} \right) ds \\ &= -\beta_n{}^2 h_n + \int_C v_n \Big[pH_s + qH_z + \tfrac{1}{2} \tan 2\theta \\ &\qquad \times \left(\frac{\partial H_s}{\partial s} + 2 \frac{\partial H_z}{\partial z} \right) \Big] ds. \quad (2.33)\end{aligned}$$

Now from (2.9),

$$\begin{aligned}\int_C v_n p H_s ds &= \int_C v_n p \left(\frac{\partial P}{\partial s} - \frac{\partial Q}{\partial \nu} \right) ds \\ &= -\int_C \left[P \frac{\partial}{\partial s}(v_n p) + v_n p \frac{\partial Q}{\partial \nu} \right] ds,\end{aligned}$$

on integrating the first term in the second integral by parts.[6] Substituting from (2.30), (2.31), we have, since the series for Q may be differentiated term by term,

$$\int_C v_n p H_s ds = \sum_m (\xi_{nm} p_m - \eta_{nm} q_m), \quad (2.34)$$

where

$$\xi_{nm} = -\int_C v_m \frac{\partial}{\partial s}(v_n p) ds = \int_C p v_n \frac{\partial v_m}{\partial s} ds,$$

$$\eta_{nm} = \int_C p v_n \frac{\partial u_m}{\partial \nu} ds,$$

the second expression for ξ_{nm} following by another integration by parts. Similarly, integrating by parts where necessary,

$$\int_C \tfrac{1}{2} \tan 2\theta v_n \frac{\partial H_s}{\partial s} ds = \sum_m (\lambda_{nm} p_m - \mu_{nm} q_m), \quad (2.35)$$

where

$$\lambda_{nm} = \tfrac{1}{2} \int_C \tan 2\theta v_n \frac{\partial^2 v_m}{\partial s^2} ds,$$

$$\mu_{nm} = \tfrac{1}{2} \int_C \tan 2\theta v_n \frac{\partial}{\partial s} \left(\frac{\partial u_m}{\partial \nu} \right) ds.$$

[6] We assume in the first place that p, q, θ are continuous functions of position on C. Our final results, however, are valid (by a limiting process) even if these quantities are discontinuous on C.

Further,

$$\int_C v_n q H_z ds = \sum_m J_{nm} h_m, \quad (2.36)$$

where

$$J_{nm} = \int_C q v_n v_m ds. \quad (2.37)$$

Also, writing

$$\frac{\partial H_z}{\partial z} = \sum_n C_n v_n, \quad (2.38)$$

we have

$$\int_C \tan 2\theta v_n \frac{\partial H_z}{\partial z} ds = \sum_m H_{nm} C_m, \quad (2.39)$$

where

$$H_{nm} = \int_C \tan 2\theta v_n v_m ds. \quad (2.40)$$

Moreover, χ being any function of (x, y, z), we have

$$\frac{d}{dz} \int_A \chi dS = \int_A \frac{\partial \chi}{\partial z} dS + \int_C \chi \tan\theta ds, \quad (2.41)$$

$$\begin{aligned}\frac{d^2}{dz^2} \int_A \chi ds &= \int_A \frac{\partial^2 \chi}{\partial z^2} dS + \int_C \frac{\partial \chi}{\partial z} \tan\theta ds \\ &\quad + \frac{d}{dz} \int_C \chi \tan\theta ds. \quad (2.42)\end{aligned}$$

Hence, from (2.38),

$$\begin{aligned}C_n &= \int_A v_n \frac{\partial H_z}{\partial z} dS = h_n' \\ &\quad - \int_A H_z \frac{\partial v_n}{\partial z} dS - \int_C \tan\theta v_n H_z ds \\ &= h_n' - \sum_m (A_{mn} + B_{nm}) h_m, \quad (2.43)\end{aligned}$$

where (here and throughout the paper) dashes stand for derivatives with respect to z, and

$$A_{mn} = \int_A v_m \frac{\partial v_n}{\partial z} dS, \quad (2.44)$$

$$B_{nm} = \int_C \tan\theta v_n v_m ds. \quad (2.45)$$

Finally, we have

$$\begin{aligned}\int_A & v_n \frac{\partial^2 H_z}{\partial z^2} dS = h_n'' - 2 \int_A \frac{\partial v_n}{\partial z} \frac{\partial H_z}{\partial z} dS \\ &- \int_A H_z \frac{\partial^2 v_n}{\partial z^2} dS - \int_C \tan\theta \left(H_z \frac{\partial v_n}{\partial z} + v_n \frac{\partial H_z}{\partial z} \right) ds \\ &- \frac{d}{dz} \int_C \tan\theta H_z v_n ds = h_n'' - 2 \sum_m A_{mn} C_m \\ &- \sum_m C_{mn} h_m - \sum_m D_{mn} h_m \\ &- \sum_m B_{mn} C_m - \frac{d}{dz} \sum_m B_{mn} h_m, \quad (2.46)\end{aligned}$$

where

$$C_{mn}=\int_A v_m\frac{\partial^2 v_n}{\partial z^2}dS, \tag{2.47}$$

$$D_{mn}=\int_C \tan\theta v_m\frac{\partial v_n}{\partial z}ds. \tag{2.48}$$

Substituting (2.33)–(2.36), (2.39), (2.43), (2.46) in (2.32), we now have

$$\begin{aligned}h_n''+(k^2-\beta_n^2)h_n+\sum_m (H_{nm}-2A_{mn}-2B_{nm})h_m'\\ +\sum_m [J_{nm}-C_{mn}-D_{mn}-B_{nm}'\\ +\sum_l (2A_{ln}+B_{ln}-H_{nl})(A_{ml}+B_{ml})]h_m\\ +\sum_m I_{nm}p_m-\sum_m K_{nm}q_m=0,\end{aligned} \tag{2.49}$$

where

$$I_{nm}=\int_C v_n\left(\tfrac{1}{2}\tan 2\theta\frac{\partial^2 v_m}{\partial s^2}+p\frac{\partial v_m}{\partial s}\right)ds, \tag{2.50}$$

$$K_{nm}=\int_C v_n\left[\tfrac{1}{2}\tan 2\theta\frac{\partial}{\partial s}\left(\frac{\partial u_m}{\partial \nu}\right)+p\frac{\partial u_m}{\partial \nu}\right]ds. \tag{2.51}$$

In a similar manner, Eqs. (2.10), (2.12)–(2.15) yield the following:

$$\begin{aligned}e_n''+(k^2-\alpha_n^2)e_n-2\sum_m E_{mn}e_m'\\ +\sum_m (-L_{mn}+2\sum_l E_{ml}E_{ln})e_m\\ +\sum_m F_{nm}f_m+\sum_m G_{nm}g_m=0,\end{aligned} \tag{2.52}$$

$$\left.\begin{aligned}f_n&=\frac{1}{\alpha_n^2}(e_n'-\sum_m E_{mn}e_m),\\ g_n&=\frac{ik}{\beta_n^2}h_n,\\ p_n&=\frac{1}{\beta_n^2}(h_n'-\sum_m A_{mn}h_m),\\ q_n&=-\frac{ik}{\alpha_n^2}e_n,\end{aligned}\right\} \tag{2.53}$$

where

$$E_{mn}=\int_A u_m\frac{\partial u_n}{\partial z}dS, \tag{2.54}$$

$$L_{mn}=\int_A u_m\frac{\partial^2 u_n}{\partial z^2}dS, \tag{2.55}$$

$$F_{nm}=\int_C (\tan\theta-\tan^3\theta)\frac{\partial u_n}{\partial \nu}\frac{\partial u_m}{\partial \nu}ds, \tag{2.56}$$

$$G_{nm}=\int_C (\tan\theta-\tan^3\theta)\frac{\partial u_n}{\partial \nu}\frac{\partial v_m}{\partial s}ds. \tag{2.57}$$

Substituting (2.53) in (2.52), (2.49), we now have

$$\boxed{\begin{aligned}e_n''+\sum_m U_{nm}e_m'+\sum_m V_{nm}e_m+\sum_m W_{nm}h_m=0,\\ h_n''+\sum_m X_{nm}h_m'+\sum_m Y_{nm}h_m+\sum_m Z_{nm}e_m=0,\end{aligned}} \tag{2.58}$$

where

$$\left.\begin{aligned}U_{nm}&=2E_{nm}+\frac{1}{\alpha_m^2}F_{nm},\\ V_{nm}&=(k^2-\alpha_n^2)\delta_{nm}+L_{nm}+\sum_l\frac{1}{\alpha_l^2}E_{lm}F_{ln},\\ W_{nm}&=\frac{ik}{\beta_m^2}G_{nm},\\ X_{nm}&=2A_{nm}+H_{nm}+\frac{1}{\beta_m^2}I_{nm},\\ Y_{nm}&=(k^2-\beta_n^2)\delta_{nm}+C_{nm}+J_{nm}\\ &\quad -\sum_l\frac{1}{\beta_l^2}A_{ml}I_{nl}+\sum_l A_{lm}H_{nl},\\ Z_{nm}&=\frac{ik}{\alpha_m^2}K_{nm}.\end{aligned}\right\} \tag{2.59}$$

(For definition of the coefficients on the right-hand sides of (2.59), see (2.54)–(2.57), (2.37), (2.40), (2.44), (2.45), (2.47), (2.48), (2.50), (2.51). δ_{nm} = Kronecker delta. For definition of p, q see (2.22).)

In reducing the equations to our final form, we have made use of the following relations between the coefficients, which are proved in Appendix II:

$$A_{mn}+A_{nm}+B_{nm}=0, \tag{2.60}$$

$$\sum_l A_{lm}A_{ln}=A_{mn}'-C_{mn}-D_{mn}, \tag{2.61}$$

$$\sum_l A_{ml}A_{ln}=C_{mn}-A_{mn}', \tag{2.62}$$

$$E_{mn}+E_{nm}=0, \tag{2.63}$$

$$2\sum_l E_{lm}E_{ln}=-(L_{mn}+L_{nm}). \tag{2.64}$$

Use has also been made of the relation,

$$\frac{\partial u_n}{\partial z}+\tan\theta\frac{\partial u_n}{\partial \nu}=0 \text{ on } C,$$

which follows from the boundary condition (2.24) on u_n.

For future reference, we may note that from (2.40), (2.44), if θ^2 be neglected,

$$H_{nm}=2B_{nm}, \tag{2.65}$$

so that, from (2.60)–(2.62), to this approximation,

$$Y_{nn}=k^2-\beta_n^2+C_{nn}+2D_{nn}+J_{nn}-\sum_l \frac{1}{\beta_l^2}A_{nl}I_{nl}. \tag{2.66}$$

Equations (2.58) constitute our final result. They are an infinite set of linear equations for the determination of the functions $e_n(z)$, $h_n(z)$. Having found them, the functions $f_n(z), \cdots, q_n(z)$ are given by (2.53). The field is then given by (2.26)–(2.31) and (2.4), (2.5).

3. DISCUSSION OF E- AND H-WAVES IN HORNS OF SMALL FLARE WHEN COUPLING IS NEGLECTED

Our Eqs. (2.58) can evidently be regarded as giving rise to an infinite number of coupled modes of propagation, these modes being analogous to the E- and H-waves in wave guides, the "coupling coefficients" being the $U_{nm}, \cdots, Z_{nm}$ for $n\neq m$. This coupling is zero for a wave guide and will therefore presumably be small for a horn of small flare. This point is investigated in detail in the next section; in this section we shall assume that the coupling can be neglected, so that $U_{nm}, \cdots, Z_{nm}$ are zero for $n\neq m$, and further, that the order of magnitude formulas (4.1)–(4.4) of the next section apply. We shall term this the "normal case."

The Eqs. (2.58) then become

$$e_n''+U_{nn}e_n'+V_{nn}e_n=0, \tag{3.1}$$

$$h_n''+X_{nn}h_n'+Y_{nn}h_n=0, \tag{3.2}$$

which are the equations for E- and H-waves, respectively. The order of magnitude formulas show that the terms in V_{nn}, Y_{nn} after the first are of the order θ^2 compared with the terms α_n^2, β_n^2, respectively (where by θ is now meant the average value of the flare angle over the boundary C of the cross section), so that we can write

$$V_{nn}=k^2-\alpha_n^2, \quad Y_{nn}=k^2-\beta_n^2, \tag{3.3}$$

with an error of the order of θ^2, except for values of z for which $k^2-\alpha_n^2$ or $k^2-\beta_n^2$ is small. But such values of z only occur over a limited range for which V_{nn} or Y_{nn} is in any case small. Thus we can use (3.3) for all values of z.

Further, using (2.60), (2.63), (2.65) we have, with an error of the order of θ^2,

$$U_{nn}=\frac{1}{\alpha_n^2}\int_C \theta\left(\frac{\partial u_n}{\partial \nu}\right)^2 ds,$$

$$X_{nn}=B_{nn}+\frac{1}{\beta_n^2}I_{nn}, \tag{3.4}$$

where

$$B_{nn}=\int_C \theta v_n^2 ds,$$

$$I_{nn}=\int_C\left(\theta v_n\frac{\partial^2 v_n}{\partial s^2}+pv_n\frac{\partial v_n}{\partial s}\right)ds. \tag{3.5}$$

Thus Eqs. (3.1)–(3.5) are the basic equations for the normal case (with neglect of θ^2).

Equations (3.1), (3.2) can be solved accurately for simple shapes of horn, as discussed in Sec. 6. For a general discussion, we can, however, use the so-called W.K.B. method.[7] Taking Eq. (3.1) for E-waves, if we reduce it to its normal form and then use the W.K.B. solution, we find as approximate solutions of this equation,

$$e_n=(k^2-\alpha_n^2)^{-\frac{1}{4}}\exp\left[-\tfrac{1}{2}\int U_{nn}dz \pm i\int(k^2-\alpha_n^2)^{\frac{1}{2}}dz\right], \quad k>\alpha_n, \tag{3.6}$$

$$=(\alpha_n^2-k^2)^{-\frac{1}{4}}\exp\left[-\tfrac{1}{2}\int U_{nn}dz \pm\int(\alpha_n^2-k^2)^{\frac{1}{2}}dz\right], \quad k<\alpha_n. \tag{3.7}$$

In deriving these solutions we have neglected U_{nn}', U_{nn}^2 in comparison with α_n^2 which, according to the order of magnitude formulas, only introduces an error of the order θ^2 in the normal case. Substitution of (3.6) or (3.7) in (3.1) shows that the differential equation is satisfied if terms of order θ^2 are neglected, except if $k\sim\alpha_n$, when the W.K.B. solution fails.

The solutions (3.6) represent waves propagated in the positive or negative z-direction (positive direction with the positive sign, negative direction with the negative sign), with a (positive or negative) attenuation given by the first two factors. The solutions (3.7), on the other hand, do not represent wave propagation at all, but standing waves with a much larger attenuation on account of the second factor in the exponential. Thus we may speak of those portions of the horn for which $\alpha_n<k$ as "transmission regions" and those portions for which $\alpha_n>k$ as "attenuation regions," this division being similar to that found by Barrow and Chu[1] for the sectoral horn. The division between the two regions is not, of course, sharp, since (3.6), (3.7) are only approximate solutions, but may conveniently be taken to be given by $\alpha_n=k$, i.e., for values of z for which the frequency is just the cut-off frequency for a wave guide

[7] See, for instance, L. I. Schiff, *Quantum Mechanics* (McGraw-Hill, Book Company, Inc., New York, 1949), pp. 178 et seq.

whose section is the same as the section of the horn for this particular value of z. This division may be termed "cutoff," so that we may speak of a "cut-off frequency" (which depends on z) for each section of the horn (Barrow and Chu[1] define cutoff somewhat differently for the sectoral horn, but this seems to be the simplest and most natural definition).

The solutions (3.6) for the transmission region must pass over into certain linear combinations of the solutions (3.7) for the attenuation region. If we choose the z-axis so that the transmission region occurs for $z>z_0$ and the attenuation region for $z<z_0$ (so that the horn flares outwards as z increases), then the solution (3.7) with the negative sign before the square root is the dominant one in the attenuation region. From the connection formulas for the W.K.B. solution,[7] we can then assert that the solution which gives an outgoing wave in the transmission region passes over into the attenuated solution in the attenuation region according to the formula,

$$(k^2-\alpha_n^2)^{-\frac{1}{4}}\exp\left(-\tfrac{1}{2}\int_{z_0}^{z}U_{nn}dz\right)$$

$$\times\exp i\int_{z_0}^{z}(k^2-\alpha_n^2)^{\frac{1}{2}}dz\rightarrow e^{-i\pi/4}(\alpha_n^2-k^2)^{-\frac{1}{4}}$$

$$\times\exp\left[-\tfrac{1}{2}\int^{z}U_{nn}dz-\int_{z_0}^{z}(\alpha_n^2-k^2)^{\frac{1}{2}}dz\right]. \quad (3.8)$$

We may also remark that a modification of the W.K.B. method, due to Langer,[7] may be given which yields an approximate solution which is valid even in the neighborhood of cutoff. Exactly similar considerations apply to Eq. (3.2) for H-waves.

The propagation properties of the horn can be conveniently expressed in terms of a phase velocity of propagation (ω/β) and an attenuation constant (α), where (see Barrow and Chu[1])

$$\alpha-i\beta=-\frac{d}{dz}\log(E_z \text{ or } H_z)$$

for E- and H-waves, respectively.

Since

$$E_z\cong e_n u_n, \quad H_z\cong h_n v_n, \quad (3.9)$$

and u_n, v_n depend on z as well as x, y, this would give a phase velocity and attenuation constant which vary over the cross section, i.e., the behavior of the field components as we go along the horn depends on the particular point on the cross section selected. This effect can be eliminated by taking an appropriate average of the field over the cross section; the main effect of the u_n, v_n factors in (3.9) is that due to the normalization factor for these functions, which according to (2.25), (2.25a) is proportional to $A^{-\frac{1}{2}}$ (where A now denotes the area of the cross section). We may therefore say that the variation of the longitudinal field components along the horn is, effectively, given by

$$E_z\propto A^{-\frac{1}{2}}e_n, \quad H_z\propto A^{-\frac{1}{2}}h_n,$$

for E- and H-waves, respectively, so that the phase velocity and attenuation constant are determined by

$$\alpha-i\beta=-\frac{d}{dz}\log[A^{-\frac{1}{2}}(e_n \text{ or } h_n)].$$

Equations (3.6), (3.7) then give as approximate expressions for α, β for E-waves in the transmission region

$$\alpha=-\frac{1}{2}\frac{A'}{A}-\frac{1}{2}\frac{\alpha_n\alpha_n'}{k^2-\alpha_n^2}+\tfrac{1}{2}U_{nn},$$
$$\beta=(k^2-\alpha_n^2)^{\frac{1}{2}}, \quad (3.10)$$

while in the attenuation region,

$$\alpha=(\alpha_n^2-k^2)^{\frac{1}{2}}+\frac{1}{2}\frac{A'}{A}+\frac{1}{2}\frac{\alpha_n\alpha_n'}{\alpha_n^2-k^2}+\tfrac{1}{2}U_{nn},$$
$$\beta=0, \quad (3.11)$$

the first term in the first of (3.11) being the major one (a more accurate solution would give a small nonzero value for β in (3.11)).

For H-waves (Eq. (3.2)), the results are the same with α_n, U_{nn} replaced by β_n, X_{nn}, respectively.

4. COUPLING OF MODES

In this section, we shall discuss the coupling between the different E- and H-waves. For this purpose we shall solve the whole system of equations (2.58) approximately, using a generalization of the W.K.B. method. We shall first give the orders of magnitude that can be expected for the various coefficients occurring in (2.58), (2.59). From dimensional considerations, and use of (2.41) with $\chi=1$, it is easily seen that we have the following orders of magnitude (in which A denotes the area of the cross section and θ the average value of the flare angle over the boundary):

$$\left.\begin{aligned}
&u_n,\ v_n,\ \alpha_n,\ \beta_n,\ 1/R\sim A^{-\frac{1}{2}},\\
&\left(\frac{\partial v}{\partial s}\right)_c,\ \left(\frac{\partial u}{\partial \nu}\right)_c\sim A^{-1},\\
&\left(\frac{\partial^2 v}{\partial s^2}\right)_c,\ \frac{\partial}{\partial s}\left(\frac{\partial u}{\partial \nu}\right)_c\sim A^{-\frac{3}{2}},\\
&A'\sim\theta A^{\frac{1}{2}},\\
&\frac{\partial u_n}{\partial z},\ \frac{\partial v_n}{\partial z}\sim\theta A^{-1}.
\end{aligned}\right\} \quad (4.1)$$

Also we shall assume that $d\theta_{av}/dz$ and $1/R_1$ are of the order $\theta^2A^{-\frac{1}{2}}$ (or smaller), as would be the case with any

reasonable shape of horn. For simplicity, we shall also assume that ψ is of the same order as θ (or smaller). We then have

$$\left.\begin{aligned} &\frac{\partial^2 u}{\partial z^2}, \ \frac{\partial^2 v}{\partial z^2} \sim \theta^2 A^{-1}, \\ &p \sim \theta A^{-1}, \ q \sim \theta^2 A^{-1}. \end{aligned}\right\} \tag{4.2}$$

From (4.1), (4.2) we now have the following orders of magnitude for the coefficients occurring in (2.59):

$$\left.\begin{aligned} &A_{nm}, \ B_{nm}, \ E_{nm}, \ H_{nm} \sim \theta A^{-1}, \\ &F_{nm}, \ G_{nm}, \ I_{nm}, \ K_{nm} \sim \theta A^{-1}, \\ &C_{nm}, \ D_{nm}, \ J_{nm} \sim \theta^2 A^{-1}. \end{aligned}\right\} \tag{4.3}$$

Hence

$$\left.\begin{aligned} &U_{nm}, \ X_{nm} \sim \theta A^{-1}, \\ &V_{nm}, \ Y_{nm} \sim \theta^2 A^{-1} (n \neq m), \\ &W_{nm}, \ Z_{nm} \sim \theta k A^{-1}. \end{aligned}\right\} \tag{4.4}$$

It should be pointed out, however, that ratios of lengths relating to the cross section may also enter into the coefficients, so that the above formulas can only be regarded as those relating to the general case, to which exceptions can occur. The occurrence of the numbers n, m defining the modes concerned may also affect the orders of magnitude. In our discussion of the coupling of modes, however, we shall assume that the formulas (4.1)–(4.4) apply. These formulas were used in the previous section in discussing the normal case. In applying the W.K.B. method, we shall further assume that we are not in the neighborhood of cutoff, so that $(k^2-\alpha_n^2)$ or $(k^2-\beta_n^2)$ are of order A^{-1} or larger.

We now attempt to find a solution of the equations (2.58) in the form,

$$e_n = \eta_n \exp\left(i\int \chi dz\right), \quad h_n = \zeta_n \exp\left(i\int \chi dz\right), \tag{4.5}$$

where η_n, ζ_n, χ are slowly varying functions. Substituting (5.5) in (2.58), and neglecting η_n'', ζ_n'', we obtain

$$\begin{aligned} \{\sum_m [&-(\chi^2+\tfrac{1}{2}U_{nn}')\delta_{nm}+V_{nm}+i\chi U_{nm}]\eta_m \\ &+\sum_m W_{nm}\zeta_m\} + \{(i\chi'+\tfrac{1}{2}U_{nn}')\eta_n \\ &+\sum_m (2i\chi\delta_{nm}+U_{nm})\eta_m'\} = 0, \end{aligned} \tag{4.6}$$

$$\begin{aligned} \{\sum_m [&-(\chi^2+\tfrac{1}{2}X_{nn}')\delta_{nm}+Y_{nm}+i\chi X_{nm}]\zeta_m \\ &+\sum_m Z_{nm}\eta_m\} + \{(i\chi'+\tfrac{1}{2}X_{nn}')\zeta_n \\ &+\sum_m (2i\chi\delta_{nm}+X_{nm})\zeta_m'\} = 0. \end{aligned} \tag{4.7}$$

The terms in the first curly brackets in (4.6), (4.7), which do not contain the derivatives of slowly varying functions, are the most important ones.[8] We shall refer to the terms in the first and second curly brackets in these equations as the major and minor terms, respectively. We now solve these equations by successive approximations as follows. If coupling is neglected, we obtain, by equating to zero the major and minor terms separately, the particular solution:

$$\left.\begin{aligned} &-(\chi^2+\tfrac{1}{2}U_{nn}')+V_{nn}+i\chi U_{nn}=0, \\ &(i\chi'+\tfrac{1}{2}U_{nn}')\eta_n+(2i\chi+U_{nn})\eta_n'=0, \\ &\eta_m=0 (m\neq n), \quad \zeta_n=0, \end{aligned}\right\} \tag{4.8}$$

or, neglecting θ^2,

$$\left.\begin{aligned} &\chi = iU_{nn}/2 \pm (k^2-\alpha_n^2)^{\frac{1}{2}}, \\ &\eta_n = (k^2-\alpha_n^2)^{-\frac{1}{4}}, \\ &\eta_m = 0 (m\neq n), \quad \zeta_n = 0, \end{aligned}\right\} \tag{4.9}$$

which is just the W.K.B. solution (3.6), (3.7) for E-waves. In the next approximation, we take account of the coupling by using the neglected equations in (4.6), (4.7), retaining only the major terms, to find approximate values of $\eta_m (m\neq n)$ and ζ_n. Substituting in the previously used equation, again treating the major and minor terms separately, we obtain improved values of χ, η_n, and so on. The minor terms can be taken into account in the neglected equations in higher approximations, derivatives of slowly varying functions higher than the first being consistently neglected.

We thus find for the next approximation corresponding to (4.9):

$$\left.\begin{aligned} \eta_m &= \frac{V_{mn}+i\chi_1 U_{mn}}{\chi_1^2+\tfrac{1}{2}U_{mm}'-V_{mm}-i\chi_1 U_{mm}}\eta_n (m\neq n), \\ \zeta_m &= \frac{Z_{mn}}{\chi_1^2+\tfrac{1}{2}X_{mm}'-Y_{mm}-i\chi_1 X_{mm}}\eta_n, \end{aligned}\right\} \tag{4.10}$$

while χ, η_n are now given by

$$\begin{aligned} &-(\chi^2+\tfrac{1}{2}U_{nn}')+V_{nn}+i\chi U_{nn} \\ &\quad+\sum_{m\neq n}\frac{(V_{nm}+i\chi_1 U_{nm})(V_{mn}+i\chi_1 U_{mn})}{\chi_1^2+\tfrac{1}{2}U_{mm}'-V_{mm}-i\chi_1 U_{mm}} \\ &\quad+\sum_m \frac{W_{nm}Z_{mn}}{\chi_1^2+\tfrac{1}{2}X_{mm}'-Y_{mm}-i\chi_1 X_{mm}}=0, \end{aligned} \tag{4.11}$$

$$\begin{aligned} &(i\chi'+\tfrac{1}{2}U_{nn}')\eta_n+(2i\chi+U_{nn})\eta_n' \\ &\qquad+\sum_{m\neq n} U_{nm}\eta_m'=0, \end{aligned} \tag{4.11a}$$

in which χ_1 is the first approximation to χ given by (4.9), and we are to substitute for η_m in the summation in (4.11a) from (4.10). We take for definiteness the positive sign before the square root in (4.9) and suppose $k>\alpha_n$, i.e., we take the solution which represents a wave propagated in the positive z-direction in the transmission region, and retain only the lowest order terms in θ. We further suppose that α_n is not equal (or nearly equal) to any of the other α's or any of the β's (i.e., the

[8] The term in U_{nn}' is included among the major terms for convenience, and so that the first approximation shall agree with the usual W.K.B. solution.

E-wave concerned has not the same cut-off frequency for all z as any of the other modes). We thus obtain from (4.10):

$$\eta_m=\frac{i(k^2-\alpha_n^2)^{\frac{1}{2}}U_{mn}}{\alpha_m^2-\alpha_n^2}\eta_n(m\neq n),$$
$$\zeta_m=\frac{Z_{mn}}{\beta_m^2-\alpha_n^2}\eta_n. \tag{4.12}$$

Further, under the same assumptions, the first summand in (4.11) is (retaining the lowest order terms in both real and imaginary parts)

$$\frac{-U_{nm}U_{mn}(k^2-\alpha_n^2)+i(k^2-\alpha_n^2)^{\frac{1}{2}}(\rho_{nm}+\rho_{mn})}{\alpha_m^2-\alpha_n^2+i(k^2-\alpha_n^2)^{\frac{1}{2}}(U_{nn}-U_{mm})},$$

where

$$\rho_{nm}=U_{nm}(V_{mn}-(1/2)U_{mn}U_{nn}).$$

This is of the form p_1+iq_1, where p_1 is of order θ^2A^{-1} and q_1 of order θ^3A^{-1}. The second summand in (4.11) yields terms of the same orders. Thus the added terms in (4.11) are of the form p_2+iq_2 where p_2 is of order θ^2A^{-1} and q_2 of order θ^3A^{-1}. It is then readily verified that the extra terms yield corrections of the order θ^2 to both the real and imaginary parts of χ for the transmission region. Similarly for the attenuation region, the correction to χ (which is now a pure imaginary) is of the order θ^2. In a similar manner, it can be shown that Eq. (4.11a) gives a correction of order θ^2 to η_n.

Thus, if θ^2 be neglected, the coupling between nodes can be neglected as far as the calculation of χ, η_n, and hence e_n, is concerned, provided that the E-wave characterized by e_n has not the same cut-off frequency (for all z) as any of the other modes. The coupling cannot be neglected, however, for modes having the same cut-off frequency. Although we have only shown this result on the assumption that we are not near cutoff and that we have the normal case, it is reasonable to suppose that it applies without these restrictions.

On the other hand, η_m/η_n and ζ_m/ζ_n as given by (4.12) are of the *first* order in θ. The main effect of this, as discussed in the next section, is on the way in which the field varies over the cross section.

In an exactly similar way, the case of an H-wave is dealt with. Neglecting θ^2, we have, in place of (4.12), for the H-wave determined by ζ_n, and under similar assumptions,

$$\zeta_m=\frac{i(k^2-\beta_n^2)X_{mn}}{\beta_m^2-\beta_n^2}\zeta_n(m\neq n),$$
$$\eta_m=\frac{W_{mn}}{\alpha_m^2-\beta_n^2}\zeta_n, \tag{4.13}$$

it being supposed that the H-wave concerned has not the same cut-off frequency as any of the other modes.

5. THE FIELD COMPONENTS CORRECT TO THE FIRST ORDER IN THE FLARE ANGLE. CALCULATION OF THE FIELD OUTSIDE THE HORN

From (2.26)–(2.31), (2.53), (4.12), (4.13) we now have, correct to the first order in θ, for the six functions defining the electromagnetic field the following expressions:

For an E-wave:

$$E_z=e_n\left[u_n+i(k^2-\alpha_n^2)^{\frac{1}{2}}\sum_{m\neq n}\frac{U_{mn}}{\alpha_m^2-\alpha_n^2}u_m\right],$$
$$H_z=e_n\sum_m\frac{Z_{mn}}{\beta_m^2-\alpha_n^2}v_m,$$
$$F=\frac{e_n'}{\alpha_n^2}u_n+i(k^2-\alpha_n^2)^{\frac{1}{2}}e_n'\sum_{m\neq n}\frac{U_{mn}}{\alpha_m^2(\alpha_m^2-\alpha_n^2)}u_m,$$
$$G=ike_n\sum_m\frac{Z_{mn}}{\beta_m^2(\beta_m^2-\alpha_n^2)}v_m, \tag{5.1}$$
$$P=ike_n'\sum_m\frac{Z_{mn}}{\beta_m^2(\beta_m^2-\alpha_n^2)}v_m,$$
$$Q=ike_n\left[(1/\alpha_n^2)u_n+i(k^2-\alpha_n^2)^{\frac{1}{2}}\times\sum_{m\neq n}\frac{U_{mn}}{\alpha_m^2(\alpha_m^2-\alpha_n^2)}u_m\right],$$

where e_n is found (by neglecting coupling) from (3.1), the solution which represents a wave propagated in the positive z-direction in the propagation region being taken.

For an H-wave:

$$H_z=h_n\left[v_n+i(k^2-\beta_n^2)^{\frac{1}{2}}\sum_{m\neq n}\frac{X_{mn}}{\beta_m^2-\beta_n^2}v_m\right],$$
$$E_z=h_n\sum_m\frac{W_{mn}}{\alpha_m^2-\beta_n^2}u_m,$$
$$P=(1/\beta_n^2)(h_n'-A_{nn}h_n)v_n+i(k^2-\beta_n^2)^{\frac{1}{2}}h_n'\times\sum_{m\neq n}\frac{X_{mn}}{\beta_m^2(\beta_m^2-\beta_n^2)}v_m,$$
$$Q=-ikh_n\sum_m\frac{W_{mn}}{\alpha_m^2(\alpha_m^2-\beta_n^2)}u_m, \tag{5.2}$$
$$F=ikh_n'\sum_m\frac{W_{mn}}{\alpha_m^2(\alpha_m^2-\beta_n^2)}u_m,$$
$$G=ikh_n\left[(1/\beta_n^2)v_n+i(k^2-\beta_n^2)^{\frac{1}{2}}\times\sum_{m\neq n}\frac{X_{mn}}{\beta_m^2(\beta_m^2-\beta_n^2)}v_m\right],$$

where h_n is found from (3.2). We may suppose that (5.1), (5.2) hold even in the neighborhood of cutoff, since they contain no factors of the form $k^2-\alpha_n^2$ or $k^2-\beta_n^2$ in the denominators.

It will be seen that, even if only the first power of θ be retained, the complete expressions for the field are quite complicated. In particular, there is a small component of **H** along the horn in an "*E*-wave," and a small component of **E** in an "*H*-wave." The small additional terms, represented by the infinite series in (5.1), (5.2) alter the way in which the field varies along the horn. But this variation depends also on the particular point on the cross section selected, and could be eliminated by taking an appropriate mean value of the field over the cross section.[9] The main dependence of the longitudinal field components on the variable z is still given by $A^{-\frac{1}{2}}e_n$ or $A^{-\frac{1}{2}}h_n$, as assumed in Sec. 3.

In calculating the field *outside* the horn, it is usual to assume that the field over the mouth of the horn is the same as if the horn were of infinite length and to use Kirchoff's method or one of its refinements.[1,10] If the flare of the horn be neglected altogether, this will, of course, give a radiation pattern which depends only on the shape of the *mouth* of the horn. But if the flare be taken into account, the pattern will depend on the shape of the horn as a whole. In this case, it is necessary to retain the complete expressions (5.1), (5.2). The calculation of the radiation pattern then becomes somewhat laborious, but it would seem that the infinite series involved are fairly rapidly convergent, and, moreover, there is some advantage in having the field given over a plane surface, rather than over a curved surface as in Barrow and Chu's[1] calculations for the sectoral horn. We may note, too, that in the case of the sectoral horn Barrow and Lewis[11] reported that surprisingly good results for the radiation pattern could be obtained by neglecting the flare, even for flare angles up to 20° or 25°.

6. SOME PARTICULAR HORNS

We shall first prove some general results relating to horns whose section is always either rectangular or circular (the centers of the sections lying on a straight line parallel to the z-axis), and shall then consider the following particular horns: sectoral, pyramidal, rectangular exponential, conical, circular exponential. Of these, the problems of the sectoral and conical horns can be solved rigorously, but it is of interest to include them in order to compare the rigorous and approximate solutions. We shall neglect θ^2 throughout this section, so that we can use (3.3)–(3.5), or, if we have not the normal case, (2.66), in place of the second of (3.3).

Horns of Rectangular Section

The E_{nm}- and H_{nm}-waves[12] ($n\neq 0$, $m\neq 0$) are coupled to each other, since they have the same cut-off frequency. On the other hand, the H_{n0}- and H_{0n}-waves are not coupled to other waves, in general. Let us discuss the H_{n0}-wave in detail (the discussion of the H_{0n}-wave is, of course, entirely similar).

Let a, b be the sides of the rectangular section, θ_1 the value of θ along the two "a" sides, and θ_2 the value of θ along the two "b" sides. a, b, θ_1, θ_2, are, of course, functions of z, and

$$2\theta_1=a', \quad 2\theta_2=b'.$$

Taking the origin at a corner,[13] with the x, y axes along the "a"- and "b"-sides, respectively, we have for the H_{n0}-wave (on dropping the subscripts on v, β):

$$v=(2/ab)^{\frac{1}{2}}\cos n\pi x/a, \quad \beta=n\pi/a.$$

It is readily seen that we have the normal case *unless* $\theta_2=0$, *i.e.*, $a=const$ (we assume that θ_1, θ_2 are of the same order unless one of them vanishes). Excluding this case, we find from (3.3)–(3.5) (again dropping the subscripts), and noting that $p=0$:

$$\begin{aligned} &B=2\theta_1/b+4\theta_2/a, \quad && I=-(2\theta_1/b)(n\pi/a)^2, \\ &X=2a'/a, && V=k^2-(n\pi/a)^2. \end{aligned} \tag{6.1}$$

Hence the equation for the propagation of the H_{n0}-wave is

$$h''+(2a'/a)h'+(k^2-n^2\pi^2/a^2)h=0, \quad (a'\neq 0). \tag{6.2}$$

We can draw two conclusions of some interest from (6.2). In the first place, the equation does not involve b, so that (to our approximation) it does not matter how the other side of the rectangle varies as far as the calculation of the coefficient h for this particular wave is concerned. This other side will only affect the variation of the field down the guide through the normalization factor $A^{-\frac{1}{2}}$. In the second place, if we use the W.K.B. approximation corresponding to (3.6) for H-waves in the transmission region of the horn, we see that the attenuation of the H_{n0}-wave in a given length of horn depends only on the dimensions of the cross sections at either end, and not on the shape of the horn in between. On the other hand, the phase difference in the transmission region, and the attenuation in the attenuation region, *do* depend on the shape of the horn in between.

[9] Namely, by replacing E_z by

$$\bar{E}_z=A^{-\frac{1}{2}}\int_A E_z u_n dS$$

in the case of E-waves, with a similar average for H_z in the case of H-waves. The transverse field components vary with z in a slightly different way.

[10] W. L. Barrow and F. M. Greene, Proc. Inst. Radio Engrs. **26**, 1498 (1938). L. J. Chu, J. Appl. Phys. **11**, 603 (1940).

[11] W. L. Barrow and F. D. Lewis, Proc. Inst. Radio Engrs. **27**, 41 (1939). Note that the flare angle as defined by us is one-half the flare angle use by these authors.

[12] There should, of course, be no confusion between the symbols E_{nm}, H_{nm} used for particular types of waves and the same symbols which occur in (2.59) giving the coefficients occurring in the fundamental equations.

[13] It is evidently permissible, for the purpose of calculating the coefficients occurring in the equations, to shift the axes in any way, provided the z-axis remains parallel to its original direction and the correct dependence of the parameters on z is preserved.

Horns of Circular Section

In this case, there is no coupling between any of the waves, and we always have the normal case. Let a be the radius of the cross section, θ being constant round the circumference, so that $\theta=a'$. Let (r, ϕ) be polar coordinates in a cross section, with origin at the center of the circle. Then for the E_{nm}-wave[14]

$$u=(2/\pi\delta_n)^{\frac{1}{2}}[aJ_{n+1}(j_{nm})]^{-1}J_n(j_{nm}r/a)\begin{matrix}\cos\\ \sin\end{matrix}n\phi,$$

$$\alpha=j_{nm}/a,$$

where j_{nm} is the mth zero of $J_n(x)$, and $\delta_n=1$ or 2 according as $n\neq 0$ or $n=0$. Then from (3.4) (dropping the subscripts) we find

$$U=2\theta/a=2a'/a.$$

Hence the equation for the propagation of the E_{nm}-wave is

$$e''+(2a'/a)e'+(k^2-j_{nm}^2/a^2)e=0. \tag{6.3}$$

For the H_{nm}-wave,[14]

$$v=(2/\pi\delta_n)^{\frac{1}{2}}[aJ_n(j_{nm}')]^{-1}(1-n^2/j_{nm}'^2)^{-\frac{1}{2}}\cdot J_n(j_{nm}'r/a)\begin{matrix}\cos\\ \sin\end{matrix}n\phi,$$

$$\beta=j_{nm}'/a,$$

where j_{nm}' is the mth zero of $J_n'(x)$.

From (3.4), (3.5) we find

$$B=(2\theta/a)(1-n^2/j_{nm}'^2)^{-1},$$
$$I=-(2\theta n^2/a)(1-n^2/j_{nm}'^2)^{-1},$$
$$X=2\theta/a=2a'/a.$$

Hence the equation for the H_{nm}-wave is

$$h''+(2a'/a)h'+(k^2-j_{nm}'^2/a^2)h=0. \tag{6.4}$$

We may draw the same conclusion regarding the attenuation in a given length of horn in the transmission region as in the case of Eq. (6.2) for both the E_{nm}- and H_{nm}-waves.

Sectoral Horn

This is a particular case of horns of rectangular section. Let 2θ be the angle between the flaring sides, and take the origin on the line of intersection of these sides. Also, let a, b be the varying and constant sides of the rectangle, so that

$$a=2\theta z, \quad b=\text{const.}$$

For the H_{n0}-wave, we have the normal case and can use (6.2), which becomes

$$h''+(2/z)h'+(k^2-n^2\pi^2/4\theta^2z^2)h=0.$$

The solution of this equation which represents outgoing waves for large z is

$$h=z^{-\frac{1}{2}}H_{n\pi/2\theta}^{(1)}(kz).$$

Since the area of the cross section is proportional to z, this gives for the variation of the field down the horn

$$H_z\propto z^{-1}H_{n\pi/2\theta}^{(1)}(kz). \tag{6.5}$$

This agrees with the result of Barrow and Chu,[1] if z be interpreted as *radial* distance from the line of intersection of the flaring sides, rather than distance along the horn, so that the approximate theory agrees with the rigorous one to the first order in θ in this case.

Consider now the case of the H_{0n}-wave. In accordance with the discussion already given, we now have an exceptional case, and we must use (2.66) instead of the second of (3.3). We now have

$$v=(2/ab)^{\frac{1}{2}}\cos(n\pi y/b), \quad \beta=n\pi/b.$$

Calculation gives (dropping the subscripts):

$$A=-B/2=-1/2z, \quad I=-n^2\pi^2/a^2z, \quad X=0,$$
$$C=3/4z^2, \quad D=-1/2z^2, \quad J=0.$$

Moreover, it is easily shown that in the summation on the right-hand side of (2.66), we need only retain the term with $l=n$, since the remaining terms are of order θ^2 compared with β_n^2. Hence

$$Y=k^2-\beta^2+C+2D-AI/\beta^2$$
$$=k^2-(n\pi/b)^2-3/4z^2.$$

The equation for the H_{0n}-wave thus becomes

$$h''+(k^2-n^2\pi^2/b^2-3/4z^2)h=0.$$

The solution representing an outgoing wave for large z is

$$h=z^{\frac{1}{2}}H_1^{(1)}[(k^2-n^2\pi^2/b^2)^{\frac{1}{2}}z].$$

Hence

$$H_z\propto H_1^{(1)}[(k^2-n^2\pi^2/b^2)^{\frac{1}{2}}z]. \tag{6.6}$$

This again agrees with the result of Barrow and Chu,[1] if a be interpreted as in (6.5).

In the case of E_{nm}- and H_{nm}-waves we have, in accordance with our previous discussion, a coupling between these two waves. We now have

$$u=(4/ab)^{\frac{1}{2}}\sin(n\pi x/a)\sin(m\pi y/b),$$
$$v=(4/ab)^{\frac{1}{2}}\cos(n\pi x/a)\cos(m\pi y/b),$$
$$\alpha=\beta=(n^2\pi^2/a^2+m^2\pi^2/b^2)^{\frac{1}{2}}.$$

We find from (3.3), (3.4)

$$U=X=m^2a^2/(m^2a^2+4n^2\theta^2z^2)(2/z).$$

Further, from (2.59), (2.51), (2.57), to the first order in θ,

$$W=-Z=4iknma\theta/(m^2a^2+4n^2\theta^2z^2).$$

Hence the equations for the propagation of this mode

[14] The modes of propagation with $\cos n\phi$ and $\sin n\phi$ for the angular factor in u or v have the same cut-off frequency, but it is readily verified that there is, nevertheless, no coupling between these two modes.

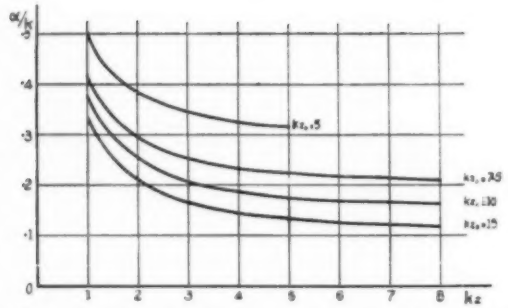

FIG. 2. Attenuation constant α (in units $k=2\pi/\lambda$) as a function of kz in the transmission region for the H_{10}-wave in rectangular exponential horns of the type (6.9) with $ka_0=\pi$, and for various values of kz_0. The cutoff for all such horns is at $z=0$.

are

$$e''+U(z)e'+(k^2-\alpha^2)e+W(z)h=0,$$
$$h''+U(z)h'+(k^2-\alpha^2)h-W(z)e=0,$$

where U, α, W are as above.

To solve these equations, we note that we can replace $k^2-\alpha^2$ by

$$k^2-\alpha^2+[m^2a^2/(m^2a^2+4n^2\theta^2z^2)-\tfrac{3}{4}]/z^2$$

with an error of the order of θ^2. Doing this, it can be shown that there are two independent solutions which represent outgoing waves for large z, namely,

$$\begin{aligned}
&e=z^{-\frac{1}{2}}H_{m\pi/2\theta}^{(1)}[(k^2-n^2\pi^2/a^2)^{\frac{1}{2}}z],\\
&h=-(2in\theta/mka)(k^2-n^2\pi^2/a^2)^{\frac{1}{2}}z^{\frac{1}{2}}\\
&\qquad\times H_{m\pi/2\theta}^{(1)\prime}[(k^2-n^2\pi^2/a^2)^{\frac{1}{2}}z],\\
&\text{and}\qquad\qquad (6.7)\\
&e=(2in\theta/mka)(k^2-n^2\pi^2/a^2)^{\frac{1}{2}}z^{\frac{1}{2}}\\
&\qquad\times H_{m\pi/2\theta}^{(1)\prime}[(k^2-n^2\pi^2/a^2)^{\frac{1}{2}}z],\\
&h=z^{-\frac{1}{2}}H_{m\pi/2\theta}^{(1)}[(k^2-n^2\pi^2/a^2)^{\frac{1}{2}}z].
\end{aligned}$$

For the variation of the field components E_z, H_z along the horn, we must multiply the right-hand sides of the above formulas by $z^{-\frac{1}{2}}$.

In their paper on the sectoral horn, Barrow and Chu[1] only considered the H_{n0}- and H_{0n}-waves. But their analysis is easily extended to cover the general case, and it is found that the longitudinal components of the field then vary precisely in accordance with (6.7), if the same modification in the interpretation of z be made as in (6.5), (6.6). In the first solution of (6.7), the longitudinal component of the electric field is the dominant one for small z, while the longitudinal component of the magnetic field is dominant for large z. In the second solution, the roles of the electric and magnetic fields are interchanged. In neither solution does a transmission region exist unless $ka>n\pi$.

Pyramidal Horn

Taking the origin at the vertex of the pyramid, we have

$$a=2\theta_1 z, \quad b=2\theta_2 z,$$

where $2\theta_1$, $2\theta_2$ are the angles between opposite sides of the pyramid. We shall consider only the H_{n0}- and H_{0n}-waves, for which we have no coupling with other modes. For the H_{n0}-wave, the equation of propagation will, in accordance with our previous discussion, be exactly the same as for the sectoral horn, with θ_1 in place of θ. The only difference is that the cross-sectional area now increases as z^2 instead of z. Hence, from (6.5),

$$H_z\propto z^{-\frac{1}{2}}H_{n\pi/2\theta_1}^{(1)}(kz). \qquad (6.8)$$

For the H_{0n}-wave, similarly,

$$H_z\propto z^{-\frac{1}{2}}H_{n\pi/2\theta_2}^{(1)}(kz).$$

The attenuation constant and phase velocity vary along the horn in a manner similar to that for the sectoral horn, the only essential difference being the factor $z^{-\frac{1}{2}}$ instead of z^{-1}.

Rectangular Exponential Horn

We shall understand by "rectangular exponential horn" a horn in which the cross section remains rectangular, either or both sides of the rectangle increasing exponentially with z. Hence either

$$a=a_0e^{z/z_0}, \quad b=\text{const}, \qquad (6.9)$$

or

$$a=a_0e^{z/z_0}, \quad b=b_0e^{z/z_0} \qquad (6.10)$$

(we assume, for simplicity, that if both sides increase exponentially, their ratio remains constant).

We shall consider only the H_{n0}-wave for both (6.9) and (6.10), for which we have the normal case. For either (6.9) or (6.10) we can then use (6.2) and obtain

$$h''+(2/z_0)h'+(k^2-n^2\pi^2/a_0^2\cdot e^{-2z/z_0})h=0.$$

The outgoing-wave solution is

$$h=e^{-z/z_0}J_{-i(k^2z_0^2-1)^{\frac{1}{2}}}(in\pi z_0/a_0\cdot e^{-z/z_0}). \qquad (6.11)$$

For the variation of H_z along the horn, we must multiply the right-hand side of (6.11) by $e^{z/2z_0}$ in the case of (6.9) and by e^{z/z_0} in the case of (6.10).

As an example, we give, in Figs. 2, 3 graphs of the attenuation constant and phase velocity for the H_{10}-

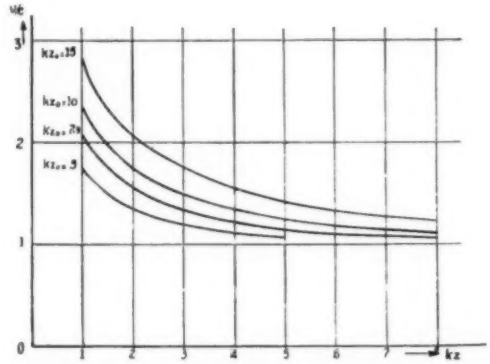

FIG. 3. Phase velocity of propagation v (in units c) as a function of kz in the transmission region for the H_{10}-wave in the same rectangular exponential horns as are considered in Fig. 1.

wave in the transmission region for various rectangular exponential horns of the type (6.9). Owing to the fact that tables of bessel functions of imaginary order were not available to the author, the W.K.B. approximation, in which α, β are given by formulas analogous to (3.10), was used. The origin for z has been chosen so that $z=0$ is the cutoff for the H_{10}-wave. This means taking $ka_0=\pi$. Figure 4 shows the shapes of the horns considered, the scales being adjusted so that the flare angle is correctly given in the graphs.[15]

Conical Horn

Taking the origin at the vertex of the cone, with the z-axis as axis of the cone, we have for the radius of the cross section

$$a=\theta z,$$

where θ is the semivertical angle of the cone. We can apply (6.3), (6.4) directly, and obtain

$$e''+(2/z)e'+(k^2-j_{nm}^2/\theta^2z^2)e=0, \qquad (6.12)$$

$$h''+(2/z)h'+(k^2-j_{nm}'^2/\theta^2z^2)h=0, \qquad (6.13)$$

for the E_{nm}- and H_{nm}-waves, respectively. The outgoing-wave solution of (6.12) is

$$e=z^{-\frac{1}{2}}Hj_{nm/\theta}^{(1)}(kz),$$

so that

$$E_z\propto z^{-\frac{1}{2}}Hj_{nm/\theta}^{(1)}(kz).$$

This agrees with the rigorous theory for E-waves,[2] provided that z be interpreted as radial distance from the vertex of the cone, and the order of the hankel function be replaced by $\lambda+\frac{1}{2}$, where λ is the mth root of the equation

$$P_\lambda^n(\cos\theta)=0.$$

Since this gives $\lambda=j_{nm}/\theta-\frac{1}{2}$ with an error of the order of θ^2,[16] we see that the rigorous and approximate theories agree to the first order in θ.

Similarly, (6.13) gives for the H_{nm}-wave

$$H_z\propto z^{-\frac{1}{2}}Hj'_{nm/\theta}{}^{(1)}(kz),$$

which again agrees with the rigorous theory[2] to the first order in θ. It is evident that the attenuation constant and phase velocity vary along the horn in a manner similar to that for the pyramidal horn.

Circular Exponential Horn

We consider finally a horn in which the cross section remains circular and increases exponentially with z, so that the radius a is given by

$$a=a_0e^{z/z_0}.$$

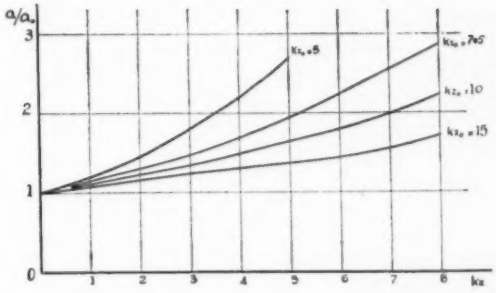

FIG. 4. The actual shapes of the horns considered in Figs. 1, 2. The ratio of the distance between the two flaring sides of the horn (a) to its value at cutoff (a_0) is shown as a function of kz, the scales being adjusted so that the flare angle is correctly shown.

For the E_{nm}-wave, (6.3) gives

$$e''+(2/z_0)e'+(k^2-j_{nm}^2/a_0^2\cdot e^{-2z/z_0})e=0.$$

The outgoing-wave solution is

$$e=e^{-z/z_0}J_{-i(k^2z_0^2-1)^{\frac{1}{2}}}(ij_{nm}z_0/a_0\cdot e^{-z/z_0}),$$

giving

$$E_z\propto e^{-2z/z_0}J_{-i(k^2z_0^2-1)^{\frac{1}{2}}}(ij_{nm}z_0/a_0\cdot e^{-z/z_0}).$$

Similarly, (6.4) gives for the H_{nm}-wave

$$H_z\propto e^{-2z/z_0}J_{-i(k^2z_0^2-1)^{\frac{1}{2}}}(ij'_{nm}z_0/a_0\cdot e^{-z/z_0}).$$

Attenuation constant and phase velocity behave in a way similar to that for the rectangular exponential horn of type (6.10).

APPENDIX I

We wish to prove the boundary condition (2.21). Taking an origin 0 on the horn, let us take axes (ξ, η, ζ) with 0ξ along the tangent s to the cross section C, 0ζ along the normal ν to C, and 0η parallel to the z-axis, the directions s, ν being as defined in Sec. 2 (see Fig. 1(b)). Also let us take another set of right-handed axes (ξ, η', ζ') with the same ξ-axis, but with $0\zeta'$ in the direction of the normal to the horn as defined in Sec. 2. Then the angle between 0ζ and $0\zeta'$ is the flare angle θ as defined in Sec. 2, θ being positive if a right-handed rotation from 0ζ to $0\zeta'$ carries us in the direction 0ξ.

Let the equation to the horn in the neighborhood of 0 be

$$\zeta'=(a/2)\xi^2+(c/2)\eta'^2+b\xi\eta' \qquad (I, 1)$$

correct to the second order in ξ, η', where a, b, c have the following geometrical meanings:

$$a=-\cos\theta/R, \quad c=1/R_1, \qquad b=-(1/2)(1/R_1+\cos\theta/R)\tan 2\psi, \qquad (I, 2)$$

R, R_1, ψ being as defined in Sec. 2 and referring to the origin 0.

Now

$$\zeta'=\zeta\cos\theta-\eta\sin\theta, \quad \eta'=\zeta\sin\theta+\eta\cos\theta.$$

Substituting in (I, 1) we have for the equation of the horn, correct to the second order in ξ, η,

$$\zeta=\eta\tan\theta+(a/2)\sec\theta\xi^2+(c/2)\sec^3\theta\eta^2+b\sec^2\theta\xi\eta.$$

[15] I am indebted to Mr. A. Moughalian for his kind assistance in drawing the curves.

[16] E. W. Hobson, *Theory of Spherical and Ellipsoidal Harmonics* (Cambridge University Press, Cambridge, 1931), p. 407.

For the direction cosines of the normal to the horn in the neighborhood of 0, we find, correct to the first order in ξ, η,

$$\begin{aligned} l &= -a\xi - b\sec\theta\eta, \\ m &= -\sin\theta - b\cos\theta\xi - c\eta, \\ n &= \cos\theta - b\sin\theta\xi - c\tan\theta\eta. \end{aligned} \tag{I, 3}$$

Now from the boundary conditions (2.2) it follows that the component of $\mathbf{H}$ normal to the horn is everywhere zero. Hence

$$lH_\xi + mH_\eta + nH_\zeta = 0. \tag{I, 4}$$

Further, to the first order in ξ, η, we have

$$H_\xi(\xi, \eta, \zeta) = (H_\xi)_0 + \xi\left(\frac{\partial H_\xi}{\partial \xi}\right)_0 + \eta\left(\frac{\partial H_\xi}{\partial \eta}\right)_0 + \zeta\left(\frac{\partial H_\xi}{\partial \zeta}\right)_0, \tag{I, 5}$$

with similar equations for $H_\eta(\xi, \eta, \zeta)$, $H_\zeta(\xi, \eta, \zeta)$. Substituting (I, 3), (I, 5) in (I, 4), and retaining only terms of the first order in ξ, η, we obtain a linear equation in ξ, η which must be satisfied identically. Equating to zero the coefficient of η in this equation, we obtain the following relation which must be satisfied at 0:

$$\frac{\partial H_\eta}{\partial \zeta}\cos 2\theta = bH_\xi + c\sec\theta H_\eta + \sin\theta\cos\theta\left(\frac{\partial H_\xi}{\partial \xi} + 2\frac{\partial H_\eta}{\partial \eta}\right). \tag{I, 6}$$

In deriving (I, 6), we have made use of the relations (at 0)

$$\frac{\partial H_\zeta}{\partial \eta} = \frac{\partial H_\eta}{\partial \zeta}, \quad H_\zeta = \tan\theta H_\eta,$$

$$\frac{\partial H_\xi}{\partial \xi} + \frac{\partial H_\eta}{\partial \eta} + \frac{\partial H_\zeta}{\partial \zeta} = 0,$$

the first two of which follow from the boundary conditions (2.2), and the last of which is the maxwell equation $\mathrm{div}\mathbf{H} = 0$.

Now bearing in mind the relation of our axes (ξ, η, ζ) to the directions ν, s, z as defined in Sec. 2, we have

$$\begin{aligned} &H_\xi = H_s, \quad H_\eta = H_z, \quad \frac{\partial H_\eta}{\partial \zeta} = \frac{\partial H_z}{\partial \nu}, \\ &\frac{\partial H_\eta}{\partial \eta} = \frac{\partial H_z}{\partial z}, \quad \frac{\partial H_\xi}{\partial \xi} = \frac{\partial H_s}{\partial s} + \frac{H_\nu}{R} = \frac{\partial H_s}{\partial s} + \frac{\tan\theta}{R}H_z, \end{aligned} \tag{I, 7}$$

where $\partial H_s/\partial s$ denotes $\partial H_s(s, z)/\partial s$. Substituting (I, 7) in (I, 6), and using (I, 2), we have Eq. (2.21) of the text.

The definition (2.22) for p becomes meaningless if $\psi = \pm\pi/4$. We see from (I, 1), however, that instead of defining b by (I, 2) we can use

$$b = (\partial^2\zeta'/\partial\xi\partial\eta')_0,$$

so that

$$p = \sec 2\theta(\partial^2\zeta'/\partial\xi\partial\eta')_0.$$

This can replace (2.22) if $\psi = \pm\pi/4$. If $\theta = \pm\pi/4$, on the other hand, the method fails, each side of (I, 6) being then equal to zero, and would have to be modified. As our main interest is in the case where θ is small, however, it does not seem worthwhile to attempt such a modification.

APPENDIX II

We wish to prove the relations (2.60)–(2.64). To prove (2.60), we differentiate the relation (2.25a) with respect to z, using (2.41). The required relation follows at once. To prove (2.61), we differentiate (2.45) with respect to z, obtaining

$$A_{mn}' = C_{mn} + D_{mn} + \int_A \frac{\partial v_m}{\partial z}\frac{\partial v_n}{\partial z}dS. \tag{II, 1}$$

But from the definition (2.45) of A_{mn} it follows that

$$\frac{\partial v_n}{\partial z} = \sum_l A_{ln}v_l. \tag{II, 2}$$

Substituting (II, 2) in (II, 1), (2.61) follows.

Again, substituting (II, 2) in the definition (2.48) of D_{mn}, and using (2.60), we have

$$D_{mn} = \sum_l A_{ln}B_{ml} = -\sum_l A_{ln}(A_{ml} + A_{lm}).$$

Combining this relation with (2.61), we have (2.62). The other relations (2.63), (2.64) follow in a similar way, using the eigenfunctions u_n instead of the v_n.

JOURNAL OF APPLIED PHYSICS VOLUME 22, NUMBER 12 DECEMBER, 1951

Exact and Approximate Equations for Wave Propagation in Acoustic Horns

A. F. STEVENSON*
Department of Mathematics, Faculty of Science, Farouk I University, Alexandria, Egypt
(Received June 8, 1951)

Exact equations are given for the propagation of acoustic waves in horns of arbitrary shape. These equations are similar to, though simpler than, the equations previously found for electromagnetic horns, and can be regarded as giving rise to an infinite number of coupled modes of propagation. If the coupling is neglected, the equation for the fundamental mode is the familiar one, but the theory also furnishes equations for the higher modes. The error involved in neglecting coupling is discussed.

1. INTRODUCTION

A RIGOROUS theory of acoustic horns can only be given for a few special cases such as the conical horn. To treat more general cases it has been usual to derive, from first principles, an approximate equation for horns of small flare, on the assumption that the waves are approximately plane.[1] This procedure makes it difficult to estimate the errors involved, while at the same time it is evident that this only gives what may be termed the principal mode of propagation, corresponding to plane waves in a cylindrical tube. There will exist other modes of propagation corresponding to the higher modes in tubes.

It seems worthwhile, therefore, to derive *exact* equations for the propagation of acoustic waves in horns of arbitrary shape, from which the errors involved in the usual treatment for horns of small flare can be estimated, and which at the same time furnish approximate equations for the propagation of the higher modes. Such a procedure can be carried out by a method quite analogous to that used for electromagnetic horns.[2] The analysis is, indeed, considerably simpler for acoustic than for electromagnetic horns, since in the former we need only consider a single scalar quantity, the velocity potential, whereas in the latter we have to deal with the six components of the electric and magnetic fields.

2. EXACT EQUATIONS FOR ACOUSTIC HORNS

We define a "horn," as in EMH, as any surface such that any plane perpendicular to a given line, which we take to be the z-axis, meets this surface in a single closed curve C, whose interior we denote by A (we shall also use A, where necessary, to denote the area of the cross section). We denote the directions of the normal and tangent to C by ν, s, respectively, the direction of s being such that a right-handed rotation from ν to s carries us in the direction z. We further define, as in EMH, the flare angle θ as the angle between the normal ν to C and the normal to the horn, θ being positive if a right-handed rotation from the direction ν to the direction of the normal to the horn carries us in the direction s, the direction of the normal to the horn being defined by requiring $|\theta|<\pi/2$.

Let ϕ denote the velocity potential of the sound waves. We shall consider only steady-state solutions with a time-factor $e^{-i\omega t}$ and put $k=\omega/c=2\pi/\lambda$, where c is the velocity of sound in the medium. The problem then is to find a solution of the wave equation

$$\nabla^2\phi+\frac{\partial^2\phi}{\partial z^2}+k^2\phi=0, \tag{2.1}$$

subject to the boundary condition

$$\frac{\partial\phi}{\partial\nu}=\tan\theta\frac{\partial\phi}{\partial z} \text{ on } C. \tag{2.2}$$

In (2.1), ∇^2 denotes the *two-dimensional* laplacian operator,

$$\nabla^2=\frac{\partial^2}{\partial x^2}+\frac{\partial^2}{\partial y^2}.$$

We now introduce the set of normalized and orthogonal eigenfunctions v_n and associated eigenvalues $\beta_n(n=0, 1, 2, \cdots)$, defined as in EMH by

$$(\nabla^2+\beta_n^2)v_n=0 \text{ in } A, \tag{2.3}$$

$$\frac{\partial v_n}{\partial\nu}=0 \text{ on } C, \tag{2.4}$$

$$\int_A v_n v_m dS=\delta_{nm}. \tag{2.5}$$

The eigenfunctions and eigenvalues depend, of course, on z, and are those required to solve the problem of the propagation of sound waves in a *tube* of cross section C. We suppose them known for all values of z. We note that one solution of (2.3)–(2.5) (which we take to be labeled by $n=0$) is

$$\beta_0=0, \quad v_0=A^{-\frac{1}{2}}. \tag{2.6}$$

(This solution can be ignored in the case of electromagnetic horns, since it does not contribute to the field.)

We now assume the expansion

$$\phi=\sum_n \phi_n(z)v_n. \tag{2.7}$$

* Now at Bishop's University, Lennoxville, Quebec, Canada.

[1] See, for instance, P. M. Morse, *Vibration and Sound* (McGraw-Hill Book Company, Inc., New York, 1936), pp. 215 et seq.

[2] A. F. Stevenson, preceding paper. We shall refer to this paper as "EMH."

We assume (2.7) to hold within and on C, but we shall not assume that we can differentiate term by term.

We now multiply (2.1) by v_n and integrate over A. Using (2.7) and (2.5) we obtain

$$k^2\phi_n+\int_A v_n\nabla^2\phi dS+\int_A v_n\frac{\partial^2\phi}{\partial z^2}dS=0. \tag{2.8}$$

Further, if we write

$$\frac{\partial\phi}{\partial z}=\sum_n C_n v_n, \tag{2.9}$$

then, by a method quite similar to that used in Sec. 2 of EMH, we can show that

$$\int_A v_n\nabla^2\phi dS=-\beta_n{}^2\phi_n+\sum_m B_{nm}C_m, \tag{2.10}$$

$$\int_A v_n\frac{\partial^2\phi}{\partial z^2}dS=\phi_n''-\sum_m (C_{mn}+D_{mn})\phi_m -\sum_m (B_{mn}+2A_{mn})C_m -\frac{d}{dz}\sum_m B_{mn}\phi_m, \tag{2.11}$$

$$C_n=\phi_n'-\sum_m (A_{mn}+B_{mn})\phi_m, \tag{2.12}$$

where (with the same notation as in EMH)

$$\left.\begin{aligned} A_{mn}&=\int_A v_m\frac{\partial v_n}{\partial z}dS, \quad B_{mn}=\int_C \tan\theta v_m v_n ds,\\ C_{mn}&=\int_A v_m\frac{\partial^2 v_n}{\partial z^2}dS, \quad D_{mn}=\int_C \tan\theta v_m\frac{\partial v_n}{\partial z}ds. \end{aligned}\right\} \tag{2.13}$$

Substituting (2.9)–(2.12) in (2.8), we obtain

$$\phi_n''+\sum_m X_{nm}\phi_m'+\sum_m Y_{nm}\phi_m=0, \tag{2.14}$$

where

$$X_{nm}=-(B_{nm}+2A_{mn},$$

$$Y_{nm}=(k^2-\beta_n{}^2)\delta_{nm}-C_{mn}-D_{mn}-B_{nm}' +2\sum_l (A_{ml}+B_{lm})A_{ln}$$

The expressions for X_{nm}, Y_{nm} can be simplified by using the relations (2.60), (2.61) of EMH which subsist between $A_{nm}, \cdots, D_{nm}$. With the help of these relations we can write

$$X_{nm}=A_{nm}-A_{mn}, \tag{2.15}$$

$$Y_{nm}=(k^2-\beta_n{}^2)\delta_{nm}+C_{nm}+D_{nm}. \tag{2.16}$$

Equations (2.14), with X_{nm}, Y_{nm} defined by (2.15), (2.16) constitute an infinite set of linear equations for the determination of the coefficients $\phi_n(z)$ in the expansion (2.7) of the velocity potential. They are quite analogous to the more complicated Eqs. (2.58) of EMH, and can evidently be regarded as giving rise to an infinite number of coupled modes of propagation, the coefficients X_{nm}, $Y_{nm}(n\neq m)$ playing the role of "coupling coefficients."

3. DISCUSSION

If coupling between modes is neglected, Eqs. (2.14) become

$$\phi_n''+Y_{nn}\phi_n=0, \tag{3.1}$$

since, from (2.15), $X_{nn}=0$. The discussion in EMH shows that, in general, C_{nn}, D_{nn} are of the order θ^2 compared with $\beta_n{}^2$, so that, neglecting θ^2, we may write

$$\phi_n''+(k^2-\beta_n{}^2)\phi_n=0. \tag{3.2}$$

The case of the principal mode ($n=0$) is, however, an exception, since $\beta_0=0$. For this case, we find from (2.6), (2.13)

$$C_{00}=(3/4)(A'/A)^2-(1/2)A''/A,$$

$$D_{00}=-(1/2)(A'/A^2)\int_C \tan\theta ds=-(1/2)(A'/A)^2,$$

the last step following from (2.41) of EMH with $\chi=1$. Equation (3.1) thus becomes, for $n=0$,

$$\phi_0''+[k^2+(1/4)(A'/A)^2-(1/2)A''/A]\phi_0=0. \tag{3.3}$$

If all the ϕ's in (2.7) other than ϕ_0 are put equal to zero, the velocity potential is given by

$$\phi=A^{-\frac{1}{2}}\phi_0. \tag{3.4}$$

From (3.3), we find that ϕ, defined by (3.4), satisfies

$$\phi''+(A'/A)\phi'+k^2\phi=0, \tag{3.5}$$

which is the usual equation for the velocity potential of approximately plane sound waves in a horn.[1] From (2.7), we see that we have *accurately*

$$\frac{1}{A}\int_A \phi dz=A^{-\frac{1}{2}}\phi_0,$$

so that the "ϕ" in (3.5) can be defined more accurately as the mean value of the velocity potential over the cross section of the horn (though Eq. (3.5) is, of course, only approximate, since coupling is neglected).

The Eqs. (3.2), (3.3) (or more generally (3.1)) can be solved approximately by the W.K.B. method as in EMH, and we have the same distinction between "transmission regions" and "attenuation regions" of the horn. For the principal mode, (3.3), for instance, cutoff (if it exists) occurs when

$$k^2+(1/4)(A'/A)^2-(1/2)A''/A=0.$$

As regards the error involved in neglecting coupling, the discussion in EMH shows that it is, in general, of the order θ^2 as regards the variation of the velocity potential

along the horn, but is of the order θ as regards the variation of the velocity potential over the cross section. If, however, two modes have the same cut-off frequency (for all z), i.e., if the eigenvalue β_n in (2.3) is degenerate, then coupling between these modes cannot be neglected. For the principal mode this cannot arise, since the eigenvalue β_0 is nondegenerate.

We shall not attempt to develop the theory further. We may, however, remark that the higher modes as determined by (3.1) or (3.2) would be of interest if it were desired to calculate reflection from the mouth of the horn more accurately than is usually done. It might also be desirable to take into account the coupling between modes to the first order in θ, as in Sec. 5 of EMH, in connection with this problem or that of finding the radiation pattern outside the horn.

JOURNAL OF APPLIED PHYSICS VOLUME 22, NUMBER 12 DECEMBER, 1951

Evaporation Rate of Liquid Helium. I*

AARON WEXLER
Westinghouse Research Laboratories, East Pittsburgh, Pennsylvania
(Received June 11, 1951)

In connection with a study of the emissivity of metals at low temperatures, a quantitative analysis has been made of the factors involved in the design of storage containers for liquid helium. Experiments confirm the analysis, which has resulted in an exceedingly simple liquid-nitrogen-protected liquid helium container having a helium evaporation rate of 1 percent per day.

The hemispherical emissivity of mechanically polished copper at 4.23°K was determined for blackbody radiation. For radiation corresponding to that emitted by a blackbody at 77.1°K and 297.1°K, the measured emissivities are 6.9×10^{-3} and 1.29×10^{-2}, respectively. These data are discussed in relation to the recent theoretical work of Reuter and Sondheimer.

The heat of vaporization of helium at 4.228°K was determined to be 4.93 cal g^{-1}, in substantial agreement with the data of Dana and Kamerlingh Onnes. Kistemaker's thermodynamic considerations questioning the accuracy of these data are evaluated in terms of the new determination.

I. INTRODUCTION

THE present study of the factors governing the rate of evaporation of liquid helium is the first phase of an investigation of the emissivity of metals at low temperatures. There are both fundamental and practical aspects of this problem. In the wavelength region of practical interest, the recent theory of Reuter and Sondheimer[1] of the anomalous skin effect in metals predicts for the low temperature emissivity of pure metals a wavelength dependence which is radically different from that implied by the classical theory. The Reuter and Sondheimer theory awaits experimental confirmation in this spectral range.

As will be demonstrated, the experimental check of the quantitative analysis of the factors involved in the flow of heat into liquid helium containers can yield data on the low temperature emissivity of metals in the interesting range mentioned above. In addition, the heat of vaporization of liquid helium may be determined concomitantly; this seemed particularly worthwhile in view of the doubts raised by Kistemaker[2] on thermodynamic grounds concerning the accuracy of the experimental determinations of Dana and Kamerlingh Onnes[3] above 4°K.

A survey of the literature indicates but a single reference[4] to a storage container for liquid helium. It is a Pyrex vessel of eight liters capacity, surrounded by liquid air; it was estimated to be able to hold helium for at least four days. Conservative estimates by us indicated that it should be possible to design an all-metal container of at least fifteen times greater efficiency; this major discrepancy, together with the facts already cited, militated for the initial approach to the problem, namely, the emphasis on container design. As is now well well known,[5] in the case of liquid hydrogen a detailed study of its evaporation rate could have led to the discovery of the ortho-para equilibrium many years before it was predicted and actually found experimentally. This fact made the study of the reasons for the large difference between the theoretically possible efficiency and the reported efficiency of helium containers all the more interesting.

The practical interests in efficient storage containers need no elaboration. The availability of such containers for liquid helium and for para hydrogen would be of value both to the research work in a field of increasing activity and to possible applications of low temperature

* This paper is based on material presented at the Low Temperature Symposium, National Bureau of Standards, March 27–29, 1951.

[1] G. E. H. Reuter and E. H. Sondheimer, Proc. Roy. Soc. (London) **A195**, 336 (1949).

[2] J. Kistemaker, Physica **12**, 281 (1946); also Communs. Kamerlingh Onnes Lab. Univ. Leiden Suppl., No. 95a.

[3] L. J. Dana and H. Kamerlingh Onnes, Communs. Kamerlingh Onnes Lab. Univ. Leiden, No. 179c.

[4] W. F. Giauque, Rev. Sci. Instr. **18**, 852 (1947).

[5] Larsen, Simon, and Swenson, Rev. Sci. Instr. **19**, 266 (1948).

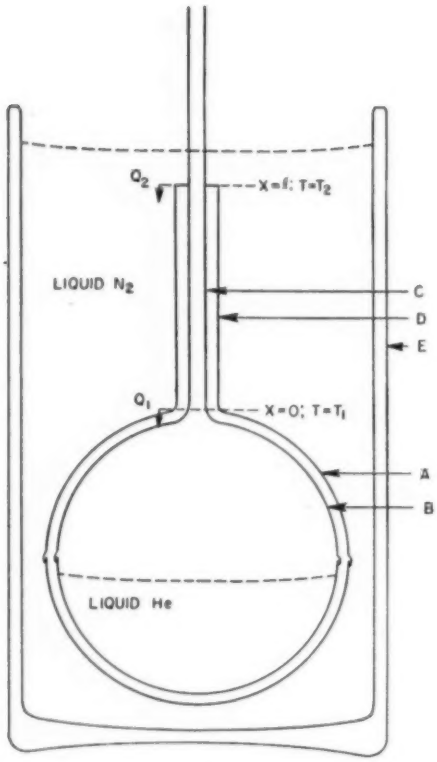

FIG. 1. Liquid helium container.

phenomena. In addition, such containers might make economical the shipping of these elements in the liquid phase and could eliminate the need for a liquefaction plant on the part of users of the refrigerants.

II. ANALYSIS OF THE PROBLEM

Our studies were based on a container of very simple design as shown in Fig. 1. The liquid helium container itself consists of two concentric spherical shells A and B, with a high vacuum between the shells. C is an Inconel neck tube of low thermal conductance. The entire container is immersed in another conventional metal Dewar vessel containing liquid nitrogen.

The physics of a vacuum vessel for the storage of liquefied gases, with special reference to the storage of liquid oxygen, has been discussed thoroughly in the *Report of the Oxygen Research Committee of Great Britain*.[6] The Report lists seven causes of heat flow to the inner vessel of a vacuum container:

(1) Conduction through the residual gas in the vacuum space.
(2) Convection through the residual gas in the vacuum space.
(3) Radiation across the vacuum space.
(4) Conduction along the neck of the flask.
(5) Radiation through the neck aperture.
(6) Conduction through supporting materials, if any, crossing the vacuum space.
(7) Convection in the interior space of the flask and neck.

[6] *The Report of the Oxygen Research Committee* (His Majesty's Stationary Office, London, 1923).

For liquid oxygen containers, whose ambient conditions are those of the atmosphere, practically the only factor of importance is radiation across the vacuum space. At the time that the Report was written, conduction through the residual vacuum had to be considered; improved vacuum technique has made this factor negligible. The only other factor of any consequence is conduction along the neck of the flask, although its contribution is minor.

It is necessary to reconsider the analysis presented in the Report, for it will be seen that for a helium container the important factors are different from those governing the efficiency of an oxygen container.

The vapor pressures of all substances, with the exception of hydrogen and helium, are so low at liquid helium temperatures that the first two factors become entirely negligible. The last two factors may also be eliminated. Radiation through the neck aperture, however, can be of real significance. If the walls of the neck tube were perfectly reflecting, the heat leak effect would be the same as that resulting from the piping into the liquid of all of the radiation from a room temperature blackbody of surface area equal to that of the neck tube opening. For a neck tube of the size which we used (about 1.5-cm diam), this would result in an evaporation rate of about three liters per day. Since our work dealt with evaporation rates of the order of 100 cc/day, the contribution by this effect had to be considered even if only a few percent of the radiation funneling down the tube reached the liquid. Our observations in this connection and the steps taken to minimize the losses due to this cause will be outlined later.

The other factors, radiation across the vacuum space and conduction along the neck of the flask are all important and must be considered together. The problem to be considered is the following: The copper vessel B may be regarded as an isothermal body at temperature T_1, the temperature at which the helium boils at the given pressure above it. At a distance l along the neck tube, the temperature is fixed at T_2, the temperature of the shielding bath. Heat is conducted down the tube at the rate Q_2 at $x=l$, Q decreasing as $x\rightarrow 0$ because of heat exchange with the effluent gas (see Fig. 1). The rate of liquid helium evaporation is thus determined by Q_1+Q_R, i.e., the sum of the rate of heat entering by conduction along the tube and that due to radiation heat transfer between surfaces A and B. The calculation of the evaporation rate may be made in a straightforward manner on the assumption that heat exchange between the effluent gas and the neck tube is perfect. Across any section of the tube, we have

$$Q=kA(dT/dx), \tag{1}$$

where k is the thermal conductivity of the tube and A is the cross-sectional area of the metal wall. If the specific heat of the gas is denoted by C_p and if n is the

number of moles per second of gas flowing out of the system, the assumption of perfect heat exchange implies

$$dQ = nC_p dT. \quad (2)$$

In practice, the thermal conductivity of the neck tube is found to be a linear function of temperature:

$$k = a + bT. \quad (3)$$

The integration of Eq. (2) yields

$$n = (A/lC_p)[\{a+b(T_1-g)\} \times \ln\{1+(T_2-T_1)/g\}+b(T_2-T_1)], \quad (4)$$

wherein $g = Q_1/nC_p$.

Since n is linearly related to Q_1+Q_R, we have

$$n = \beta(Q_1+Q_R), \quad (5)$$

so that

$$Q_R = n[(1/\beta)-C_p g]. \quad (6)$$

C_p is assumed to be temperature independent and equal to the specific heat at constant pressure of an ideal monatomic gas. The value of β is related to the reciprocal of the heat of vaporization L. If all of the liquid evaporated were to contribute to n, then $\beta = L^{-1}$. Actually, because the space occupied by the evaporating liquid is taken up by the vapor, not all of the evaporating liquid contributes to the gas current. In fact, it may be shown[7] that

$$\beta = (1-\rho_v/\rho_l)/L, \quad (7)$$

where ρ_v and ρ_l are the respective densities of the vapor and liquid.

Calculations based on the foregoing may be made as follows. The most interesting calculations are those for the evaporation rate as a function of the radiation heat transfer Q_R. Equation (4) permits the calculation of n as a function of g. For given combinations of n and g thus determined, the corresponding values of Q_R are calculable from Eq. (6). The highest value of g appearing in the calculations is $g = 1/\beta C_p$.

The application of these considerations indicated the possibility of making a highly efficient container for liquid helium. The design indicated in Fig. 1 was chosen for its simplicity and for the possibility it offered of permitting the determination of the radiation heat transfer to a polished copper surface at the helium boiling point. The approximately spherical shells were made of spun hemispheres which were soldered together. Two containers were studied. Both had inner spheres which were made of copper whose outer surface was made highly reflecting by buffing and hand polishing with a commercial polish. The outer sphere of one of the containers, hereinafter called container A, was made of monel having a sandblasted inner surface. The other container, container B, had a copper outer sphere whose inner surface was highly polished by the same method used for the outer surface of the inner spheres. At the joining diameter of the inner spheres there was a band of solder; its width was kept less than 0.5 cm. Its surface, which was highly polished, represented less than 6 percent of the surface area of the inner sphere. The inner spheres had a volume of 9250 cc and the outer ones a volume of 12,500 cc. The corresponding surfaces facing the vacuum, therefore, were 2140 cm² and 2610 cm², respectively. The neck tube was a 20.0-cm length of hard drawn Inconel tubing, $\frac{5}{8}$ in. o.d.×0.0105-in. wall. In the range of temperatures involved, the thermal conductivity of the metal is well represented by $k = 1.21T - 2.28$ milliwatts cm^{-1} deg^{-1}.†

It is assumed that the bath temperature is at 77.1°K and that that of the helium is 4.23°K. The other values used are 20.8 watt-sec mole^{-1} deg^{-1} for C_p; 0.0107 mole·joule^{-1} for β; and 4.87 cal g^{-1} for the heat of vaporization of the liquid.

One extreme case is that for zero heat exchange between the effluent gas and the wall of the neck tube. Under these circumstances, the evaporation rate is

$$Q_1+Q_R = (A/l)[a(T_2-T_1)+\tfrac{1}{2}b(T_2^2-T_1^2)]+Q_R. \quad (8)$$

If $Q_R = 0$, the upper limit of the evaporation rate for our container would be 770 cc/day, corresponding to $Q_1 = 0.0227$ watt.

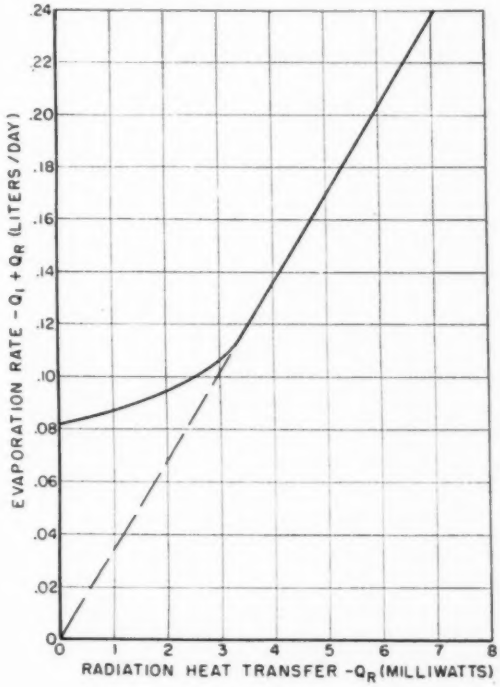

FIG. 2. Calculated evaporation rate.

[7] Scott, Ferguson, and Brickwedde, J. Research Natl. Bur. Standards **33**, 1 (1944).

† This relation was deduced from data kindly supplied in advance of publication by Dr. J. E. Zimmerman, of Carnegie Institute of Technology. His measurements were made on a sample of metal from the same lot as that from which our tubing originated. While the data are good to better than 5 percent, Dr. Zimmerman has found large differences in the thermal conductivity depending upon the temper of the alloy. Due care must therefore be taken in the application of this relation to other samples of Inconel.

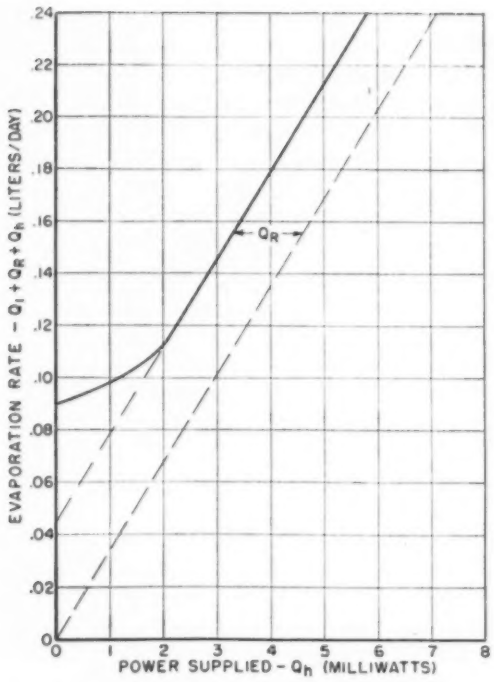

FIG. 3. Determination of radiation heat transfer.

The other extreme case is the one for perfect heat exchange which is a condition very likely to be approached at low rates of flow of a gas whose thermal conductivity is high. Figure 2 shows the results of the application of Eqs. (4) and (6) to our container. The predicted evaporation rate for $Q_R=0$ is 82 cc/day, corresponding to $Q_1=2.41\times10^{-3}$ watt. Thus, the importance of good heat exchange is emphasized by a comparison of this number with that deduced for zero heat exchange.

The implications of the analysis as indicated in Fig. 2 are very interesting. It will be seen that as Q_R increases from zero, the evaporation rate (Q_1+Q_R) changes rather slowly. This results, of course, from the fact that the increased flow of effluent gas is effective in substantially reducing Q_1. The calculations show that when the radiation heat transfer rises to a value which is equal to the rate of heat entering the helium container when $Q_R=0$, the evaporation rate increases by only 20 percent over that for $Q_R=0$. Hence, if for a given container Q_R happens to be of the order of or less than Q_1 when $Q_R=0$, attempts to decrease Q_R by using better reflecting materials or by incorporating radiation shields would not appreciably decrease the evaporation rate.

The method for the determination of the heat of vaporization and of the radiation heat transfer follows directly from Eq. (6). If the evaporation rate is plotted as a function of the power Q_h dissipated in a heater immersed in the liquid helium, then, when $Q_1\rightarrow0$, the evaporation rate will be proportional to Q_h. The slope of the straight line is β, from which the heat of vaporization may be calculated by means of Eq. (7). Moreover, the radiation heat transfer is just the separation between the experimental straight line and that parallel to it and passing through the origin. Thus, the intercept of the experimental straight line on the evaporation rate axis is indeed Q_R.

These remarks may be made more concrete by referring to Fig. 3 which was obtained from the same calculations as those on which Fig. 2 is based. The curve was drawn for the initial condition $Q_1=Q_R$.

This method of determining Q_R makes the assumption that the heat dissipated in the heater results in isothermal boiling away of liquid helium. If the heat not only evaporates helium but also raises its temperature, the effect of Q_h upon the evaporation rate would be less than that shown in Fig. 3; and, in fact, for large values of Q_h the curve of Fig. 3 would curve towards the Q_h axis. On the other hand, the possibility of the removal of liquid in an amount greater than that corresponding to isothermal boiling by mist and spray which is carried along with the evaporated vapor was discussed by Dana and Kamerlingh Onnes,[3] from whose paper we have taken the heat of vaporization data for liquid helium. These workers found no evidence for either of these effects; and in the application of the method outlined above, it would appear that if for large values of Q_h the evaporation rate is accurately linearly dependent on Q_h and if the slope is derivable from the heat of vaporization, this would constitute a confirmation of the absence of these undesired effects.

The existence of the initial interval of small slope in Fig. 2 is a consequence of the large value of β for helium. For other liquefied gases, this interval will be smaller. It is important to note, nevertheless, that the method, indicated in Fig. 3, of separating heat transfer across the vacuum space from other sources of heat influx is usable even for small values of β or if the heat exchange is not perfect. For maximum accuracy in deducing Q_R by this method, however, it is manifestly desirable to reduce to a minimum the initial value of Q_1.

III. THE RADIATION HEAT TRANSFER

Radiation heat transfer to a metallic surface, whose resistivity lies in the residual resistivity range, involves fundamental problems with respect to the emissivity of the surface. The radiation heat transfer H between two concentric spheres is readily calculable[5] if the emissivities of the surfaces are known:

$$H=[A_i\sigma e_i e_o/\{e_o+e_i(1-e_o)\rho\}](T_o^4-T_i^4). \qquad (9)$$

In this relation, the subscripts i and o refer to the inner and outer surfaces, respectively. A_i is the surface area of the inner spherical shell, $\sigma=5.72\times10^{-12}$ watt·cm^{-2}·deg^{-4} is the Stefan-Boltzmann constant, e_i and e_o are the emissivities, T_i and T_o are the absolute temperatures of the surfaces, and $\rho=A_i/A_o$ is the fraction of the

[5] O. A. Saunders, Proc. Phys. Soc. (London) 41, 569 (1929).

radiation reflected from the outer surfaces which strikes the inner surface directly. In our work $T_o^4 \gg T_i^4$, so that $T_o^4 \simeq T_o^4 - T_i^4$ to a good approximation. If the internal surface of the outer sphere is regularly reflecting, we have $\rho = 1$. If $e_i \ll e_o$, then we have

$$H = A_i \sigma e_i T_o^4, \tag{10}$$

which means, of course, that the radiation flux in the interspace between the two surfaces is essentially blackbody radiation corresponding to the temperature T_o; if H is measured under these conditions, then a knowledge of e_o is not necessary for an evaluation of e_i.

The classical work of Drude and of Hagen and Rubens[9] established the relation,

$$(1-R) = e = 36.5(\rho/\lambda)^{\frac{1}{2}}, \tag{11}$$

where R is the reflectivity at normal incidence on the surface of a metal, e its emissivity, ρ its resistivity in ohm-cm, and λ the wavelength in microns of the radiation used. Considered as a function of wavelength, the emissivity of a metal at constant temperature will thus vary as $\lambda^{-\frac{1}{2}}$. When the wavelength decreases, however, and the period of the radiation becomes comparable with or less than the time of relaxation of the conduction electrons, the emissivity is independent of the wavelength. At low temperatures new phenomena are possible, for the mean free path of the electrons may become comparable with or greater than the skin depth for penetration of the electric field. Under these circumstances, the assumption implicit in the classical theory that the electric field may be considered as spatially constant, as far as the motion of electrons is concerned, is not valid except at sufficiently long wavelengths for which the skin depth is large compared with the free path and at sufficiently short wavelengths at which the penetration depth is large compared with the distance travelled by an electron during one cycle of the electric field. At intermediate wavelengths, the recent theory of the anomalous skin effect of Reuter and Sondheimer[1] is applicable. The predictions of this theory may be indicated by referring to the authors' calculations of $(1-R)$ at normal incidence as a function of λ for pure silver at liquid helium temperatures. At the long wavelength end of the spectrum, $(1-R)$ varies classically as $\lambda^{-\frac{1}{2}}$. In the microwave region between 4 cm and 0.1 cm, the variation is as $\lambda^{-\frac{3}{2}}$. The curve rises to a maximum of 1.5×10^{-3} at 69μ; and beyond this point $(1-R)$ drops to the classical value in the visible range, beyond which it goes to zero. The classical theory for wavelengths in the region of maximum yields a wavelength-independent value of $(1-R) < 10^{-5}$. A wavelength range of special interest is that between *ca* 40μ and 3μ. For the case of perfectly specular surface reflection of electrons, the Reuter and Sondheimer computation gives $(1-R)$ in this range as varying as λ^n, where $n > 1$.‡ This is the spectral range which is encountered in the design of liquid helium containing apparatus. In the microwave region, the theory of Reuter and Sondheimer finds experimental support.[10–12] The only datum which we have been able to find in the micron range is that given by Scott *et al.*[13] for chemically deposited silver at 20°K encompassed by a similar surface at room temperature. The value given for the hemispherical emissivity is 0.03, being a factor of twenty greater than the maximum emissivity expected theoretically. It is possible that this number is appreciably higher than the actual value of e for such a surface; for at the time that this work was done, the effect of the ortho-para conversion of the liquid hydrogen, possibly catalyzed by frozen oxygen, was not recognized. Further, these workers assumed that the emissivities of the warm and cold surfaces were equal. This could lead to an estimate of the emissivity of the cold surface which is too large by a factor of two.§ In view of the state of the experimental data in the micron range, there is clearly a need for experimental work.

For a calculation of the evaporation rate of our container B on the basis of Fig. 2, the emissivities of the surfaces were required. Conservative estimates could be made on the basis of experimental data available at elevated temperatures.

The Hagen-Rubens Eq. (11) pertains to normally emitted monochromatic radiation and has received experimental confirmation in the micron range at temperatures above room temperature.[9,14] The extension to polychromatic hemispherical emissivity in the micron range at elevated temperatures also finds reasonably good experimental verification.[15] At lower temperatures, on the other hand, the observed hemispherical emissivities are several-fold larger than the calculated values.[16] Thus, the lowest observed emissivity for a copper surface at 90°K, exposed to room temperature blackbody radiation, is given by Blackman *et al.* as 0.019, a value 2.5 times greater than the theoretical one. These authors attributed the discrepancy to the presence of surface films, particularly oxide films, and

[9] E. Hagen and H. Rubens, Ann. Physik **11**, 873 (1903).

‡ T. Holstein has treated the problem in this wavelength region and finds that the wavelength dependence is critically dependent upon p, the fraction of electrons which are reflected specularly. If $p=0$, his result is that $(1-R)$ is independent of λ at a level corresponding to $(1-R)_{\max}$. The details of this work are to be published.

[10] A. B. Pippard, Proc. Roy. Soc. (London) **A191**, 370–84 (1947).

[11] Maxwell, Marcus, and Slater, Phys. Rev. **76**, 1332 (1949).

[12] W. B. Nowak and J. C. Slater, Phys. Rev. **76**, 469(A) (1949).

[13] Scott, Cook, and Brickwedde, J. Research Natl. Bur. Standards **7**, 935 (1931).

§ In a communication to the author, R. B. Scott has pointed out that one has to consider also the fact that the surfaces facing the vacuum were not polished; they had a slightly dull appearance, probably because of microscopic roughness and also the possible adherence of some of the so-called "bloom" that appears in the silvering process.

[14] C. Hurst, Proc. Roy. Soc. (London) **A142**, 466 (1933).

[15] C. Davisson and J. R. Weeks, Jr., J. Opt. Soc. Am. **8**, 581 (1924).

[16] Blackman, Egerton, and Truter, Proc. Roy. Soc. (London) **A194**, 1947 (1948).

TABLE I. Evaporation rate of liquid helium at 4.228°K.

Container *A*		Container *B*	
Inner surface	Polished copper	Polished copper	
Outer surface	Sandblasted Monel	Polished copper	
Ambient temp. (°K)	77.08±0.02	77.05±0.02	
ΔH_v (cal/gm)	4.93	4.93	
Q_R (Milliwatts)	3.00	1.67	
Heater power (milliwatts)	Evap. rate (CFH at NTP)	Heater power (milliwatts)	Evap. rate (CFH at NTP)
0.000	0.1462	0.000	0.1417
1.839	0.1597	1.785	0.1530
2.265	0.1638	2.374	0.1570
4.223	0.2152	3.299	0.1649
8.876	0.3568	4.216	0.1783
12.613	0.4706	8.862	0.3161
17.786	0.6256	12.590	0.4285
23.272	0.7894	17.896	0.5877
		23.556	0.7571

possibly to the difference in resistivity of the surface layers as compared with that of the bulk of the material. It was in view of the foregoing that for the estimate of the evaporation rate of our container, we took 0.02 for the emissivity of both surfaces. Actually, on the basis of the theory of Reuter and Sondheimer, this estimate for the copper surface at liquid helium temperature could be too high by a factor of ten. From Eq. (9), the maximum radiation heat transfer expected is thus 4.3×10^{-3} watt for container *B*. From Fig. 2, it is seen that this corresponds to an evaporation rate of 146 cc per day. Hence, we expected an evaporation rate between 82 cc per day and 146 cc per day, which implies the possibility of more than an order of magnitude improvement in the efficiency of liquid helium storage containers as compared with the one which has been described in the literature.

IV. EXPERIMENTAL

The experiments consisted of measuring the evaporation rates of liquid helium in the containers *A* and *B*, whose construction was indicated in Sec. II. The liquid helium in the containers was maintained at 772.0±0.1 mm Hg with the aid of a thermostatted manostat.‖ Thus, our experiments all refer to helium boiling at 4.228°K. Gas flow measurements were made with a wet test meter;¶ one revolution of the meter's pointer corresponds to 0.1 cu ft. The calibration of the meter made before and after the experiments was constant to ±0.2 percent; the calibrations were made with a 0.1-cu ft meter prover which was standardized by the National Bureau of Standards. In order to maintain constant the water level in the wet test meter, the gas issuing from the container was passed through a water saturator before it entered the meter.

‖ For this purpose, we have found the Model Number 5 Cartesian Manostat manufactured by The Emil Greiner Company very useful. The manostat was thermostatted at about 300°K to a constancy of ±0.02°.

¶ Manufactured by Precision Scientific Company.

In the measurement of rates of evaporation of low boiling liquids, pressure control is of paramount importance. Changes in the pressure have marked effects on the flow rate,[17] and it is important to note that these effects are proportional to the mass of the liquid. It is necessary to meter an amount of gas which is sufficiently high to give the desired precision. In view of the pressure control and the fact that for each flow rate determination we metered at least 1.0 cu ft, possible errors due to this factor were made entirely negligible.

The temperature of the nitrogen bath was determined by fluctuations of the atmospheric pressure which led to a temperature fluctuation of ±0.02°. Actually, at any given pressure, measurements with a platinum resistance thermometer probe showed that the bath temperature was constant to ±0.005°.

The initial experiments gave erratic results; the fluctuations in the evaporation rate were traced to the funneling of radiation down the neck tube. This could be completely eliminated by the simple expedient of blackening the inside of the neck tube with Aquadag down to the liquid nitrogen temperature level. The introduction into the neck tube of a metal test tube, which provided a radiation shield at the liquid nitrogen level, also resulted in consistently reproducible data. In practice, both of these precautions were taken; and, under these circumstances, the evaporation rates for the containers *A* and *B* were 112 cc/day and 96 cc/day, respectively. These values are entirely in accord with the analysis presented in Sec. II; it was thus very desirable to check for quantitative agreement with the analysis by experiments which yield data of the type indicated by Fig. 3.

In order to facilitate the installation of a heater whose leads did not contribute to the heat leak and in order to improve heat exchange[18] between the gas and the wall of the neck tube, a ½-in. o.d. by 0.010-in.

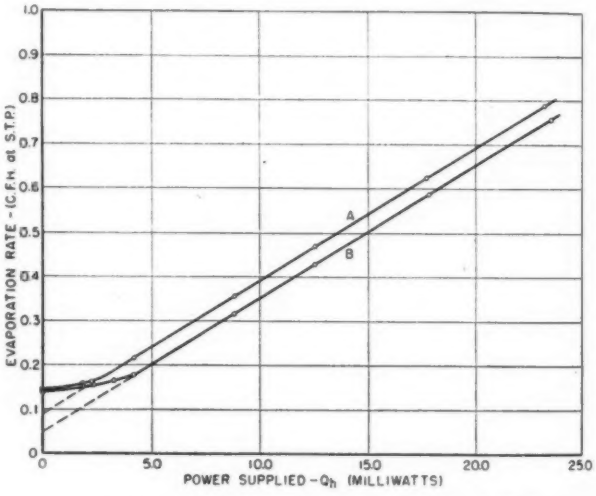

FIG. 4. Liquid helium evaporation rates at 4.228°K.

[17] A. Wexler and W. S. Corak, Rev. Sci. Instr. **21**, 583 (1950).
[18] R. B. Jacobs and S. C. Collins, J. Appl. Phys. **11**, 491 (1940).

wall Inconel tube (from the same lot and of the same temper as the neck tube) was inserted into the neck tube. The leads, each a ten foot length of Number 40 constantan wire, were spiraled about the inserted tube and the evaporating gas was made to pass up the annulus between the two tubes. The heater was a 50,000-ohm wire wound constantan resistor. With a regulated dc power supply,** the power dissipated in the heater could be kept constant for many hours to ± 0.01 percent. A Leeds and Northrup Type K-2 potentiometer was used to measure the current through the heater and the potential drop across it; it is estimated that the power measurements are accurate to ± 0.02 percent. The data obtained are tabulated in Table I and are plotted in Fig. 4.

The last four points on the straight line portions of the curves of Fig. 4 can be fitted by a linear equation which reproduces all of the points to ± 0.1 percent. The slopes of the two straight lines agree within these limits and have the value 30.03 CFH(NTP)/watt. As a check on the method, curve A was redetermined with a 500,000-ohm heater; the experimental points coincided with those obtained with the 50,000 ohm heater to ± 0.1 percent. With the aid of Eq. (7) and the densities of the liquid[19] and vapor[20] phases, we calculate that the heat of vaporization of helium at 4.228°K is 4.93 cal/g. A discussion of this determination will be given in the next section.

The intercepts of the straight lines on the evaporation rate axis give the radiation heat transfer for containers A and B to be 3.00×10^{-3} watt and 1.67×10^{-3} watt, respectively. These values of Q_R may be inserted in the equations developed in Sec. II; and, if one adjusts suitably the parameter A/l, which may be in error by as much as 5 percent, one can reproduce the curves A and B identically. The values of Q_R thus determined may also be used for a calculation of the evaporation rates of the containers themselves, i.e., without the added heat exchange tube. The evaporation rates may in fact be obtained from Fig. 3; the calculated values for containers A and B are 106 cc/day and 92 cc/day, which are in fair agreement with observed values of 112 cc/day and 96 cc/day. While the discrepancies correspond to the maximum differences attributable to the uncertainty in A/l, there is the suggestion that at least part of the differences is due to imperfect heat exchange in the neck tube.

The hemispherical emissivity of polished copper at 4.228°K for radiation corresponding to that emitted by a blackbody at 77.1°K may be calculated from the determined value of $Q_R=3.00\times10^{-3}$ watt for container A. This calculation may be made with the aid of Eq. (9) on the assumption that $e_o \gg e_i$. It may be estimated that such an assumption will lead to an uncertainty in e_i of less than 5 percent. The calculated value of the emissivity under these conditions is 6.9×10^{-3} and corresponds to a blackbody radiation spectrum having a maximum intensity at 37.4μ. Since, in addition to the absolute value of the emissivity, the wavelength dependence is of crucial interest, the evaporation rate was determined for a 297.1°K blackbody radiation spectrum having a maximum intensity at 9.71μ. The flow rate had to be measured with a different flow meter arrangement whose accuracy was estimated as ± 4 percent. With this arrangement the observed flow rate was 36.9 CFH (NTP) and corresponds to $e_i=1.2_9\times10^{-2}$.

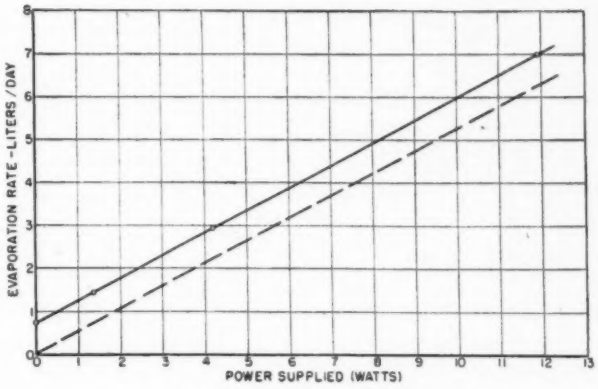

FIG. 5. Liquid nitrogen evaporation rate at 77.12°K.

It may be worth noting here our observations of the effects of spontaneous vibrations of the helium gas column between the liquid level and the vent tube of a given container. Such oscillations have been observed many times,[21] and an attempt has been made to treat the problem theoretically.[22] If the vent tube of the container is closed or restricted with a rubber tube, for example, oscillations within the container may be felt by holding the rubber tube. It was found that the intensity of such oscillations, which are accompanied by an influx of heat at a rate which may be a thousand times that due to normal heat leak, is a function of the liquid helium level. We were careful to work under such conditions that the effects of this phenomenon could be neglected.

For completeness Fig. 5, which is based on data obtained early in the work in order to check the principle of the method used in determining Q_R and ΔH_v, is included. In Fig. 5 is presented the evaporation rate of liquid nitrogen at 77.12°K in a container which differed from container B in that incorporated in it was a copper-shielded activated charcoal pump in contact with the liquid nitrogen cooled surface. The outer surface of this container was at room temperature, 297.1°K. The ac-

** We are indebted to Mr. D. J. Grove, of our Laboratories, for making available to us this power supply of his own design.

[19] H. Kamerlingh Onnes and J. D. A. Boks, Communs. Kamerlingh Onnes Lab. Univ. Leiden No. 170b.

[20] Mathias, Crommelin, Kamerlingh Onnes, and Swallow, Communs. Kamerlingh Onnes Lab. Univ. Leiden No. 172b.

[21] K. W. Taconis *et al.*, Physica **15**, 733 (1949), also Communs. Kamerlingh Onnes Lab. Univ. Leiden No. 279a.

[22] H. A. Kramers, Physica **15**, 971 (1949); also Communs. Kamerlingh Onnes Lab. Univ. Leiden Suppl. No. 100a.

curacy of the evaporation rate measurements was ±1 percent. From the data it was estimated that 97 percent of the initial losses is due to heat transfer across the vacuum space, which is consistent with known facts. The heat of evaporation calculated from these data is 1345±13 cal·mole^{-1}, which includes a correction of 0.5 percent made in accordance with Eq. (7). This determination is in satisfactory agreement with the value deduced from the data of Giauque and Clayton[23] for the same temperature, namely, 1344.2±1 cal·mole^{-1}.

V. DISCUSSION

The emissivities determined for polished copper at 4.228°K are 6.9×10^{-3} for blackbody radiation at 77.1°K and $1.2_9\times10^{-2}$ for blackbody radiation at 297.1°K. The theoretical expectations should not be appreciably different from those computed for silver at liquid helium temperatures at the wavelengths corresponding to the maximum intensities in the blackbody spectrum, namely, 37.4μ and 9.71μ, on the basis of the Reuter and Sondheimer theory. The calculated values are 1.0×10^{-3} and 2.0×10^{-4}, respectively. Not only is absolute agreement lacking, but the experimentally determined emissivities increase as λ^{-1} and do not decrease. It is, of course, possible that the surface is not representative of the bulk metal and that surface roughness is responsible for the large values of the absorption. Such considerations have, in fact, been offered to explain anomalously high resistive losses in the microwave region.[9–11] The difficulty here is that in order to obtain a λ^{-1} wavelength dependence, the absolute values of e must be much higher than those which are observed. These questions which require further experimental study and more precise determinations of the emissivities of metals as a function of their temperature and of the frequency of the radiation, with special emphasis on the treatment of the surface, are in progress.

Recently Kistemaker,[2] on the basis of an equation which results from the equating of the Gibbs free energies of the liquid and the saturated vapor, concluded that above 3.5°K the values of the heat of vaporization of helium measured by Dana and Kamerlingh Onnes[3] are 6 percent too low. The thermodynamic relation used by Kistemaker involves the virial coefficients of helium as well as the specific heat of the liquid. The experimental determinations of Dana and Kamerlingh Onnes may be assumed to be accurate to 1 percent; the only data they required was the densities of the liquid under its saturated pressure.[19]

The heat of vaporization of helium at 4.228°K as extrapolated from the data of Dana and Kamerlingh Onnes, is 4.87 cal·g^{-1}. The accuracy of our value of 4.93 cal·g^{-1} depends on that of the determinations of both the liquid density,[19] $\rho_l=0.1253$, and the vapor density,[20] $\rho_v=0.01637$ g cm^{-3}. Except for errors due to inaccuracies in ρ_l or ρ_v, our determination is considered to be accurate to better than 0.5 percent. The Clausius-Clapeyron equation

$$\Delta H_v=T(1/\rho_v-1/\rho_l)dp/dT$$

yields the value 5.31 cal·g^{-1}. This strongly suggests that the vapor density is in error; and if, indeed, ρ_v is taken as 0.01755, all three values become identical.

With respect to container design, the experimental results confirm the analysis and demonstrate the possibility of making extremely efficient storage containers for liquid helium. It would be quite feasible to build storage containers of moderate size which would hold liquid helium for a year or more after the initial filling.

VI. ACKNOWLEDGMENTS

We wish to thank T. Holstein for very helpful discussions concerning the theoretical aspects of this work. Our thanks are also due to Hofman Laboratories, Inc., Newark, New Jersey, for providing the containers designed on the basis of the analysis contained in this paper and, in particular, to H. Jacket, of Hofman Laboratories, Inc., who supervised their construction and assisted in taking the initial data. We are also grateful for valuable discussions with K. Mendelssohn, R. B. Scott, and D. Shoenberg at the Low Temperature Symposium held at the National Bureau of Standards. Finally, we wish to acknowledge the assistance of our colleagues, particularly W. S. Corak and G. T. Cunningham.

[23] W. F. Giauque and J. O. Clayton, J. Am. Chem. Soc. **55**, 4875 (1933).

JOURNAL OF APPLIED PHYSICS VOLUME 22, NUMBER 12 DECEMBER, 1951

Studies in Newtonian Flow. II. The Dependence of the Viscosity of Liquids on Free-Space

ARTHUR K. DOOLITTLE
Carbide and Carbon Chemicals Company, A Division of Union Carbide and Carbon Corporation, South Charleston, West Virginia
(Received June 14, 1951)

In this paper it is shown that the viscosity of the liquid normal paraffins can be accurately defined as a simple function of relative free-space except for values in the neighborhood of the freezing points of each compound. A novel method of extrapolating the specific volumes of this family of compounds to absolute zero is described which permits the calculation of reliable values of the relative free-space from density data.

An expression of the same form as the author's function, but in which temperature rather than free-space is the primary variable (the so-called Andrade equation), fails to reproduce the viscosity of *n*-heptadecane over the same range of temperatures within the limits of the known accuracy of the measurements.

THE idea that the resistance to flow in a liquid depends upon the relative volume of molecules present per unit of free-space is a concept that is intuitively acceptable. Some consideration has been given to this point of view by prior investigators, but in comparison with the voluminous literature on the temperature dependence of viscosity, one concludes that this concept has been somewhat neglected. It is surprising indeed that so promising an approach to the subject should have received so little attention, particularly when one considers that the idea was first introduced by Batschinski[1] thirty-five years ago. For a review of some of the more prominent free-space relationships, the reader is referred to a chapter by the author in Alexander's *Colloid Chemistry*.[2]

The study that is described in part in this paper is based on high precision measurements of the densities and viscosities of pure members of the homologous series of *n*-alkanes. A description of the synthesis and measurement of these compounds has recently been published,[3] which presents the original data together with a conservative estimate of the accuracy of the measurements.

The first paper[4] of the current series (published in this Journal) employed these data to show that expressions previously proposed in the literature relating the viscosity of liquids to temperature are not adequate to reproduce the observed values with a validity corresponding to the known accuracy of the measurements when the temperature range of these measurements is considerable. It was shown further that certain relationships that do reproduce the measured values with satisfactory validity are complicated and therefore useless in a practical sense.

It is the purpose of the present paper to show that if relative free-space rather than temperature is considered to be the primary variable, very satisfactory reproduction of the measured values may be obtained by use of a relatively simple relationship. It will be shown that values calculated by this equation fall well within the limits of the accuracy of the measurements over a range of temperatures extending from the boiling point down to within 100 Centigrade degrees of the freezing point of each of the compounds studied.

The "free-space" in a liquid is considered by us to be that space seemingly arising from the total thermal expansion of the liquid without change of phase. Relative free-space is therefore the fractional increase in volume resulting from expansion, and is defined as

$$v_f/v_0=(v-v_0)/v_0, \tag{1}$$

where v_f = volume of free-space per gram of liquid at any temperature; v_0 = volume of 1 gram of liquid extrapolated to absolute zero without change of phase; and v = volume of 1 gram of liquid at any temperature. Presumably changes in relative free-space result from changes in pressure as well as from changes in temperature, but data have not so far been obtained that could be used in a similar study of the pressure variable.

It appeared from our study of the literature that not only were the temperature ranges narrower and the methods of measurement used by prior investigators in some cases less highly refined than those reported by us, but a limitation of even greater significance was the fact that no reliable means was at hand for determining the free-space in a liquid. Our attention was therefore directed to the problem of the accurate calculation of the total thermal expansion (without change of phase) of our *n*-alkanes from absolute zero to the temperatures of measurement. Since measurements at absolute zero are impossible or at least impractical, and since supercooling to absolute zero without freezing would be quite improbable, our approach was to devise a method of extrapolating our measured specific volumes to the values that presumably would have been obtained at absolute zero if the contraction were to have followed the same pattern throughout its course.

Several methods of estimating the density (or its reciprocal, the specific volume) of liquids at absolute zero have been proposed in the literature. Of these,

[1] A. J. Batschinski, Z. physik Chem. **84**, 644 (1913).
[2] J. Alexander, *Colloid Chemistry* (Reinhold, New York, 1950), Vol. VII, pp. 154–155.
[3] A. K. Doolittle and R. H. Peterson, J. Am. Chem. Soc. **73**, 2145 (1951).
[4] A. K. Doolittle, J. Appl. Phys. **22**, 1031 (1951).

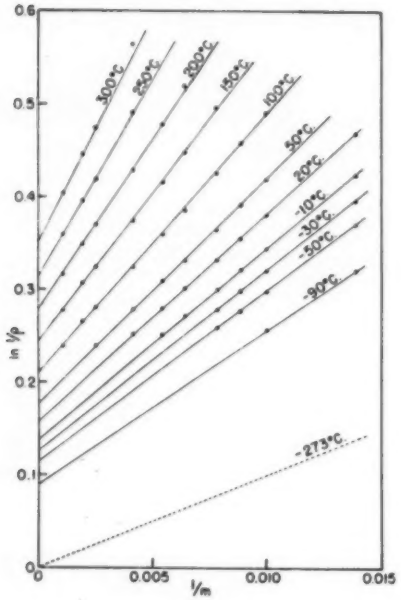

FIG. 1. Specific volume of *n*-paraffin hydrocarbons $\ln(1/\rho)$ *vs* $1/m$ at various temperatures.

Goldhammer's rule,[5]

$$\rho_l-\rho_v=C(T_c-T)^{\frac{1}{3}}, \tag{2}$$

where ρ_l = density of the liquid; ρ_v = density of the vapor; T_c = critical temperature; and T = absolute temperature of the measurements, is generally considered to be the most reliable. Obviously Goldhammer's rule can be applied only when the critical temperature can be determined.

Van der Waals'[6] rule,

$$\rho_0=\rho_c(RT_c/P_cV_c), \tag{3}$$

where ρ_0 = density at absolute zero, ρ_c = critical density, T_c = critical temperature, P_c = critical pressure, V_c = critical volume, has an equally sound theoretical basis but requires several critical measurements in addition to the critical temperature.

Cailletet and Mathias' Law of the Rectilinear Diameter,[7]

$$(\rho_l+\rho_v)/2=aT+b, \tag{4}$$

where ρ_l = density of the liquid and ρ_v = density of the vapor, becomes equivalent to a linear function as the temperature scale is descended, since the density of the vapor is negligible at low temperatures. We were led to abandon this relatively simple method of determining the density at absolute zero, however, because the work of others has shown that the extrapolation of these lines to absolute zero gives values that do not correspond to those obtained by other, more reliable methods. Such early workers as Sydney Young[8] and J. Timmermans[9] have pointed out that the averages of the liquid and vapor densities, if plotted over a sufficiently extended range of temperatures, do not define straight lines, but rather, curves. Mathews[6] finds that the values obtained by extrapolation of the Law of the Rectilinear Diameter to very low temperatures are always consistently higher than those obtained by other methods.

Perhaps the most obvious method of extrapolating densities to absolute zero would be to set up a density function in the form of a Taylor expansion, such as

$$\rho=\rho_0+\alpha T+\beta T^2+\gamma T^3+\cdots \tag{5}$$

and determine the constants by means of least squares calculations. Extrapolation of such an equation to $T=0$ should give ρ_0. However, the method involving least squares calculations would be laborious and would be of doubtful validity for our higher molecular weight paraffins because the extrapolation would have to extend over too great a range of temperatures. An even greater limitation to the usefulness of the Taylor expansion method is that a separate calculation would have to be made for each compound under review, thus affording no means of taking advantage of the fact that we are dealing with an homologous series of compounds. In the method finally adopted, the accuracy of each extrapolated value is enhanced by the fact that it is determined by measurements made on a number of our compounds, not by measurements made on a single compound.

In addition to the four methods mentioned above, consideration was also given to the measurement of molar refractivity as a means of determining the volume occupied by the molecules. There is some reason to believe that the Lorenz-Lorentz molar refractivity should be proportional to the occupied volume.[10] That is, if

$$R_L=(n_D^2-1/n_D^2+2)\cdot m/\rho, \tag{6}$$

where R_L = Lorenz-Lorentz molar refractivity, n_D = refractive index at sodium line, m = molecular weight, ρ = density at temperature of measurement, then v_0m should equal aR_L or

$$v_0=a(n_D^2-1/n_D^2+2)\cdot 1/\rho. \tag{7}$$

This approach proved entirely too uncertain for our purposes, but it is interesting to observe that when the molar refractive indices were plotted against v_0m, using values of v_0 obtained by the method to be described below, very good straight lines were obtained.

[5] D. A. Goldhammer, Z. physik Chem. **71**, 577 (1910).
[6] A. P. Mathews, J. Phys. Chem. **20**, 554 (1916).
[7] L. Cailletet and E. Mathias, Compt. rend. acad. sci. U.R.S.S., Paris **102**, 1202 (1886).
[8] S. Young, Phil. Mag. **50**, 291 (1900).
[9] J. Timmermans, Bull. Soc. Chim. Belges **26**, 205 (1917).
[10] Samuel Glasstone, *Textbook of Physical Chemistry* (D. Van Nostrand Company, New York, New York), second edition, p. 529.

TABLE I. *n*-Paraffin hydrocarbons. Specific volume as a function of molecular weight. $\ln(1/\rho)$ *vs* $1/m$. (Experimental values.)

	$m\rightarrow$	72.15	100.20	114.14	128.25	156.30	184.35	240.46	394.74	506.95	899.68
	$1/m\rightarrow$	0.01386	0.00998	0.00876	0.00780	0.00640	0.00542	0.00416	0.00253	0.00197	0.00111
t, °C	T, Abs.	$\ln(1/\rho)$	$\ln(1/\rho)$	$\ln(1/\rho)$	$\ln(1/\rho)$	$\ln(1/\rho)$	$\ln(1/\rho)$	$\ln(1/\rho)$	$\ln(1/\rho)$	$\ln(1/\rho)$	$\ln(1/\rho)$
−136.5	136.7	0.2637[a]									
−90	183.2	0.3206[b]	0.2564[b]								
−50	223.2	0.3699[b]	0.2984[b]	0.2760[b]	0.2580[b]						
−30	243.2	0.3963[b]	0.3208[b]	0.2968[b]	0.2780[b]						
−10	263.2	0.4234	0.3443	0.3195	0.3000	0.2714	0.2513[c]				
20	293.2	0.4679	0.3799	0.3530	0.3317	0.3008	0.2793	0.2510[d]			
50	323.2		0.4183	0.3883	0.3645	0.3313	0.3080	0.2777	0.2388[e]		
100	373.2		0.4912	0.4541	0.4259	0.3857	0.3588	0.3241	0.2804	0.2657	0.2385[f]
150	423.2				0.4966	0.4474	0.4149	0.3740	0.3237	0.3069	0.2772
200	473.2					0.5197	0.4779	0.4289	0.3696	0.3498	0.3170
250	523.2							0.4912	0.4189	0.3960	0.3594
300	573.2							0.5644	0.4739	0.4464	0.4035

[a] J. Timmermans, Bull. Soc. Chim. Belges **26**, 205 (1917).
[b] R. W. Dornte and C. P. Smyth, J. Am. Chem. Soc. **52**, 3546 (1930).
[c] Extrapolated from −5.4°C.
[d] Extrapolated from 22.0°C.
[e] Extrapolated from 62.0°C.
[f] Extrapolated from 110.0°C.

DETERMINATION OF THE VOLUME PER GRAM OF MOLECULES

The volume of a gram of a substance is the reciprocal of its density. Our problem was to devise the most accurate method possible of extrapolating our specific volumes (reciprocal densities) to absolute zero. After considerable study it was discovered that when the logarithm of reciprocal density was plotted *vs* reciprocal molecular weight in the homologous series of normal alkanes, a family of straight lines resulted—one line for each temperature of measurement. Such a family of lines is represented by

$$\ln(1/\rho)=a/m+b. \tag{8}$$

Where ρ=density, m=molecular weight, and a and b=functions of temperature alone. The plot of Eq. (8) is shown in Fig. 1. The data from which this plot is made are shown in Table I which includes some results of measurements by others. The agreement is seen to be good except for a few points at the lower molecular weight end of the higher temperature lines.

Empirical equations defining a and b as functions of T took the form of

$$\ln a=C_1T+C_2 \tag{9}$$

and

$$b=C_3T^{C_4}+C_5. \tag{10}$$

The values of the constants were found to be: $C_1=0.00275$, $C_2=2.303$, $C_3=0.000182$, $C_4=1.19$, $C_5=0$. When $T=0$, $\ln a=2.303$, $a=10$, $b=0$. Therefore,

$$\ln(1/\rho_0)=10/m \quad \text{or} \quad v_0=e^{10/m}. \tag{11}$$

No significance is attached to the fact that the volume of one gram of *n*-paraffin molecules of infinite molecular weight appears, according to Eq. (11), to equal one cubic centimeter. As a matter of fact the constant C_5 could be read as slightly less than zero, say, −0.005, but the accuracy is not seriously impaired by using the value of zero and the calculations are somewhat simplified.

The extrapolation to absolute zero of the slopes and intercepts of the $\ln(1/\rho)$ *vs* $1/m$ lines is regarded by us as much more reliable than the extrapolation of the data for any single substance because each point on the lines defined by Eqs. (9) and (10) is weighted by virtue of the fact that it represents all molecular weights. Furthermore, the values of the densities at absolute zero for the lower members of the homologous series (those compounds whose critical temperature can be measured) approximately check the values calculated by Goldhammer's rule, and calculated densities also approximately check several other measured values including the lowest measured value of *n*-pentane recorded in the literature.

The calculations according to Goldhammer's rule were made for *n*-pentane, *n*-heptane, *n*-octane, and *n*-nonane. For *n*-pentane and *n*-octane, the results of Mathews[6] were used. For *n*-heptane, the value of C in Eq. (2) was determined to be 0.1123, and for *n*-nonane, 0.1100. The critical temperature for *n*-heptane is 266.9°C (Sydney Young[11]), and for *n*-nonane, 322.8°C (Prudhomme[12]). The calculated densities compared with those obtained by our extrapolation become, then

Densities at Absolute Zero

Molecular weight of compound	72	100	114	128
Density from Goldhammer's rule	0.8751	0.9140	0.9119	0.9250
Density from our extrapolation	0.8706	0.9050	0.9162	0.9250

The lowest measured value found in the literature applicable to the *n*-alkanes used in this study is the density of *n*-pentane determined at −136.5°C by Timmermans.[9] This figure is 0.7682. Our extrapolation gives 0.7671. Since our values of a and b of Eqs. (9) and (10) were determined by the employment of density values representing all molecular weights, we feel that checks obtained on low molecular weight

[11] S. Young, Sci. Proc. Roy. Dublin Soc. **12**, 374 (1910).
[12] M. Prudhomme, J. chim. phys. **18**, 94 (1920).

TABLE II. *n*-Paraffin hydrocarbons. (Observed viscosities, specific volumes, and the reciprocal relative free space.)

$m \rightarrow$			72.15				100.20				114.22				128.25				156.30			
$v_0 \rightarrow$			1.1487				1.1049				1.0915				1.0811				1.0661			
t, °C	T Abs.	$\eta_{obs.}$	$\ln\eta_{obs.}$	$1/\rho$	v_0/v_f	$\eta_{obs.}$	$\ln\eta_{obs.}$	$1/\rho$	v_0/v_f	$\eta_{obs.}$	$\ln\eta_{obs.}$	$1/\rho$	v_0/v_f	$\eta_{obs.}$	$\ln\eta_{obs.}$	$1/\rho$	v_0/v_f	$\eta_{obs.}$	$\ln\eta_{obs.}$	$1/\rho$	v_0/v_f
−10	263.2	0.003114	−5.772	1.5272	3.035	0.006008	−5.115	1.4110	3.610	0.008314	−4.790	1.3765	3.830	0.01150	−4.465	1.3499	4.022	0.02167	−3.832	1.3118	4.338
20	293.2	0.002404	−6.031	1.5967	2.564	0.004180	−5.477	1.4622	3.093	0.005479	−5.207	1.4232	3.291	0.007165	−4.939	1.3933	3.462	0.01186	−4.435	1.3510	3.742
50	323.2					0.003100	−5.776	1.5193	2.667	0.003928	−5.540	1.4746	2.849	0.004968	−5.305	1.4405	3.008	0.007609	−4.878	1.3928	3.263
100	373.2					0.002099	−6.166	1.6343	2.088	0.002554	−5.970	1.5747	2.259	0.003087	−5.781	1.5309	2.403	0.004384	−5.430	1.4706	2.635
150	423.2													0.002136	−6.149	1.6431	1.924	0.002894	−5.845	1.5642	2.140
200	473.2																	0.002048	−6.191	1.6815	1.732
$m \rightarrow$			184.35				240.46				394.74				506.95				899.68			
$v_0 \rightarrow$			1.0557				1.0425				1.0257				1.0199				1.0112			
t, °C	T Abs.	$\eta_{obs.}$	$\ln\eta_{obs.}$	$1/\rho$	v_0/v_f	$\eta_{obs.}$	$\ln\eta_{obs.}$	$1/\rho$	v_0/v_f	$\eta_{obs.}$	$\ln\eta_{obs.}$	$1/\rho$	v_0/v_f	$\eta_{obs.}$	$\ln\eta_{obs.}$	$1/\rho$	v_0/v_f	$\eta_{obs.}$	$\ln\eta_{obs.}$	$1/\rho$	v_0/v_f
−10	263.2	0.03922[a]	−3.239	1.2857[a]	4.591																
20	293.2	0.01883	−3.972	1.3222	3.962	0.04209[a]	−3.168	1.2853[a]	4.292												
50	323.2	0.01118	−4.494	1.3607	3.462	0.02170	−3.830	1.3201	3.754												
100	373.2	0.006001	−5.116	1.4316	2.809	0.01018	−4.587	1.3827	3.064	0.02872	−3.550	1.3236	3.442	0.04884	−3.019	1.3043	3.587	0.1785[a]	−1.723	1.2694[a]	3.916
150	423.2	0.003765	−5.582	1.5142	2.303	0.005984	−5.119	1.4535	2.536	0.01460	−4.227	1.3822	2.877	0.02315	−3.766	1.3592	3.006	0.07144	−2.639	1.3194	3.280
200	473.2	0.002615	−5.947	1.6126	1.896	0.003938	−5.537	1.5356	2.114	0.008856	−4.727	1.4472	2.433	0.01344	−4.309	1.4188	2.557	0.03757	−3.282	1.3731	2.794
250	523.2					0.002785	−5.884	1.6343	1.762	0.005920	−5.129	1.5202	2.074	0.008749	−4.739	1.4859	2.189	0.02292	−3.776	1.4325	2.400
300	573.2					0.002030	−6.200	1.7584	1.456	0.004173	−5.479	1.6062	1.767	0.006083	−5.102	1.5627	1.879	0.01525	−4.183	1.4970	2.081

[a] By extrapolation.

members of the homologous series of *n*-alkanes mean that our method of extrapolation gives reliable estimates of the density at absolute zero of all members of the series over the entire range of the molecular weights used. It is of interest to note in connection with this study that Goldhammer's rule could be employed in conjunction with our densities at absolute zero for estimating the critical temperatures of the higher molecular weight paraffins whose critical constants cannot be measured. Table II presents values of viscosity, specific volume, and reciprocal relative free-space for the even temperatures over the range of our measurements.

DETERMINATION OF THE VISCOSITY—FREE-SPACE FUNCTION

Earlier investigators, notably Batschinski[1] and Macleod[13] who pioneered the relation between viscosity and free-space, attempted to establish a direct relationship between these two variables. Our study disclosed, however, that the relationship is logarithmic rather than direct. Thus, when the logarithm of the viscosity (at various temperatures) of each of our *n*-alkanes is plotted against reciprocal relative free-space, v_0/v_f, straight lines are very precisely determined for each compound in the series over a range of temperatures extending from their boiling points to somewhat less than 100 Centigrade degrees above their freezing points.

Thus, the relationship found by us upon which the viscosity of nonassociated pure liquids depends proves to be

$$\eta = A\, e^{B/(v_f/v_0)} \quad \text{or} \quad \ln\eta = B(v_0/v_f) + \ln A, \qquad (12)$$

where η = coefficient of viscosity, v_f/v_0 = relative free-space for a single substance, and A and B = constants for a single substance. At fixed pressure, v_f/v_0 is a function of temperature only. In a later paper the case where v_f/v_0 varies as one goes from member to member in an homologous series of compounds will be considered.

Equation (12) was applied to all of our normal alkane data and the slopes and intercepts of the "best" straight lines through the points were calculated by trial and error methods. Calculation in this manner was resorted to because Eq. (12) is transcendental with respect to η and conventional least squares calculations could not be applied. The "best" line chosen in each case is the locus of points representing actual viscosities (not logarithms of viscosities) that differ from the measured values by amounts such that the sum of the squares of these deviations is a minimum. Points in the neighborhood of the freezing points of each compound were rejected, limiting the calculations to points clearly falling on the straight lines.

The experimental measurements were made on members of the homologous series of *n*-alkanes from molecular weights 72 to 900 and over a temperature range of

[13] R. B. Macleod, Trans. Faraday Soc. **19**, 6 (1923).

TABLE III. Viscosity of *n*-heptadecane. (Comparison of observed values with those calculated by (1) Free-space and (2) Andrade temperature equations.)

			Free-space equation[a]		Andrade temperature equation[b]	
T	$\eta_{obs.}$	% accuracy	$\eta_{calc.}$	% error	$\eta_{calc.}$	% error
293.2	0.04209	0.2	0.03472	−17.5	0.03621	−14.0
323.2	0.02170	0.2	0.02028	− 6.5	0.02099	− 3.3
373.2	0.01018	0.2	0.01017	−0.1	0.01030	+1.2
423.2	0.005984	0.3	0.006001	+0.3	0.005970	−0.2
473.2	0.003938	0.5	0.003936	−0.1	0.003883	−1.1
523.2	0.002785	0.6	0.002769	−0.6	0.002743	−1.5
573.2	0.002030	0.8	0.002039	+0.4	0.002062	+1.6
Σ[% error]²(373 to 573° range only)→				0.6		6.5

[a] $\ln\eta_{calc.} = 0.9995 v_0/v_f - 7.6505$.
[b] $\ln\eta_{calc.} = 1720/T - 9.1855$.
Coefficients in above equations approximate least square values, as determined by repeated trial and error calculations using only experimental values from 373 to 573°A, inclusive.

from −10° to 300°C. Obviously, the highest temperature of measurement is well above the boiling points of many of the lower members of the series whereas the lowest temperature of measurement is below the freezing points of several of the higher members of the series. Thus, for the temperature range chosen for our measurements, it so happens that heptadecane, $m=240$, provides the greatest spread between the freezing and boiling points, since its freezing point is 21.95° and its boiling point is 302.56°C.[14] We therefore base our case on heptadecane in this instance, although there is no reason to believe that the evidence would be any less convincing had a different temperature range been chosen for our measurements and the compound selected for study which gave the greatest spread under those conditions.

For heptadecane, it was found that all values measured between 100° and 300°C inclusive lay on a straight line, whereas values below 100°C gradually deviated from it, reaching a maximum difference of 16.6 percent at the freezing point, approximately 22°C. Considering only the values between 100° and 300°C inclusive, reference to Table III will show that the deviations of the calculated from the measured viscosity values are well within the accuracy of the measurements. For comparison, the Andrade temperature equation,

$$\eta = Ae^{B/T} \quad \text{or} \quad \ln\eta = B/T + \ln A, \qquad (13)$$

was applied to the data covering the same range of temperatures. These results are also presented in Table III. It is obvious that Eq. (12) defines the relationship well within the accuracy of the measurements, whereas Eq. (13) does not. Furthermore, the sum of the squares of the percent deviations calculated according to the temperature equation is more than ten times as great as the corresponding figure for the free-space equation. The error chart, Fig. 2, makes the comparison evident at a glance.

[14] American Petroleum Institute Research Project 44, Carnegie Institute of Technology, "Selected Values of Properties of Hydrocarbons," Table 20a, June 30, 1948.

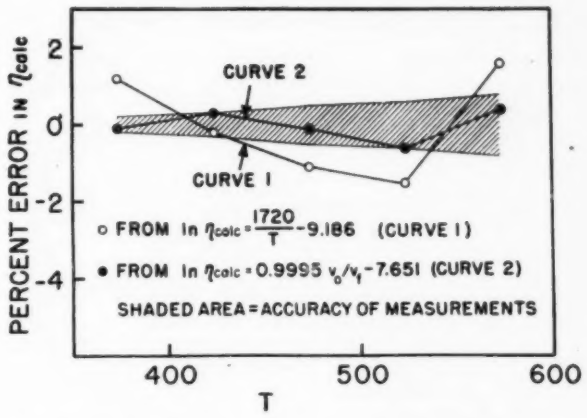

FIG. 2. *n*-Heptadecane. Error curve showing deviations of values calculated by 1, the reciprocal temperature and 2, the reciprocal relative free-space functions compared with the known accuracy of the measurements.

SUMMARY

1. A method of extrapolating the specific volumes (reciprocal densities) of the *n*-alkanes to absolute zero is presented which is believed to give reliable values for all molecular weights studied.

2. It is shown that an equation of the same form as the Andrade temperature equation, but in which relative free-space is the direct variable instead of absolute temperature, defines the viscosity of *n*-heptadecane (as the temperature is varied at constant pressure) as precisely as the accuracy of the measurements themselves except for values measured in the neighborhood of the freezing points. The Andrade equation is not capable of this degree of accuracy over the same range of temperatures.

ACKNOWLEDGMENT

Several individuals contributed to the development of the method for estimating the specific volume at absolute zero. Among these, the author desires particularly to recognize Doctors H. Morawetz and G. J. Dienes, formerly of the Bakelite Company, and T. P. Wilson of the Carbide and Carbon Chemicals Company.

Convection Currents in Porous Media. IV.* Remarks on the Theory

F. T. ROGERS, JR., AND L. E. SCHILBERG
U. S. Naval Ordnance Test Station, Inyokern,† California

AND

H. L. MORRISON‡
North Carolina State College of Engineering, Raleigh, North Carolina

(Received June 14, 1951)

Differential equations for critical stability of a fluid in a porous medium and heated from below are solved by an approximate method not hitherto used. A single formula is obtained for the thermal environment at critical stability, apparently valid over a wide range of conditions, which allows for temperature dependence of viscosity and nonlinear temperature distributions. New experiments are reported in which initial convection has been detected by visual, thermal, and radioactive-trace means. Experimental mean thermal gradients for critical stability deviated from values predicted by the new solution of theory by the following average amounts: visual, 150 percent; thermal, 32 percent; radioisotopic, 11 percent.

THE theory of instability of a fluid in a porous medium and heated from below, has essentially been defined.[1,2] It has even been solved[1,2] with precision for a fluid of constant viscosity in a thermal environment which varies only linearly with vertical distance, the solution being patterned after Rayleigh's for a fluid not in a porous medium.[3] However, efforts toward solution for nonconstant viscosity and for different thermal environments have met with limited success[4] at most, and this paper seeks to advance them somewhat. It is a matter of experimental experience[4] that, if viscosity is temperature dependent and if temperature is suitably nonlinear in vertical distance, then critical stability is more "easily" achieved than simple theory would suggest; and it seems relatively certain[4] that the extended theory is capable, if solved with precision, of accounting for this experience. Prof. O. G. Sutton has recently treated[5] a similar situation with respect to critical stability in CO_2 but not in a porous medium.

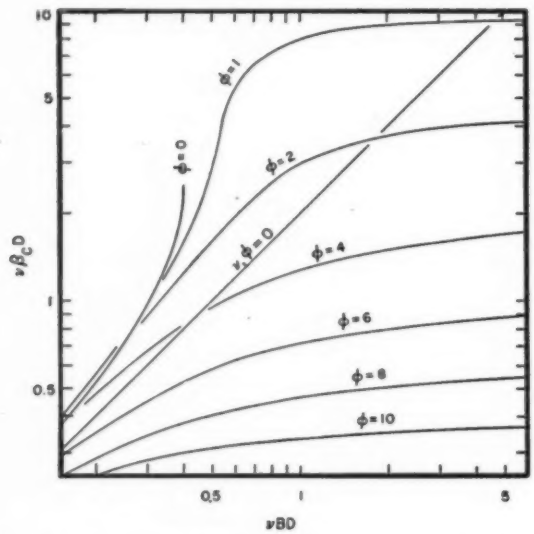

FIG. 1. Relation of the dimensionless quantity, $\nu\beta_c D$, which contains the (negative) mean thermal gradient at critical stability, to the dimensionless νBD according to Eqs. (8). The straight line represents the simple theory in reference 1 and 2.

Improving upon the discussion in reference 4, we denote temperature by

$$\Theta=\Theta_0(l)+T(z,l)+\theta(x,y,z,l), \tag{1}$$

where Θ_0 is bottom ($z=0$) temperature, T is additive in whatever way the equation of heat conduction may require, and $\theta \ll T$ represents the alteration of heat flow which is attributed to fluid motion subsequent to critical stability.[6] We correspondingly modify the potential function[1] to read

$$\Omega=p+g\rho_0 z-g\rho_0\alpha\int T\partial z; \tag{2}$$

p is hydrostatic pressure; g, the acceleration of gravity; ρ_0, density of fluid at $z=0$; and α, coefficient of cubical expansion of fluid relative to porous medium. Repeating the analysis in references 1, 2, and 4, we now find the following system of differential equations,

$$\left.\begin{aligned}(\partial^2 w/\partial z^2)-\nu(\partial T/\partial z)(\partial w/\partial z)-Aw+A\lambda\theta e^{\nu T}=0,\\ h^2[(\partial^2\theta/\partial z^2)-A\theta]=w(\partial T/\partial z).\end{aligned}\right\} \tag{3}$$

Here w is vertical component of flow velocity, $A=l^2+m^2$ is a measure of flow-cell cross section, $\lambda=kg\rho_0\alpha/\mu_0$,

* The theoretical details in this paper were read (F.T.R. and H.L.M.) 20 June 1951 before the Fourth Annual Heat Transfer and Fluid Mechanics Institute, Stanford University, under the title "Remarks on the Theory for Convection in Porous Media," and subsequently communicated by the Institute.

† Post office, China Lake, California.

‡ Present address: U. S. Naval Ordnance Test Station, Inyokern, P. O. China Lake, California.

[1] C. W. Horton and F. T. Rogers, Jr., J. Appl. Phys. **16**, 367 (1945).

[2] E. R. Lapwood, Proc. Cambridge Phil. Soc. **44**, 508 (1948).

[3] Lord Rayleigh, Pil. Mag. **32**, 529 (1916).

[4] F. T. Rogers, Jr., and H. L. Morrison, J. Appl. Phys. **21**, 1177 (1950).

[5] O. G. Sutton, Proc. Roy Soc. (London), **A204**, 297 (1950).

[6] What appears as θ in Eq. (3) and Fig. 1 of reference 4 is really T as here defined.

h^2 is thermal diffusivity, μ_0 is viscosity at $z=0$, and $\nu=d(\ln\mu)/d\Theta$ is a constant for a given fluid. Equations (3), taken together with the boundary conditions, $w(0)=w(D)=0$ and $\theta(0)=\theta(D)=0$, suffice[7] to determine eigenfunctions for $w(z)$ and $\theta(z)$ and corresponding eigenvalues for parameters in T, which are appropriate to that initial flow occurring when critical stability has passed to instability.

Following our recent findings,[8] we take

$$T=-\beta_c D[1-\exp(-z/\tau)]/[1-\exp(-\phi)], \quad (4)$$

where $\beta_c=-(1/D)T_{z=D}$ is the negative mean thermal gradient when flow begins, and τ and $\phi=D/\tau$ are empirical constants largely related to the rate at which heat is applied at $z=0$. More precise forms for T may be had from heat-conduction theory, but we feel that the added manipulative complications are not warranted by present experimental methods.[9]

For $\nu=0$ and $\phi=0$, w and θ eigenfunctions for Eqs. (3) are[1,2] proportional to $\sin sz$, where $s=\pi z/D$, and the least eigenvalue for β_c is $4\pi^2h^2\mu_0/kg\rho_0\alpha D^2$. As the basis of the present treatment we take $w=w_m\sin sz$; even though this is not precisely correct, it has, at least in an integral sense, most of the properties of the true w-eigenfunction. From the second of Eqs. (3), then,

$$\theta=-\{w_m\beta_c D\tau/h^2[1-\exp(-\phi)]\}\cdot H(z;\phi), \quad (5a)$$

where

$$H=\frac{2\pi/\phi}{(1-2\pi^2/\phi^2)^2+4\pi^2/\phi^2}\left[\frac{e^{-\phi}+e^{\pi}}{\sinh\pi}\sinh\frac{\pi z}{D}-e^{\pi z/D}\right.$$
$$\left.+e^{\phi z/D}\left(\frac{1-2\pi^2/\phi^2}{2\pi/\phi}\sin\frac{\pi z}{D}+\cos\frac{\pi z}{D}\right)\right]. \quad (5b)$$

Inasmuch as $w_m\sin sz$ does not satisfy the first of Eqs. (3), we replace this equation by the integral form,

$$\int_0^D T'w''dz-\nu\int_0^D T'^2w'dz-A\int_0^D T'wdz$$
$$+A\lambda\int_0^D T'\theta e^{\tau}dz=0, \quad (6)$$

which it can satisfy.[10] In this way we find four integrals

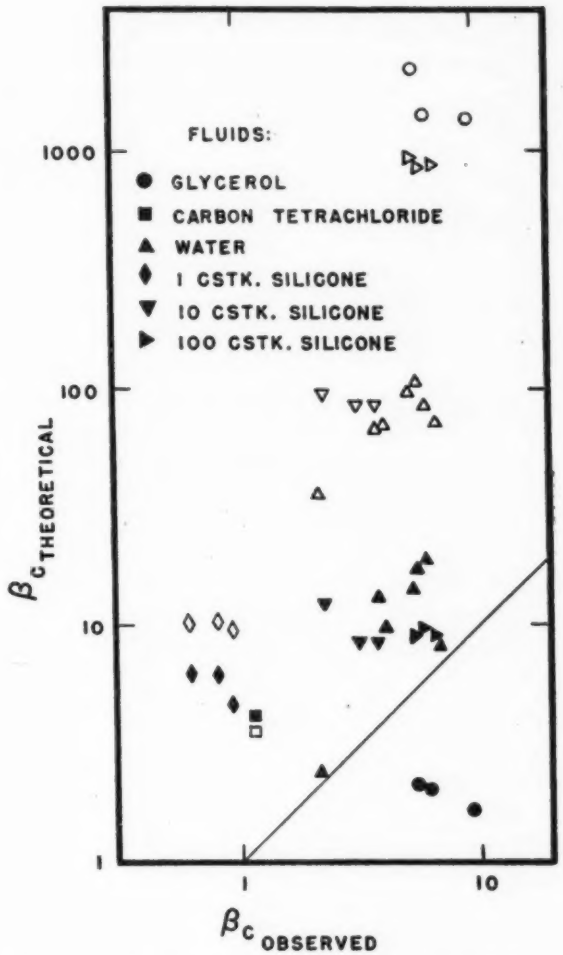

FIG. 2. Comparison of the theory with the visually obtained data reported in reference 4; corrections have been made for new values of thermal diffusivity, as noted in footnote 14. Units are degrees C/cm. Ordinates for filled points are calculated by Eqs. (8), those for open points by references 1 and 2. Points on the straight line represent perfect agreement of theory with experiment.

with the following respective values:

$$\left.\begin{aligned}
&-[w_m\beta_c\phi D/(1+\pi^2/\phi^2)]\coth\tfrac{1}{2}\phi,\\
&[2\pi w_m\beta_c^2\phi/(4+\pi^2/\phi^2)][(1+e^{-2\phi})/(1-e^{-\phi})^2],\\
&[\pi^2 w_m\beta_c/\phi D(1+\pi^2/\phi^2)]\coth\tfrac{1}{2}\phi,\\
&-(w_m\beta_c D^2\phi^2 e^{-\phi/8}/\pi^3h^2)(0.59e^{-\nu\beta_c D/1.5}\\
&\qquad+0.41e^{-\nu\beta_c D/3.7}).
\end{aligned}\right\} \quad (7)$$

The last of these was obtained in the form shown, by numerical integration, and by fitting the functions used to the numerical values.

[7] Attention is called to the fact that Eq. (6) in reference 4 should not be read as equal to zero.

[8] See, for example, F. T. Rogers, Jr., and L. E. Schilberg, J. Appl. Phys. **22**, 233 (1951).

[9] Equation (4) represents experimental data somewhat better than the form $\theta_1\sin\pi z/D+\theta_2\sin 2\pi z/D$ suggested in reference 4, and much better than the $\theta_m\sin\pi z/D$ used therein.

[10] Prof. L. M. Grossman of the University of California has pointed out (reference *) that an alternative procedure exists, in which Eqs. (3) may be transformed into Fredholm integral equations which may then be solved numerically. We wish to point out beyond this, that Eqs. (3) have enough in common with the Sturm-Liouville system as to render them largely soluble by variational means. Either of these alternative methods would be much more rigorously correct than the one used in this paper; on the other hand, the present method yields results which are in excellent agreement with experimental findings, and is certainly simple.

Note added in proof: Dr. W. M. Whyburn has pointed out to the authors that the procedure used in Eqs.(5)–(7) represents the beginning of successive approximations after the method of Picard.

TABLE I. Data obtained in new tests of initial convective flow of water ($\nu = 0.0142°C^{-1}$) in sand.

No. of test	D (cm)	$10^8 k$ (cgs)	ϕ	μ_0 (poise)	h^2 [a] (cgs)	νBD (cgs)	β_c(°C/cm) Eqs. (8)	Visual	Thermal	P-32
...	~10	~250	...	...	...	...	...	...	...	[b]
N-8[c]	11.7	256	14.6	0.0064	0.0031	1.07	1.14	2.42	1.15	0.97
N-9	13.1	433	13.1	0.0058	0.004	0.66	1.34	2.15	1.28	1.23
N-10	12.2	433	8.7_1	0.0065	0.004	0.79_5	2.43	1.22	1.40	[d]
N-11	12.2	433	6.4_2	0.0064	0.004	0.79	3.64	1.13	1.89	[d]
N-12	11±.5	433	11.6	0.0062	0.0027	0.56_8	1.81	2.40	1.86	1.75
N-13	10.3	433	10.8_5	0.0058	0.0036	0.75_8	2.09	3.02	1.96	1.95
N-14	11.9	433	12.1_5	0.0057	0.0038	0.68	1.51	2.66	2.62	1.80
N-15	10.6	433	8.8_5	0.0059	0.005	1.04	2.78	2.56	1.76	[e]
N-16	11.4	433	8.2_0	0.0050	0.006	0.98_5	2.81	3.44	2.53	2.22
N-17	11.2	433	9.3_4	0.0058	0.005	0.96_7	2.48	3.04	1.57	2.35
N-18	11.5	433	8.5_9	0.0060	0.004	0.77_9	2.27	2.53	1.74	2.23
N-19	10.6	433	9.6_4	0.0052	0.004	0.73_2	2.42	3.18	3.00	2.61
Average of percent deviations of theory:								150	32	11

[a] Method of Penrod, J. Appl. Phys. **21**, 425 (1950).
[b] Zn-65 used to verify nonsuitability of gamma-activity.
[c] Counter tube outside of vessel.
[d] Excessive settling during initial convective flow.
[e] Inoculation in contact with counter wall.

Combined, Eqs. (6) and (7) yield a formula which may be taken to determine the (negative) mean thermal gradient at critical stability, in terms of ϕ, ν, D, and $B = 2\pi^2 h^2 \mu_0 / kg\rho_0 \alpha D^2$:

$$\nu\beta_c D \cdot K(\nu\beta_c D) - \nu BD \cdot L(\phi)[1 - \nu\beta_c D \cdot M(\phi)] = 0, \quad (8a)$$

where

$$\left.\begin{aligned} K &= 0.59e^{+\nu\beta_c D/1.5} + 0.41e^{-\nu\beta_c D/3.7}, \\ L &= [\phi e^{-\phi/8}/(1+\phi^2/\pi^2)] \coth \tfrac{1}{2}\phi, \\ \text{and} \\ M &= [\phi^2(1+\phi^2/\pi^2)/\pi^2(1+4\phi^2/\pi^2)] \coth\phi. \end{aligned}\right\} \quad (8b)$$

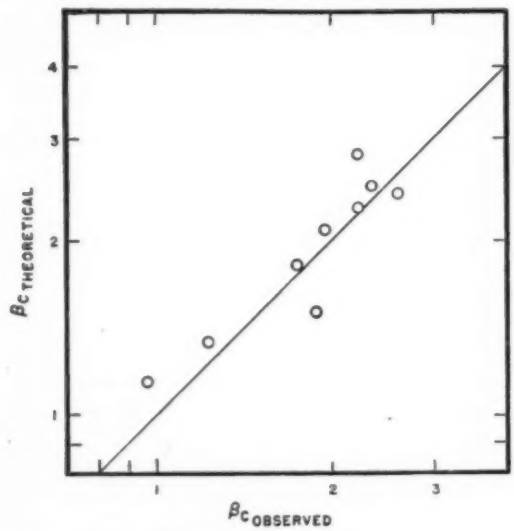

FIG. 3. Comparison of the theory with those new data in Table I which were obtained by radioisotopic-trace means. Units are degrees C/cm. A similar plot of the corresponding visual data shows scatter comparable to that in Fig. 2, while a plot of points representing thermally obtained data is rather like Fig. 3 but with somewhat greater scattering. Points on the straight line represent perfect agreement of theory with experiment.

Figure 1 illustrates Eqs. (8) graphically. Clearly,

$$\lim_{\nu BD \doteq 0} \nu\beta_c D/\nu BD = 2,$$

so that Eqs. (8) converge to solutions previously obtained,[1,2] under appropriate conditions. Moreover,

$$\nu\beta_c D|_{\nu BD > 1} \cong \text{fn. } (\phi),$$

a result demonstrated previously in different form.[4] That

$$\lim_{\nu BD \doteq \infty} \nu\beta_c D \text{ is finite,}$$

is a definite limitation to Eqs. (8), although it does not seem (see subsequently) to be operative in experimental experience to date.

In searching for data of increased reliability and precision, for use in testing the validity of Eqs. (8), we have carried out a new series of tests, using water in sand. The techniques are discussed elsewhere.[10,11,12] Briefly, they have involved the determination of initial convection for each of twelve tests, by three means: visual observation of dissolved dye,[4] significant alterations in[10] $d\Theta_0/dt$, and changes[10] in counting rate of a small Geiger counter located near a radioactive inoculation[13] of fluid. References 11 and 12 should be consulted for typical charts of test records which were obtained; in particular, Fig. 2 of reference 11 illustrates the choice which we have made for T in Eq. (4). Table I presents all pertinent reduced data.

Two bodies of data are thus available for comparison with the theory embodied in Eqs. (8); those reported in

[10] F. T. Rogers, Jr., and H. L. Morrison, Bull. SE Sec. Am. Phys. Soc. (1950), p. 10.
[11] F. T. Rogers, Jr., and L. E. Schilberg, J. Appl. Phys. **22**, 233 (1951).
[12] F. T. Rogers, Jr., and L. E. Schilberg, Nucleonics (to be published).
[13] The active material, $H_3P^{32}O_4$, was furnished by the Oak Ridge National Laboratory under authorization number 5849 of the AEC.

reference 4 were obtained by visual methods by one group of observers, and those in Table I were obtained independently. Figure 2 compares the earlier data[14] with Eqs. (8) and with the simple theory.[1,2] Figure 3, on the other hand, compares the new data as obtained by radioactive trace means, with Eqs. (8); the new visual data accord about as well with Eqs. (8) as do the points shown in Fig. 2, while the thermal data are of intermediate accuracy in comparison with Eqs. (8), for which reasons these two groups are not plotted. Figure 2 shows that Eqs. (8) agree with experiment as well as do the more complicated and fragmentary formulas in reference 4. Figure 3 shows that Eqs. (8) are in very good agreement indeed with experimental data obtained with the most sensitive experimental method, namely, the radioisotopic, based upon the beta-active P^{32} tracer.

Quantitatively, the summaries of average deviations of theory from experiment, listed in Table I, are in satisfactory agreement with experience. The 11 percent A. D. relative to radioisotopically determined initial flow reflects the fact that these determinations were generally the most prompt, while the 150 percent value for visual determinations is in accord with the facts that visual evidences of flow were generally most delayed and most difficult to detect. We feel that the 32 percent based upon $d\Theta_0/dt$ is probably capable of considerable reduction, and probably represents nonoptimum location of thermocouples.

[14] New values of thermal diffusivities for the data in reference 4 have been adopted on the basis of findings in Table I and of reexaminations of the few sets of original data capable of yielding h^2. For tests with glycerol, $h^2=0.005$ cgs.; CCl_4, 0.0025; H_2O and 1-centistoke silicone, 0.005; and 10- and 100-centistoke silicone, 0.004. It should be borne in mind that μ_{Av} is used rather than μ_0 in comparing data against the simple theory.

JOURNAL OF APPLIED PHYSICS VOLUME 22, NUMBER 12 DECEMBER, 1951

Dosimetry of X-Rays and Gamma-Rays by Radiophotoluminescence

JAMES H. SCHULMAN, ROBERT J. GINTHER, AND CLIFFORD C. KLICK
Naval Research Laboratory, Washington, D. C.

AND

RAYMOND S. ALGER AND ROBERT A. LEVY
Naval Radiological Defense Laboratory, San Francisco, California

(Received May 31, 1951)

The effects of high energy radiation on the luminescence properties of solids are surveyed. Of the four effects considered—radiophotoluminescence, radiophotostimulation, radiothermoluminescence, and the "killing" of luminescence by x-rays or gamma-rays—the first effect is shown to have advantages in principle over the others as a basis for dosimetry.

The absorption, excitation, emission, sensitivity, energy dependence, and stability characteristics of a radiophotoluminescent Ag-activated phosphate glass are described. It is shown that dosage measurements can be made with this material, employing a simple fluorophotometer, from 10 roentgens to a few thousand roentgens of gamma-rays. By proper shielding, such a dosimeter element can be made reasonably independent of energy. The dosage indication obtained is quite stable with time and is not seriously affected by exposure of the glass to visible or ultraviolet light or to temperatures in the range of $-70°$ to $+100°$C. Because of its sensitivity range and its stability over a wide range of ambient conditions, the dosimeter appears to be particularly suited for monitoring personnel that may be exposed to rather high doses of gamma-rays, such as may be encountered in A-bomb explosions.

INTRODUCTION

THE absorption of radiant energy by matter can result in dissipation of the absorbed energy as heat, in re-radiation of the absorbed energy as luminescence, or in the production of photochemical changes in the absorbing material. The occurrence of photochemical changes on irradiation of a solid is most frequently manifested by a change in its absorption spectrum as, for example, in the formation of *F*-bands by treatment of the alkali halides with x-rays or gamma-rays. A number of solids, on exposure to such high energy radiations, undergo photochemical changes that alter not only their absorption spectra but their luminescent properties as well. An alteration of the ultraviolet-excited luminescence spectrum of numerous organic compounds by exposure to cathode-rays or gamma-rays was first noted by Goldstein.[1] Similar effects in minerals and synthetic inorganic solids were observed by Przibram, and were studied extensively by him and his students at the Vienna Institut für Radiumforschung from about 1920.[2] The purpose of this paper is twofold: first, to discuss a number of the most prominent effects of high-energy radiation on the luminescence of solids, and second, to describe a proposed system of dosimetry based upon one of these effects.[3,4]

[1] E. Goldstein, Physik Z. **13**, 188 (1912).

[2] K. Przibram (Review of work done at Institut f. Radiumforschung, Vienna), Z. Physik **20**, 196 (1924); **41**, 833 (1927); **44**, 542 (1927); **68**, 403 (1931); **102**, 331 (1936).

[3] Schulman, Ginther, and Evans, U. S. Patent No. 2,524,839, October 10 (1950).

[4] Weyl, Schulman, Ginther, and Evans, J. Electrochem. Soc. **95**, 70 (1949).

The effects of high energy radiation on the luminescence of solids are many and varied, and no standard nomenclature has been adopted to describe them all. We owe to Przibram the term "radiophotoluminescence" which has been generally applied to the alteration of photoluminescence properties by treatment with high energy radiations. He initially used this term to characterize the increase in ultraviolet-excited afterglow observed in some materials after they had been exposed to gamma-rays.[5] As his researches continued, Przibram recognized that the alterations of luminescence properties provoked by gamma-ray irradiation could be more far-reaching than merely a change in the afterglow characteristics, and could in effect consist of the actual creation of new luminescent centers by the photochemical action of the gamma-rays. He therefore redefined "radiophotoluminescence" to describe the phenomenon where a material, originally non-luminescent under ultraviolet or visible light, is made responsive to such excitation by pretreatment with gamma-rays or x-rays.[6] This definition of radiophotoluminescence, however, made no distinction between the creation of new stable luminescent centers, which are not destroyed by the long wavelength radiation that is subsequently employed to excite them, and the creation of centers whose subsequent destruction by long wavelength radiation is necessary to produce luminescence. The designation "radiophotoluminescence" will be restricted in this paper to the first of the aforementioned cases. The term "radiophotostimulation" will be used in this paper to describe the latter case, because of its similarity to the well-known effects observed on the excitation and stimulation of infrared stimulable phosphors. It is true, of course, that even the "stable" centers created by high-energy radiation in radiophotoluminescent materials may slowly be destroyed by reversal of the photochemical reaction that generated them, and that the action of exciting long wavelength radiation on these centers may even accelerate this destruction to some extent. However, in such systems this destruction of the centers is to be regarded as an undesirable side effect which is not involved in the luminescence emission, whereas in radiophotostimulable materials the destruction of the centers by the stimulating light is a necessary part of the process.

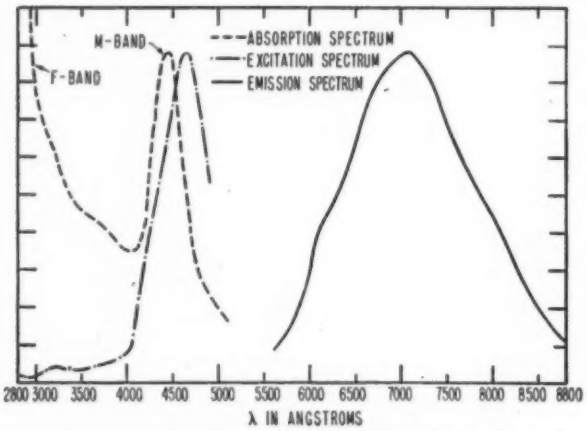

FIG. 1. Absorption, excitation and emission bands in x-rayed lithium fluoride.

Another phenomenon, recognized by Przibram and called by him "radiothermoluminescence," is the production of thermoluminescent properties in a solid by treatment with x-rays or gamma-rays. The effect is basically the same as the thermoluminescence observed in many phosphors after excitation by ultraviolet or visible light. In view of the extensive literature on thermoluminescence and "glow" curves of phosphors,[6a] a detailed discussion of radiothermoluminescence is not required here.

The final major effect of high energy radiation on luminescence that we shall mention is the reverse of radiophotoluminescence, namely, the destruction of the response of a phosphor to light that normally excites its luminescence. The deterioration of phosphors under ultraviolet or cathode rays is a well-known phenomenon. In most cases, however, it is not altogether clear that the "killing" effect of the destructive radiation is a photochemical change involving only the phosphor. For example, water vapor plays an important role in the deterioration of ZnS phosphors,[7] and chemical effects involving the active gases or reaction with the glass walls may play a part in the brightness loss of phosphors in fluorescent lamps.[7,8] Cases have been found, however, where the "killing" of luminescence response by high energy radiation is definitely due to photochemical changes in the phosphor itself.[9,10]

RADIOPHOTOLUMINESCENT SYSTEMS

Upon irradiation with x-rays or gamma-rays the alkali halides acquire new absorption bands lying to the long wavelength side of their fundamental lattice absorption edge.[11] The visible discoloration produced in most of the alkali halides by moderate x-ray exposure is called the "*F*"-band.* More intense irradiation produces additional absorption bands at longer wavelengths than the *F*-band, these new bands being desig-

[5] K. Przibram and E. Kara-Michailova, Wien. Ber. IIa, **131**, 511, (1922).

[6] K. Przibram, Wien. Ber. IIa, **134**, 233 (1925).

[6a] G. R. Fonda and F. Seitz, Editors, *Solid Luminescent Materials* (John Wiley & Sons, Inc., New York, 1945).

[7] H. W. Leverenz, *Luminescence of Solids* (John Wiley & Sons, Inc., New York 1950), pp. 376–377, 418–419, 448–452.

[8] W. Forsythe and E. Adams, *Fluorescent Lamps* (Murray Hill Books Inc., New York, 1948), p. 196.

[9] Schulman, Ginther, and Evans, U. S. Patent No. 2,506,749, May 9 (1950).

[10] Schulman, Ginther, Klick, and Evans, Phys. Rev. **76**, 459 (1949).

[11] N. F. Mott and R. W. Gurney, *Electronic Processes in Ionic Crystals* (Oxford University Press, London, 1940), pp. 111–113.

* The *F*-band of LiF lies entirely in the ultraviolet, with a peak at 2570A (see reference 12). Visible coloration produced on x-irradiation of LiF is due to a band at longer wavelengths than its *F*-band.

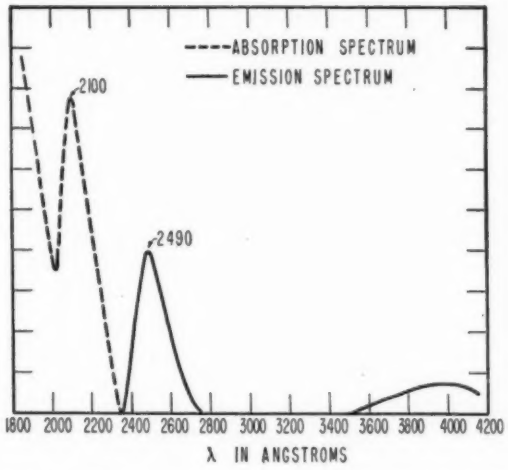

FIG. 2. Absorption and emission bands in NaCl:Ag (after Kato).

nated by *M*, *R*, *N*, etc.[12] There is considerable evidence that the "center" giving rise to the "*F*" absorption band of an alkali halide is an electron trapped at a vacant anion position in the crystal.[11,13] In the formation of this center by x-irradiation an electron must be stripped off one of the ions of the crystal, presumably a halide ion, leaving a "positive hole" (i.e., neutral atom). Absorption of light by the *F*-center at room temperature ejects the electron from its trap and allows it to wander through the crystal giving rise to photoconductivity. If the freed electron recombines with a positive hole, a normal anion is formed again. Mott and Gurney[14] have suggested that, at low temperatures, absorption of light in the *F*-band causes excitation of the *F*-centers, rather than complete ionization, and that the excited electrons in the *F*-centers return to the ground state with the emission of luminescent near infrared radiation. If this prediction were correct, one would have in the alkali halides perhaps the simplest radiophotoluminescent materials—x-ray or gamma-ray irradiation of the nonluminescent crystals producing new centers, the *F*-centers, which would be stable at the temperatures in question and which could be excited to luminescence by light absorbed by these centers. Experiment has not verified Mott and Gurney's hypothesis,[15] and this ideal case of radiophotoluminescence does not seem to exist. An example of radiophotoluminescence very similar to this ideal case is found, however, in at least one of the alkali halides, LiF. Although the comparatively simple *F*-center created by x-irradiation of this crystal is nonluminescent, a somewhat more complex but probably similar center, likewise created by the x-ray treatment, was found by Molnar to give a red luminescence† (Fig. 1).[15,16]

The addition of impurities to crystals opens up the possibility of forming, on x-ray irradiation, new types of centers involving the impurities, in addition to the centers formed from the constitutents and defects of the host crystal itself. Thus, while the centers formed on x-irradiation of the pure crystal may be either unstable or nonluminescent, the centers formed from the impurity in the same crystal may be both stable and luminescent, and a radiophotoluminescence may be achieved in this way. Examples of such behavior are the silver-activated alkali halides, typified by NaCl:Ag of low silver content. Of course, NaCl:Ag, when crystallized from the melt, is already a phosphor without any further treatment. However, this luminescence is excited only by short wave ultraviolet in the neighborhood of 2100A, luminescence emission under these conditions consisting of two bands peaking at 2490A and 4000A (Fig. 2).[17] The crystal shows no luminescence under near ultraviolet excitation, in the neighborhood of 3650A. If such a Ag-activated crystal is treated with x-rays, it acquires a yellow coloration due to the formation of *F*-centers, exactly as the pure NaCl crystal does. As with the pure crystal, the *F*-band can be bleached by exposure to light in the *F*-band, the system being apparently returned to its original condition. If the x-rayed and bleached NaCl:Ag crystal is examined under near ultraviolet illumination, however, a very bright orange to yellow fluorescence is observed (Fig. 3). This ability to fluoresce under near ultraviolet radiation is an essentially stable effect as long as the crystal is stored in the neighborhood of room temperature. It is possible to excite the crystal continuously with strong near ultraviolet radiation (15-watt Sylvania

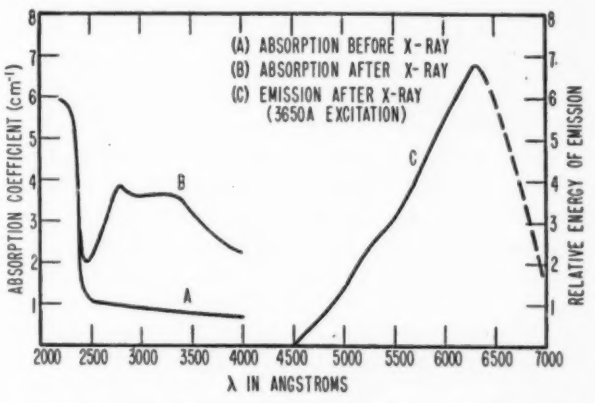

FIG. 3. Absorption and emission bands in x-rayed NaCl:Ag.

[12] J. P. Molnar, thesis (Massachusetts Institute of Technology, 1940), pp. 53–54.
[13] F. Seitz, Revs. Modern Phys. **18**, 384 (1946).
[14] See reference 11, pp. 135–137.
[15] C. C. Klick, Phys. Rev. **79**, 894 (1950).

† This center produces an absorption band between 4100 and 4800A (peak at about 4450A) in x-rayed LiF, and may be the "*M*" center for this material (see reference 16). Seitz (see reference 13), has suggested that the "*M*" center may be an electron trapped at a complex lattice defect consisting of a cation and two anion vacancies.
[16] See reference 12 pp. 69–71.
[17] M. Kato, Sci. Papers Inst. Phys. Chem. Research (Tokyo) **41**, 113 (1943).

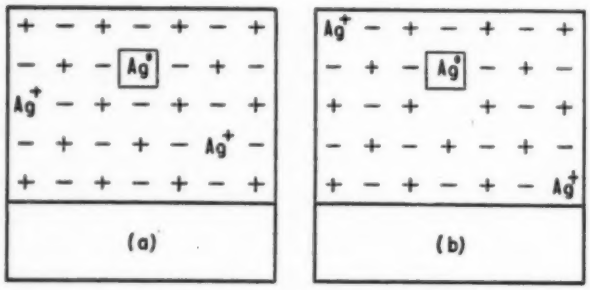

FIG. 4. Possible structure of "atomic silver" centers created by x-irradiation of NaCl:Ag. (a) Electrons trapped at Ag^+-ions occupying normal cation sites. (b) Electrons trapped at Ag^+-ions adjacent to a halogen-ion vacancy.

"Blacklight" lamp with red-purple glass envelope, at a distance of 10 cms) for days without any large loss of its fluorescence brightness.

The excitation and emission bands observed in unx-rayed NaCl:Ag are due to Ag^+-ion, while the new excitation and emission bands found in x-rayed NaCl:Ag are presumably the result of centers containing reduced Ag, or "atomic" silver.[3,4] Such centers are formed when the Ag^+-ions trap electrons that have been liberated in the crystal by absorption of the x-rays. Electrons trapped by the Ag^+-ions are apparently more strongly bound than those trapped at halogen ion vacancies, and the former centers are therefore much more stable than the *F*-centers. The principal effect of light absorption in these centers is evidently not the freeing of the electron and destruction of the center, but rather the raising of the electron to an excited state, from which it can return with luminescence emission. It is not known at present whether these "atomic" silver centers are formed from Ag^+-ions situated at any position in the lattice, or whether they are formed only from Ag^+-ions that happen to be located adjacent to a halogen-ion vacancy. In the latter case the "atomic" silver center would be very closely analogous to the normal *F*-center, with the exception that one of the six cations surrounding the vacancy would be a silver ion. In this case one would expect a stronger binding between the silver-ion and the electron than between the five alkali ions and the electron. The center might, therefore, be considered either as an "atomic" silver center or as a special type of *F*-center. The above two possible positions of the silver traps are illustrated in Fig. 4.

The creation of the relatively stable "atomic" silver centers by the x-ray reduction of Ag-ion, with corresponding changes in the absorption and emission spectra, occurs in other alkali halides, in potassium sulfate, and in various glasses containing silver as an impurity.[3,4] New stable fluorescent centers, emitting in the yellow region of the spectrum under short ultraviolet excitation, can similarly be created by x-ray treatment of NaCl:Cd.[10] Many further examples of this "radiophotoluminescence," involving principally the rare earth impurities in a number of minerals and synthetic crystals, have been described by Przibram in the numerous publications to which reference has already been made.[2]

RADIOPHOTOSTIMULABLE SYSTEMS

As previously indicated, the phenomenon of radiophotostimulation is basically the same as that observed in the well-known infrared stimulable phosphors. An example of such a case is NaCl:Mn.[18] On treatment with x-rays or gamma-rays, NaCl:Mn acquires a yellow discoloration due to the formation of the *F*-band, which for NaCl lies in the blue (peak at 4600A at room temperature). Irradiation of the discolored NaCl:Mn with light in the *F*-band excites an orange luminescence characteristic of Mn^{+2} and at the same time bleaches the *F*-band. The luminescence intensity grows progressively weaker as the irradiation with blue light continues, and finally ceases when the *F*-band has been completely bleached. In this case, at least part of the energy released by the recombination of electrons and holes, is transferred to Mn^{+2}-ions, exciting them to luminescence. In the presence of an activator other than manganese, say Ag^+, the energy of recomination of the electrons and holes can be transferred to this activator, resulting in an ultraviolet emission characteristic of the Ag^+.[19] The blue-green photoluminescence observed by Urbach with various x-rayed alkali halides may similarly be due to an impurity.[20] In the complete absence of any impurity in the crystal, presumably the recombination of electrons and holes under stimulation by blue light could give rise to a luminescence in the ultraviolet, corresponding to the "edge" or resonance luminescence emitted by ZnS and CdS on excitation in their fundamental absorption bands at low temperature,[21] or recombination may take place without the emission of radiation. Kudryavtseva[22] claimed to have found such a far ultraviolet emission on irradiating x-rayed NaCl with light in its *F*-band, but the validity of her results has been questioned by Pringsheim.‡ [23]

[18] E. Jahoda, Wien. Ber. IIa, **193**, 675 (1926).
[19] A. Polonsky, C. R. Acad. Sci. USSR **31**, 543 (1941).
[20] F. Urbach Wien. Ber. IIa, **135**, 149 (1926).
[21] F. A. Kröger, thesis (Amsterdam, 1940).
[22] V. Kudryavtseva, Z. Physik **90**, 489 (1934).

‡ One of the ultraviolet emission bands observed by Kudryavtseva peaked at 2500A. We have not been able to confirm this with pure NaCl. Furthermore, we have found, in agreement with the work of Polonsky (see reference 19), that stimulation of x-rayed NaCl:Ag with light in the *F*-band gives an extremely intense emission at 2500A. This indicates that Kudryavtseva's observations may be due to contamination of her NaCl with a trace of Ag. Kudryavtseva also reports a second, less intense emission band at 1500A on stimulation of x-rayed NaCl with blue light. Pringsheim has shown that light of this wavelength could hardly have been observed by Kudryavtseva with her experimental arrangement.

[23] P. Pringsheim, *Fluorescence and Phosphorescence* (Interscience Publishers, Inc., New York, 1949), p. 658.

SYSTEMS SHOWING KILLING OF LUMINESCENCE BY HIGH ENERGY RADIATION

In addition to creating new stable luminescent centers or filling electron traps in crystals which can later be emptied by long wavelength light to stimulate emission, x-rays and gamma-rays can also exercise a destructive effect on luminescent centers already existing in a phosphor. This can be inferred, of course, from the interpretation given to the observations on NaCl:Ag. The creation of "atomic" silver from Ag^+-ions necessarily involves the "destruction" of the Ag^+-ion as such. The growth of atomic silver absorption and emission bands should thus be paralleled by a decrease in the Ag^+-ion absorption and emission. Although the experimental confirmation of this behavior is not available for this system, similar observations have been made in the systems NaCl:Pb and NaCl:(Pb+Mn).[9,10] NaCl:Pb has absorption bands at 2730A and 2900A due to Pb^{+2}-ion with corresponding emission bands in the near ultraviolet and visible.[17,24,25] X-irradiation of this phosphor, besides producing the usual *F*-band peaking at 4600A, bleaches the ultraviolet absorption bands characteristic of the Pb^{+2}-ion. Because of the second effect, the phosphor no longer luminesces under 2730A or 2900A excitation.[25] It has been postulated[25] that the destruction of the Pb^{+2}-ion is due to its reduction to "atomic" lead by the electrons released by the x-rays, and that the lead in this form shows no ultraviolet absorption in NaCl. When heavy x-ray dosages are used the reduced lead appears as a stain of colloidal lead dispersed in the crystal.§

APPLICATION TO DOSIMETRY

Any one of the above effects of x-rays and gamma-rays may, in principle, be used as a basis for dosimetry. Certain rather obvious practical considerations, however, tend to make the radiophotostimulation and radiothermoluminescence schemes less desirable *a priori* than the other two methods. Dosage determination with a radiophotostimulable phosphor would involve a reading of either the brightness or the light sum under appropriate stimulation. The emptying of electron traps that occurs under stimulating light should, in principle, give lower apparent readings on successive brightness measurements and would completely prevent a repetition of the light sum determination. Furthermore, any accidental exposure of the phosphor to stimulating radiation would tend to exhaust the phosphor and vitiate later readings. Similar limitations apply to the use of a radiothermoluminescent phosphor, in the use of which the trapped electrons are released by heating the phosphor. Here again the dosage can be read only once. These practical disadvantages can be eliminated by use of radiophotoluminescent materials or of phosphors whose luminescence is killed by high energy radiations. Proper choice of such materials should allow repeated reading of the dosage indication, and it should be possible to expose x-rayed specimens to light or to moderately elevated temperatures without introducing excessive error in the subsequent reading of the dosage.

Of the two remaining effects, radiophotoluminescence appeared to hold promise of greater sensitivity for dosimetry than the "killing" effect. In the former case contrast between a weakly luminescent x-rayed sample and a completely nonluminescent reference sample can be increased approximately in proportion to the increase of exciting ultraviolet used for observation, limited only by saturation of the centers. In the latter case contrast of the fluorescence of a slightly "killed" phosphor with that of an un-x-rayed sample cannot be improved proportionately by increase in exciting ultraviolet intensity over that required to yield a reasonable brightness level.

Other practical considerations involved in the choice of a dosimeter material are the ease of reproducible preparation of large quantities of the substance and of fabrication of the material into desirable shapes and sizes. With respect to both of these points it seemed fairly obvious that glass or plastic were to be preferred over crystalline material if the latter had to be prepared in the form of large single crystals.

A silver-activated potassium-barium-aluminum phosphate glass, the radiophotoluminescence of which had previously been suggested as a basis for dosimetry,[3,4] appeared to fulfill most of the *a priori* requirements for this purpose. The mechanism of the effect in this glass is presumably the same as that described for NaCl:Ag, namely, the x-ray induced photochemical reaction $Ag^+ \rightarrow Ag^0$, with subsequent excitation of the Ag^0 by near ultraviolet. A detailed study of the properties of this glass was accordingly undertaken.

PREPARATION AND PROPERTIES OF RADIOPHOTOLUMINESCENT GLASS

Preparation

The glass samples were prepared by melting together the component metaphosphates at 1200°C in fused silica crucibles, casting the melt into metal molds, annealing, and finally cutting, grinding, and polishing them to the desired size.

The base glass is of the following composition:

[21] A. Arsanjewa, Z. Physik **57**, 163 (1929).

[25] Schulman, Ginther, and Klick, J. Opt. Soc. Am. **40**, 854 (1950).

§ The "killing" effect of x-rays on luminescence may be made more striking to the unaided eye by employing NaCl:(Pb+Mn) instead of NaCl:Pb (see reference 10). NaCl:(Pb+Mn) is a sensitized phosphor, that is, the energy absorbed by the lead upon irradiation with 2730A–2900A ultraviolet, is transferred in large part to the Mn^{+2}-ion [Schulman, Burstein, Evans, Ginther, and White, Phys. Rev. **76**, 178 (1949)]. This ion luminesces in the visible with a characteristic yellow-orange color, in contrast to the luminescence of Pb^{+2}, which is principally in the ultraviolet. The orange luminescence of NaCl:(Pb+Mn) under 2730A excitation is very markedly diminished by the x-ray exposure, which changes the Pb^{+2}-ion to Pb^0, thus eliminating the ultraviolet excitation bands of the crystal.

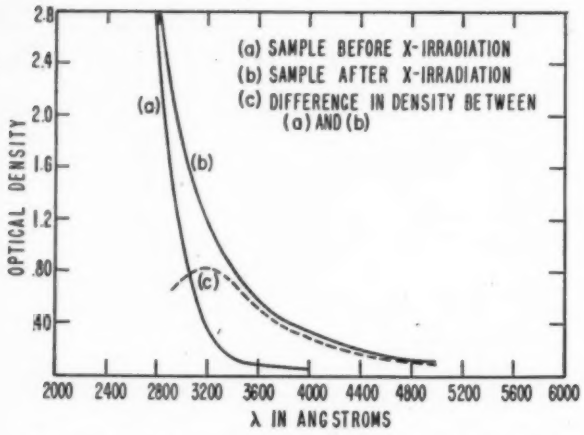
(a) SAMPLE BEFORE X-IRRADIATION
(b) SAMPLE AFTER X-IRRADIATION
(c) DIFFERENCE IN DENSITY BETWEEN (a) AND (b)
OPTICAL DENSITY
λ IN ANGSTROMS

FIG. 5. Absorption spectrum of silver-activated phosphate glass before and after x-irradiation.

$Al(PO_3)_3$, 50 percent; $Ba(PO_3)_2$, 25 percent; KPO_3, 25 percent. In this base glass up to 16 percent $AgPO_3$ has been incorporated. A commercial grade of aluminum, barium, and potassium metaphosphates as supplied for glass manufacture has been used. However, some selection of raw material is required. Titanium and iron have been found to have a deleterious effect upon the radiophotoluminescent properties of the glass. Manganese impurity should be particularly avoided, since it produces a permanent red luminescence which is similar to that of the "atomic" silver formed by the x-radiation. In order to maintain reproducibility it is desirable to take the usual precautions as to impurities and contamination observed in phosphor preparation. With proper care in selection of raw materials it appears that the sensitivity of the glass can be reproduced within ±5 percent.

Optical Properties

The absorption spectrum of the untreated 8 percent silver-activated phosphate glass is shown in Fig. 5 along with that of the same glass after exposure to x-rays. It may be seen that the effect of the x-rays is to increase the long wavelength tail of the base glass absorption. By subtracting the absorption of the unirradiated glass in this region from the absorption curve of the x-rayed glass, it is shown that the x-rays cause the growth of a new absorption band, which peaks at about 3200A and extends into the visible. On strong x-irradiation the glass accordingly acquires a distinctly yellow color. Figure 6 is a plot of the intensity of the new absorption band as a function of x-ray dosage.

The excitation spectra of the untreated and x-rayed 8 percent Ag glass are shown in Fig. 7. To obtain these curves, the samples were irradiated with monochromatic light from a Beckman spectrophotometer using a hydrogen lamp source, and viewed by a 1P21 photomultiplier through an appropriate Corning glass filter. The data obtained in this way constitute only rough excitation spectra, since they are uncorrected for the spectral

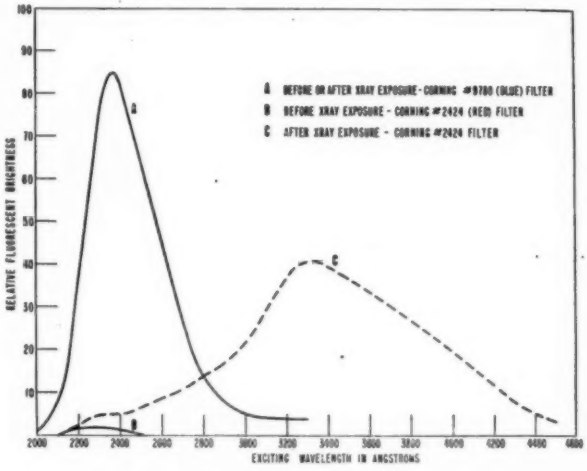
A BEFORE OR AFTER XRAY EXPOSURE - CORNING #9780 (BLUE) FILTER
B BEFORE XRAY EXPOSURE - CORNING #2424 (RED) FILTER
C AFTER XRAY EXPOSURE - CORNING #2424 FILTER
RELATIVE FLUORESCENT BRIGHTNESS
EXCITING WAVELENGTH IN ANGSTROMS

FIG. 7. Excitation spectra of silver-activated phosphate glass before and after x-irradiation.

energy distribution of the lamp and the transmission of the monochromator. As shown in the figure, the untreated glass luminesces on excitation by light lying in the region of 2400A. By visual observation and by interposing various filters between the phototube and the glass sample, it was established that this luminescence lies principally in the blue region of the spectrum. After x-irradiation, the luminescence excited by short wavelength ultraviolet is not significantly diminished in intensity, but a new 3300A-peaked excitation band appears practically coincident with the new absorption band. Excitation in this new band gives an orange-red luminescence.

The spectral distribution of the luminescence of x-rayed samples of the glass of various silver contents under near ultraviolet excitation (3650A) is shown in Fig. 8. There is a greater component of green and blue in the emission of the x-rayed preparations of higher silver concentration.

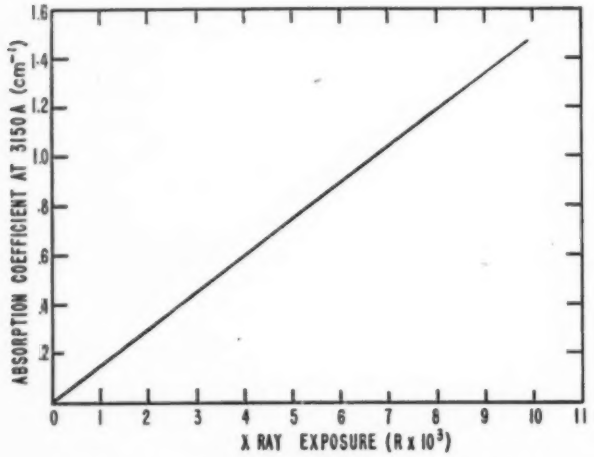

FIG. 6. Growth of near-ultraviolet absorption band in silver-activated phosphate glass with x-ray dosage.

The temperature coefficient of luminescence efficiency of the x-rayed glass was measured between 0° and 70°C and found to be −0.7 percent of the intensity at 25°C per degree Centigrade. This temperature dependence is fairly small, and can be neglected for the most part. If desired, a luminescent reference standard with the same temperature coefficient of luminescence efficiency as the phosphate glass can be employed in the fluorophotometer to compensate automatically for this effect.

Sensitivity to X-Rays

Figure 9 illustrates the relative sensitivities of glasses of different silver concentrations to x-irradiation. To obtain this data plaques of glass powder were x-rayed and their fluorescence was measured in a modification of the fluorophotometer described by Price[26] and illustrated in Fig. 10. Light from a GE AH-4 lamp is filtered through two Corning 5860 filters and focused on the glass plaque. Fluorescent light from the plaque is received by a 1P21 photomultiplier through a Corning 3480 filter. A 30-μ ampere meter with an Ayrton shunt is used to measure the photocurrent. The dynode voltage on the photomultiplier is set to give a fixed current with a luminescent reference standard‖ and then the sample under test is inserted in place of the standard. The glass containing 8 percent of silver was found to exhibit the greatest sensitivity when its luminescence was measured through the 3480 filter, but other filters can be chosen to favor the higher silver concentrations. It may be seen from Fig. 9 that the luminescence intensity increases fairly linearly with x-ray dosage.

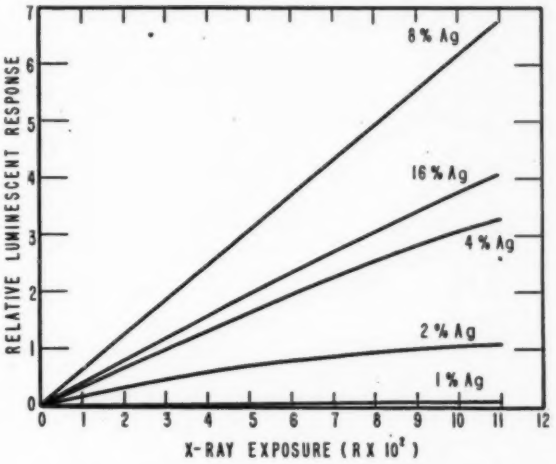

FIG. 9. Sensitivity of silver-activated phosphate glass to x-rays as function of silver concentration.

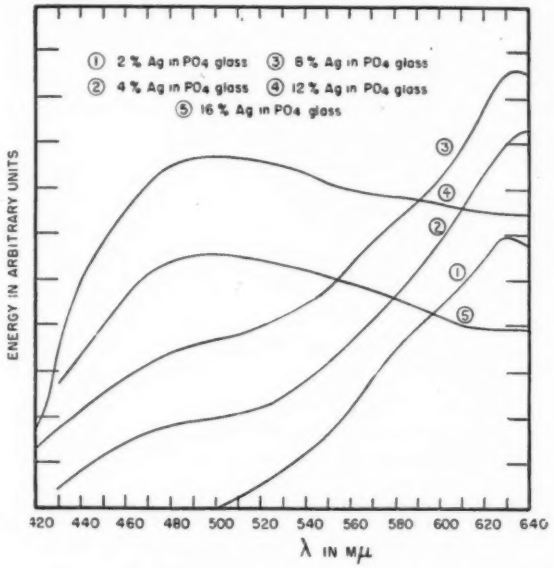

FIG. 8. Spectral distribution of luminescence of silver-activated phosphate glass as function of silver concentration.

The dependence of the luminescence intensity on the wavelength of the x-rays is given in Fig. 11. For this purpose plaques of ground glass, containing 12 percent silver, were exposed to a dose of 500±25 roentgens of x-rays of various effective energies,¶ and the lumines-

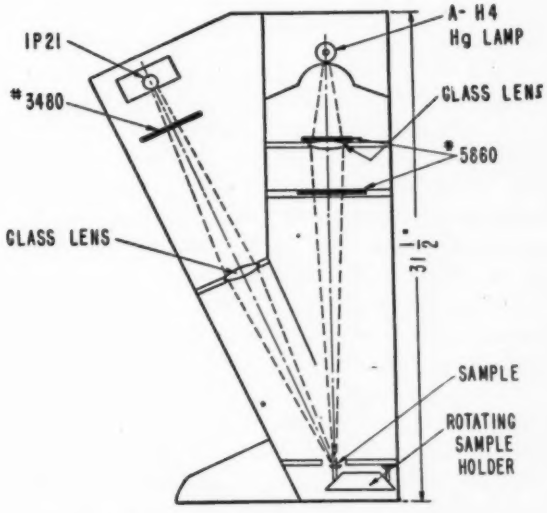

FIG. 10. Schematic diagram of fluorophotometer.

[26] G. R. Price, *The Design and Construction of Sensitive Fluorophotometers*, Part I, Principles, AECD-2677, April (1948).

‖ At NRDL a reference standard of ZnS:Ag embedded in lucite was used. At NRL a standard of a red-luminescing ZnO:Pr phosphor was used.

¶ The effective energies in the figure were calculated from measured half-value layers of copper and the absorption coefficient of copper as a function of monochromatic x-ray energy [J. A. Victoreen, J. Appl. Phys. **19**, 855 (1948)]. The half-value layers were determined for a given accelerating voltage and various beam filters as the thickness of copper required to reduce the x-ray beam intensity by one-half. The effective energy was then taken as the energy of a beam of monochromatic x-rays having the same half-value layer as calculated from the absorption coefficient of copper for this wavelength of x-ray. The exposure to 1.2 Mev radiation was made with a Co^{60} source.

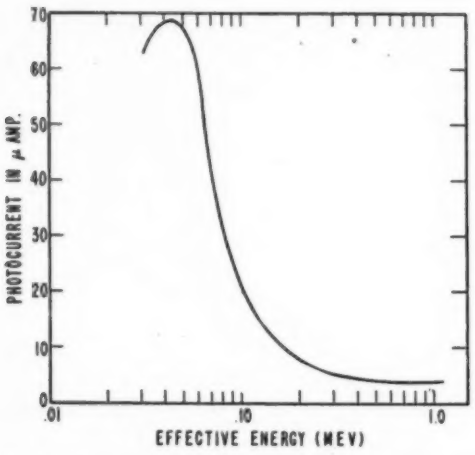

FIG. 11. Dependence of sensitivity of silver-activated phosphate glass on x-ray energy.

cence measured with the arrangement previously described. The dependence of the sensitivity of the glass on the energy of the x-rays is quite great, as one might expect from x-ray absorption considerations. In the region of low x-ray energies, corresponding to photoelectric absorption of the x-rays, the glass is much more sensitive than in the region of higher x-ray energies, where absorption is principally by the Compton effect. This energy dependence can be reduced to ±20 percent over the range of 100 kv to 1.2 mev by encasing the glass in appropriate metal filters.

Stability

In the use of a dosimeter under field conditions a number of contingencies may arise which, ideally, should have no effect on the dosage indicated by the device. For example, considerable time may elapse between the exposure to high energy radiation and the reading of the dosage, and during this time the exposed dosimeter element may be subjected to temperatures that are considerably above or below body temperature, or to bright sunlight. In the case of the radiophotoluminescent dosimeter, the glass is necessarily exposed to near ultraviolet light in order to excite its fluorescence, and this ultraviolet light should not destroy the luminescent centers appreciably. Tests of the stability of the luminescent centers in the Ag-activated phosphate glass as a function of storage time, temperature, and exposure to sunlight and ultraviolet were accordingly undertaken.

Figure 12 shows the luminescence intensity as a function of time for 8 percent Ag-activated phosphate glass plates exposed at room temperature to 150 r of 67.5 kv effective x-rays at a rate of 420 r/minute, and subsequently stored in the dark at various temperatures. In order to measure their luminescence response, the samples stored above and below room temperature, were brought to 24°C as quickly as possible, and then returned to their storage temperature immediately after the measurement. It may be seen from the figure that a rise time of the order of hours is required before the "final" value of fluorescence response is attained at room temperature. About 83 percent of the final response at this temperature is observed, however, three minutes after the end of the x-ray exposure, 90 percent of the final value is observed after 30 minutes to one hour, and more than 95 percent in 5 hours after the end of exposure. The initial growth of luminescence response is observed only when high dosage rates are employed. With a low dosage rate of the order of 0.5 r/minute of Co^{60} radiation and with dosage times of the order of hours, the initial growth occurs during the exposure and only a negligible increase is observed on storage. With high dosage rates such as those employed in obtaining data for Fig. 12, initial fluorescence intensities as low as 66 percent of the final value have been observed when the reading was taken within 30 seconds after the termination of a short exposure. At 0°C and −75°C the growth rates of the luminescence are progressively smaller, about 25 hours being required at 0°C and 40 hours at −75°C for the attainment of the final fluorescence response, which at these temperatures is about 8 percent lower than the final response observed at 24°C. The growth of luminescence after x-irradiation, and the variation of the growth rate with temperature indicates that a considerable fraction of the electrons liberated by the x-rays are captured in shallow traps in the glass to form nonluminescent centers, from which they are liberated by thermal energy and recaptured by Ag^+-ions to form luminescent Ag^0 centers. The lower final value at 0° and −75°C may indicate that some of the traps are considerably deeper than others, and that the deeper ones are not emptied appreciably at these low temperatures. At 100°C the growth period is noticeably shorter than at the lower temperatures and the luminescence response that is achieved within 5 hours is about 8 percent higher than the final value observed for glasses maintained at room temperature. At 100°C, however, thermal bleaching occurs at a measurable rate, for in about a week the fluorescence response of glasses stored at this temperature has decreased to a few percent less than the response of glasses stored at room temperature, and is still decreasing. Further studies of growth and thermal bleaching appear worthwhile in order to obtain a better understanding of the mechanism of these phenomena. It seems clear, however, that the disturbing effect of a slow growth rate occurs at much lower temperatures than a personnel-type dosimeter need be subjected to, while the effect of thermal bleaching occurs at much higher temperatures than are reasonably to be expected for such a dosimeter. For practical purposes, it appears that the stability of the phosphate glass dosimeter is quite satisfactory, and that the final dosage indication should not vary more than ±8 percent due to variations in storage temperature of the irradiated glass.

Stability of the x-rayed glass to light that may be

encountered in use as a dosimeter was tested in two ways. Samples were exposed to bright sunlight on successive days and the luminescence intensity was measured after different exposure times. After 12 hours of such exposure the dosage indication was reduced by 15 percent. In practice the dosimeter glass would be mounted in an essentially light-tight container surrounded by lead or other metallic shielding. Exposure to sunlight should occur in practice only if the glass is accidentally removed from its case. The error that such accidental "optical" bleaching might introduce in the dosage indication is not considered excessive.

While exposure of the dosimeter glass to sunlight may be considered an accidental occurrence, exposure to near ultraviolet is a necessity in measuring the dosage. In the second test of the light-stability of the x-rayed glass it was accordingly exposed continuously to the radiation from a 15-watt "Blacklight" lamp (Sylvania "360B1" with red-purple glass envelope) at a distance of 10 cm from the axis of the lamp. A reduction of 10 percent in luminescence intensity was observed after 48 hours of exposure. Since the time of exposure to near ultraviolet during measurement of dosage in the fluorophotometer is of the order of a few seconds, no significant decrease of luminescence by the measurement procedure is to be expected even after many successive readings.

The "optical" bleaching, like the thermal bleaching, appears worthy of more study of a fundamental nature. Studies are planned of the effect of the spectral distribution of bleaching efficiency at various temperatures, and the effect of bleaching by simultaneous irradiation with ultraviolet and visible or infrared light.

The stability of the un-x-rayed glass on storage has not been quantitatively investigated. Samples stored in the laboratory for a period of two years before x-raying have not lost their ability to radiophotoluminesce. There is no theoretical or experimental basis for expecting any alteration of the sensitivity of the un-x-rayed glass on storage.

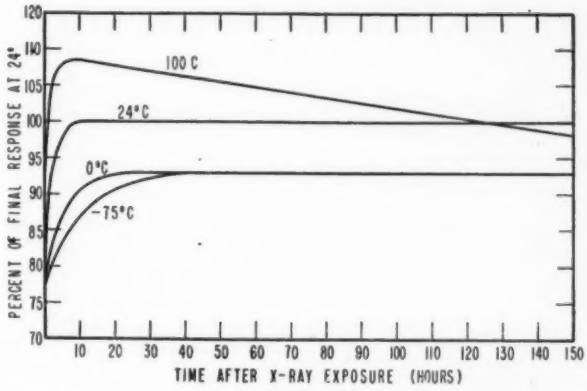

FIG. 12. Variation of luminescence response of x-rayed silver-activated phosphate glass with storage time in the dark.

CONCLUSIONS

The above-described experiments confirm the feasibility of using the phenomenon of radiophotoluminescence, with the Ag-activated phosphate glass as the sensitive element, for dosimetry of personnel that may be exposed to rather high x-ray or gamma-ray dosages. With glass plates $1\times1\times0.1$ cm in size a dosage of 10 *r* of radium gamma-rays can be measured in a suitable fluorophotometer. The method is suitable for measurement of dosages up to several thousand roentgens of such gamma-rays, at which dosage levels the direct coloration of the glass can probably be used for dosimetry.

ACKNOWLEDGMENTS

The authors gratefully acknowledge the assistance of Dr. Howard Etzel and Mrs. Esther W. Claffy who participated in the work at the Naval Research Laboratory.

The Crystallographic Aspect of Slip in Body-Centered Cubic Single Crystals. II. Interpretation of Experiments

A. J. Opinsky* and R. Smoluchowski
Carnegie Institute of Technology, Pittsburgh, Pennsylvania
(Received July 9, 1951)

A new method for determining the ratios of the critical shear stresses has been applied to data taken from the literature and to original results. Measurements of yield strength were found to be not too satisfactory for the investigation of the slip behavior of the body-centered cubic materials. On the other hand, any method which determined the slip plane and the orientation of the tensile axis gave useful results. In all instances where the data were available, the ratio of the critical shear stresses on {123} and {112} was very close to one, and did not change with temperature. The ratio of the critical shear stresses on {123} and {110} changes with temperature and composition, with the value of S_{123} generally being higher than that for S_{110}.

A PREVIOUS paper[1] was concerned with the fundamental aspects of slip in body-centered cubic lattices, and in particular with the ratios of the critical shear stresses. Results of these considerations will be applied now to data from the literature and to some new data obtained with iron-silicon alloys. The process of determining the ratio of the critical shears, as described in *I*, is briefly as follows:

(a) By observing traces of the slip bands on the surface of specimens or by measuring directly yield strength values, the indices of the operative slip planes as a function of the orientation of the tensile axis are determined.

(b) The results are then projected, along great circles passing through the original orientations of the tensile axes and the slip directions, onto the base line [001]–[011] of a unit stereographic triangle.

(c) On that base line, the boundaries between regions of various active slip planes are found and the ratios of the critical shear stresses read off the plot in Fig. 1.

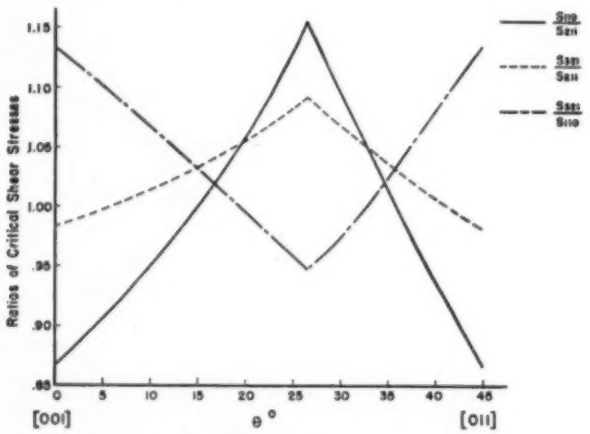

FIG. 1. Ratios of the critical shear stresses as a function of the orientation of the tensile axis along the line [001]–[011].

* Now associated with Research Laboratory Division, General Motors Corporation. Submitted in partial fulfillment of the requirements for the degree of Doctor of Science at Carnegie Institute of Technology.

[1] A. J. Opinsky and R. Smoluchowski, J. Appl. Phys. **22**, 1380 (1951) (referred to as I).

1. EARLY EXPERIMENTAL DATA

Probably the first data suitable for our analysis are those of Fahrenhorst and Schmid[2] for iron. An examination of their plot of the experimental yield strength *versus* the orientation of the tensile axis, Fig. 2, yields no definite conclusions concerning the actual operative slip plane (or planes) although supplementary lattice rotation data indicate that probably planes of the types {112} or {123} were operative; Fahrenhorst and Schmid themselves concluded that the iron slipped only on {123}.

In order to apply our analysis, all the points of Fig. 2 should be projected onto the base line [001]–[011]. Then the real variation of the yield strength due to the operation of several slip planes may become evident. The projected yield strength at the projected point along the line [001]–[011] is calculated in the following manner: At the initiation of yielding in point *P* (Fig. 3), the resolved shear stress τ is equal to the critical shear stress *S*. Thus,

$$Y = S/\cos\lambda \cos\phi. \tag{1}$$

On the other hand, the yield strength at the projected

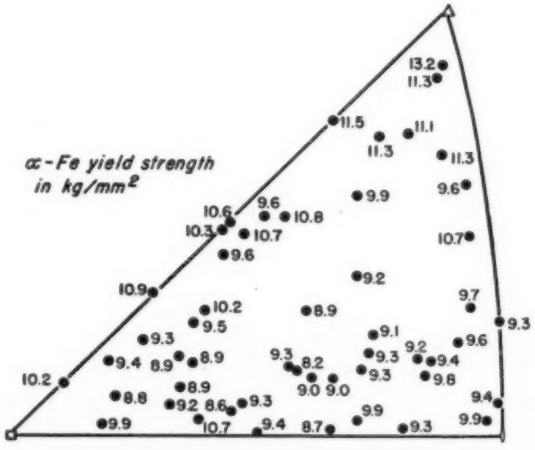

FIG. 2. Experimental yield strength as a function of the orientation of the tensile axis.

[2] W. Fahrenhorst and E. Schmid, Z. Phys. **78**, 383 (1932).

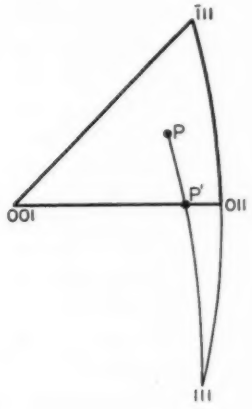

FIG. 3. The projection method.

point P' will obey a similar relation, with the primes denoting the various quantities at the point P': $Y'=S'/\cos\lambda'\cos\phi'$. Since $S=S'$, we have

$$Y'=Y\cos\lambda\cos\phi/\cos\lambda'\cos\phi', \qquad (2)$$

assuming that the operative slip plane did not change during the rotation. This is a justified assumption, as long as the tensile axis lies in regions where the crystal, during elongation, rotates toward [111] (see Fig. 4, which represents the regions of maximum resolved shear stress for plane and direction combinations within one unit stereographic triangle). All the slip-direction combinations marked "111" satisfy that requirement. It follows that determinations of ratios of the critical shear stresses should be made preferentially in the region of the unit triangle where the [111] direction is the operative slip direction. Also, it is suggested that planes possessing nearly the maximum resolved shear stress be used in order to minimize errors.

Figures 5 and 6 show the $[\bar{1}11]$ and [111] projections of data of Fig. 2. The small numbers next to the points

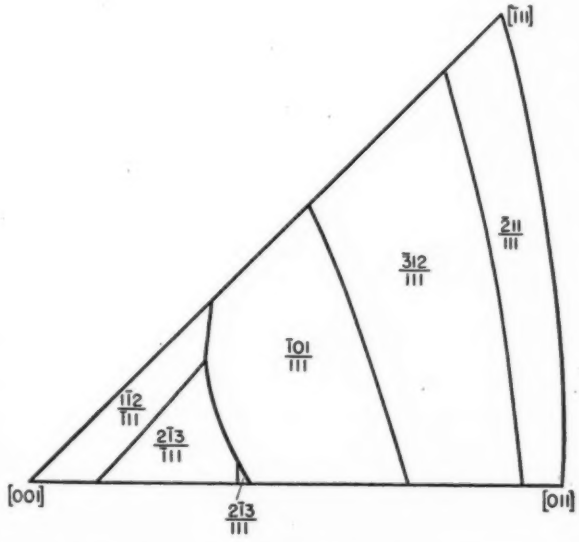

FIG. 4. Regions of maximum resolved shear stress, three families of planes.

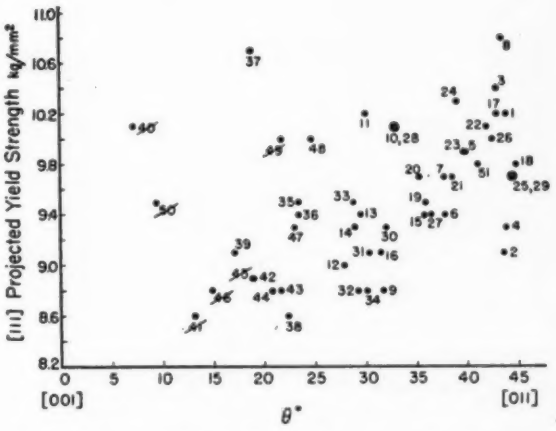

FIG. 5. [111] projection of Fahrenhorst and Schmid data.

serve to identify them and some of the points had to be projected along both possible slip directions. The choice of the proper projection was based on the following two requirements:

(a) All points projected along $[\bar{1}11]$ great circles had to fall to the left of the points projected along [111] great circles since the operative region of $[\bar{1}11]$ falls to the left of that for [111] (Fig. 4).

(b) Points which could be assigned to either direction were placed so as to give the best continuity.

Figure 7 shows the complete projection, with the full dots corresponding to projection along great circles through [111] and the open dots corresponding to projection along great circles through $[\bar{1}11]$. It appears that there is a definite trend toward a minimum in the center of the plot. A comparison with Fig. 8, which shows the shapes of curves which might be expected if any of the three planes were active, indicates that planes of the type {110} must have been operative, because the {110} curve alone has a minimum in the middle of the diagram. However, the rotation data mentioned earlier make it necessary that also another type of plane was operating because otherwise all rotation should be toward [111], which was not observed.

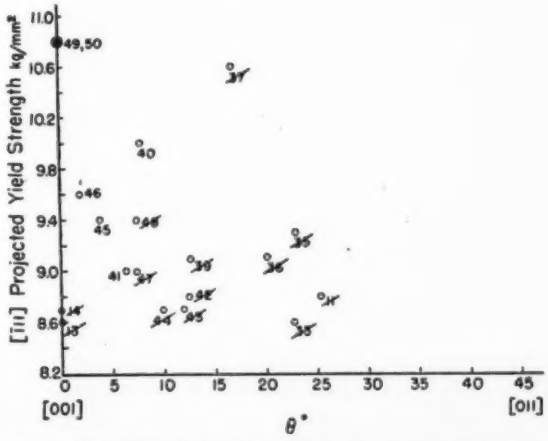

FIG 6. $[\bar{1}11]$ projection of Fahrenhorst and Schmid data.

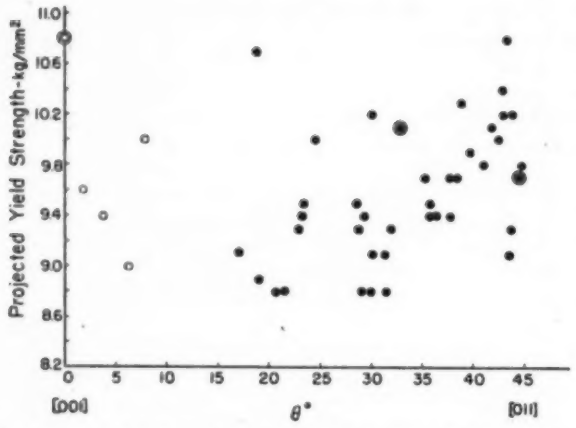

FIG. 7. Completed projection of Fahrenhorst and Schmid data.

On the basis of Fahrenhorst and Schmid's conclusions, this second plane was drawn in as {123}, although in the particular region there is not much choice between {123} and {112}. The curves, in the proper position, are shown in Fig. 9, together with estimated precision of the data shown in dotted lines.

A determination of the ratios of the critical shear stresses from Fig. 9 is not possible because of uncertainty both of the index of the second plane and of the boundary between the regions of operation of the two planes. It appears that in general the yield strength is not a particularly good variable for this type of investigation.

Another group of experimental results to which our theory can be applied is the unstretched cone data of Taylor and Elam[3–5] who investigated the slip behavior of iron. From their data, which are plotted on stereographic projections in the original paper, the active slip plane and the orientation of the tensile axis can be obtained as shown in Figs. 10 and 11. In the region investigated, no slip was found on the {110} planes. The boundary between the {123} and {112} regions is about 42½° from [001] toward [011]; reference to

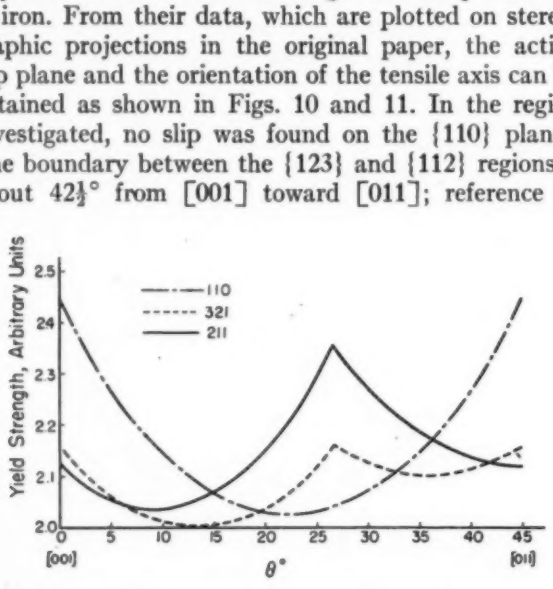

FIG. 8. Yield strength along the line [001]–[011].

[3] G. I. Taylor and C. F. Elam, Proc. Roy. Soc. (London) **A102**, 643 (1923).
[4] G. I. Taylor and C. F. Elam, Proc. Roy. Soc. (London) **A112**, 337 (1926).
[5] G. I. Taylor, Proc. Roy. Soc. (London) **A118**, 1 (1928).

Fig. 1 indicates that $S_{123}=0.99\ S_{112}$. The only inference which can be made concerning S_{110} is that, since the furthermost point of {123} projects to 33° along the line [001]–[011], S_{123} must be less than S_{110}.

Later investigations of Taylor[5] of the slip behavior of beta-brass over a fairly narrow range of composition are shown in Fig. 12. Here it is necessary only to put all the tensile axes into one unit stereographic triangle as shown in Fig. 13. Again two active slip planes appear. However, they are different from those found in Fig. 11. The boundary between {123} and {110} is 37½° from [001] toward [011], which corresponds to $S_{123}=1.05\ S_{110}$. Unfortunately, no slip was observed on {112}, presumably because the tensile axes were too far from the [011]–[$\bar{1}$11] line. The two last examples indicate that unstretched cone data are quite satisfactory for determination of the ratio of the critical shear stresses.

2. NEW DATA

Silicon ferrite is the obvious choice for the working material, because of the ease of production of large

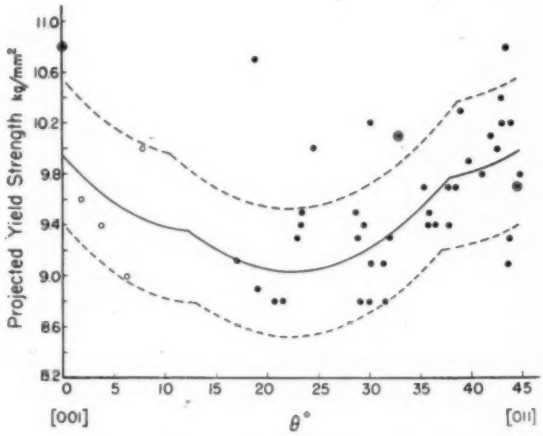

FIG. 9. Analysis of the completed projection of Fahrenhorst and Schmid data.

grains and because we know, from the work of Barrett, Ansel, and Mehl[6] that up to about 4 percent silicon all three types of slip planes can be active. On the basis of the previous discussion of the experimental material available in literature, it was decided to use standard metallographic techniques to determine the active slip planes rather than to measure the yield strengths.

(a) Experimental Procedure

Single crystal samples can be obtained either by transforming prepared samples into single crystals by the strain-anneal method, or by cutting specimens from a larger single crystal. Both procedures were used. The advantages of the strain anneal crystals were that the specimen could be cut to shape beforehand,

[6] Barrett, Ansel, and Mehl, Trans. Am. Soc. Metals **25**, 702 (1937).

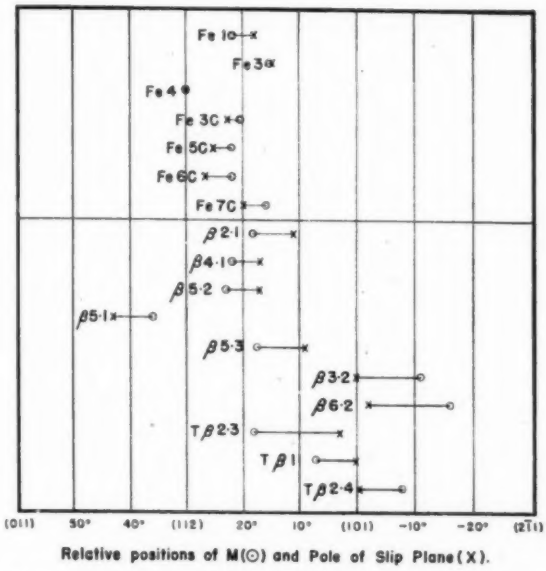

FIG. 10. Positions of the poles of planes having maximum resolved shear stress and slip planes.

the surface of the crystal was not strained by cutting, and the crystals were fairly perfect. On the other hand, the crystals grown by strain-anneal methods provided little choice of tensile axes. Using a larger single crystal, the choice of tensile axis was almost unlimited, but unfortunately the crystals were much less perfect than those grown by the strain-anneal method, because the original large single crystal was grown from the melt.

In the strain-anneal treatment elongations between 2 and 3 percent gave best results. The material was annealed in two steps from room temperature to 1000°C and then from 1000°C to 1300°C with slowly increasing temperature. The material, furnished by Allegheny-Ludlum Steel Corporation, was a 3.4 percent silicon ferrite in the form of a 0.100-inch-thick sheet which was reduced to strips 0.150 inch wide by 8 inches long for the treatment. The single crystals were over one inch long.

The large single crystals of 3.3 percent silicon ferite ($1\frac{1}{8}$ inches in diameter) furnished by Dr. J. K. Stanley of Westinghouse, were first cut in disks on a small water-cooled cut-off wheel. Then back reflection Laue

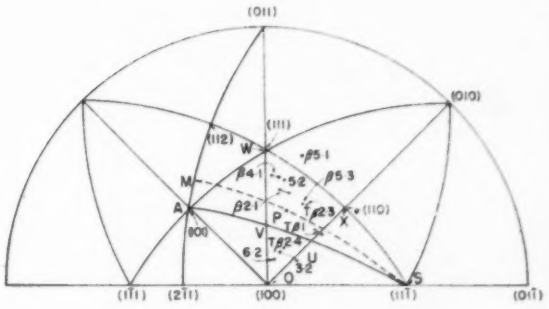

FIG. 12. The data of Taylor.

x-ray photograms were taken, and the orientation of each disk determined. The small specimens were then cut from the disk by means of a surface grinder in which the grinding wheel was replaced by a cut-off wheel. These small single crystals had about the same length and width as the specimens grown by the strain-anneal method, and had predetermined tensile axes. They were then polished by standard technique into small rectangular parallelopipeds and finally electropolished in a 10 percent solution of chromic acid in orthophosphoric acid at a current density of ten amperes per square inch.

The precise orientations of the tensile axes of the various crystals were then determined with the aid of a special back reflection Laue camera and it is estimated that the error in the determination of the tensile axis should be no more than 1°. The accuracy in the determination of the tensile axes of the strain-anneal crystals is about 2°. The crystals, placed in templin sheet grips, were then strained on the low (2400-pound) range of a Baldwin-Southwark testing machine at slow rates of straining. Specimens which gave evidence of nonaxial loading were discarded. Low temperature experiments were performed by siphoning liquid nitrogen from a Dewar flask onto the specimen, and the high temperature work was done by placing a small resistor around the specimen while it was in the grips. After extension, the traces of the slip planes were measured on two perpendicular surfaces, and the index of the plane causing the traces was determined by standard crystallographic methods.

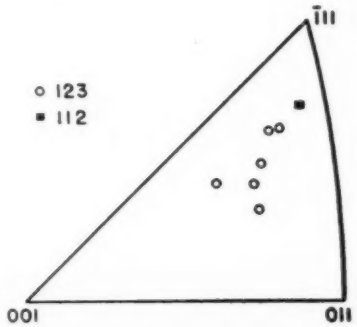

FIG. 11 Replotting of data of Taylor and Elam (reference 4). Material—iron.

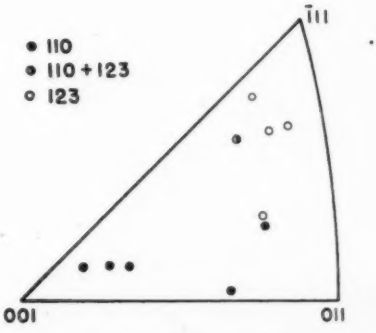

FIG. 13. Replotting of Fig. 12 (reference 5). Material—β-brass.

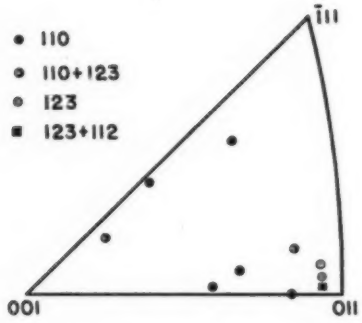

FIG. 14. Strain-anneal crystals, room temperature testing.

(b) Results

The strain-anneal crystals were tested only at room temperature. Fig. 14 presents the data which show that all three types of planes were active at room temperature. The boundaries on the right side of Fig. 14 are 39° from [001] for the boundary between $(\bar{1}01)$ and $(\bar{3}21)$, and 43° from [001] for the boundary between $(\bar{3}21)$ and $(\bar{2}11)$. (Notation is described in Fig. 4.) This gives $S_{123}=1.07\ S_{110}$ and $S_{123}=0.99\ S_{112}$, respectively. The

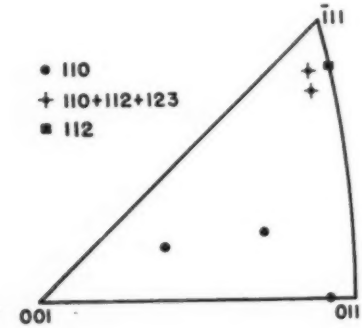

FIG. 15. Cut single crystals, room temperature testing.

room temperature data for the cut single crystals, Fig. 15, are slightly different. Here the boundaries between the three types of planes merge at 43°; consequently, $S_{123}=1.11\ S_{110}$ and $S_{123}=0.99\ S_{112}$.

High temperature testing at 190±15°C, Fig. 16, shows results similar to those obtained at room temperature, in that all three slip planes were operative, but the boundary between $(\bar{1}01)$ and $(\bar{3}21)$ is displaced to 38° from [001] along [001]–[011]; the ratio here is $S_{123}=1.06\ S_{110}$. On the other hand, the boundary between (123) and (112) remains the same: $S_{123}=0.99\ S_{112}$.

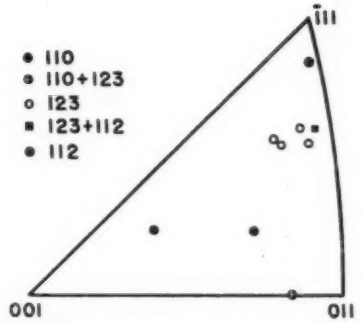

FIG. 16. Cut single crystals, high temperature testing.

Finally at the temperature of −140±15°C only {110} slip was observed (see Fig. 17). As evident from Fig. 8, if {110} slip occurs at the edge of the unit stereographic triangle (at 45° or [011]), it will occur everywhere within the triangle. Thus, one can say only that, at the low temperature used, $S_{123}>1.13\ S_{110}$ and $S_{112}>1.16\ S_{110}$.

The relative error in the numerical values of these ratios is quite small although it should be kept in mind that small variations of these ratios may radically affect the slip behavior. An error of one degree in the

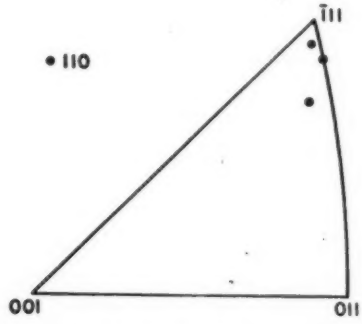

FIG. 17. Cut single crystals, low temperature testing.

orientation determination of the tensile axis, in proximity of the middle of the diagram, produces an uncertainty about one percent in the value of the ratio. Nevertheless, this method of determining the ratios of the critical shear stresses is much more accurate than any other which has been heretofore devised and should be satisfactory for the treatment of various experimental data.

This work has been sponsored by an AEC contract. One of the authors (A. J. O) wishes to express his appreciation to the Atomic Energy Commission for a fellowship.

JOURNAL OF APPLIED PHYSICS VOLUME 22, NUMBER 12 DECEMBER, 1951

Atomic Size Effect in the X-Ray Scattering by Alloys*

B. E. WARREN, B. L. AVERBACH, AND B. W. ROBERTS
Massachusetts Institute of Technology, Cambridge, Massachusetts

(Received July 23, 1951)

In a random solid solution, if the two atoms have appreciably different sizes, the nearest-neighbor distances and to a lesser extent the higher neighbor distances will be of three kinds, r_{AA}, r_{AB}, and r_{BB}. The effect produces modulations in the diffuse intensity similar to those produced by short-range order. The size effect is important when the difference in scattering power is large, the difference in size is large, and the short-range order is small. The size effect is illustrated by a single crystal pattern of Cu_3Au and a powder pattern of Ni_3Au_2. An asymmetry in the wings about a fundamental reflection is a result of the size effect.

I. INTRODUCTION

THE usual treatment of diffuse scattering by an AB alloy assumes that the atoms are precisely at the lattice points $R_m=m_1a_1+m_2a_2+m_3a_3$. If N is the total number of atoms in the sample, m_A and m_B are the fractions of A and B atoms, and the atoms are assumed to be distributed at random on the lattice points R_m, Laue[1] has shown that there will be a monotonic diffuse scattering which is expressed in electron units by

$$I=Nm_Am_B(f_B-f_A)^2. \tag{1}$$

If short-range order exists, the distribution is not completely random. About a particular kind of atom, the average composition of surrounding atoms depends on the kind of atom. The diffuse intensity is given by

$$I=Nm_Am_B(f_B-f_A)^2\sum_{ij}\alpha_{ij}\exp[i\mathbf{k}\cdot\mathbf{r}_{ij}] \tag{2}$$

where $\mathbf{k}=(2\pi/\lambda)(\mathbf{s}-\mathbf{s}_0)$, r_{ij} is the vector distance from the origin atom to the jth neighbor of the ith shell, and α_{ij} is the short-range order parameter defined by $\alpha_{ij}=1-p_{ij}/m_A$ where p_{ij} is the probability of finding an A atom as the ij neighbor of a B atom. Since $\alpha_{00}=1.0$, the Laue monotonic scattering is included in Eq. (2) as the special case for all $\alpha_{ij}=0$ except α_{00}.

The derivation of Eq. (2) assumes that all atoms are precisely at the average lattice points R_m. It completely neglects the fact that if there is an appreciable difference in size of the two atoms, the interatomic distances for nearest neighbors and to a lesser extent for remote neighbors will be of three kinds $r_{AA}{}^i$, $r_{AB}{}^i$, and $r_{BB}{}^i$ depending on the pair of atoms considered. The purpose of this paper is to show that if there are appreciable differences in both size and scattering power of the two atoms, the size effect can produce modulations in the diffuse intensity which are comparable in size to those produced by short range order. The existence of a size effect has already been suggested by von Laue,[1] Guinier,[2] and Wasastjerna.[3]

* Research sponsored by the ONR under Contract N5ori-07832 and by the AEC under Contract No. AT(30-1)-gen-368.

[1] M. von Laue, *Röntgenstrahl Interferenzen* (Edwards Brothers, Inc., Ann Arbor, Michigan, 1943), p. 175.

[2] A. J. Guinier, Proc. Phys. Soc. (London) **LVII**, 310 (1945).

[3] J. A. Wasastjerna, Soc. Sci. Fennica, Commentationes Phys. Math. **13**, 5 (1947).

II. THEORY OF THE SIZE EFFECT

If all atoms are at lattice points the intensity is given by

$$I=\sum_m\sum_{m'}f_mf_{m'}\exp[i\mathbf{k}\cdot(\mathbf{R}_m-\mathbf{R}_{m'})]. \tag{3}$$

To allow for differences in size we represent the interatomic distances by

$$r_{AA}{}^i=r_i(1+\epsilon_{AA}{}^i)\quad r_{AB}{}^i=r_i(1+\epsilon_{AB}{}^i)\quad r_{BB}{}^i=r_i(1+\epsilon_{BB}{}^i)$$

where r_i is the average distance between two lattice points such that one is in the ith shell with respect to the other. To allow for partial short-range order we let p_i represent the probability of finding an A atom at a distance r_i from a B atom, and p_i' the probability of a B atom at a distance r_i from an A atom. The probabilities are related by $m_Ap_1'=m_Bp_i$.

Separating the terms with $m=m'$ Eq. (3) becomes

$$\begin{aligned}I=N(m_Af_A{}^2+m_Bf_B{}^2)+\sum_m\sum_{m\neq m'}[&m_Af_A\{(1-p_i')f_A\\&\times\exp[i\mathbf{k}\cdot(\mathbf{R}_m-\mathbf{R}_{m'})(1+\epsilon_{AA}{}^i)]\\&+p_i'f_B\exp[i\mathbf{k}\cdot(\mathbf{R}_m-\mathbf{R}_{m'})(1+\epsilon_{AB}{}^i)]\}\\&+m_Bf_B\{p_if_A\exp[i\mathbf{k}\cdot(\mathbf{R}_m-\mathbf{R}_{m'})(1+\epsilon_{AB}{}^i)]\\&+(1-p_i)f_B\exp[i\mathbf{k}\cdot(\mathbf{R}_m-\mathbf{R}_{m'})(1+\epsilon_{BB}{}^i)]\}].\end{aligned} \tag{4}$$

Since ϵ can be assumed to be small

$$\exp[i\mathbf{k}\cdot\mathbf{R}(1+\epsilon)]=(1+i\mathbf{k}\cdot\mathbf{R}\epsilon)\exp[i\mathbf{k}\cdot\mathbf{R}].$$

If we add and subtract the quantity

$$\sum_m\sum_{m'}(m_Af_A+m_Bf_B)^2\exp[i\mathbf{k}\cdot(\mathbf{R}_m-\mathbf{R}_{m'})].$$

Equation (4) becomes

$$\begin{aligned}I=Nm_Am_B(f_B-f_A)^2+\sum_m\sum_{m\neq m'}&m_Am_B(f_B-f_A)^2(1-p_i/m_A)\\&\times\exp[i\mathbf{k}\cdot(\mathbf{R}_m-\mathbf{R}_{m'})]+\sum_m\sum_{m\neq m'}\{(m_A-m_Bp_i)f_A{}^2\epsilon_{AA}{}^i\\&+2m_Bp_if_Af_B\epsilon_{AB}{}^i+m_B(1-p_i)f_B{}^2\epsilon_{BB}{}^i\}\\&\times i\mathbf{k}\cdot(\mathbf{R}_m-\mathbf{R}_{m'})\exp[i\mathbf{k}\cdot(\mathbf{R}_m-\mathbf{R}_{m'})]\\&+\sum_m\sum_{m'}(m_Af_A+m_Bf_B)^2\exp[i\mathbf{k}\cdot(\mathbf{R}_m-\mathbf{R}_{m'})].\end{aligned} \tag{5}$$

In Eq. (5) the first term represents the monotonic diffuse scattering which arises from complete randomness, the second term gives the modulations in the diffuse scattering due to short-range order, the third term gives the modulations due to the difference in size of the atoms, and the fourth term represents the sharp crystalline reflections. Assuming that the second and third terms converge rapidly for increasing values of $|R_m-R_{m'}|$, the double sums can be replaced by N times a single sum over neighboring atoms.

Let

$$\eta=f_B/f_A, \quad r_{ij}=R_m-R_{m'}, \quad \alpha_i=(1-p_i/m_A),$$

$$\beta_i=\left(\frac{1}{\eta-1}\right)^2\left\{\left(\frac{m_A}{m_B}+\alpha_i\right)\epsilon_{AA}{}^i+2(1-\alpha_i)\eta\epsilon_{AB}{}^i+\left(\frac{m_B}{m_A}+\alpha_i\right)\eta^2\epsilon_{BB}{}^i\right\}. \quad (6)$$

The diffuse intensity is then given by

$$\frac{I_D}{Nm_Am_B(f_B-f_A)^2}=\sum_{ij}\alpha_i\exp[i\mathbf{k}\cdot\mathbf{r}_{ij}]+\sum_{ij}\beta_i i\mathbf{k}\cdot\mathbf{r}_{ij}\exp[i\mathbf{k}\cdot\mathbf{r}_{ij}]. \quad (7)$$

The distortion due to difference in size has been expressed in terms of the three quantities $\epsilon_{AA}{}^i$, $\epsilon_{AB}{}^i$, and $\epsilon_{BB}{}^i$. There is necessarily a relation between these, since the weighted average interatomic distance must equal the average lattice distance which determines the sharp crystalline reflections.

$$m_A(1-p_i')r_i(1+\epsilon_{AA}{}^i)+(m_Ap_i'+m_Bp_i)r_i(1+\epsilon_{AB}{}^i)+m_B(1-p_i)r_i(1+\epsilon_{BBi})=r_i. \quad (8)$$

Incorporating this restriction in Eq. (6) the size effect parameter becomes

$$\beta_i=\left(\frac{1}{\eta-1}\right)\left\{-\left(\frac{m_A}{m_B}+\alpha_i\right)\epsilon_{AA}{}^i+\left(\frac{m_B}{m_A}+\alpha_i\right)\eta\epsilon_{BB}{}^i\right\}. \quad (9)$$

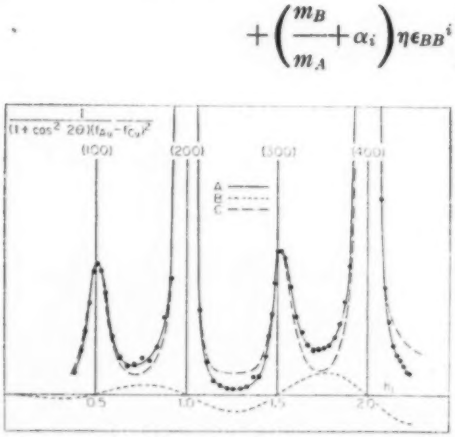

FIG. 1. Measurements along the h_1 00 line for a single crystal of Cu_3Au quenched from 500°C, using crystal monochromated CuKα. A. Experimental readings. B. Nearest-neighbor size effect term. C. Difference.

If $f_B>f_A$, then $\eta>1.0$. If the atom B is larger than the A atom, $\epsilon_{BB}{}^i$ is positive and $\epsilon_{AA}{}^i$ is negative and β_i is a positive quantity. Rough magnitudes for $\epsilon_{AA}{}^i$ and $\epsilon_{BB}{}^i$ can be obtained by comparing the cell dimensions of the alloy with those of the A and B constituents. The values probably vary with both composition and the degree of order.

We have considered that the distance $|R_m-R_{m'}|$ between atoms m and m' will depend upon the kind of atom at position m and m'. If m and m' are not nearest neighbors of one another, it can also depend upon the composition of the region between them. If atom B is the larger in both scattering power and size, then a region which is B rich in composition will contribute terms involving larger distances and these terms will be weighted by the higher scattering factors. In this paper we assume that there is no appreciable segregation and hence that contributions to the diffuse intensity from composition fluctuations can be neglected.

To express the diffuse intensity in terms of a position in reciprocal space, we represent the vector from one atom to another by

$$r_{ij}=la_1'+ma_2'+na_3'$$

where $a_1'a_2'a_3'$ are each half of the usual cubic axes $a_1a_2a_3$ and lmn are integers. For the face-centered cubic lattice $l+m+n=$ even and for the body-centered cubic lattice lmn are unmixed. In terms of the $a_1'a_2'a_3'$ there are corresponding reciprocal vectors $b_1'b_2'b_3'$ and the diffraction vector $(s-s_0)/\lambda$ can be represented by

$$\frac{s-s_0}{\lambda}=h_1b_1'+h_2b_2'+h_3b_3'$$

where $h_1h_2h_3$ are continuous variables. For each neighbor at l, m, n there is a corresponding neighbor at $-l, -m, -n$ with the same values of α_i and β_i. Expressed in terms of $h_1h_2h_3$, Eq. (7) becomes

$$\frac{I_D}{Nm_Am_B(f_B-f_A)^2}=\sum_l\sum_m\sum_n\alpha_{lmn}\cos2\pi(lh_1+mh_2+nh_3)-\sum_l\sum_m\sum_n\beta_{lmn}2\pi(lh_1+mh_2+nh_3)\times\sin2\pi(lh_1+mh_2+nh_3). \quad (10)$$

The first term represents the effect of short-range order and is periodic in reciprocal space, the second term is due to the difference in size of the atoms and increases in magnitude with increasing distance from the origin.

For a powder pattern we wish to express the diffuse intensity in terms of the usual θ. This involves averaging the terms of Eq. (7) letting the vector r_{ij} take with equal probability all orientations relative to the vector k. The summation over j is expressed by multiplying by C_i the coordination number for the ith shell of neighbors. For a powder pattern the diffuse intensity

can be written

$$\frac{I_D}{Nm_Am_B(f_B-f_A)^2}=\sum_i C_i\alpha_i\frac{\sin sr_i}{sr_i}$$

$$-\sum_i C_i\beta_i\left\{\frac{\sin sr_i}{sr_i}-\cos sr_i\right\} \quad (11)$$

where $s=(4\pi\sin\theta)/\lambda$. On a powder pattern the modulations in intensity due to short-range order decrease rapidly with increasing angle, while those due to the size effect persist.

III. EXAMPLES OF THE SIZE EFFECT

A set of spectrometer measurements along the $h_1\,00$ line of reciprocal space for a single crystal of Cu_3Au quenched from 500°C is shown by Fig. 1. The radiation was crystal monochromated CuKα. The strong fundamental reflections (200) and (400) occur at the positions $h_1=1.0$ and $h_1=2.0$. The peaks in the diffuse scattering which are due to short-range order occur approximately at the positions where (100) and (300) superstructure lines would occur if the material were in the long-range ordered form. Quenching a large single crystal of Cu_3Au from 500°C does not maintain a short-range order characteristic of 500°C, and the (100) and (300) peaks are about two or three times as high as they would be if measured at temperature.

A striking feature of the figure is the alternating background; high between (100) and (200), low between (200) and (300) and high between (300) and (400). From Eq. (10) the size effect term for the 12 nearest neighbors only is $-16\pi\beta_1h_1\sin2\pi h_1$. The sinusoidal curve of Fig. 1 is a plot of this term with β_1 chosen so that when the size effect term is subtracted from the measured curve the background between peaks will be about the same. Within a factor of 2 this corresponds to $\beta_1=0.015$. From Eq. (9) this rough value gives $\epsilon_{BB}{}^1-5.2\epsilon_{AA}{}^1=0.055$. For Cu_3Au where A represents copper and B represents gold, we would expect $\epsilon_{AA}{}^1$ to be negative and quite small in magnitude compared with $\epsilon_{BB}{}^1$. Hence we can conclude that $\epsilon_{BB}{}^1<0.055$. From the cell dimensions Au=4.07A and Cu_3Au =3.74A, if we were to assume that the Au-Au distance in Cu_3Au is the same as in Au we would compute $\epsilon_{BB}{}^1=0.089$. The rough upper value obtained from Fig. 1 is about one-half of this. It is probably reasonable that the value should be smaller since in a mixture of atoms of two different sizes the large atoms will be squeezed together and the small ones pulled apart.

Figure 2 shows spectrometer measurements with CoKα from a powder sample of approximate composition Ni_3Au_2 quenched from 900°C. At 900°C the material is a solid solution with a face-centered cubic lattice. At lower temperatures it segregates into Ni rich and Au rich phases. Because of this tendency to segregate it would be expected that short-range order in this system would be very small.

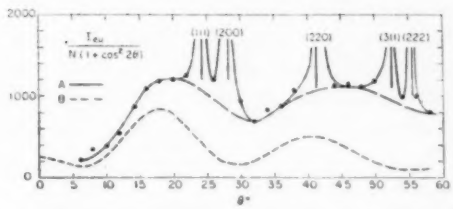

FIG. 2. Spectrometer measurements on Ni_3Au_2 powder quenched from 900°C, using crystal monochromated CoKα. A. Experimental readings. B. Diffuse intensity computed from $\alpha_1=-0.05$ and $\beta_1=+0.05$.

There are two pronounced peaks in the measured diffuse scattering. The second exists in a high angle region where peaks due to short-range order are usually not observable on powder patterns. The first peak is at a larger angle than is usually found for the first short-range order peak. It does not appear to be possible to explain the measured curve in terms of any reasonable combination of short-range order parameters. The fact that the intensity drops to small values at small angle indicates that there is some short-range order, and the intense peak at large angle suggests a size effect term. The calculated curve of Fig. 2 is a first rough approximation using a nearest-neighbor short-range order parameter $\alpha_1=-0.05$, and a nearest-neighbor size effect parameter $\beta_1=+0.05$. The agreement is good enough to suggest that these are the dominant terms. The Ni-Au system is probably ideally suited to showing the size effect since the difference in scattering power is large, the difference in size of the atoms is about 15 percent, and the short range order is small.

IV. DISCUSSION

A size effect in the diffuse scattering is most likely to be observed when there is a large difference in both scattering power and atomic size, and when the short-range order is small. In the two examples given in this paper, it cannot be claimed that the existence of a size effect term in the diffuse scattering has been rigorously proved. We can only say that it does not appear to be possible to explain the observed curve by the usual short-range order coefficients, and that the introduction of a nearest-neighbor size effect term, with a reasonable value for the size effect coefficient β_1, gives approximate agreement between the calculated and observed curves.

The size effect term puts a positive peak on one side of each fundamental reflection and a negative peak on the other side. The inclusion of higher terms than β_1 moves the two diffuse peaks closer to the fundamental reflection. The result is an asymmetry in the wings about each fundamental reflection. In the two examples quoted in this paper, the atom with the larger scattering power is also the larger in size and the coefficient β is positive. For this case the wings about the fundamental reflections are high on the small angle side and low on

the large angle side. When the atom with the higher scattering power is the smaller in size, the coefficient β is negative, and the wings about a fundamental reflection should be low on the small angle side and high on the large angle side. Although Preston's[4] observations on Al-Cu in the early stages of aging are of this type, it seems evident that in this case the effect is largely a result of segregation rather than the simple size effect.

The authors are grateful to Mr. Paul Flinn for his assistance in obtaining the data on the nickel-gold sample.

[4] G. D. Preston, Proc. Roy. Soc. (London) **167**, 526 (1938).

JOURNAL OF APPLIED PHYSICS VOLUME 22, NUMBER 12 DECEMBER, 1951

Propagation of Disturbances in One-Dimensional Accelerated Electron Streams*

L. D. SMULLIN
Research Laboratory of Electronics, Massachusetts Institute of Technology, Cambridge, Massachusetts
(Received July 16, 1951)

The propagation of small sinusoidal modulations in the infinite, parallel-plane diode is studied. A second-order differential equation is obtained for the ac convection current. Solutions are found in closed form for the cases of a drift-stream, space-charge-limited acceleration, and acceleration with an arbitrary current density less than the space-charge-limited value.

INTRODUCTION

THIS paper is concerned with the propagation of small ac signals or disturbances in one-dimensional electron streams. The electron flow is assumed to be in the z direction, and there are no variations of any quantities in the x or y directions. It is further assumed that the velocity is single-valued at every point (the region between the cathode and virtual cathode is thus excluded). We shall be concerned only with small signals: i.e., fluctuations whose amplitude is small compared with the dc current or velocity, as the case may be.

A second-order differential equation is derived, giving the variation of the ac convection current density with z as a function of the dc current density and the dc velocity, v_0. This equation is solved for three cases: (1) The drift space, $(dv_0)/dz=0$; (2) space-charge limited flow, $v_0 \sim z^{\frac{1}{3}}$; and (3) arbitrary space-charge conditions. The solutions, thus obtained, give the familiar space-charge waves for the drift region and for the accelerated stream case; the final results are the same as those obtained by Llewellyn[1,2] and Benham.[3]

Although the final results of this analysis are the same as those previously obtained by other authors, it is felt that the form of the solution is such as to throw new light on the nature of the phenomenon under consideration. The differential equation for the ac convection current has already found application in a number of specific problems which will be discussed in future publications.

II. THE DIFFERENTIAL EQUATION

The now familiar technique of describing the various electrical quantities as sums of dc and small ac components will be used as follows:

$$\begin{aligned}&\text{Electron velocity}=v=v_0+v_1e^{j\omega t}.\\&\text{Charge density}=\rho=\rho_0+\rho_1e^{j\omega t}.\\&\text{Potential}=V=V_0+V_1e^{j\omega t}.\\&\text{Convection current density}=J=J_0+J_1e^{j\omega t}.\end{aligned}\tag{1}$$

All quantities with subscripts are assumed to be functions of z only, where z is measured in the direction of electron flow. J_0 is, of course, independent of z.

The fundamental equations are:

$$J=\rho v\simeq\rho_0v_0+(\rho_0v_1+\rho_1v_0)e^{j\omega t},\tag{2}$$

$$\partial\rho/\partial t=-\partial J/\partial z,\tag{3}$$

$$\partial^2V/\partial z^2=-\rho/\epsilon,\tag{4}$$

$$-\eta\frac{\partial V}{\partial z}=\frac{dv}{dt}=\frac{\partial v}{\partial t}+\frac{\partial v}{\partial z}\frac{\partial z}{\partial t},\tag{5}$$

where $\eta=e/m$.

It is assumed that the solution of the dc problem is known for the particular diode being studied, so that we are only interested in finding the ac solutions for current density, velocity, etc. Thus, separating out the ac terms and replacing $\partial/\partial t$ by $j\omega$, we find that (5) becomes

$$-\eta\frac{dV_1}{dz}=j\omega v_1+v_0\frac{dv_1}{dz}+v_1\frac{dv_0}{dz}.\tag{6}$$

* This work has been supported in part by the Signal Corps, the Air Materiel Command, and ONR.

[1] F. B. Llewellyn, *Electron Inertia Effects* (Cambridge University Press, New York, 1939).

[2] F. B. Llewellyn and L. C. Peterson, Proc. Inst. Radio Engrs. **32**, 144 (1944).

[3] W. E. Benham, Phil. Mag. (March, 1928); Phil. Mag. Supp. II (February, 1931).

Equations (3) and (4) combine to give

$$\frac{d^2V_1}{dz^2}=\frac{1}{j\omega\epsilon}\frac{dJ_1}{dz}. \tag{7}$$

Integration of (7) results in

$$dV_1/dz=(J_1/j\omega\epsilon)-E. \tag{8}$$

The constant of integration E is independent of z and represents an impressed field $Ee^{j\omega t}$. The total ac current density is the sum of the convection and displacement current densities

$$J_T=J_1-j\omega\epsilon\frac{dV_1}{dz}=j\omega\epsilon E. \tag{9}$$

Thus, the total current in the infinite parallel-plane diode is just the displacement current resulting from the impressed field E. E may be caused by an external source, or it may be the result of induced currents in the electrodes, flowing through an external impedance.

Since J_0 is independent of z, it follows from (2) that

$$\frac{1}{\rho_0}\frac{d\rho_0}{dz}=-\frac{1}{v_0}\frac{dv_0}{dz}. \tag{10}$$

By combining Eqs. (2), (3), (6), (8), and (10), a differential equation in J_1 and z is obtained:

$$J_1''+J_1'\left(\frac{2j\omega}{v_0}+\frac{3}{v_0}\frac{dv_0}{dz}\right)+J_1\left(-\frac{\omega^2}{v_0^2}+\frac{2j\omega}{v_0^2}\frac{dv_0}{dz}+\frac{\eta J_0}{\epsilon v_0^3}\right)=\frac{-j\omega\eta J_0}{v_0^3}E. \tag{11}$$

The solution of this equation can be found by the usual technique of first solving the homogeneous differential equation ($E=0$). The ac velocity can be found, once J_1 is known, from

$$v_1=\frac{v_0}{J_0}\left(J_1+\frac{v_0}{j\omega}\frac{dJ_1}{dz}\right). \tag{12}$$

III. SOLUTION OF THE HOMOGENEOUS DIFFERENTIAL EQUATION (ZERO TOTAL CURRENT, $E=0$)

Solutions of the form

$$J_1=\mathcal{J}\exp\left(-j\omega\int\frac{dz}{v_0}\right)=\mathcal{J}e^{-j\omega T} \tag{13}$$

will be sought, where both J_1 and $\mathcal{J}$ are functions of z only, and T is the transit time between any two planes in the absence of an ac signal. The substitution of Eq. (13) into Eq. (11), with $E=0$, gives us

$$\mathcal{J}''+\frac{3}{v_0}\frac{dv_0}{dz}\mathcal{J}'+\frac{\eta J_0}{\epsilon v_0^3}\mathcal{J}=0. \tag{14}$$

1. The Drift Space

Assume a drift region in which only the longitudinal dc space-charge forces are neutralized; then with $(dv_0)/dz=0$, we find

$$\mathcal{J}=e^{\pm j\beta_p z}, \tag{15}$$

where

$$\omega_p=\left(\frac{\eta\rho_0}{\epsilon}\right)^{\frac{1}{2}}=\left(\frac{\eta J_0}{\epsilon v_0}\right)^{\frac{1}{2}} \quad \text{and} \quad \beta_p=\frac{\omega_p}{v_0}.$$

From Eqs. (12) and (13) we find the well-known solutions for the ac current density and the ac velocity

$$J_1=(Ae^{-j\beta_p z}+Be^{j\beta_p z})e^{-j\beta z}, \tag{16}$$

$$v_1=\frac{-v_0}{J_0}\frac{\omega_p}{\omega}(Ae^{-j\beta_p z}-Be^{j\beta_p z})e^{-j\beta z}, \tag{17}$$

where $\beta=\omega/v_0$.

2. Space Charge Limited Flow

In space charge limited flow, $v_0=kz^{\frac{2}{3}}$, where $k=(9\eta J_0/2\epsilon)^{\frac{1}{2}}$, and $(\eta J_0)/\epsilon v_0^3=2/9z^2$ if the potential minimum is at $z=0$. Equation (14) becomes

$$\mathcal{J}''+\frac{2}{z}\mathcal{J}'+\frac{2}{9z^2}\mathcal{J}=0. \tag{18}$$

The solutions of (18) are

$$\mathcal{J}=Az^{-\frac{1}{3}}+Bz^{-\frac{2}{3}}. \tag{19}$$

Thus, the current density and velocity are found to be

$$J_1=[Az^{-\frac{1}{3}}+Bz^{-\frac{2}{3}}]e^{-j\omega T}, \tag{20}$$

$$v_1=-\frac{k^2}{3j\omega J_0}[A+2Bz^{-\frac{1}{3}}]e^{-j\omega T}, \tag{21}$$

where $T=3z/v_0=3z^{\frac{1}{3}}/k$.

The constants A and B can be found from the known values J_s and v_s at a plane $z=s$.

$$J_1=\left\{J_s\left[2\left(\frac{s}{z}\right)^{\frac{1}{2}}-\left(\frac{s}{z}\right)^{\frac{1}{3}}\right]+\frac{3j\omega J_0}{k^2s^{\frac{1}{3}}}v_s\left[\left(\frac{s}{z}\right)^{\frac{1}{3}}-\left(\frac{s}{z}\right)^{\frac{2}{3}}\right]\right\}e^{-j\phi}, \tag{22}$$

$$v_1=-\left\{\frac{2J_sk^2z^{\frac{1}{3}}}{3j\omega J_0}\left[\left(\frac{s}{z}\right)^{\frac{1}{3}}-\left(\frac{s}{z}\right)^{\frac{2}{3}}\right]+v_s\left[1-2\left(\frac{s}{z}\right)^{\frac{1}{3}}\right]\right\}e^{-j\phi}, \tag{23}$$

where $\phi=(3j\omega/k)(z^{\frac{1}{3}}-s^{\frac{1}{3}})$.†

† Since the entire derivation has been based upon the small signal approximation $v_1\ll v_0$, it is not clear what happens as $s\to 0$ where $v_0\to 0$. It should be noted, however, that reasonably good quantitative computations, based on A. J. Rack's (Bell System Tech. J. 17, 592–619 (1938)) and Llewellyn's analysis, have been made for high frequency tubes, in which it has been assumed that the equations can be used where $v_0=0$.

3. Arbitrary Space Charge

Now let the diode operate at a current density $J_0<J_{max}$, where J_{max} is the space-charge limited current. It can be shown that z and v_0 are related by

$$(z-z_0)^2=\frac{2\epsilon}{9\eta J_0}(v_0-2b)^2(v_0+b), \tag{24}$$

where $z_0=(-\epsilon^2\eta C_1^{\frac{1}{2}}/3J_0^2)$, $b=(\epsilon\eta C_1/2J_0)$, $v_0=0$ at $z=0$, and C_1 is the electric gradient at $z=0$. Since v_0 is not given explicitly in (24), we can help matters by changing the independent variable in (14) from z to v_0.

$$\frac{d^2\mathcal{J}}{dv_0^2}+\frac{d\mathcal{J}}{dv_0}\left[\frac{d^2v_0}{dz^2}\left(\frac{dv_0}{dz}\right)^{-2}+\frac{3}{v_0}\right]+\mathcal{J}\frac{\eta J_0}{\epsilon v_0^3}\left(\frac{dv_0}{dz}\right)^{-2}=0. \tag{25}$$

Then, using Eq. (24),

$$\frac{d^2\mathcal{J}}{dv_0^2}+\frac{d\mathcal{J}}{dv_0}\left[\frac{5v_0+4b}{2v_0(v_0+b)}\right]+\frac{\mathcal{J}}{2v_0(v_0+b)}=0. \tag{26}$$

Thus the current and velocity are found to be

$$J_1=\left[\frac{A}{v_0}+\frac{B(v_0+b)^{\frac{1}{2}}}{v_0}\right]e^{-j\omega T}, \tag{27}$$

$$v_1=-\frac{1}{j\omega}\left(\frac{2\eta}{J_0\epsilon}\right)^{\frac{1}{2}}\left[A\frac{(v_0+b)^{\frac{1}{2}}}{v_0}+B\frac{v_0+2b}{2v_0}\right]e^{-j\omega T}, \tag{28}$$

where v_0 is the dc velocity at z. If the flow is space-charge limited, $C_1=b=0$, and the equations reduce to (20) and (21).

IV. THE INHOMOGENEOUS EQUATION ($E\neq 0$)

The method of variation of constants[4] may be used to solve the equations for $E\neq 0$. When this is done for the drift space, we find

$$J_1=(Ae^{-j\beta_p z}+Be^{j\beta_p z})e^{-j\beta z}+j\omega\epsilon E\frac{\omega_p^2}{\omega^2-\omega_p^2}. \tag{29}$$

$$v_1=\frac{-v_0\omega_p}{J_0\omega}(Ae^{-j\beta_p z}-Be^{j\beta_p z})e^{-j\beta z}+jv_0\frac{\omega\epsilon E}{J_0}\frac{\omega_p^2}{\omega^2-\omega_p^2}. \tag{30}$$

[4] F. S. Woods, *Advanced Calculus* (Ginn and Company, New York, 1926).

In the same way the complete solution for the accelerated diode with arbitrary space charge is found to be

$$J_1=\left[\frac{A}{v_0}+\frac{B(v_0+b)^{\frac{1}{2}}}{v_0}\right]e^{-j\omega T}+\frac{j\eta J_0 E}{\omega v_0}, \tag{31}$$

$$v_1=\frac{-1}{j\omega}\left(\frac{2\eta}{J_0\epsilon}\right)^{\frac{1}{2}}\left[A\frac{(v_0+b)^{\frac{1}{2}}}{v_0}+B\frac{(v_0+2b)}{2v_0}\right]e^{-j\omega T}+\frac{j\eta E}{\omega}\left[1-\frac{1}{j\omega v_0}\left(\frac{2(v_0+b)\eta J_0}{\epsilon}\right)^{\frac{1}{2}}\right]. \tag{32}$$

When the current is space-charge limited, $b=0$ and Eqs. (31) and (32) become

$$J_1=\left[\frac{A}{v_0}+\frac{B}{(v_0)^{\frac{1}{2}}}\right]e^{-j\omega T}+j\frac{\eta J_0 E}{\omega v_0} \tag{33}$$

$$v_1=\frac{j}{\omega}\left(\frac{2\eta}{J_0\epsilon}\right)^{\frac{1}{2}}\left[\frac{A}{(v_0)^{\frac{1}{2}}}+\frac{B}{2}\right]e^{-j\omega T}+\frac{j\eta E}{\omega}\left[1+\frac{j}{\omega}\left(\frac{2\eta J_0}{\epsilon v_0}\right)^{\frac{1}{2}}\right]. \tag{34}$$

To be symmetrical with Eqs. (29) and (30), these may be rewritten

$$J_1=\left[\frac{A}{v_0}+\frac{B}{(v_0)^{\frac{1}{2}}}\right]e^{-j\omega T}+j\omega\epsilon E\frac{\omega_p^2}{\omega^2} \tag{33a}$$

$$v_1=j\frac{v_0}{J_0}\sqrt{2}\frac{\omega_p}{\omega}\left(\frac{A}{v_0}+\frac{B}{2}\right)e^{-j\omega T}+jv_0\frac{\omega\epsilon E}{J_0}\frac{\omega_p^2}{\omega^2}\left(1+j\sqrt{2}\frac{\omega_p}{\omega}\right), \tag{34a}$$

where $\omega_p^2=\eta J_0/\epsilon v_0$.

ACKNOWLEDGMENT

The author would like to thank Professor L. J. Chu for many helpful discussions and suggestions.

JOURNAL OF APPLIED PHYSICS VOLUME 22, NUMBER 12 DECEMBER, 1951

The Capacitance of a Circular Annulus

W. R. SMYTHE
California Institute of Technology, Pasadena, California
(Received July 16, 1951)

Two formulas are derived for the capacitance of a flat circular annulus. The first has an accuracy of 1 part in 1000 or better when the ratio of the external to the internal radius lies between 1.1 and ∞ and is exact at ∞. The second, $C=34.96R/\ln(32R/c)$ $\mu\mu$f, has an accuracy of 1 part in 1000 when the ratio lies between 1.000 and 1.1 and is exact at 1.000. In this formula c is the difference of the radii and R their mean value in meters. An approximate expression for the charge density is given in the first case.

AT an American Institute of Electrical Engineers meeting in Madison, Wisconsin, on May 17–19, 1951, T. J. Higgins and D. K. Reitan described the calculation of the capacitance C of a circular annulus by their method of subareas,[1] and pointed out the futile efforts of several mathematicians to solve the problem.[2–4] The annulus is an infinitely thin plane conducting area bounded by concentric circles of internal and external radii a and b. They found a lower limit for C for seven values of b/a ranging from 1.0213 to 1.5000. In the discussion the author presented a lower limit formula valid when b/a is large. Since then he has improved it to provide both upper and lower limits. The insertion of a simple correction factor gives a formula for C which is accurate to 1 part in 1000 or better over a range of b/a from 1.1 to ∞. A second formula of equal accuracy covers the remainder of the range from 1.000 to 1.1.

METHOD OF APPROXIMATION

Consider a freely charged plane conducting disk of radius b at potential V. The charge density in coulombs per square meter including both faces, on such a disk is[5,6]

$$\sigma_0=4\epsilon V[\pi(b^2-\rho^2)^{\frac{1}{2}}]^{-1}, \tag{1}$$

where ρ is the distance from the center and $\epsilon=8.855\times10^{-12}$. The charge inside $\rho=a$ is q_0, and that between $\rho=a$ and $\rho=b$ is Q_0. This is shown in Fig. 1a. Now calculate the charge density σ_1 (including both faces) on an infinite plane conducting sheet at potential zero having a hole bounded by $\rho=a$ in which there is a fixed charge distribution of density $-\sigma_0$, as shown in Fig. 1b. Superposition gives Fig. 1c in which the annulus between a and b is at potential V under the influence of a small coplanar positive charge q_1 in the region $\rho>b$. The charge Q_0+Q_1 on the annulus is less than if q_1 were removed so the ratio $(Q_0+Q_1)/V$ gives a lower limit C_1 for C. As b/a increases, q_1 decreases and C_1 approaches C. The induced charge cannot exceed $-q_1$ so the charge on the annulus at potential V cannot exceed $q_1+Q_0+Q_1$ which was the original charge on the disk. Thus C is less than $8\epsilon b$, the capacitance of a disk.

Now calculate the charge density σ_2 (including both faces) on a disk or radius b at potential zero when there is a coplanar fixed charge distribution of density $-\sigma_1$ in the region $\rho>b$ as shown in Fig. 1d. The induced charge inside $\rho=a$ is q_2 and that between $\rho=a$ and $\rho=b$ is Q_2. Superposition of Fig. 1c and Fig. 1d gives Fig. 1e in which the annulus at potential V is influenced by a very small coplanar charge q_2 in the hole. Evidently C is greater than $(Q_0+Q_1+Q_2)/V$ and less than $(Q_0+Q_1+Q_2+q_2)/V$. In theory this process could be repeated indefinitely to give a rigorous result. Because the integrals become increasingly complicated we have carried it out only as far as described.

CALCULATION

A ring charge $2\pi\sigma_0 dc$ at $\rho=c$ in a hole $\rho=a$ in an infinite coplanar sheet at potential zero induces at ρ a charge density σ_1 which is,[7] including both faces,

$$\sigma_1=-2\sigma_0(a^2-c^2)^{\frac{1}{2}}[\pi(\rho^2-a^2)^{\frac{1}{2}}(\rho^2-c^2)]^{-1}dc. \tag{2}$$

The first approximation to the charge on the annulus is then

$$Q_0+Q_1=\int_a^b 2\pi(\sigma_0-\sigma_1)\rho d\rho. \tag{3}$$

The integrations are straightforward and division of the result by V gives

$$C_1=16\epsilon b\pi^{-1}[\cos^{-1}(a/b)+(1-(a^2/b^2))^{\frac{1}{2}}\tanh^{-1}(a/b)]. \tag{4}$$

This obviously gives $8\epsilon b$, the capacitance of a disk, if $a=0$.

Inversion of (2) shows that a ring charge $2\pi\sigma_1 dc$ at $\rho=c$ will induce at ρ on a coplanar disk at potential zero bounded by $\rho=b$ a charge density σ_2 which is, including both faces,

$$\sigma_2=-2\sigma_1(c^2-b^2)^{\frac{1}{2}}[\pi(b^2-\rho^2)^{\frac{1}{2}}(c^2-\rho^2)]^{-1}dc. \tag{5}$$

[1] T. J. Higgins and D. K. Reitan, Am. Inst. Elec. Engrs. Trans. **70**, 1 (1951).
[2] J. W. Nicholson, Proc. Roy. Soc. (London) **101A**, 195 (1922).
[3] E. G. C. Poole, Proc. London Math. Soc. **29**, 342 (1929) and **30**, 174 (1930).
[4] N. Lebedev, J. Tech. Phys. (U.S.S.R.) **4**, 1 (1937).
[5] W. R. Smythe, *Static and Dynamic Electricity* (McGraw-Hill Book Company, Inc., New York, 1950), p. 114.
[6] Mks units are used throughout.
[7] Reference 5, p. 203, last line.

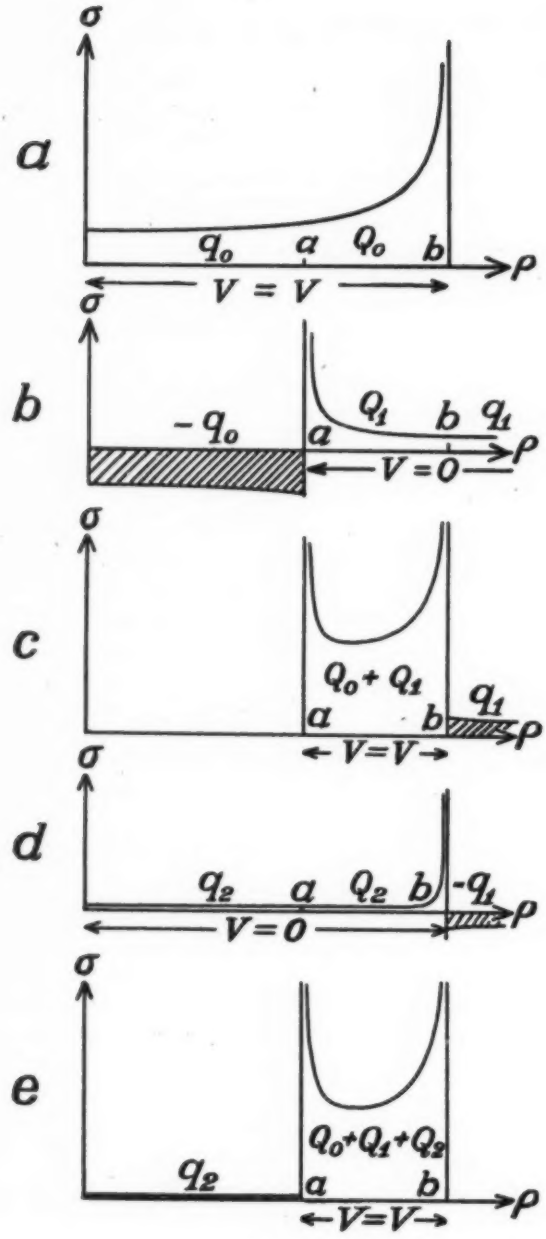

FIG. 1.

The charge to be added to (3) for a better lower limit is,

$$Q_2=\int_a^b 2\pi\sigma_2\rho d\rho \tag{6}$$

and for a better upper limit it is,

$$q_2+Q_2=\int_0^b 2\pi\sigma_2\rho d\rho. \tag{7}$$

We could not obtain the integrals of (6) and (7) in closed form. Since this method works best for large values of b/a we expressed them as a power series in a/b. The integrations were carried out twice independently and the lower limit result was further verified by a different method of integration. Thus we have

$$C_1+\Delta C'<C<C_1+\Delta C'', \tag{8}$$

where $\Delta C'$ and $\Delta C''$ have the form

$$\Delta C=0.12112(16\epsilon b/\pi)\sum_{n=0}^{\infty}A_n(a/b)^{2n+3}. \tag{9}$$

The coefficients A_0' and A_0'' are 1 and the rest are given in Table I. Numerical results for several values of b/a appear in Table II.

CORRECTION FOR SUBANNULAR METHOD

The foregoing method is inaccurate for ratios of b/a much less than 1.2. To get better values for small ratios a correction is added to the results of Higgins and Reitan. They divide the annulus into several uniformly charged subannuluses of equal width, the charge on each being such that all have the same potential on their center lines. The chief effect of making the annulus conducting is to redistribute the charge on each subannulus. This lowers the local potential but has little effect on the potential at more remote points. This drop of potential will therefore be nearly independent of the curvature of the annulus and may be calculated for an infinite straight strip. The resultant corrected capacitance turns out to be very close, being only 1 percent too low in the most unfavorable case of a disk.

An infinite strip of width c which carries a total charge Q_1 per unit length and whose inner and outer quarters have uniform charge densities $0.6847c^{-1}Q_1$ and $1.3151c^{-1}Q_1$, respectively, has, at the center of each quarter, the potential

$$V'=(2\pi\epsilon)^{-1}Q_1[\ln(cR^{-1})-1.4743]. \tag{10}$$

Here R is the distance from the center of the strip to a distant parallel reference line at zero potential. When one, two, or three subareas are used instead of four the last number is replaced by 1.6931, 1.5621, or 1.5034. For a conducting strip of the same width and charge per unit length the potential is given by a conformal transformation to be[8]

$$V=(2\pi\epsilon)^{-1}Q_1\sinh^{-1}(2c^{-1}R)$$
$$\approx(2\pi\epsilon)^{-1}Q_1[\ln(cR^{-1})-1.3863]. \tag{11}$$

The difference, which is the correction to the subarea approximation, is

$$\Delta V=\alpha_n Q(a+b)^{-1}\times 10^{12}, \tag{12}$$

TABLE I.

n	1	2	3	4	5	6
A_n'	0.3832	0.1960	0.1435	0.0582	0.0446	0.0357
A_n''	0.6752	0.4910	0.3794	0.3050	0.2544	0.2212

[8] Reference 5, page 90.

TABLE II. Capacitance of annulus in $\mu\mu$f. Outer radius is b meters.

b/a	Sub areas	Lower limits Original H. and R.	Lower limits H. and R. (Eq. (14))	Eq. (4)	Eq. (8)	Upper limit Eq. (8)	Best values Eq. (15)	Best values Eq. (18)
∞	4	67.60b	69.97b	70.73b	70.73b	70.73b	70.73b	...
2.0000	..	...	...	68.68b	69.44b	69.51b	69.49b	...
1.5000	4	65.71b	67.03b	64.98b	66.97b	67.33b	67.08b	...
1.2500	3	61.97b	63.44b	58.75b	62.61b	63.90b	63.41b	...
1.2000	2	59.94b	62.09b	56.30b	60.84b	62.63b	62.05b	62.00b
1.1250	1	55.77b	58.82b	50.73b	56.8b	61.3b	58.99b	58.99b
1.0909	1	53.82b	56.61b	46.80b	...	...	56.69b	56.73b
1.0445	1	49.30b	51.58b	37.86b	...	...	...	51.69b
1.0213	1	45.25b	47.15b	30.07b	...	...	...	47.20b

where Q, the charge on the annulus, is the product of Q_1 by its mean circumference $\pi(a+b)$. The values of α_n when n, the number of subannuluses, ranges from 1 to 4, are

$$\alpha_1=0.001755, \quad \alpha_2=0.001060,$$
$$\alpha_3=0.000671, \quad \alpha_4=0.000503. \tag{13}$$

If the subarea capacitance is $C_0=Q/V_0$ then the corrected capacitance is

$$C=Q(V_0-\Delta V)^{-1}=C_0[1-\alpha_n(a+b)^{-1}C_0\times 10^{12}]^{-1}. \tag{14}$$

The values obtained by application of this formula to the Higgins and Reitan results appear in the fourth column of Table II. For 2, 3, and 4 subareas the apparent accuracy is 0.01 percent and for 1 subarea 0.05 percent although in the last case the original values are 4 percent too low.

GENERAL FORMULA

Addition of a simple correction factor to Eq. (4) gives the following formula for the annulus capacitance which is certainly good to 1 part in 1000 over the range $1.1<b/a<\infty$ and much better in the range $2<b/a\lesssim\infty$.

$$C=C_1[1+(0.0143b/a)\tan^3(1.28a/b)]. \tag{15}$$

The values given by this formula appear in Table II. It is not reliable when b/a is less than 1.09.

NARROW ANNULUS

The very narrow annulus is best approached from the side of the infinite straight strip for which the exact solution is known. Equation (11) shows that the potential of an infinite conducting strip of width $c=b-a$ is

$$V=(2\pi\epsilon)^{-1}Q_1\ln(\tfrac{1}{4}cR^{-1}), \tag{16}$$

where R is the distance from its center to a distant parallel reference line at zero potential. This is exactly the same as would be produced by a line charge of strength Q_1 per unit length at a distance $\frac{1}{4}c$ from the center line. If a finite length of the charged strip is bent into a ring so that its axis lies on a circle of radius R, then the potential on its center line will be nearly that of a circular ring charge of the same linear strength and radius but displaced a distance $\frac{1}{4}c$ from it. Thus, we have

$$V\approx\frac{Q}{4\pi^2\epsilon}\int_0^\pi\frac{d\phi}{[(\tfrac{1}{4}c)^2+(2R\sin\tfrac{1}{2}\phi)^2]^{\frac{1}{2}}}=\frac{2QK(k)}{\pi^2\epsilon(c^2+64R^2)^{\frac{1}{2}}}, \tag{17}$$

where the modulus k of the complete elliptic integral K is $8R(c^2+64R^2)^{-\frac{1}{2}}$. When c/R is small, k is close to one so that $k'=(1-k^2)^{\frac{1}{2}}$ is nearly zero and K may be replaced with great accuracy by $\ln(4/k')$.[9] Thus, we get

$$C=\frac{Q}{V}\approx\frac{4\pi^2\epsilon R}{\ln(32R/c)}=\frac{34.96R}{\ln(32R/c)}\times 10^{-12}\text{ farad}. \tag{18}$$

Here $2R$ is $a+b$ and c is $b-a$. The accuracy is about 1 part in 1000 when b/a is 1.1 and increases as the band narrows and b/a approaches unity.

CHARGE DENSITY ON ANNULUS

A first approximation to the charge density on the annulus is found by putting Eq. (1) into Eq. (2), integrating from $c=0$ to $c=a$, adding σ_0 from Eq. (1), and dividing by 2. This gives the charge density at the radius ρ on one surface of the annulus to be

$$\frac{2\epsilon V}{\pi(b^2-\rho^2)^{\frac{1}{2}}}\left[1+\frac{2(b^2-\rho^2)^{\frac{1}{2}}}{\pi(\rho^2-a^2)^{\frac{1}{2}}}\tanh^{-1}\frac{a}{b}+\frac{2}{\pi}\tan^{-1}\frac{a(b^2-\rho^2)^{\frac{1}{2}}}{b(\rho^2-a^2)^{\frac{1}{2}}}\right]. \tag{19}$$

This is a lower limit. When multiplied by the last factor in Eq. (15), the average density is correct but the density near the inside edge is slightly too high and that near the outer edge is too low.

[9] H. B. Dwight, *Tables of Integrals* (Macmillan Company, New York, 1947), Formula number 773.3.

Letters to the Editor

Electron Diffraction Study on the Ordered Alloy Au_3Cu

S. OGAWA AND D. WATANABE
The Research Institute for Iron, Steel and Other Metals, Tohoku University, Sendai, Japan
(Received May 11, 1951)

IN the alloy system of gold and copper two kinds of superlattice, namely, Cu_3Au and CuAu, are well known. From the viewpoint of the crystal structure, the existence of the superlattice Au_3Cu with a face-centered cubic type is predictable, but no reliable report on this point has been given till recently. Cowley[1] calculated the critical temperatures of order-disorder transition in this alloy system and obtained 190°C for Au_3Cu. Recently, Hirabayashi[2] investigated the specific heat-temperature relation for the gold-copper alloy of 74 atomic percent of gold which had been annealed at 200°C for 20 days, and observed a peak of λ-type at 243°C. Moreover, the specimen after annealing at 200°C for 20 days has clearly shown several superlattice lines in the microphotometer trace of its x-ray back reflection photograph.

For the study of a superlattice of such a low critical temperature, the electron diffraction method is surely valid, because the ordered region, which is hardly formed by a low temperature annealing, can be detected in its early stage of formation on account of the short wavelength of electron. Germer[3] first applied the electron diffraction method to the problem of order in an alloy and studied with success the behavior of Cu_3Au at high temperatures, while it is because of the low critical temperature that he failed to detect the ordered structure of Au_3Cu.

In our experiment, double films of metal were made on the cleavage surfaces of rocksalt by successive evaporations of gold and copper in vacuum, each quantity being so controlled that the atomic ratio of the former to the latter is 3 to 1. They were homogenized at 400°C for 30 min after being removed from the substrata and were annealed at 200°C or 210°C for a long time in vacuum; and then the diffraction photographs were taken, in which several clear signs of the ordered lattice were seen. Among several heat-treated films, the one annealed at 200°C for 210 hr indicated the most distinct superlattice rings of (100), (110), (210), (211), and (321), which were considerably broader than normal rings, and the extent of the ordered region estimated from (110) rings breadth was about 50A. In every photograph, (110) was the most intense superlattice ring rather than (100) because of a strong orientation of the film, which made the consideration about the ring intensities impossible; nevertheless, it gave a quite good indication of an early stage of order. These incompletely ordered films were heated step by step up to 500°C and examined by electron diffraction after being quenched from several temperatures in the course of the heating. The estimated extent of the ordered region decreased monotonically with temperature rise: for example, it was 19A at 250°C and 16A at 300°C. At high temperatures far beyond the critical point on the specific heat-temperature curve, photographs still showed faint broad bands of (110), which indicate the persisted small ordered region extending 14A at 400°C and 11A at 500°C. These results coincide well with what Germer obtained for Cu_3Au and seem to be a property common to all 3-to-1 superlattices of a face-centered cubic structure. On the other hand, Germer reported that no trace of the ordered region could be found in CuAu above 400°C. Such a distinct difference between the 3-to-1 and the 1-to-1 superlattices also exists in the measurements of specific heat: in Cu_3Au[4] or in Au_3Cu[2] an excess specific heat appeared above the critical temperature, but none appeared in CuAu.[5] These facts concerning specific heat seem to confirm the results obtained by the electron diffraction experiments. A report in detail will be published in the *Journal of the Physical Society of Japan*, or in the *Science Reports of the Research Institutes*, Tohoku University, Sendai, Japan.

[1] J. M. Cowley, Phys. Rev. **77**, 669 (1950).
[2] M. Hirabayashi, J. Phys. Soc. Japan. **6**, 129 (1951).
[3] Germer, Haworth, and Lander, Phys. Rev. **61**, 614 (1942).
[4] C. Sykes and F. W. Jones, Proc. Roy. Soc. (London) **A157**, 213 (1936).
[5] Hirabayashi, Nagasaki, and Maniwa, Japan. Inst. Metals **14**, No. 3, 1 (1950).

On the Reliability of Geiger-Counter Response at Moderately High Rates*

L. G. PARRATT AND C. F. HEMPSTEAD
Cornell University, Ithaca, New York
(Received July 25, 1951)

SELF-QUENCHING Geiger counters are being used in many applications requiring measurement of ionizing events at a rate N above a few hundred per second with an accuracy of better than 2 percent. The common practice is to record a rate N_c for a time t seconds such that, after correction for "lost counts" by $N=N_c/(1-N_cT)$, the fractional standard deviation $(Nt)^{-\frac{1}{2}}$ is equal to or less than the required accuracy. T, the effective resolving time of the counter and detecting circuit, is assumed to be known, or is measured by varying N in a known way with the assumption that T is constant. This practice, possibly valid for counting rates less than about 100 cps, leads to a false sense of security for rates above a few hundred cps.

The basic difficulty lies in the inconstancy of the ratio of spurious counts to valid counts. Spurious counts are commonly recognized as the multiple counts that occur at the time the positive ion sheath reaches the cathode (other mechanisms for spurious counts have also been proposed), and as the "monkey business" responsible for part of the slope of the plateau curve, especially for the abrupt increase in slope at the upper end of the curve. At low rates, the slope of the plateau (if expressed as a percentage per volt) is very nearly constant and is more or less independent of rate; these facts suggest that, at least for operation at the middle of the plateau, the ratio of spurious to valid counts is constant, although at high rates some experiments have indicated that the ratio increases with rate.[1]

Typical calibration curves[2] are shown in Fig. 1 for plain wire counters at each of two discrimination voltages, 0.25 and 0.063. The figure also includes calibration curves for two beaded wire counters, one with 8.7-mm bead spacing (10 beads) and one with 15-mm spacing (5 beads), both at the same discrimination voltage.

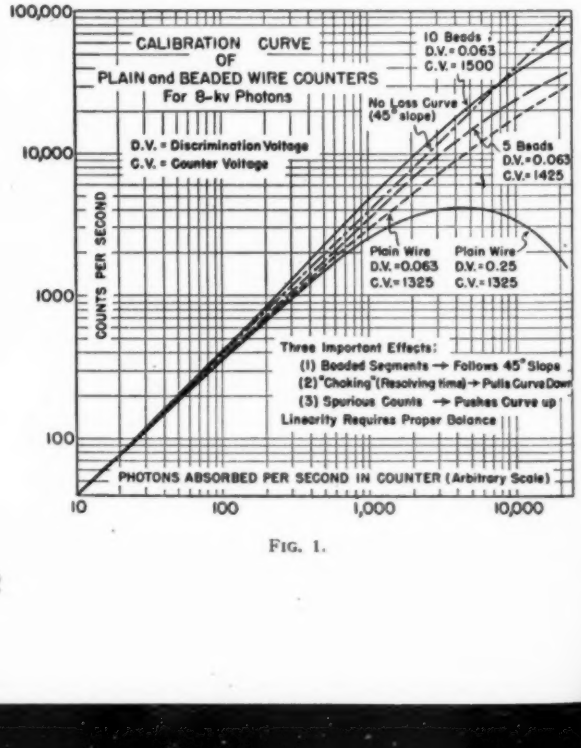

FIG. 1.

From such a curve for a particular counter the rate dependence of the effective resolving time may be determined. Typically, T initially decreases with N, reaches a minimum, then increases as N is further increased. For the beaded wire counter with 8.7-mm spacing, the effective resolving time is actually *negative* for the rate range of about a hundred to 20,000 cps. A negative resolving time means, of course, that there are more spurious counts than lost counts. (In the upper range, the 5-microsecond resolving time of the detector circuit is a significant factor in pulling the curve down.) Other aspects of these curves are explainable qualitatively on the basis of current Geiger-counter theory.

The curves of Fig. 1 were taken with 8-kv photons entering the counter axially. For such a triggering photon in a beaded wire counter, the probability is negligible of having more than two segments of the anode discharged, whereas in the case of the plain wire the entire anode length is discharged. The ratio of spurious to valid counts increases with the length of the discharge; therefore, the ratio of spurious to valid counts with the plain wire counter must be alarmingly large at moderate to high rates. No adequate statistical theory of lost counts, taking into account the simultaneous multiple sheaths of positive ions and the voltage drop across the input resistor, has been made so one cannot say to what extent the loss is compensated by the increase in spurious counts.

A clear demonstration of the increase in the ratio of spurious to valid counts is afforded by a series of plateau curves run at successively increased rate. Such curves are presented in Fig. 2.

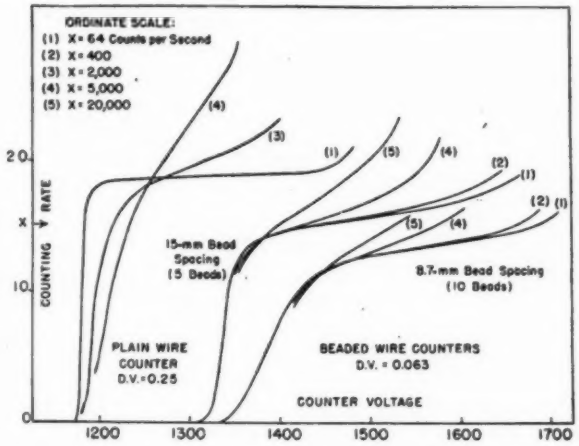

FIG. 2. "Plateau" *vs* counting rate, plain and beaded wire counters for 8-kv photons.

The linear ordinate scale for the plain and beaded wire counters is indicated for each curve by the scale position "x." The fact that the plateaux for the beaded wire counters do not deteriorate with rate as readily as do the plateaux for the plain wire counters supports the observation[3] that the ratio of spurious to valid counts depends upon the length of the discharge.

When an attempt was made to repeat the cycle of plateau curves, with no appreciable rest time between cycles, the curves did not repeat. It was necessary to let the plain wire counter rest for several hours before near-identical repetition of the low rate curves was possible; and, following a high rate curve, the necessary rest period was sometimes extended to a day or two. With the beaded wire counters, a much shorter but still definitely noticeable rest period was required for satisfactory repetition. This dependence of the ratio of spurious to valid counts upon the immediate past history of counting rate is a very serious problem in many applications, and by itself precludes 2 percent accuracy when a range of rate of about a thousand to one cps is involved in a time interval less than many (perhaps 30) minutes.

After several cycles with the plain wire counter, the plateau curves would not repeat. The counter showed the usual effects of age—presumably of consumption of the quenching gas. As might be expected, the beaded wire counter would repeat through many more cycles than would the plain wire counter before showing age effects. This age phenomenon is also a serious obstacle to accuracy if a repetition of rather large rates is unavoidable.

It is further evident from the plateau curves, that, to minimize the inconstancy of the ratio of spurious to valid counts, one should operate his counter at a small overvoltage, closer to the voltage for onset of the plateau than the current general practice of operating at about the middle. In other words, the inconstancy of spurious counts is much more serious in preventing accuracy than is inconstancy in the voltage supplied to the counter by a modern stabilized power supply.

The inconstancy of the ratio of spurious to valid counts thus depends upon counting rate, length of the discharge, immediate past counting history, tube age, and the overvoltage. These factors are a source of inconstancy of Geiger-counter response and a *menace to accuracy, even after correction*, at rates in excess of a few hundred cps. The authors believe that investigators experienced with Geiger counters are more or less acquainted with these vagaries and would avoid using Geiger counters at these rates, but the dangers have not been adequately emphasized.

* Supported in part by the ONR.

[1] See D. H. Wilkinson, *Ionisation Chambers and Counters* (Cambridge University Press, London, 1950), pp. 225–237.

[2] Most of the many counters used in this study were constructed with currently popular gases and electrode materials, *viz.*, argon with either ethyl alcohol or ethylene quenching vapor, brass cathodes (1.9 cm inside diameter, 12 cm long), and tungsten wire anodes (4 mil diameter, 10.5 cm long). The cathode was carefully cleaned and "passivized," then the counter was filled with 1.6 mm Hg of quenching vapor, and argon (99.6 percent pure and 0.4 percent nitrogen) to a total pressure of 16 mm Hg. Brief studies with stainless steel cathodes, and of a few commercial plain wire counters of unspecified gases and cathode coatings showed similar results. The slope of the plateau curves for all new plain wire counters studied was 0.02 to 0.03 percent per volt at about 90 cps. As observed on an oscilloscope, the pulses were of uniform size and shape, and the number of multiple spurious counts was satisfactorily small. All counters were kept and used at room temperature.

[3] Also see A. G. Fenton and E. W. Fuller, Proc. Phys. Soc. (London) **A62**, 32 (1949).

The Transmission of Hydrogen through Metals

H. B. WAHLIN
Department of Physics, The University of Wisconsin, Madison, Wisconsin
(Received November 5, 1951)

IT is, of course, a well-known fact that hydrogen diffuses into some metals, but some uncertainty exists as to the mechanism of the process. In order to test the hypothesis that the process consists of a surface dissociation followed by a diffusion of the atomic hydrogen into the metal, the following experiment was tried.

Palladium was made the cathode in an ordinary sulfuric acid bath, and it was found that the hydrogen passed through the metal at room temperature and in appreciable quantities (as much as 1.5 cc per cm² per min). The diffusion rate increases rapidly with the temperature.

A palladium tube connected to a pressure gauge was made the cathode in the bath, and a hydrogen pressure of 700 psi was built up. This is not the limiting pressure and the indications are that the limiting pressure, which would be when the pressure dissociation equals the electrolytic, is several thousand pounds.

The work has been extended to a number of other metals and it has been found that Ni, Nb, Ta, and Mo all show a slight transmission. Iron also transmits. This has been known for some time. Copper transmits hydrogen so slowly (if at all) that so far no positive results have been obtained. The work is being extended to other metals. It is hoped that more quantitative results will be obtained in the near future.

A number of obvious applications immediately suggest themselves. As examples:

(1) The electrolytic method can be substituted for the heated palladium tube in a palladium hydrogen source.

(2) A method of getting high pressure, pure hydrogen, at least on a laboratory scale, is obvious.

Other possible applications are being investigated.

A Method of Producing an Electric Current from Radioactivity

P. E. OHMART*
The Ohmart Corporation, Cincinnati, Ohio
(Received September 5, 1951)

EXPERIMENTS have shown that if a cell, made up of two electrochemically dissimilar materials separated by a gas, is connected to a current measuring device, a small continuous current will be caused to flow from the more noble to the more active electrode without an external source of voltage when the separating gas is forcibly ionized by exposure to nuclear radiation. The current thus produced has been found to be dependent upon the nature of the electrodes and their surfaces, the type and flux density of the energizing radiation, the type and pressure of the filling gas, and (when excited by gamma-radiation) the gamma-stopping power of the electrodes.

It has been found, for example, that if a cell with one electrode made of gold and the other of lead with air as the filling gas is energized by gamma-radiation, a small, continuous current will flow from the gold to the lead. If a copper electrode is substituted for the gold, the current is smaller but the polarity is the same. When the surface of the copper is oxidized the current increases and is greater than that originally obtained with the gold. When a lead electrode having a surface that is identical with the other lead electrode is substituted for the gold electrode, no current flows. When an aluminum electrode is substituted for the gold, the current is weaker and is reversed in polarity.

By connecting a potentiometer with such a polarity that increasing the voltage of the potentiometer caused a reduction in the current flow and adjusting it until the current dropped to zero, it was found to be possible to measure the open-circuit voltage of the cell. By carrying out a number of measurements with various types of filling gases at different pressures, with various types of energizing radiation on a number of different electrode combinations, it was found that the open-circuit voltage of the cell is apparently dependent upon the character of the surfaces of the electrodes only and is essentially independent of the type and pressure of the filling gas, the geometry of the cell, and the type of energizing radiation. A list of open-circuit voltages of cells with aluminum negative electrodes (Al_2O_3 surfaces) and different positive electrodes is given in Table I. It will be noted that these fall in the same general position as they appear in the electrochemical series.

TABLE I. Open-circuit voltages of cells with aluminum (Al_2O_3) negative electrodes.

Positive electrodes	Characteristic potential (volts)
PbO_2 plated on gold	1.34
Oxidized copper	0.975
Gold plated on copper	0.95
Silver	0.67
Copper	0.64
Brass	0.64
Lead	0.2
Chromium	0.18
Zinc	−0.01

The current, on the other hand, was found to increase as the flux density increased, to increase as the molecular weight of the filling gas increased (ionization potential of the gas also seems to be an influencing factor), to approach zero as the gas pressure approached zero, and to depend on the type of energizing radiation. Also, when a cell was energized by gamma-radiation, it was found that the gamma-stopping power of the electrodes was an important factor since some ionization of the filling gas is produced by secondary electrons emitted from the surfaces of the electrodes. For example, a gold:lead cell gives greater current flow from gamma-radiation than a copper oxide:aluminum oxide cell even though its open-circuit voltage is lower.

The fact that the current approaches zero as the pressure of the gas approaches zero and an experiment carried out with alpha-activity in which the cell was so arranged that current flow was caused by ionization of the gas alone (since none of the alpha-particles could strike either electrode) indicate that practically none of the total current is produced by selective secondary electron emission from the electrodes. Also it should be noted that when a light metal is employed as the positive electrode and a heavy metal as the negative electrode, tendencies for current flow caused by secondary electron emission from the electrodes will be in opposition to the direction that the current actually has been observed to flow.

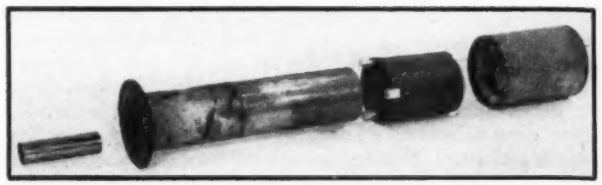

FIG. 1. Coaxial type cell, disassembled.

From the foregoing it appears as if these cells are essentially constant-voltage generators with variable internal impedances and that there is a close analogy between these and the ordinary electrolytic cells. The voltage in both types of cells is dependent upon the nature of the electrodes, and the current is dependent upon the concentration of ions between the electrodes as well as the external load resistance. Also there is an analogy to the behavior of an ordinary ionization chamber. In the ionization chamber the electrodes may be identical, and an external potential is required to make the radiation-produced gas ions move and thus produce a current. Whereas, in this cell the inherent potential difference between the electrodes produces the necessary potential.

Also it is interesting to note the similarity of the method of measuring the open-circuit voltages of the cells and the Kelvin Null method of measuring contact differences of potential. In the Kelvin Null method contact potentials are made to produce a current flow by vibrating a reed in the electrostatic field produced by the contact potential of the electrodes. In these cells, the current flow is produced by ionizing the gas in the field between the electrodes.

Initial efficiencies of conversion of radioactive energy to electrical energy that were achieved were only of the order of 1×10^{-11} percent when an air cell was excited by gamma-radiation from a 24.8 milligram radium source. In order to improve these efficiencies the co-axial type cell, shown in Figs. 1 and 2, was constructed.

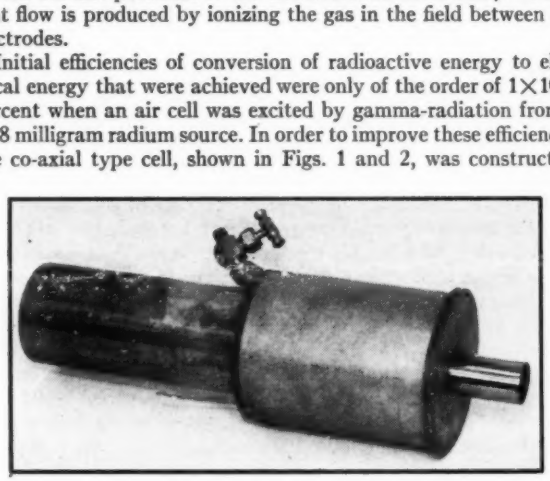

FIG. 2. Coaxial type cell, assembled.

In this cell the negative electrode was prepared by first plating the brass case with lead and then coating the lead with magnesium by metal evaporation. Thus, since no efforts were made to protect it from oxygen, the negative electrode had a magnesium oxide surface. The positive electrode was made by plating brass shim stock first with gold and then with lead-dioxide. The characteristic potential of the cell was 1.24 volts. The cell was filled with argon gas at 70 pounds per square inch gauge. The sample was mounted

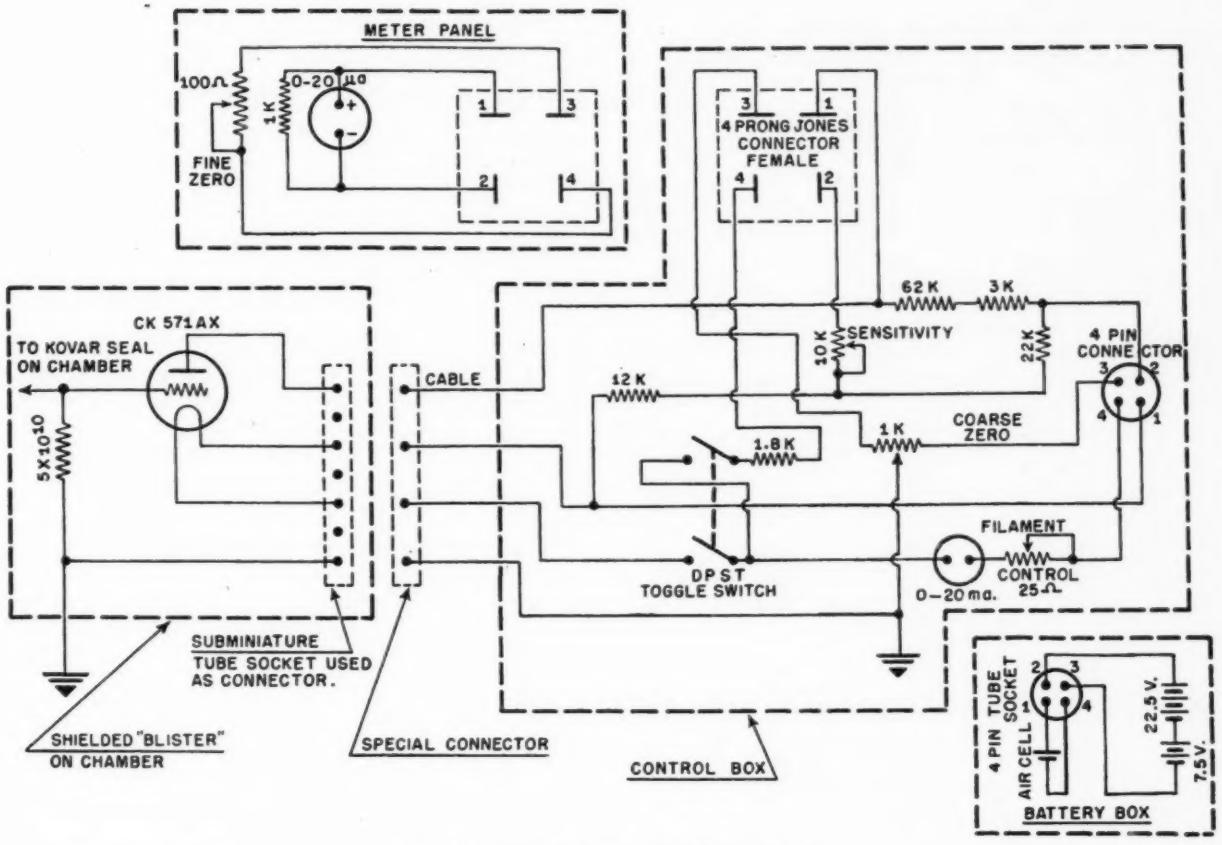

FIG. 3. Electrometer circuit used with coaxial cell.

in the center of the cylinder so that greater than 50 percent geometry was obtained.

When this cell was connected to the simple electrometer circuit shown in Fig. 3 and was checked for sensitivity and linearity with several calibrated Co^{60} sources the curve shown in Fig. 4 resulted.

When the cell was excited with approximately 11 microcuries of Ag^{110}, 0.86 volt was developed across 1×10^{11} ohms, thus the electrical power that was received from the cell was 7.3×10^{-12} watt. If the assumption is made that the gamma-radiation from Ag^{110} has an average energy of 1.0 million electron volts, then the power that would be available from the source would be (number of disintegrations per second)$\times$(the energy of the gamma-photons)$\times$(charge on an electron). In numerical values this would give

$$(11.0\times10^{-6}\times3.7\times10^{10})\times(1.0\times10^{6})\times(1.59\times10^{-19})$$
$$=6.49\times10^{-8}\text{ watt.}$$

So the over-all efficiency would be

$$(7.3\times10^{-12})/(6.49\times10^{-8})\times10^{2}=0.011\text{ percent.}$$

If this is corrected by a geometry factor so that only the gamma-energy that is available for conversion to electrical energy is considered, then the efficiency would be about 0.02 percent.

For recoil-proton or alpha-detection where it is desirable to discriminate against gamma-radiation, it has been found desirable to make electrodes of light materials such as aluminum for the negative electrode and copper-oxide-on-copper or carbon for the positive electrode to reduce the number of secondary electrons emitted from the electrodes.

Although this effect may be found to have many uses, so far its applications mainly have been confined to the measurement of electrode potentials, to the measurement of the rate of growth of oxide films, and to the measurement of gamma-radiation in a portable gamma-monitor. It has been possible to build a gamma-monitor that has an over-all size of $3\frac{1}{8}$ inches by $3\frac{1}{8}$ inches by $7\frac{1}{4}$ inches. Compared with the well-known "Cutie Pie," it is smaller, more sensitive, and simpler in that no high voltage battery is required. It should be pointed out however that the energy-sensitivity of the detector is not, as yet, known. A complete description of this device will appear later in the literature.

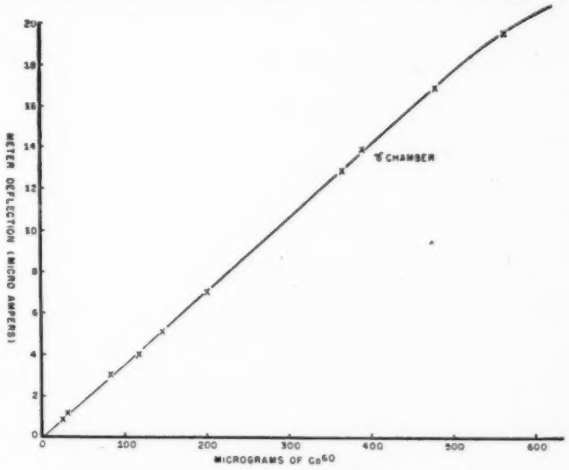

FIG. 4. Calibration curve of coaxial cell.

Experiments performed to date in this work have been of a preliminary and exploratory nature. It is planned to repeat all experiments discussed here with greater attention to detail and control so that greater precision will result.

* Formerly of Mound Laboratory, Monsanto Chemical Company, Miamisburg, Ohio.

A New Point of View on Magnetic Losses in Anisotropic Bars of Ferrite at Ultra-High Frequencies

H. G. Beljers, W. J. van de Lindt, and J. J. Went*
Philips Research Laboratories, N. V. Philips' Gloeilampenfabrieken, Eindhoven-Netherlands
(Received September 17, 1951)

We recently found that several ferrite bars, when adequately prepared, show magnetic losses at frequencies between 100 and 10,000 mc/sec which can be greatly reduced (in some cases down to 10 percent) by a relatively small, axially directed, polarizing magnetostatic field. The magnetic losses were measured in a TE_0 cavity resonator with the ferrite bars exposed to the transverse magnetic microwave field and a variable axial dc field. Figure 1 gives a curve of the losses of these ferrite bars in terms of

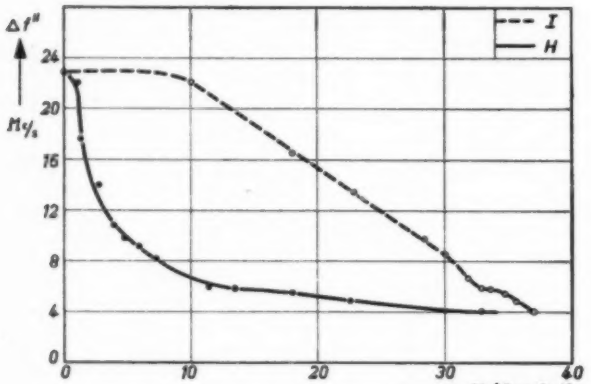

Fig. 1.

the half-width value of the resonance curve of the cavity as a function of the magnetostatic field H, and also as a function of the polarization I, the latter showing a more gradual decrease of the losses.

More particularly, an appreciable decrease in the losses is found in the following circumstances:

1. The specific resistance is sufficiently high, which condition is fulfilled in most Ni—Zn ferrites.

2. Bars that have been extruded with a binding agent show a much greater effect than pressed bars. Especially "Electrocol" (a partly hydrolyzed potato starch product manufactured by Scholten's Aardappelmeelfabrieken) appears to be a good binding agent for this purpose.

3. The sintering process should be carried out in such a way that the apparent density is not too high.

Ferrite bars not suitably prepared show losses nearly independent of the polarization. Generally these losses are on the same level as the rest-losses of the polarized bars that have additional losses in the unpolarized state as already mentioned. Moreover, there seems to be an upper frequency limit, as measurements at 24,000 Mc/sec at room temperature did not show the effect at all.

Measurements at 9300 Mc/sec carried out at increasing temperatures showed a sudden decrease in magnetic losses at a temperature apparently below the Curie temperature of the specimen.

Amplitude modulation of microwaves when using these bars in cavity resonators coupled to a wave guide proves to be possible, with a suitably designed apparatus up to modulation frequencies, of at least 1.3 Mc/sec.

The following explanation of the observed phenomena is suggested. We think that the extrusion causes elongated air inclusions giving rise to an anistropic structure, a certain nonrandom orientation of the magnetic domains.

It may be possible that, as a result of this orientation, polarizing fields are generated giving rise to gyromagnetic resonance effects and additional magnetic losses.[1,2]

As it is reasonable to relate these polarizing fields to the saturation magnetization, which is known to decrease at increasing temperatures, it may be expected (as experiments prove) that the additional magnetic losses disappear at the temperature at which the saturation magnetization reaches a value connected with the applied frequency according to the Larmor relation. Magnetic saturation of the material destroys the above-mentioned orientation and the additional magnetic losses disappear.

A more detailed account of the phenomena will be published in *Physica*.

* Present address N. V. Kema, Arnhem, Netherlands.
[1] J. L. Snoek, Nature **160**, 60–61 (1947) and Physica **14**, 207–217 (1948).
[2] H. G. Beljers and J. L. Snoek, Philips tech. Rev. **11**, 317–325 (1949).

On the Anomalous Magnus Effect

Itiro Tani
Institute of Industrial Science, University of Tokyo, Chiba, Japan
(Received September 21, 1951)

In this Journal, September, 1949, J. M. Davies reported results of measurements on golf balls spinning in a wind stream. The most interesting result is the effect of surface roughness on the cross-wind force. For a standard ball with dimple or mesh the cross-wind force increased monotonously with the rotational speed, while for a smooth ball the force was negative for low rotational speeds, opposite in direction to that expected from the Magnus effect. At high rotational speeds the force became positive, but was smaller than for the smooth ball.

The present writer, unaware of the aforementioned study, started early in 1949 similar measurements on baseballs spinning in a wind tunnel. The results were published in a Japanese scientific journal *Kagaku*, September, 1950. The test failed to show the negative force at low rotational speeds, but it agreed with Davies's result in indicating that the force is much larger for a standard ball with stitching than for a smooth ball.

The existence of negative cross-wind force has already been observed by Lafay (1912), Reid (1924), Thom (1927), and Maccoll (1928). However, no explanation has ever been given why the force is produced in the direction just opposite to that expected from the usual Magnus effect. Davies suggested a possibility such that the effective Reynolds number is higher on the side rotating against the wind than that rotating with the wind, but he gave no explanation why such a difference should occur. The following consideration, although speculative as yet, appears to make the situation clearer.

Since the fluid layer in contact with the surface has no velocity relative to it, the fluid particle should describe a flattened closed circuit on the side rotating against the wind, as shown in Fig. 1. Probably, the thickness of the circuit will be of the same order of magnitude as that of the usual boundary layer. If it is assumed that such a circuit is stable and extends far downstream, there would be a tendency for the flow to follow the surface for a longer

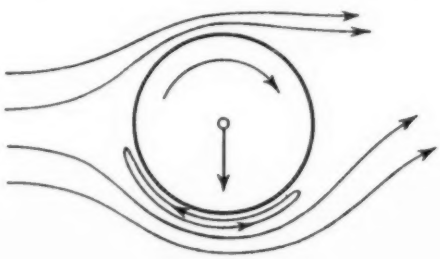

Fig. 1.

distance on the side rotating against the wind than that rotating with the wind, leaving a circulation round the ball in the opposite sense to the rotation. This accounts for the production of negative cross-wind force. In order that the flattened circuit remain stable, however, it may perhaps be required that the rotational speed be low, that the surface be sufficiently smooth, and that the stream turbulence be small. If one of these conditions is not satisfied, the circuit would split up into vortices, and a circulation would be produced in the same sense as the rotation, thus resulting in the normal Magnus effect. These considerations account for the disappearance of negative force for rough balls. The reason for not finding the negative force in the writer's test may probably be the result of the effect of turbulence in the wind stream.

Radioactive Tracers for Rapid Measurement of Cutting Tool Life

M. Eugene Merchant and E. J. Krabacher
Research Department, The Cincinnati Milling Machine Company, Cincinnati, Ohio
(Received August 20, 1951)

THE life of cutting tools in machining is a major factor influencing the costs of most manufacturing operations. Research designed to discover and develop ways of increasing tool life requires means for accurate measurement of tool wear and life. Such measurements, normally made as controlled laboratory tests, require hours of time and hundreds of pounds of metal, when carried out by conventional means. Testing under accelerated conditions, as by using abnormally high cutting speeds, gives results which do not agree with practice.

In looking for ways to circumvent the use of the costly conventional methods of measuring tool life, the idea was conceived of using radioactive tracers to measure the "instantaneous" rate of tool wear. This method has now been investigated, with promising results.

The method consists, in essence, of machining with a cutting tool which has been rendered radioactive by neutron irradiation in a nuclear reactor and measuring the radioactivity of the collected particles worn from the tool during a few seconds of cutting. This latter is conveniently done by measuring the radioactivity of the chips removed during that few seconds of cutting, since it has been found from the present study that well over 90 percent of the radioactive tool material worn away during cutting remains attached to the chips.

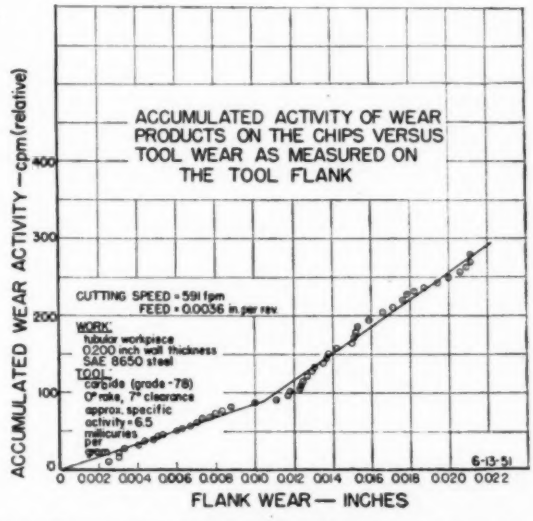
ACCUMULATED ACTIVITY OF WEAR PRODUCTS ON THE CHIPS VERSUS TOOL WEAR AS MEASURED ON THE TOOL FLANK
CUTTING SPEED = 591 fpm
FEED = 0.0036 in per rev
WORK:
tubular workpiece
0.200 inch wall thickness
SAE 8650 steel
TOOL:
carbide (grade -78)
0° rake, 7° clearance
approx. specific activity = 6.5 millicuries per gram
6-13-51
ACCUMULATED WEAR ACTIVITY — cpm (relative)
0
100
200
300
400
0 0002 0004 0006 0008 0010 0012 0014 0016 0018 0020 0022
FLANK WEAR — INCHES

FIG. 1. The accumulated radioactivity of the wear products on the chips, throughout a life test on the cutting tool, correlates well with the wear of the tool as measured on the flank with a microscope in the conventional way.

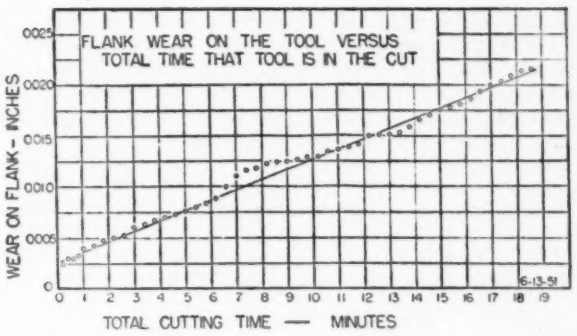
FLANK WEAR ON THE TOOL VERSUS TOTAL TIME THAT TOOL IS IN THE CUT
WEAR ON FLANK - INCHES
0
0005
0010
0015
0020
0025
6-13-51
0 1 2 3 4 5 6 7 8 9 10 11 12 13 14 15 16 17 18 19
TOTAL CUTTING TIME — MINUTES

FIG. 2. The wear on the flank of the cutting tool, when measured with a microscope in the conventional way throughout the life test, exhibits "cascading." This cascading effect is a usual occurrence.

In the initial investigation discussed here, the cutting tool material used was a sintered carbide composed of WC, TiC, TaC, and Co. The service irradiation of this material was carried out by the Oak Ridge National Laboratory on authorization from the Isotopes Division, U. S. Atomic Energy Commission. The resulting effective tracer radioisotopes were W 185, Ta 182, and Co 60. The results of a series of cuts taken on SAE 8650 steel, starting with a sharp tool, are shown in Fig. 1. Here the accumulation, throughout the test, of the radioactivity of the chips (which is proportional to the amount of radioactive tool material present on the chips) is plotted against the wear of the tool as measured on the flank of the tool with a microscope in the conventional way. (The activity of the chips was measured with a heavy-wall Geiger tube and thus represents gamma-radiation only.) The correlation and its linearity are evident. While the scatter of the experimental points may seem disturbing at first, Figs. 2 and 3 show that this

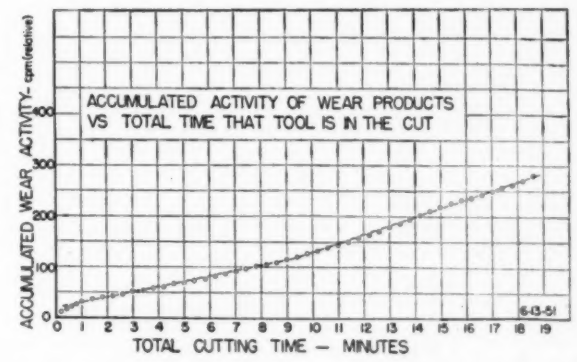
ACCUMULATED ACTIVITY OF WEAR PRODUCTS VS TOTAL TIME THAT TOOL IS IN THE CUT
ACCUMULATED WEAR ACTIVITY - cpm (relative)
0
100
200
300
400
6-13-51
0 1 2 3 4 5 6 7 8 9 10 11 12 13 14 15 16 17 18 19
TOTAL CUTTING TIME — MINUTES

FIG. 3. A smooth, linear relationship exists between the activity of the wear products on the chips and the elapsed cutting time in the life test. The rate of tool wear can thus be measured by making a few cuts of a few seconds duration each; by this means relative tool life values for different cutting conditions can be quickly obtained.

effect is due to the "cascading" of the gross wear on the flank (as measured with the microscope) (Fig. 2) and not to any irregularity in the over-all actual wear rate as measured by the activity of the chips (Fig. 3).

The "cascading" effect seen in Fig. 2 is well known and is one of the important factors preventing the obtaining of reliable measurements of the rate of tool wear from short-time tests, covering only a small portion of the wear curve, when using conventional methods. Because this "cascading" effect is absent in Fig. 3, it is apparent that an accurate measure of the rate of tool wear can be obtained by averaging the values for the activity of the chips (counts per minute per gram of chips) obtained from only a few runs of a few seconds duration each. It is evident that the method is especially well suited to the rapid determination of relative

values of tool wear and tool life when evaluating the effect of a series of different cutting conditions, as for instance a series of different cutting fluids or different work materials.

The authors wish to acknowledge the many important contributions of Mr. Hans Ernst, Research Director, to the practical realization of this method of measuring tool wear.

Deformation of Body-Centered Cubic Metals

E. A. CALNAN
AND
C. J. B. CLEWS
National Physical Laboratory, Metallurgy Division, Teddington, England
(Received September 17, 1951)

IN a recent publication on the deformation textures of body-centered cubic metals,[1] reference was made to the preliminary results of Opinsky and Smoluchowski which provide a very useful addition to the knowledge of deformation modes. At the time of going to press only an indirect report summarizing their results was available to the authors, and the ratios

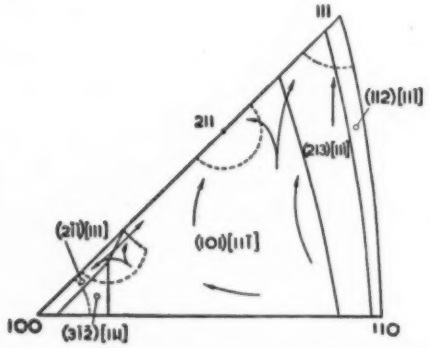

FIG. 1. Operative slip systems for critical shear stresses in the ratios: $C_{123}/C_{110}=1.07$; $C_{111}/C_{112}=0.99$. Arrows indicate slip rotations under compression.

of critical resolved shear stresses in silicon ferrite quoted were in error. These erroneous values were used to determine the regions of different operative slip systems within a stereographic

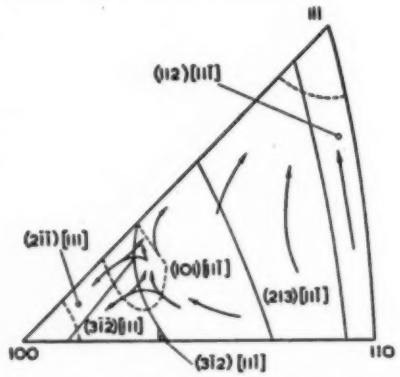

FIG. 2. Operative slip systems for equal critical shear stresses. Arrows indicate slip rotations under compression.

unit triangle, and the calculation has now been repeated using the correct ratios (Fig. 1). The corresponding diagram when the three operative slip systems have equal critical shear stresses is shown in Fig. 2. It is clear that comparatively small variations in the critical stresses alter the positions of the boundaries between the regions considerably. The rotations associated with slip are very similar for the case of applied tension, but the rotations in the case of applied compression, which are indicated by arrows in the diagrams, are somewhat different and lead to the conclusion that in the compression of silicon ferrite an additional [211] texture will appear. This in turn will increase the (211)[110] component in the rolling texture at the expense of the (111)[110] texture, a prediction which is in good agreement with the experimental observations of Barrett, Ansel, and Mehl.[2] Further work on the refinement of the method by which rolling textures may be derived from tension and compression textures is in hand.

The authors wish to point out that the method by which the regions of different most favorable slip systems are determined is essentially the same as that of Opinsky and Smoluchowski;[3] but it is gratifying to find independent confirmation of the results, since they differ from the previously published work of Fahrenhorst and Schmid.[4]

[1] E. A. Calnan and C. J. B. Clews, Phil. Mag. **41**, 1085 (1951).
[2] Barrett, Ansel, and Mehl, Trans. Am. Inst. Mining Met. Eng. **125**, 516 (1937).
[3] A. J. Opinsky and R. Smoluchowski, J. Appl. Phys. **22**, 1488 (1951).
[4] W. Fahrenhorst and E. Schmid, Z. Physik. **78**, 383 (1932).

On the Ratio of the Critical Shear Stresses

A. J. OPINSKY AND R. SMOLUCHOWSKI
Carnegie Institute of Technology, Pittsburgh, Pennsylvania
(Received September 17, 1951)

IN connection with the preceding note by Calnan and Clews[1] it should be pointed out that one can assume the critical shear stresses on the (123) and (112) planes to be equal. The value 0.99 for the ratio of the two stresses given in our paper[2] differs from unity within the limit of experimental error.

The agreement between the interesting results of Calnan and Clews[3] and ours is very pleasing.

[1] E. A. Calnan and C. J. B. Clews, preceding note.
[2] A. J. Opinsky and R. Smoluchowski, J. Appl. Phys. **22**, 1488 (1951).
[3] E. A. Calnan and C. J. B. Clews, Phil. Mag. **41**, 1085 (1951).

A Problem in Heat Conduction

WILLIAM SQUIRE
Cornell Aeronautical Laboratory, Inc., Buffalo, New York
(Received May 31, 1951)

THE steady-state temperature field due to a heat source moving with constant velocity has been found for a source of constant strength[1-3] and for a source varying as $1-\cos\omega t$.[4] In the present note a simple derivation is given for a source varying as $e^{i\omega t}$. This enables the field due to an arbitrarily varying source to be found by superposition.

A fixed source in a moving medium is considered. By a galilean transformation this gives the case of a moving source. The equation of heat conduction with sources is

$$\rho c[(\partial T/\partial t)+v(\partial T/\partial z)]=k\nabla^2 T+F(x,y,z,t), \tag{1}$$

in which ρ is the density, c is the heat capacity, k is the conductivity, and v is the flow velocity. $F(x,y,z,t)$ is the heat input per unit volume per unit time. For the present problem

$$F(x,y,z,t)=\delta(\mathbf{r})e^{i\omega t}, \tag{2}$$

where $\delta(\mathbf{r})$ is the Dirac delta-function which is zero everywhere but at the location of the source, which will be taken at the origin. Here $\delta(\mathbf{r})$ is infinite in such a way that

$$\int \delta(\mathbf{r})f(\mathbf{r})dV=f(0). \tag{3}$$

We therefore must solve

$$1/\kappa[(\partial T/\partial t)+v(\partial T/\partial z)]=\nabla^2 T+(1/k)\delta(\mathbf{r})e^{i\omega t}, \quad (4)$$

where $\kappa=k/\rho c$ subject to $T\to 0$ at infinity.

It is easily shown that the time dependence of T is $e^{i\omega t}$ and the first derivative term can be removed by a device similar to that used for ordinary differential equations. By the substitution,

$$T=\exp[(i\omega t+(vz/2\kappa)]\varphi(x, y, z) \quad (5)$$

the equation,

$$\nabla^2\varphi+\lambda^2\varphi=-(\delta(\mathbf{r})/k)\exp[-(vZ/2\kappa)] \quad (6)$$

where

$$\lambda=\frac{v}{2\kappa}\left[\left(\frac{R+1}{2}\right)^{\frac{1}{2}}+i\left(\frac{R-1}{2}\right)^{\frac{1}{2}}\right]$$

$$R=\left(1+\frac{16\omega^2\kappa^2}{v^4}\right)^{\frac{1}{2}}$$

is obtained. The solution of Eq. (6) is[5]

$$\varphi(x, y, z)=\frac{1}{4\pi k}\int\exp[-(vz/2\kappa)]\delta(\mathbf{r})\times\frac{\exp[\pm\lambda((x-x_1)^2+(y-y_1)^2+(z-z_1)^2)^{\frac{1}{2}}]}{((x-x_1)^2+(y-y_1)^2+(z-z_1)^2)^{\frac{1}{2}}}dV_1 \quad (7)$$

by using Eq. (3) the integral is easily evaluated. Only the negative sign satisfies the boundary condition giving:

$$\varphi=(1/4\pi kr)\exp\{-(v/2\kappa)[(R+1)/2]^{\frac{1}{2}}+i[(R-1)/2]^{\frac{1}{2}}r\}$$

$$T=(1/4\pi kr)\exp\{(vz/2\kappa)-(vr/2\kappa)[(R+1)/2]^{\frac{1}{2}}+i(\omega t-[(R-1)/2]^{\frac{1}{2}}r)\} \quad (8a)$$

$$r=(x^2+y^2+z^2)^{\frac{1}{2}}. \quad (8b)$$

For a constant source, $\omega=0$ and $R=1$ this reduces to

$$T=(1/4\pi kr)\exp[(v/2\kappa)(z-r)]. \quad (9)$$

By taking the real and imaginary parts of Eq. (8b) the response to cosine and sine sources are obtained:

$$T=(1/4\pi kr)\exp\{(v/2\kappa)[[(R-1)/2]^{\frac{1}{2}}r-z]\}\times\cos(\omega t-[(R-1)/2]^{\frac{1}{2}}r) \quad (10a)$$

$$T=(1/4\pi kr)\exp\{(v/2\kappa)[[(R+1)/2]^{\frac{1}{2}}r-z]\}\times\sin(\omega t-[(R-1)/2]^{\frac{1}{2}}r). \quad (10b)$$

By combining (9) and (10a) Podolsky's solution[4] for a $(1-\cos\omega t)$ source is obtained.

Dr. Podolsky's valuable criticism is gratefully acknowledged.

[1] Wilson, Proc. Cambridge Phil. Soc. **12**, 406 (1904).
[2] H. S. Carslaw and J. C. Jaeger, *Conduction of Heat in Solids* (Oxford University Press, London, 1947), Sec. 106.
[3] D. Rosenthal, Trans. Am. Soc. Mech. Engrs. **68**, 849–66 (1940).
[4] B. Podolsky, J. Appl. Phys. **22**, 581–84 (1951).
[5] A. G. Webster, *Partial Differential Equations* (New York, 1933), Sect. 65.

JOURNAL OF APPLIED PHYSICS VOLUME 22, NUMBER 12 DECEMBER, 1951

Author Index to Volume 22

References with (L) are to Letters to the Editor

Achter, M. R. and R. Smoluchowski. Diffusion in grain boundaries and their structure—1260

Aden, A. L. Electromagnetic scattering from spheres with sizes comparable to the wavelength—601

Aden, Arthur L. and Milton Kerker. Scattering of electromagnetic waves from two concentric spheres—1242

Affleck, John H. (see Hensley, Eugene B.)—359(L)

Aldrich, L. T. Evaporation products of barium oxide from various base metals and of strontium oxide from platinum—1168

Alexander, B. H. (see Kuczynski, G. C.)—344

——, **M. H. Dawson, and H. P. Kling.** Deformation of gold wire at high temperature—439

Alexanderson, E. L. (see Gemant, Andrew)—460

Alger, Raymond S. (see Schulman, James H.)—1479

Allmand, D. E. (see McMillen, J. H.)—360(L)

Anderson, R. B. (see McCartney, J. T.)—1441

Andrews, C. L. Diffraction pattern of microwaves near rods—465

—— Erratum: Diffraction pattern in a circular aperture measured in the microwave region—520

Angelakos, D. J. Current and charge distributions on antennas and open-wire lines—910

Antes, Leland L. and Norman Hackerman. Contact potential variations on freshly condensed metal films at low pressures—1395

Anthony, Robert L. (see Witte, Robert S.)—689

Artman, Robert A. and Donald O. Thompson. Elastic parameters of beta-brass—358(L)

Attwood, Stephen S. Surface-wave propagation over a coated plane conductor—504

Austin, A. E. and C. M. Schwartz. Modification of a positive-replica technique for electron microscopy—847(L)

Averbach, B. L. X-ray detection of long-range order in Ni_3Mn—1088(L)

—— (see Warren, B. E.)—1493

Bachman, C. H., Harold Eubank, and George Hall. Hollow cathode for positive ion studies in cathode-ray tubes—1208

Balent, R. (see Iversen, H. W.)—324

Bandel, Herman W. Corona from ice points—984(L)

Baños, Alfredo, Jr., David S. Saxon, and H. Gruen. Propagation characteristics in a coaxial structure with two dielectrics—117

Barnes, B. T. (see Kenty, C.)—1006

Beams, J. W. and H. S. Morton, Jr. Transmission line Kerr cell—523(L)

Bear, Richard S. and Orvil E. A. Bolduan. Periodic statistical distortion of unidirectionally ordered diffractors, with application to collagen—191

Becker, Herbert (see Gerard, George)—1298(L)

Belanger, J. R. (see Kasper, J. S.)—361(L)

Beljers, H. G., W. J. van de Lindt, and J. J. Went. A new point of view on magnetic losses in anisotropic bars of ferrite at ultra-high frequencies—1506(L)

Bennett, F. D. Optimum source size for the Mach-Zehnder interferometer—184

—— Effect of size and spectral purity of source on fringe pattern of the Mach-Zehnder interferometer—776

Bennett, R. R. and A. S. Fulton. Generation and measurement of low frequency random noise—1187

Benson, W. H., Jr. (see LaGrone, A. H.)—672

Beth, Richard A. and Charles P. Wells. Finite deflections of a cantilever-strut—742

Bever, M. B. and L. B. Ticknor. Method for determining the energy stored during cold-working of metals—1297(L)

—— (see Michael, A. B.)—1403

Birnbaum, George, S. J. Kryder, and Harold Lyons. Microwave measurements of the dielectric properties of gases—95

Blaha, F. and J. A. Schedling. Improvements in visual depiction of magnetic lines of force by means of a gas discharge—11

Blair, G. W. Scott (see Reiner, M.)—236

Bleil, Carl E. (see Howard, Robert A.)—360(L)

Blizard, Robert B. Visco-elasticity of rubber—730

Boadway, J. D. Condenser aperture device for electron microscopes—104(L)
Bolduan, Orvil E. A. (see Bear, Richard S.)—191
Bonfiglioli, G. and G. Montalenti. On linear expansion coefficient and melting point of metals—1089(L)
Bowen, R. J. (see Šimon, I.)—177
—— (see Šimon, I.)—848
Boyer, R. F. Relation of tensile strength to brittle temperature in plasticized polymers—723
Brackett, F. S. (see Daniel, J. H.)—542
Brillouin, L. Maxwell's demon cannot operate: Information and entropy. I—334
—— Physical entropy and information. II—338
—— Information theory and most efficient codings for communication or memory devices—1108
Brockhouse, B. N. (see Peppiatt, H. J.)—985(L)
Brown, F. W. (see Parkins, W. E.)—1012
Buchdahl, Rolf and Lawrence E. Nielsen. Application of Nutting's equation to the viscoelastic behavior of certain polymeric systems—1344
Bundy, F. P., H. M. Strong, and A. B. Gregg. Measurement of velocity and pressure of gases in rocket flames by spectroscopic methods—1069

Cagle, F. Wm., Jr. and Henry Eyring. Application of the absolute reaction rate theory to some problems in annealing—771
Caldecourt, V. J. (see Matheson, L. A.)—1176
Calnan, E. A. and C. J. B. Clews. Deformation of body-centered cubic metals—1508(L)
Campbell, H. N. X-ray absorption in a crystal set at the Bragg angle—1139
Carruthers, J. A. (see Woonton, G. A.)—390
Chaney, Jesse Gerald. A critical study of the circuit concept—1429
Chang, Lo-Ching. Coefficients of thermal expansion of Au-Cd alloys containing 47.5 atomic percent Cd—525(L)
Cheney, M. G., Jr., and Robert B. Watson. Diffraction of electromagnetic waves by two conducting parallel half-planes—675
Clark, O. H., W. W. Woods, and J. R. White. Lubrication at extreme pressures with mineral oil films—474
Clews, C. J. B. (see Calnan, E. A.)—1508(L)
Cobine, J. D. and D. A. Wilbur. Electronic torch and related high freqiency phenomena—835
Coburn, N. Compressible supersonic flow in jets under the Kármán-Tsien pressure-volume relation—124
Codrington, R. S. (see Holroyd, L. V.)—696
Cohen, S. T. (see Plesset, M. S.)—350
Cohn, Seymour B. Electric and magnetic constants of metallic delay media containing obstacles of arbitrary shape and thickness—628
Collins, S. C. (see Eldin, A. S.)—1296(L)
Coolidge, John E. and George Schulz. Static electrification of dust particles on dispersion into a cloud—103(L)
Corney, G. M. Comment on nomenclature in "Electron microradiography of electrodeposited metals"—682(L)
Corrsin, Stanley. On the spectrum of isotropic temperature fluctuations in an isotropic turbulence—469; erratum—1292
Czyzewski, Harry. Branching of slip lines in alpha-brass—846(L)

Daniel, J. H. and F. S. Brackett. Electrical method for investigating the nature and behavior of small, airborne, charged particles—542
Dawson, M. H. (see Alexander, B. H.)—439
Decker, B. F. (see Kasper, J. S.)—361(L)
—— **and David Harker.** Relations between initial and final orientations in rolling and annealing of silicon ferrite—900
Dienes, G. J. On the volume diffusion of metals—848(L)
—— (see Parkins, W. E.)—1012
—— Kinetics of ordering in the alloy AuCu—1020
Doolittle, Arthur K. Studies in Newtonian flow. I. The dependence of the viscosity of liquids on temperature—1031
—— Studies in Newtonian flow. II. The dependence of the viscosity of liquids on free-space—1471
Dow, W. G. (see Welch, H. W., Jr.)—433
Dunbar, A. S. General formulation for calculation of shaped-beam antennas—1217(L)
Dunning, Kenneth L. and Rufus G. Fellers. Susceptance of a thin iris in circular wave guide with the TM_{01} mode incident—1316
Duwez, Pol. Allotropic transformation of hafnium—1174

Easley, M. A. Probe technique for the measurement of electron temperature—590
—— **and W. W. Mumford.** Electron temperature *vs* noise temperature in low pressure mercury-argon discharges—846(L)
—— (see Kenty, C.)—1006
Edwards, James W., Rudolph Speiser, and Herrick L. Johnston. High temperature structure and thermal expansion of some metals as determined by x-ray diffraction data. I. Platinum, tantalum, niobium, and molybdenum—424
Eisenstein, A. Leaky-condenser oxide cathode interface—138
Ekstein, H. and T. Schiffman. Elastic vibrations of almost cubic parallelepipeds—1215(L)
Eldin, A. S. and S. C. Collins. Fracture and yield stress of 1020 steel at low temperatures—1296(L)
Elliott, H. A. (see Woonton, G. A.)—390
Emrich, R. J. (see Laponsky, A. B.)—1297(L)
Eubank, Harold (see Bachman, C. H.)—1208
Eubanks, R. A. (see Sternberg, E.)—1121
Evans, Warren W. (see Schremp, Frederic W.)—711
Ewing Maurice (see Press, Frank)—892
Eyring, Henry (see Cagle, F. Wm., Jr.)—771

Fano, U. (see Goldstein, N.)—417
Farber, Erich A. Free convection heat transfer from electrically heated wires—1437
Farnsworth, H. E. and M. J. Lun. Secondary emission of nickel-barium mixtures and rhenium when bombarded by electrons with energies from 50 to 8000 electron volts—77
Faro, I. D. V., T. R. Small, and F. K. Hill. Hypersonic flow at a Mach number of 10—220
Feinstein, J. Tropospheric propagation beyond the horizon—1292(L)
Fellers, Rufus G. (see Dunning, Kenneth L.)—1316
Feng, I-Ming. Applications of polystyrene particles in conjunction with shadow casting to the study of polished metallic surfaces—820
Ferro, A. and G. Montalenti. Internal friction of ferromagnetic materials—565
Ferry, John D. (see Schremp, Frederic W.)—711
——, **Edwin R. Fitzgerald, Myrle F. Johnson, and Lester D. Grandine, Jr.** Mechanical properties of substances of high molecular weight. X. The relaxation distribution function in polyisobutylene and its solutions—717
Field, J. E. and S. D. Gehman. Noncontact temperature measuring device—106(L)
Fifer, Stanley. Studies in nonlinear vibration theory—1421
Fisher, J. C. Calculation of diffusion penetration curves for surface and grain boundary diffusion—74
—— (see Fullman, R. L.)—1350
Fitzgerald, Edwin R. (see Ferry, John D.)—717
Flynn, T. (see Reich, H. J.)—682(L)
Foner, S. (see Pugh, E. M.)—487
Forrester, Jay W. Digital information storage in three dimensions using magnetic cores—44
Forster, Michael J. and Darwin J. Mead. Electrical properties of some carbon black-oil suspensions—705

Frank, F. C. Distribution of slip in metal crystals—1386(L)
French, Rolland Sydney. Plasticity and conductivity, analogous flow phenomena in copper alloys—105(L)
Friedman, Bernard. Amplification of the traveling wave tube —443
Fry, Ruth Baumann and William J. Fry. Crystal systems with low loss—198
Fry William J. (see Fry, Ruth Baumann)—198
Frye, W. E. Accuracy of the long-range ballistic rocket—585
Fullman, R. L. Interfacial free energy of coherent twin boundaries in copper—448
—— Crystallography and interfacial free energy of noncoherent twin boundaries in copper—456
—— **and J. C. Fisher.** Formation of annealing twins during grain growth—1350
Fulton, A. S. (see Bennett, R. R.)—1187

Gamble, E. H. and B. W. Hatten. Design and analysis of a conservative dynamic load simulator—1250
Garrett, Milan Wayne. Axially symmetric systems for generating and measuring magnetic fields. Part I—1091
Gehman, S. D. (see Field, J. E.)—106(L)
Geisler, A. H. (see Newkirk, J. B.)—290
Gemant, Andrew, Edward Hines, and E. L. Alexanderson. Leak location by radioactive gases in buried pipes—460
Gerard, George and Herbert Becker. Column behavior under conditions of compressive stress wave propagation—1298(L)
Germer, L. H. Arcing at electrical contacts on closure. Part I. Dependence upon surface condition and circuit parameters —955
—— Arcing at electrical contacts on closure. Part II. The initiation of an arc—1133
Gibson, J. E. (see Reich, H. J.)—682(L)
Ginther, Robert J. (see Schulman, James H.)—1479
Glaser, Frank W. Note on the metallic behavior of $MoSi_2$—103(L)
Glass, W. G. (see Smullin, L. D.)—1124
Gleichauf, Paul H. Electrical breakdown over insulators in high vacuum—535
—— Electrical breakdown over insulators in high vacuum—766
Goertz, Matilda. Iron-silicon alloys heat treated in a magnetic field—964
Goldstein, Ladislas. (see Parzen, Philip)—398
Goldstein, N., U. Fano, and H. O. Wyckoff. Directional distribution of 1040-Kev radiation from a high voltage x-ray tube—417
Goldwater, D. L. and R. E. Haddad. Certain refractory compounds as thermionic emitters—70
Grandine, Lester D., Jr. (see Ferry, John D.)—717
Green, L., Jr. (see Malmstrom, C.)—593
Gregg, A. B. (see Bundy, F. P.)—1069
Grieco, A. (see Rorden, H. C.)—842
Gross, G. and H. Pelzer. On creep and relaxation. III—1035
Gruen, H. (see Baños, Alfredo, Jr.)—117
Guth, E. (see Holroyd, L. V.)—696

Hackerman, Norman (see Antes, Leland L.)—1395
Haddad, R. E. (see Goldwater, D. L.)—70
Hahn, E. E. Some electrical properties of zinc oxide semiconductor—855
Hall, C. E. Scattering phenomena in electron microscope image formation—655
Hall, George (see Bachman, C. H.)—1208
Harker, David (see Decker, B. F.)—900
Harris, R. L. (see Ritter, H. L.)—169
Hart, Robert W. and Elliott W. Montroll. On the scattering of plane waves by soft obstacles. I. Spherical obstacles—376
—— (see Montroll, Elliott W.)—1278
Hasiguti, Ryukiti Robert and Tadamasa Hirai. Internal friction of cold-worked single crystals of copper—1084(L)
Haskell, N. A. Asymptotic approximation for the normal modes in sound channel wave propagation—157
Hatoyama, Mitio (see Komagata, Sakuji)—1290(L)
Hatten, B. W. (see Gamble, E. H.)—1250
Haworth, F. E. Electrode reactions in the glow discharge—606
Hein, C. C. and W. M. Hickam. Carbon, oxygen, and sulfur content of Chilean coppers as related to cuprous-oxide rectifiers—1192
Heine-Geldern, R. v. (see Pugh, E. M.)—487
Hempstead, C. F. (see Parratt, L. G.)—1502(L)
Henkels, H. W. Electrical properties of selenium: I. Single crystals—916
—— Electrical properties of selenium. II. Microcrystalline selenium—1265
Henry, Warren E. A finite difference treatment of a helium cryostat design problem—1439
Hensley, Eugene B. and John H. Affleck. Barium oxide on tungsten cathode interface—359(L)
Hertz, Hellmuth. Magnetic scaling circuit—107(L)
Hetherington, F. E. and James Reekie. Electrical resistivity of cold-worked copper-iron alloys—1293(L)
Hibi, T. and K. Ishikawa. On the initial decay of oxide-coated cathodes—986(L)
Hickam, W. M. (see Hein, C. C.)—1192
Higgins, Thomas James (see Reitan, Daniel Kinseth)—223
—— (see Van Bladel, J.)—329
—— Epitomization of the basic theory of the generalized Schwarz-Christoffel transformations as used in applied physics—365(L)
Hill, F. K. (see Faro, I. D. V.)—220
Hillier, James. Objective for use in the electron microscopy of ultrathin sections—135
Hines, Edward (see Gemant, Andrew)—460
Hines, M. E. Equivalent temperature of an electron beam—1385(L)
Hirai, Tadamasa (see Hasiguti, Ryukiti Robert)—1084(L)
Hoffman, R. E. and D. Turnbull. Lattice and grain boundary self-diffusion in silver—634
—— **and D. Turnbull.** Erratum: Lattice and grain-boundary self-diffusion in silver—984(L)
Holden, A. N. Yielding behavior of iron single crystals—1290(L)
Holm, Ragnar. Electric tunnel effect across thin insulator films in contacts—569; errata—1217
Holroyd, L. V., R. S. Codrington, B. A. Mrowca, and E. Guth. Nuclear magnetic resonance study of transitions in polymers —696
Holton, Gerald. Ultrasonic propagation in liquids under high pressures: Velocity measurements on water— 1407
Horio, M., S. Onogi, C. Nakayama, and K. Yamamoto. Viscoelastic properties of several high polymers—966
—— **and S. Onogi.** Dynamic measurements of physical properties of pulp and paper by audiofrequency sound—971
—— **and S. Onogi.** Forced vibration of reed as a method of determining viscoelasticity—977
Horn, F. Hubbard. On asymmetric heat conduction in copper-copper oxide rectifiers—1214(L)
Horton, C. W. Semiconductor bornite—364(L)
—— **and F. C. Karal, Jr.** On the diffraction of a plane electromagnetic wave by a paraboloid of revolution—575
—— **and C. M. McKinney, Jr.** Experimental investigation of the dielectric rod antenna of circular cross section excited in the dominant mode—1246
Householder, A. S. (see Sheppard, C. W.)—510
Houston, Robert E. and Robert H. Noble. Edge effects in a circular aperture—1295(L)
Howard, Robert A. and Carl E. Bleil. Water movement induced by compaction of clastic sediments—360(L)
Hsu, En-Yun (see McNown, John S.)—864
Hubbard, C. P. (see Smyth, J. B.)—1387(L)

Hudson, G. E. Theory of the dynamic plastic deformation of a thin diaphragm—1

Ishikawa, K. (see Hibi, T.)—986(L)
Iversen, H. W. and R. Balent. Correlating modulus for fluid resistance in accelerated motion—324

Jacob, L. (see Shah, J. R.)—1236
Jacobs, Robert B. Design of molecular pumps—217
Jakob, M. (see Wilson, L. H.)—1027
Jaumot, Frank E., Jr. and Foster C. Nix. Note on a simple technique for obtaining absorption coefficients of metals and alloys for complex radioactive spectra—1294(L)
Jepsen, Robert L. and Marcel W. Muller. Enhanced emission from magnetron cathodes—1196
Johnson, G. W. Epitaxy of alkali chlorides on metals—797
Johnson, Myrle F. (see Ferry, John D.)—717
Johnston, Herrick L. (see Edwards, James W.)—424

Kane, Evan O. Optical absorption of barium oxide with excess barium—1214(L)
Kantrowitz, Arthur (see Perry, Robert W.)—878
Karal, F. C., Jr. (see Horton, C. W.)—575
Kasper, J. S., B. F. Decker, and J. R. Belanger. Crystal structure of the sigma-phase in the Co-Cr system—361(L)
Keating, D. T. and B. E. Warren. Long-range order in beta-brass and Cu_3Au—286
Kedesdy, H. (see Lehovec, K.)—65
Keen, R. (see Malmstrom, C.)—593
Kenty, C., M. A. Easley, and B. T. Barnes. Gas temperatures and elastic losses in low pressure mercury-argon discharges—1006
Kerker, Milton (see Aden, Arthur L.)—1242
Kikuchi, Makoto (see Komagata, Sakuji)—1290(L)
King, Allen L. (see Lawton, Richard W.)—1340
King, Ronold. Theory of V-antennas—1111
Klick, Clifford C. (see Schulman, James H.)—1479
Kling, H. P. (see Alexander, B. H.)—439
Knudsen, H. Lottrup. Necessary number of elements in a directional ring aerial—1299
Koehler, James S. (see Neurath, Peter W.)—621
Komagata, Sakuji, M. Hatoyama, M. Shibuya, W. Sasaki, T. Yamamoto, and M. Kikuchi. AC characteristics of Si *p-n* junction—1290(L)
Kornhauser, E. T. Propagation on dielectric coated wires—525(L)
—— Radiation field of helical antennas with sinusoidal current—887
Krabacher, E. J. (see Merchant, M. Eugene)—1507(L)
Kramer, R. L. (see McMillen, J. H.)—360(L)
Kryder, S. J. (see Birnbaum, George)—95
Kuczynski, G. C. and B. H. Alexander. Metallographic study of diffusion interfaces—344
—— **and R. Landauer.** Measurement of carbon diffusion in metallic carbides—952
Kunkel, Wulf B. Static electrification of dust particles on dispersion into a cloud—103(L)

Lafferty, J. M. Boride cathodes—299
LaGrone, A. H., W. H. Benson, Jr., and A. W. Straiton. Attenuation of radio signals caused by scattering—672
—— Reply to J. B. Smyth and C. P. Hubbard—1387(L)
Laitone, E. V. Experimental measurement of incompressible flow along a cylinder with a conical nose—63
Landauer, R. Associated Legendre polynomial approximations—87
—— (see Kuczynski, G. C.)—952
Laponsky, A. B. and R. J. Emrich. New method for the production of air shocks in a tube—1297(L)
Larach, S. and R. E. Shrader. Cathodoluminescence of zinc orthosilicate with manganese activator—362(L)
Lawson, W. D. A method of growing single crystals of lead telluride and lead selenide—1444
Lawton, Richard W. and Allen L. King. Free longitudinal vibrations of rubber and tissue strips—1340
Leavitt, W. Z. (see Michael, A. B.)—1403
Lee, T. D. Difference between turbulence in a two-dimensional fluid and in a three-dimensional fluid—524(L)
Lehan, Frank W. Expected number of crossings of axis by linearly increasing function plus noise—1067
Lehovec, K. and H. Kedesdy. Graphical determination of the Fermi level in a simple impurity semiconductor—65
—— Recovery of selenium rectifiers after a voltage pulse in the blocking direction—934
Lengyel, Bela A. Note on reflection and transmission—263
—— Reflection and transmission at the surface of metal-plate media—265
Levine, Harold and Charles H. Papas. Theory of the circular diffraction antenna—29
Levy, Robert A. (see Schulman, James H.)—1479
Liang, S. Chu. Some measurements of thermal transpiration—148
Lin, Wei-guan. Microwave filters employing a single cavity excited in more than one mode—989
Loeb, Arthur L. Theory of the envelope type of thermal conductivity tests—282
—— Erratum: A theory of the envelope type of thermal conductivity tests—849
Loeb, Leonard B. (see Miller, Charles G.)—494
—— (see Miller, Charles G.)—614
—— (see Miller, Charles G.)—740
Lucke, Winston S. Electric dipoles in the presence of elliptic and circular cylinders—14
Ludeke, Carl A. Predominantly subharmonic oscillations—1321
Lukesh, Joseph S. (see Seybolt, A. U.)—986(L)
Lun, M. J. (see Farnsworth, H. E.)—77
Lundquist, G. (see Wegener, P.)—233(L)
—— (see Wegener, P.)—1077
Lyons, Harold (see Birnbaum, George)—95

McCartney, J. T. and R. B. Anderson. Electron microscopic replica studies of porosity in fused iron catalysts—1441
McKay, Kenneth G. Pulse method of determining the energy distribution of secondary electrons from insulators—89
McKinley, D. W. R. Deceleration and ionizing efficiency of radar meteors—202
McKinney, C. M., Jr. (see Horton, C. W.)—1246
McLucas, John L. and Richard C. Raymond. Power spectrum of a narrow band noise passed through a nonlinear impedance element—1211
McMahon, H. O. (see Šimon, I.)—177
—— (see Šimon, I.)—848
McMillen, J. H., R. L. Kramer, and D. E. Allmand. Impact flash at high speed water entry—360(L)
McNown, John S. and En-Yun Hsu. Approximation of axisymmetric body forms for specified pressure distributions—864
McPherson, J. C. (see Millsaps, Knox)—429
Malmstrom, C., R. Keen, and L. Green, Jr. Some mechanical properties of graphite at elevated temperatures—593
Marcuvitz, N. and J. Schwinger. On the representation of the electric and magnetic fields produced by currents and discontinuities in wave guides. I—806
Martin, D. L. (see Newkirk, J. B.)—290
Mason, J. H. Random noise in dielectric materials—235(L)
Matheson, L. A. and V. J. Caldecourt. Electrical charge storage in polystyrene capacitors—1176
Mathews, W. E. Transmission-line equivalent of electronic traveling-wave systems—310
Mathis, H. F. On a theorem of Brouwer—1084(L)

May, Albert. Effect of surface condition of a sphere on its water-entry cavity—1219
Mead, Darwin J. (see Forster, Michael J.)—705
Medicus, G. and G. Wehner. Noble gas hot cathode diodes with negative arc drop—1388(L)
Merchant, M. Eugene and E. J. Krabacher. Radioactive tracers for rapid measurement of cutting tool life—1507(L)
Michael, A. B., W. Z. Leavitt, M. B. Bever, and H. R. Spedden. A technique for preparing beta-ray autoradiographs of metals and minerals—1403
Middleton, David. On the theory of random noise. Phenomenological models. I—1143
—— On the theory of random noise. Phenomenological models. II—1153
—— Errata: On the theory of random noise. Phenomenological models. I—1326
Miller, Charles G. and Leonard B. Loeb. Positive coaxial cylindrical corona discharges in pure N_2, O_2, and mixtures thereof—494
—— **and Leonard B. Loeb.** Negative coaxial cylindrical discharges in pure N_2, O_2, and mixtures thereof—614
—— **and Leonard B. Loeb.** Starting potentials of positive and negative coronas with coaxial geometry in pure N_2, pure O_2, and various mixtures at pressures from atmospheric to 27 mm—740
Miller, Kenneth S. One-sided Green's function—1054
Miller, William. Effective earth's radius for radiowave propagation beyond the horizon—55
Millsaps, Knox and J. C. McPherson. Oscillations of magnetic suspensions—429
Mindlin, Raymond D. Thickness-shear and flexural vibrations of crystal plates—316
Minorsky, N. Parametric excitation—49
Montalenti, G. (see Ferro, A.)—565
—— (see Bonfiglioli, G.)—1089(L)
Montgomery, G. Franklin. Cascaded binary counter with feedback—780
Montroll, Elliott W. (see Hart, Robert W.)—376
—— **and Robert W. Hart.** Scattering of plane waves by soft obstacles. II. Scattering by cylinders, spheroids, and disks—1278
Moran, James H. Discrete energy levels of a nonlinear oscillator—1355
Morgan, F. H. Spectral emissivity of coatings of thoria and other refractories as a function of temperature—108(L)
Morrison, H. L. (see Rogers, F. T., Jr.)—1476
Morton, H. S., Jr. (see Beams, J. W.)—523(L)
Motz, H. Applications of the radiation from fast electron beams—527; errata—1217
Mrowca, B. A. (see Holroyd, L. V.)—696
Mukherjee, N. R. and Oliver Row. Studies of thin films by electron diffraction—681(L)
—— Surface tension of liquid metals—1215(L)
Muldawer, L. X-ray measurement of long-range order in β-AgZn—663
Muller, Marcel W. (see Jepsen, Robert L.)—1196
Mumford, W. W. (see Easley, M. A.)—846(L)
Munk, Max M. Generality of mixed gas flows—524(L)
Mutschler, E. C. (see Pugh, E. M.)—487

Nakayama, C. (see Horio, M.)—966
Nathan, Alan M. Dynamic method for measuring the specific heat of metals—234(L)
Neurath, Peter W. and James S. Koehler. Plastic deformation of pure single crystals of lead and copper—621
Newkirk, J. B., R. Smoluchowski, A. H. Geisler, and D. L. Martin. Phase equilibria in an ordering alloy system—290
Nielsen, Lawrence E. (see Buchdahl, Rolf)—1344
Nix, Foster C. (see Jaumot, Frank E., Jr.)—1294(L)
Noble, Robert H. (see Houston, Robert E.)—1295(L)
Norman, N. and B. E. Warren. X-ray measurement of short range order in Ag-Au—483
Nowick, A. S. Anelastic effects arising from precipitation in aluminum-zinc alloys—925
—— Reinterpretation of experiments on intermetallic diffusion—1182

Ogawa, S. and D. Watanabe. Electron diffraction study on the ordered alloy Au_3Cu—1502(L)
Ohmart, P. E. A method of producing an electric current from radioactivity—1504(L)
Onogi, S. (see Horio, M.)—966
—— (see Horio, M.)—971
—— (see Horio, M.)—977
Opinsky, A. J. and R. Smoluchowski. Crystallographic aspect of slip in body-centered cubic single crystals. I. Theoretical considerations—1380
—— **and R. Smoluchowski.** The crystallographic aspect of slip in body-centered cubic single crystals. II. Interpretation of experiments—1488
—— **and R. Smoluchowski.** On the ratio of the critical shear stresses—1508(L)
O'Rourke, R. C. Three-dimensional photoelasticity—872

Pakswer, Serge and William O. Reed. Photoconductivity of composite photoemissive cathodes—987(L)
Papas, Charles H. (see Levine, Harold)—29
Parkins, W. E., G. J. Dienes, and F. W. Brown. Pulse-annealing for the study of relaxation processes in solids—1012
Parratt, L. G. and C. F. Hempstead. On the reliability of Geiger counter response at moderately high rates—1502(L)
Parzen, Philip and Ladislas Goldstein. Effect of hydrostatic pressure in an electron beam on the operation of traveling-wave devices—398
—— Comments on "Equivalent temperature of an electron beam"—1387(L)
Peach, M. O. Concept of force in dislocation theory—1359
Pelzer, H. (see Gross, G.)—1035
Penner, S. S. and D. Weber. Emission of radiation from diatomic gases. II. Experimental determination of effective average absorption coefficients of CO—1164
—— Erratum: The emission of radiation from diatomic gases. I. Approximate calculations—1298
Peppiatt, H. J. and B. N. Brockhouse. Initial susceptibility of nickel under tension—985(L)
Perry, Robert W. and Arthur Kantrowitz. Production and stability of converging shock waves—878
Philpott, Delbert E. Portrait shadow-casting—982(L)
Plesset, M. S. and S. T. Cohen. Scattering and absorption of gamma-rays—350
Podolsky, Boris. Problem in heat conduction—581
Pohl, Herbert A. Motion and precipitation of suspenoids in divergent electric fields—869
Polachek, H. (see Seeger, R. J.)—640
Poritsky, H. and H. Weil. Conduction of current in a metallic pipe filled with a conducting liquid—1002
Press, Frank and Maurice Ewing. Theory of air-coupled flexural waves—892
Preston, F. W. Erratum: Mechanical properties of glass—48
Prim, R. C. Note on the partial differential equations describing steady current flow in intrinsic semiconductors—1388(L)
Pugh, E. M., R. v. Heine-Geldern, S. Foner, and E. C. Mutschler. Kerr cell photography of high speed phenomena—487
Pulvari, Charles F. Electrostatically induced permanent memory—1039

Quinn, Fred A., Jr., Donald E. Roberts, and R. N. Work. Volume-temperature relationships for the room temperature transition in Teflon—1085(L)

Rabinowicz, Ernest. Nature of the static and kinetic coefficients of friction—1373
Radavich, John and Charles Wert. Study of precipitates of C and N in iron with an electron microscope—367
Raff, S. J. Reflecting surface to simulate an infinite conducting plane—610
Rauch, S. E. Mathematical data for electron drain on positive ion sources—1128
Raymond, Richard C. (see McLucas, John L.)—1211
Read, W. T., Jr. (see Treuting, R. G.)—130
—— Formulas for the determination of residual stress in wires by the layer removal method—415
Reed, S., Jr. (see Wegener, P.)—1077
Reed, William O. (see Pakswer, Serge)—987(L)
Reekie, James (see Hetherington, F. E.)—1293(L)
Reich, H. J., P. M. Schultheiss, J. G. Skalnik, T. Flynn, and J. E. Gibson. Effect of auxiliary current on transistor operation—682(L)
Reiner, M. and G. W. Scott Blair. Erratum: Original authorship of formulas given in Clark and Deutsch's paper—236
Reis, Alfred J., Jerome J. Slade, and Sigmund Weissmann. New x-ray diffraction method for studying imperfections of crystal structure in polycrystalline specimens—665
Reisner, John H. Permanent magnet lenses—561
Reitan, Daniel Kinseth and Thomas James Higgins. Calculation of the electrical capacitance of a cube—223
Reverdin, D. L. Electron optical exploration of space change in a cut-off magnetron—257
Rigby, E. Caroline (see Woonton, G. A.)—390
Rigrod, W. W. Behavior of the resistance ignitor in mercury—787
Rinehart, John S. Some quantitative data bearing on the scabbing of metals under explosive attack—555
—— Work-hardening of mild steel by explosive attack—1086(L)
—— Remark on the composition dependence of the elastic parameters of beta-brass—1089
—— Some experimental indications of the stresses produced in a body by an exploding charge—1178
Ritchie, R. H. Temperature function in a moving medium—1389(L)
Ritter, H. L., R. L. Harris, and R. E. Wood. On the x-ray absorption correction for encased diffractors in the Debye-Scherrer technique—169
Roberts, B. W. (see Warren, B. E.)—1493
Roberts, Donald E. (see Quinn, Fred A., Jr.)—1085(L)
Robinson, Kenneth. Elastic energy of an ellipsoidal inclusion in an infinite solid—1045
Rogers, F. T., Jr. and L. E. Schilberg. Observation of initial flow in a fluid obeying Darcy's law by radioactive-tracer techniques—233(L)
—— **L. E. Schilberg and H. L. Morrison.** Convection currents in porous media. IV. Remarks on the theory—1476
Rooksby, H. P. and E. G. Steward. Barium oxide on tungsten cathode interface—358(L)
Rorden, H. C. and A. Grieco. Measurement of dynamic internal dissipation and elasticity of soft plastics—842
Rosen, Philip (see Stuart, George W., Jr.)—236(L)
Ross, Frederick W. The propagation in a compressible fluid of finite oblique disturbances with energy exchange and change of state—1414
Row, Oliver (see Mukherjee, N. R.)—681(L)
Ruze, J. and M. Young. Experimental determination of the reflection coefficient of metal-plate media—277

Sadowsky, M. A. (see Sternberg, E.)—1121
Sasaki, Wataru (see Komagata, Sakuji)—1290(L)
Sato, Hiroshi. Decay of spectra components in isotropic turbulence—525(L)
Saxon, David S. (see Baños, Alfredo, Jr.)—117
Schedling, J. A. (see Blaha, F.)—11
Schelkunoff, S. A. General theory of symmetric biconical antennas—1330
Schiffman, T. (see Ekstein, H.)—1215(L)
Schilberg, L. E. (see Rogers, F. T., Jr.)—233(L)
—— (see Rogers, F. T., Jr.)—1476
Schissel, Paul. Radiofrequency mass spectrometer—680(L)
Schremp, Frederic W., John D. Ferry, and Warren W. Evans. Mechanical properties of substances of high molecular weight. IX. Non-Newtonian flow and stress relaxation in concentrated polyisobutylene and polystyrene solutions—711
Schulman, James H., Robert J. Ginther, Clifford C. Klick, Raymond S. Alger, and Robert A. Levy. Dosimetry of x-rays and gamma-rays by radiophotoluminescence—1479
Schultheiss, P. M. (see Reich, H. J.)—682(L)
Schulz, George (see Coolidge, John E.)—103(L)
Schwartz, C. M. (see Austin, A. E.)—847(L)
Schwinger, J. (see Marcuvitz, N.)—806
Seeger, R. J. and H. Polachek. Shock-wave phenomena: Waterlike substances—640
Serbin, H. Response of an aerodynamic system under external harmonic force—1307
Seybolt, A. U., Joseph S. Lukesh, and D. W. White. Allotropy of beryllium—986(L)
Shah, J. R. and L. Jacob. Investigation of field distribution in symmetrical electron lens—1236
Sheppard, C. W. and A. S. Householder. Mathematical basis of the interpretation of tracer experiments in closed steady-state systems—510
Shibuya, Motoichi (see Komagata, Sakuji)—1290(L)
Shrader, R. E. (see Larach, S.)—362(L)
Sibbitt, W. L. (see Wilson, L. H.)—1027
Siefert, Arthur V. and Francis T. Worrell. Role of tetragonal twins in the internal friction of copper manganese alloys—1257
Simon, Dorothy Martin. Comparison of quenching distance and inflammability limit data for propane-air flame—103(L)
Šimon, I., H. O. McMahon, and R. J. Bowen. Dry metallic friction as a function of temperature between 4.2°K and 600°K—177
—— **H. O. McMahon, and R. J. Bowen.** Erratum: Dry metallic friction as a function of temperature between 4.2°K and 600°K—848
Skalnik, J. G. (see Reich, H. J.)—682(L)
Slade, Jerome J. (see Reis, Alfred J.)—665
Slater, J. C. Effects of radiation on materials—237
Slifkin, L. M. On the orientations of zinc crystals produced by the Bridgman method—1216(L)
Small, T. R. (see Faro, I. D. V.)—220
Smith, Donald P. Catalysis by metal powders—1291(L)
Smoluchowski, R. (see Newkirk, J. B.)—290
—— (see Achter, M. R.)—1260
—— (see Opinsky, A. J.)—1380
—— (see Opinsky, A. J.)—1488
—— (see Opinsky, A. J.)—1508(L)
Smullin, L. D. and W. G. Glass. Offset wave-guide junction as a reactive element—1124
—— Propagation of disturbances in one-dimensional accelerated electron streams—1496
Smyth, J. B. and C. P. Hubbard. Note on the "Attenuation of radio signals caused by scattering"—1387(L)
Smythe, W. R. Electric and magnetic forces between sphere and wire—521
—— On Kerr cell construction—1087(L)
—— The capacitance of a circular annulus—1499
Snoek, J. L. Natural width of a grain boundary in a metal—109(L)
Sollfrey, William. Wave propagation on helical wires—905

Spedden, H. R. (see Michael, A. B.)—1403
Speiser, Rudolph. (see Edwards, James W.)—424
Spencer, Domina Eberle. Separation of variables in electromagnetic theory—386
Squire, William. A problem in heat conduction—1508(L)
Sternberg, E., R. A. Eubanks, and M. A. Sadowsky. On the stress-function approaches of Boussinesq and Timpe to the axisymmetric problem of elasticity theory—1121
Stevenson, A. F. Exact and approximate equations for wave propagation in acoustic horns—1461
—— General theory of electromagnetic horns—1447
Steward, E. G. (see Rooksby, H. P.)—358(L)
Stollenwerk, E. (see Wegener, P.)—1077
Storer, James E. Impedance of an antenna over a large circular screen—1058
Storm, M. L. Heat conduction in simple metals—940
Straiton, A. W. (see LaGrone, A. H.)—672
Strong, H. M. (see Bundy, F. P.)—1069
Stuart, George W., Jr. and Philip Rosen. Cylindrical cavity filled with a dc discharge—236(L)
Szebehely, V. G. Relation between gas evolution and physical properties of liquids—627

Tai, C. T. Effect of a grounded slab on the radiation from a line source—405
Tani, Itiro. On the anomalous Magnus effect—1506(L)
Taub, A. H. and Nelson Wax. Erratum: Theory of the parallel plane diode—108
Taylor, Thomas T. and John R. Whinnery. Applications of potential theory to the design of linear arrays—19
Thompson, A. S. Numerical computation of neutron distribution and critical size—1223
Thompson, Donald O. (see Artman, Robert A.)—358(L)
Ticknor, L. B. (see Bever, M. B.)—1297(L)
Townes, C. H. Atomic clocks and frequency stabilization on microwave spectral lines—1365
Treuting, R. G. and W. T. Read, Jr. Mechanical determination of biaxial residual stress in sheet materials—130
Turnbull, D. (see Hoffman, R. E.)—634
—— (see Hoffman, R. E.)—984(L)
Twersky, Victor. On the nonspecular reflection of electromagnetic waves—825

Uhlig, Herbert H. Volta potentials of the copper-nickel alloys and several metals in air—1399

Van Bladel, J. Expandability of a wave-guide field in terms of normal modes—68
—— **and Thomas J. Higgins.** Cut-off frequency in two-dielectric layered rectangular wave guides—329
van de Lindt, W. J. (see Beljers, H. G.)—1506(L)
van der Reyden, D. Thermal expansion coefficients and the melting point of cubic elements—363(L)

Wahlin, H. B. The transmission of hydrogen through metals—1503(L)
Wales, M. Sedimentation equilibrium in concentrated polymer solutions—735
Warren, B. E. (see Keating, D. T.)—286
—— (see Norman, N.)—483
—— **B. L. Averbach, and B. W. Roberts.** Atomic size effect in the x-ray scattering by alloys—1493
Watanabe, D. (see Ogawa, S.)—1502(L)
Watson, John H. L. Negative charging of glass fibers under electron bombardment—1386(L)
Watson, R. B. On the directional patterns of polystyrene rod antennas—154
—— (see Cheney, M. G., Jr.)—675
Wax, Nelson (see Taub, A. H.)—108
—— Amplitude bounds for certain relaxation oscillations—278
Waymouth, J. F., Jr. Deterioration of oxide-coated cathodes under low duty-factor operation—80
Weber, D. (see Penner, S. S.)—1164
Wegener, P. and G. Lundquist. Condensation of water vapor in the shock tube below 150°K—233(L)
—— **S. Reed, Jr., E. Stollenwerk, and G. Lundquist.** Air condensation in hypersonic flow—1077
Wehner, G. (see Medicus, G.)—1388(L)
Wehner, Gottfried. Electron plasma oscillations—761
Weil, H. (see Poritsky, H.)—1002
Weissmann, Sigmund (see Reis, Alfred J.)—665
Welch, H. W., Jr., and W. G. Dow. Analysis of synchronous conditions in the cylindrical magnetron space charge—433
Wells, Charles P. (see Beth, Richard A.)—742
Went, J. J. (see Beljers, H. G.)—1506(L)
Wert, Charles (see Radavich, John)—367
Wexler, Aaron. Evaporation rate of liquid helium. I—1463
Whinnery, John R. (see Taylor, Thomas T.)—19
White, D. W. (see Seybolt, A. U.)—986(L)
White, J. R. (see Clark, O. H.)—474
Wicher, E. R. Influence of magnetic fields upon the propagation of electromagnetic waves in artificial dielectrics—1327
Wideröe, R. Investigations on the capturing of electrons in a 30-Mev betatron—362(L)
Wilbur, D. A. (see Cobine, J. D.)—835
Wilkinson, P. G. Properties of evaporated gold and tungsten oxides—226
—— Lattice distortion spectrum of evaporated gold—419
Wilson, L. H., W. L. Sibbitt, and M. Jakob. Flow of gases in porous media—1027
Winkler, Eva M. Density measurements in supersonic flow by means of the x-ray absorption method—201
Witte, Robert S. and Robert L. Anthony. Stress-temperature studies of transitions in rubbers—689
Woo, Way Dong. Transit time effect in a cylindrical diode—1333
Wood, R. E. (see Ritter, H. L.)—169
Woods, W. W. (see Clark, O. H.)—474
Woonton, G. A., J. A. Carruthers, H. A. Elliott, and E. Caroline Rigby. Diffraction errors in an optical measurement at radio wavelengths—390
Work, R. N. (see Quinn, Fred A., Jr.)—1085(L)
Worrell, Francis T. (see Siefert, Arthur V.)—1257
Wyckoff, H. O. (see Goldstein, N.)—417

Yamaguchi, Shigeto. Oriented crystals in the rolled plates of alloys—680(L)
—— On the etched surfaces of nickel single crystals—983(L)
—— Structure of oxide replica for electron microscopy—1295(L)
Yamaka, Eiso. Study of oxide-coated cathode by x-ray diffraction method—1087(L)
Yamamoto, K. (see Horio, M.)—966
Yamamoto, Takaaki (see Komagata, Sakuji)—1290(L)
Yeagley, Henry L. Preliminary study of a physical basis of bird navigation. Part II—746
Young, D. R. Temporary enhancement of hysteresis in barium titanate samples—523(L)
Young, M. (see Ruze, J.)—277
Yudowitch, K. L. Latex particle size from x-ray diffraction peaks—214

Zadeh, Lotfi A. On stability of linear varying-parameter systems—402
—— Initial conditions in linear varying-parameter systems—782
—— Note on the initial excitation of linear systems—1216(L)
Zener, Clarence. Theory of D_0 for atomic diffusion in metals—372

Subject Index to Volume 22

References with (L) are to Letters to the Editor

Ac characteristics of Si *p-n* junction, S. Komagata, M. Hatoyama, M. Shibuya, W. Sasaki, T. Yamamoto, and M. Kikuchi—1290(L)
Absolute reaction rate theory to some problems in annealing, Application of the, F. Wm. Cagle, Jr., and Henry Eyring—771
Absorption coefficients of metals and alloys for complex radioactive spectra, Simple technique for obtaining, Frank E. Jaumot, Jr., and Foster C. Nix—1294(L)
Acoustic horns, Exact and approximate equations for wave propagation in, A. F. Stevenson—1461
Aerodynamic system under external harmonic force, Response of an, H. Serbin—1307
Air condensation in hypersonic flow, P. Wegener, S. Reed, Jr., E. Stollenwerk, and G. Lundquist—1077
Air-coupled flexural waves, Theory of, Frank Press and Maurice Ewing—892
Air shocks in a tube, New method for the production of, A. B. Laponsky and R. J. Emrich—1297(L)
Allotropic transformation of hafnium, Pol Duwez—1174
Allotropy of beryllium, A. U. Seybolt, Joseph S. Lukesh, and D. W. White—986(L)
Alloys, copper, Plasticity and conductivity, analogous flow phenomena in, Rolland Sydney French—105(L)
Aluminum-zinc alloys, Anelastic effects arising from precipitation in, A. S. Nowick—925
Amplitude bounds for certain relaxation oscillations, Nelson Wax—278
Anelastic effects arising from precipitation in aluminum-zinc alloys, A. S. Nowick—925
Annealing twins during grain growth, Formation of, R. L. Fullman and J. C. Fisher—1350
Announcements—371, 414, 428, 554, 560, 574, 609, 654, 679, 722, 739, 988, 1090, and 1218
Anomalous Magnus effect, Itiro Tani—1506(L)
Antenna over a large circular screen, Impedance of, James E. Storer—1058
Antenna, Theory of the circular diffraction, Harold Levine and Charles H. Papas—29
Antennas and open-wire lines, Current and charge distributions on, D. J. Angelakos—910
Antennas, General theory of symmetric biconical, S. A. Schelkunoff—1330
Antennas, shaped-beam, General formulation for calculation of, A. S. Dunbar—1217(L)
Aperture, circular, Edge effects in a, Robert E. Houston and Robert H. Noble—1295(L)
Applications of potential theory to the design of linear arrays, Thomas T. Taylor and John R. Whinnery—19
Arcing at electrical contacts on closure. Part I. Dependence upon surface conditions and circuit parameters, L. H. Germer—955
Arcing at electrical contacts on closure. Part II. The initiation of an arc, L. H. Germer—1133
Asymptotic approximation for the normal modes in sound channel wave propagation, N. A. Haskell—157
Atomic clocks and frequency stabilization on microwave spectral lines, C. H. Townes—1365
Atomic diffusion in metals, Theory of D_0 for, Clarence Zener—372
Atomic size effect in the x-ray scattering by alloys, B. E. Warren, B. L. Averbach, and B. W. Roberts—1493
Attenuation of radio signals caused by scattering, J. B. Smyth and C. P. Hubbard—1387(L)
Attenuation of radio signals caused by scattering, Reply to, A. H. LaGrone—1387(L)
Auxiliary current on transistor operation, Effect of, H. J. Reich, P. M. Schultheiss, J. G. Skalnik, T. Flynn, and J. E. Gibson—682(L)
Axially symmetric systems for generating and measuring magnetic fields. Part I, Milan Wayne Garrett—1091
Axisymmetric body forms for specified pressure distributions, Approximation of, John S. McNown and En-Yun Hsu—864
Axisymmetric problem of elasticity theory, Stress-function approaches of Boussinesq and Timpe to, E. Sternberg, R. A. Eubanks, and M. A. Sadowsky—1121

Barium oxide from various base metals and of strontium oxide from platinum, The evaporation products of, L. T. Aldrich—1168
Barium oxide on tungsten cathode interface, Eugene B. Hensley and John H. Affleck—359(L)
Barium oxide with excess barium, Optical absorption, Evan O. Kane—1214(L)
Barium oxide on tungsten cathode interface, H. P. Rooksby and E. G. Steward—358(L)
Behavior of the resistance ignitor in mercury, W. W. Rigrod—787
Beryllium, Allotropy of, A. U. Seybolt, Joseph S. Lukesh, and D. W. White—986(L)
Beta-ray autoradiographs of metals and minerals, A technique for preparing, A. B. Michael, W. Z. Leavitt, M. B. Bever, and H. R. Spedden—1403
Bird navigation, Preliminary study of a physical basis of, Part II, Henry L. Yeagley—746
Books—94, 682, 849, and 1390
Boride cathodes, J. M. Lafferty—299
Branching of slip lines in alpha-brass, Harry Czyzewski—846(L)

Calculation of diffusion penetration curves for surface and grain boundary diffusion, J. C. Fisher—74
Calculation of the electrical capacitance of a cube, Daniel Kinseth Reitan and Thomas James Higgins—223
Cantilever-strut, Finite deflections of, Richard A. Beth and Charles P. Wells—742
Capacitance of a circular annulus, W. R. Smythe—1499
Carbon black-oil suspensions, Electrical properties of some, Michael J. Forster and Darwin J. Mead—705
Carbon diffusion in metallic carbides, Measurement of, G. C. Kuczynski and R. Landauer—952
Carbon, oxygen, and sulfur content of Chilean coppers as related to cuprous-oxide rectifiers, C. C. Hein and W. M. Hickam—1192
Cascaded binary counter with feedback, G. Franklin Montgomery—780
Catalysis by metal powders, Donald P. Smith—1291(L)
Cathodes, oxide-coated, Deterioration of, under low duty-factor operation, J. F. Waymouth, Jr.—80
Cathodoluminescence of zinc orthosilicate with manganese activator, S. Larach and R. E. Shrader—362(L)
Circuit concept, A critical study of the, Jesse Gerald Chaney—1429
Coefficients of friction, static and kinetic, Nature of, Ernest Rabinowicz—1373
Coherent twin boundaries in copper, Interfacial free energy of, R. L. Fullman—448
Column behavior under conditions of compressive stress wave propagation, George Gerard and Herbert Becker—1298(L)
Comparison of quenching distance and inflammability limit data for propane-air flames, Dorothy Martin Simon—103(L)

Composition dependence of the elastic parameters of beta-brass, John S. Rinehart—1089(L)
Compressible supersonic flow in jets under the Kármán-Tsien pressure-volume relation, N. Coburn—124
Condensation of water vapor in the shock tube below 150°K, P. Wegener and G. Lundquist—233(L)
Condenser aperture device for electron microscopes, J. D. Boadway—104(L)
Contact potential variations on freshly condensed metal films at low pressures, Leland L. Antes and Norman Hackerman—1395
Convection currents in porous media. IV. Remarks on the theory, F. T. Rogers, Jr., L. E. Schilberg, and H. L. Morrison—1476
Copper alloys, Plasticity and conductivity, analogous flow phenomena in, Rolland Sydney French—105(L)
Copper-copper oxide rectifiers, Asymmetric heat conduction in, F. Hubbard Horn—1214(L)
Corona discharges in pure N_2, O_2, and mixtures thereof, Negative coaxial cylindrical, Charles G. Miller and Leonard B. Loeb—614
Corona discharges in pure N_2, O_2, and mixtures thereof, Positive coaxial cylindrical, Charles G. Miller and Leonard B. Loeb—494
Corona from ice points, Herman W. Bandel—984(L)
Coronas with coaxial geometry in pure N_2, pure O_2, and various mixtures at pressures from atmospheric to 27 mm, Starting potentials of positive and negative, Charles G. Miller and Leonard B. Loeb—740
Correlating modulus for fluid resistance in accelerated motion, H. W. Iversen and R. Balent—324
Creep and relaxation. III, B. Gross and H. Pelzer—1035
Crystal structure of the sigma-phase in the Co-Cr system, J. S. Kasper, B. F. Decker, and J. R. Belanger—361(L)
Crystal systems with low loss, Ruth Baumann Fry and William J. Fry—198
Crystallographic aspect of slip in body-centered cubic single crystals. I. Theoretical considerations, A. J. Opinsky and R. Smoluchowski—1380
Crystallographic aspect of slip in body-centered cubic single crystals. II. Interpretation of experiments, A. J. Opinsky and R. Smoluchowski—1488
Crystallography and interfacial free energy of noncoherent twin boundaries in copper, R. L. Fullman—456
Crystals, iron single, Yielding behavior of, A. N. Holden—1290(L)
Crystals, nickel single, On the etched surfaces of, Shigeto Yamaguchi—983(L)
Crystals of copper, cold-worked single, Internal friction of, Ryukiti Robert Hasiguti and Tadamasa Hirai—1084(L)
Crystals, oriented, in the rolled plates of alloys, Shigeto Yamaguchi—680(L)
Cuprous-oxide rectifiers, Carbon, oxygen, and sulfur content of Chilean coppers as related to, C. C. Hein and W. M. Hickam—1192
Current and charge distributions on antennas and open-wire lines, D. J. Angelakos—910
Cut-off frequency in two-dielectric layered rectangular wave guides, J. Van Bladel and Thomas J. Higgins—329
Cylinder with a conical nose, Experimental measurement of incompressible flow along a, E. V. Laitone—63
Cylindrical cavity filled with a dc discharge, George W. Stuart, Jr., and Philip Rosen—236(L)

Decay of spectra components in isotropic turbulence, Hiroshi Sato—525(L)
Deceleration and ionizing efficiency of radar meteors, D. W. R. McKinley—202
Deformation of body-centered cubic metals, E. A. Calnan and C. J. B. Clews—1508(L)
Density measurements in supersonic flow by means of the x-ray absorption method, Eva M. Winkler—201
Design of molecular pumps, Robert B. Jacobs—217
Deterioration of oxide-coated cathodes under low duty-factor operation, J. F. Waymouth, Jr.—80
Diaphragm, thin, Theory of the dynamic plastic deformation of, G. E. Hudson—1
Diatomic gases, Emission of radiation from. I. Approximate calculations, S. S. Penner—1298 (erratum)
Diatomic gases, Emission of radiation from. II. Experimental determination of effective average absorption coefficients of CO, S. S. Penner and D. Weber—1164
Dielectric coated wires, Propagation on, E. T. Kornhauser—525(L)
Dielectric properties of glass, Microwave measurements of, George Birnbaum, S. J. Kryder, and Harold Lyons—95
Dielectric rod antenna of circular cross section excited in the dominant mode, Experimental investigation of, C. W. Horton and C. M. McKinney, Jr.—1246
Dielectrics, artificial, Influence of magnetic fields upon the propagation of magnetic waves in, E. R. Wicher—1327
Difference between turbulence in a two-dimensional fluid and in a three-dimensional fluid, T. D. Lee—524(L)
Differential equations, Partial, describing steady current flow in intrinsic semiconductors, R. C. Prim—1388(L)
Diffraction errors in an optical measurement at radio wavelengths, G. A. Woonton, J. A. Carruthers, H. A. Elliott, and E. Caroline Rigby—390
Diffraction of a plane electromagnetic wave by a paraboloid of revolution, C. W. Horton and F. C. Karal, Jr.—575
Diffraction of electromagnetic waves by two conducting parallel half-planes, M. G. Cheney, Jr., and Robert B. Watson—675
Diffraction pattern in a circular aperture measured in the microwave region, C. L. Andrews—520 (erratum)
Diffraction pattern of microwaves near rods, C. L. Andrews—465
Diffusion, surface and grain boundary, Calculation of penetration curves for, J. C. Fisher—74
Digital information storage in three dimensions using magnetic cores, Jay W. Forrester—44
Directional distribution of 1040-kev radiation from a high voltage x-ray tube, N. Goldstein, U. Fano, and H. O. Wyckoff—417
Directional patterns of polystyrene rod antennas, R. B. Watson—154
Distribution of slip in metal crystals, F. C. Frank—1386(L)
Dosimetry of x-rays and gamma-rays by radiophotoluminescence, J. H. Schulman, R. J. Ginther, C. C. Klick, R. S. Alger, and R. A. Levy—1479
Dry metallic friction as a function of temperature between 4.2°K and 600°K, I. Šimon, H. O. McMahon, and R. J. Bowen—177
—— I. Šimon, H. O. McMahon, and R. J. Bowen—848 (erratum)
Dust particles, Static electrification of, on dispersion into a cloud, John E. Coolidge and George Schulz—103(L)
Dust particles, Static electrification of, on dispersion into a cloud, Wulf B. Kunkel—103(L)
Dynamic internal dissipation and elasticity of soft plastics, Measurement of, H. C. Rorden and A. Grieco—842
Dynamic load simulator, conservative, Design and analysis of, E. H. Gamble and B. W. Hatten—1250
Dynamic measurements of physical properties of pulp and paper by audiofrequency sound, M. Horio and S. Onogi—971
Dynamic method for measuring the specific heat of metals, Alan M. Nathan—234(L)

Effect of size and spectral purity of source on fringe pattern of the Mach-Zehnder interferometer, F. D. Bennett—776

Effective earth's radius for radiowave propagation beyond the horizon, William Miller—55
Effects of radiation on materials, J. C. Slater—237
Elastic energy of an ellipsoidal inclusion in an infinite solid, Kenneth Robinson—1045
Elastic parameters of beta-brass, Robert A. Artman and Donald O. Thompson—358(L)
Electric and magnetic constants of metallic delay media containing obstacles of arbitrary shape and thickness, Seymour B. Cohn—628
Electric and magnetic forces between sphere and wire, W. R. Smythe—521
Electric dipoles in the presence of elliptic and circular cylinders, Winston S. Lucke—14
Electric tunnel effect across thin insulator films in contacts, Ragnar Holm—569
——Ragnar Holm—1217 (errata)
Electrical breakdown over insulators in high vacuum, Paul H. Gleichauf—535
Electrical breakdown over insulators in high vacuum, Paul H. Gleichauf—766
Electrical charge storage in polystyrene capacitors, L. A. Matheson and V. J. Caldecourt—1176
Electrical method for investigating the nature and behavior of small, airborne, charged particles, J. H. Daniel and F. S. Brackett—542
Electrical properties of selenium. I. Single crystals, H. W. Henkels—916
Electrical properties of selenium. II. Microcrystalline selenium, H. W. Henkels—1265
Electrical properties of some carbon black-oil suspensions, Michael J. Forster and Darwin J. Mead—705
Electrical properties of zinc oxide semiconductors, E. E. Hahn —855
Electrical resistivity of cold-worked copper-iron alloys, F. E. Hetherington and James Reekie—1293(L)
Electrode reactions in the glow discharge, F. E. Haworth—606
Electromagnetic horns, General theory of, A. F. Stevenson—1447
Electromagnetic scattering from spheres with sizes comparable to the wavelength, A. L. Aden—601
Electromagnetic waves from two concentric spheres, Scattering of, Arthur L. Aden and Milton Kerker—1242
Electron beam, Equivalent temperature of, M. E. Hines—1385(L)
Electron beam, Equivalent temperature of, Philip Parzen—1387(L)
Electron diffraction study on the ordered alloy Au_3Cu, S. Ogawa and D. Watanabe—1502(L)
Electron microradiography of electrodeposited metals, Comment on nomenclature in, G. M. Corney—682(L)
Electron Microscope Society of America, Program of the—110
Electron microscopes, Condenser aperture device for, J. D. Boadway—104(L)
Electron microscopic replica studies of porosity in fused iron catalysts, J. T. McCartney and R. B. Anderson—1441
Electron optical exploration of space charge in a cut-off magnetron, D. L. Reverdin—257
Electron plasma oscillations, Gottfried Wehner—761
Electron temperature *vs* noise temperature in low pressure mercury-argon discharges, M. A. Easley and W. W. Mumford—846(L)
Electronic torch and related high frequency phenomena, J. D. Cobine and D. A. Wilbur—835
Electrons from insulators, secondary, Pulse method of determining the energy distribution of, Kenneth G. McKay—89
Electrons in a 30-Mev betatron, Investigations on the capturing of, R. Wideröe—362(L)
Electrostatically induced permanent memory, Charles F. Pulvari—1039
Elliptic and circular cylinders, Electric dipoles in the presence of, Winston S. Lucke—14
Emission of radiation from diatomic gases. I. Approximate calculations, S. S. Penner—1298 (erratum)
Emission of radiation from diatomic gases. II. Experimental determination of effective average absorption coefficients of CO, S. S. Penner and D. Weber—1164
Emission, Secondary, of nickel-barium mixtures and rhenium when bombarded by electrons with energies from 50 to 8000 electron-volts, H. E. Farnsworth and M. J. Lun—77
Energy distribution of secondary electrons from insulators, Pulse method of determining, Kenneth G. McKay—89
Energy stored during cold-working of metals, Method for determining the, M. B. Bever and L. B. Ticknor—1297(L)
Envelope type of thermal conductivity tests, Theory of the, Arthur L. Loeb—282
—— Arthur L. Loeb—849 (erratum)
Epitaxy of alkali chlorides on metals, G. W. Johnson—797
Epitomization of the basic theory of the generalized Schwarz-Christoffel transformations as used in applied physics, Thomas James Higgins—365(L)
Etched surfaces of nickel single crystals, Shigeto Yamaguchi—983(L)
Evaporation products of barium oxide from various base metals and of strontium oxide from platinum, L. T. Aldrich —1168
Expandability of a wave-guide field in terms of normal modes, J. Van Bladel—68
Expected number of crossings of axis by linearly increasing function plus noise, Frank W. Lehan—1067
Experimental determination of the reflection coefficient of metal-plate media, J. Ruze and M. Young—277
Experimental measurement of incompressible flow along a cylinder with a conical nose, E. V. Laitone—63

Fermi level in a simple impurity semiconductor, Graphical determination of the, K. Lehovec and H. Kedesdy—65
Ferromagnetic materials, Internal friction of, A. Ferro and G. Montalenti—565
Force in dislocation theory, Concept of, M. O. Peach—1359
Forced vibration of reed as a method of determining viscoelasticity, M. Horio and S. Onogi—977
Fracture and yield stress of 1020 steel at low temperatures, A. S. Eldin and S. C. Collins—1296(L)
Free convection heat transfer from electrically heated wires, Erich A. Farber—1437

Gas evolution and physical properties of liquids, Relation between, V. G. Szebehely—627
Gas temperatures and elastic losses in low pressure mercury-argon discharges, C. Kenty, M. A. Easley, and B. T. Barnes —1006
Gases in porous media, Flow of, L. H. Wilson, W. L. Sibbitt, and M. Jakob—1027
Gases in rocket flames, Measurement of velocity and pressure by spectroscopic methods, F. P. Bundy, H. M. Strong, and A. B. Gregg—1069
Geiger counter response at moderately high rates, Reliability of, L. G. Parratt and C. F. Hempstead—1502(L)
Glass fibers under electron bombardment, Negative charging of, John H. L. Watson—1386(L)
Glass, Mechanical properties of, F. W. Preston—48 (erratum)
Glass, Microwave measurements of the dielectric properties of, George Birnbaum, S. J. Kryder, and Harold Lyons—95
Gold wire at high temperatures, Deformation of, B. H. Alexander, M. H. Dawson, and H. P. Kling—439
Grain boundaries and their structure, Diffusion in, M. R. Achter and R. Smoluchowski—1260
Grain boundary in a metal, Natural width of, J. L. Snoek—109(L)

Grain growth, Formation of annealing twins during, R. L. Fullman and J. C. Fisher—1350
Graphical determination of the Fermi level in a simple impurity semiconductor, K. Lehovec and H. Kedesdy—65
Graphite at elevated temperatures, Mechanical properties of, C. Malmstrom, R. Keen, and L. Green, Jr.—593
Grounded slab on the radiation from a line source, Effect of a, C. T. Tai—405

Hafnium, Allotropic transformation of, Pol Duwez—1174
Heat conduction, A problem in, William Squire—1508(L)
Heat conduction, asymmetric, in copper-copper oxide rectifiers, F. Hubbard Horn—1214(L)
Heat conduction in simple metals, M. L. Storm—940
Heat conduction, Problem in, Boris Podolsky—581
Helical antennas with sinusoidal current, Radiation field of, E. T. Kornhauser—887
Helical wires, Wave propagation on, William Sollfrey—905
Helium cryostat design problem, A finite difference treatment of, Warren E. Henry—1439
Helium, liquid, Evaporation rate of. I, Aaron Wexler—1463
High temperature structure and thermal expansion of some metals as determined by x-ray diffraction data. I. Platinum, tantalum, niobium, and molybdenum, James W. Edwards, Rudolph Speiser, and Herrick L. Johnston—424
Hollow cathode for positive ion studies in cathode-ray tubes, C. H. Bachman, Harold Eubank, and George Hall—1208
Hydrogen through metals, Transmission of, H. B. Wahlin—1503(L)
Hydrostatic pressure in an electron beam on the operation of traveling-wave devices, Effect of, Philip Parzen and Ladislas Goldstein—398
Hypersonic flow at a Mach number of 10, I. D. V. Faro, T. R. Small, and F. K. Hill—220
Hysteresis in barium titanate samples, Temporary enhancement of, D. R. Young—523(L)

Impact flash at high speed water entry, J. H. McMillen, R. L. Kramer, and D. E. Allmand—360(L)
Improvements in visual depiction of magnetic lines of force by means of a gas discharge, F. Blaha and J. A. Schedling—11
Influence of magnetic fields upon the propagation of electromagnetic waves in artificial dielectrics, E. R. Wicher—1327
Information theory and most efficient codings for communication or memory devices, L. Brillouin—1108
Initial conditions in linear varying-parameter systems, Lotfi A. Zadeh—782
Interfacial free energy of coherent twin boundaries in copper, R. L. Fullman—448
Intermetallic diffusion, Reinterpretation of experiments on, A. S. Nowick—1182
Internal friction of cold-worked single crystals of copper, Ryukiti Robert Hasiguti and Tadamasa Hirai—1084(L)
Internal friction of copper manganese alloys, Role of tetragonal twins in, Arthur V. Siefert and Francis T. Worrell—1257
Investigations on the capturing of electrons in a 30-Mev betatron, R. Wideröe—362(L)
Iron-silicon alloys heat treated in a magnetic field, Matilda Goertz—964
Iron single crystals, Yielding behavior of, A. N. Holden—1290(L)

Kerr cell construction, W. R. Smythe—1087(L)
Kerr cell photography of high speed phenomena, E. M. Pugh, R. v. Heine-Geldern, S. Foner, and E. C. Mutschler—487
Kerr cell, Transmission line, J. W. Beams and H. S. Morton, Jr.—523(L)
Kinetics of ordering the alloy AuCu, G. J. Dienes—1020

Latex particle size from x-ray diffraction peaks, K. L. Yudowitch—214
Lattice and grain boundary self-diffusion in silver, R. E. Hoffman and D. Turnbull—634
—— R. E. Hoffman and D. Turnbull—984 (erratum)
Lattice distortion spectrum of evaporated gold, P. G. Wilkinson—419
Lead telluride and lead selenide, Method of growing single crystals of, W. D. Lawson—1444
Leaky condenser oxide cathode interface, A. Eisenstein—138
Legendre polynomial approximations, Associated, R. Landauer—87
Linear arrays, Applications of potential theory to the design of, Thomas T. Taylor and John R. Whinnery—19
Linear expansion coefficient and melting point of metals, G. Bonfiglioli and G. Montalenti—1089(L)
Linear systems, Initial excitation of, L. A. Zadeh—1216(L)
Linear varying-parameter systems, Initial conditions in, Lotfi A. Zadeh—782
Linear varying-parameter systems, Stability of, Lotfi A. Zadeh—402
Linearly increasing function plus noise, Expected number of crossings of axis, Frank W. Lehan—1067
Long-range ballistic rocket, Accuracy of the, W. E. Frye—585
Long-range order in beta-brass and Cu_3Au, D. T. Keating and B. E. Warren—286
Lubrication at extreme pressures with mineral oil films, O. H. Clark, W. W. Woods, and J. R. White—474

Mach number of 10, Hypersonic flow at, I. D. V. Faro, T. R. Small, and F. K. Hill—220
Mach-Zehnder interferometer, Effect of size and spectral purity of source on fringe pattern of the, F. D. Bennett—776
Magnetic cores, Digital information storage in three dimensions using, Jay W. Forrester—44
Magnetic lines of force by means of a gas discharge, Improvements in visual depiction of, F. Blaha and J. A. Schedling—11
Magnetic losses in anisotropic bars of ferrite at ultra-high frequencies, H. G. Beljers, W. J. van de Lindt, and J. J. Went—1506(L)
Magnetic scaling circuit, Hellmuth Hertz—107(L)
Magnetron cathodes, Enhanced emission from, Robert L. Jepsen and Marcel W. Muller—1196
Mathematical basis of the interpretation of tracer experiments in closed steady-state systems, C. W. Sheppard and A. S. Householder—510
Mathematical data for electron drain on positive ion sources, S. E. Rauch—1128
Maxwell's demon cannot operate: Information and entropy. I, L. Brillouin—334
Measurement of velocity and pressure of gases in rocket flames by spectroscopic methods, F. P. Bundy, H. M. Strong, and A. B. Gregg—1069
Mechanical determination of biaxial residual stress in sheet materials, R. G. Treuting and W. T. Read, Jr.—130
Mechanical properties of glass, F. W. Preston—48 (erratum)
Mechanical properties of graphite at elevated temperatures, C. Malmstrom, R. Keen, and L. Green, Jr.—593
Mechanical properties of substances of high molecular weight. IX. Non-Newtonian flow and stress relaxation in concentrated polyisobutylene and polystyrene solutions, Frederic W. Schremp, John D. Ferry, and Warren W. Evans—711
Mechanical properties of substances of high molecular weight. X. The relaxation distribution function in polyisobutylene and its solutions, John D. Ferry, Edwin R. Fitzgerald, Myrle F. Johnson, and Lester D. Grandine, Jr.—717
Memory devices, Information theory and most efficient codings for, L. Brillouin—1108

Memory, permanent, Electrostatically induced, Charles F. Pulvari—1039
Metallic behavior of $MoSi_2$, Frank W. Glaser—103(L)
Metallic delay media containing obstacles of arbitrary shape and thickness, Electric and magnetic constants of, Seymour B. Cohn—628
Metallic pipe filled with a conducting liquid, Conduction of current in a, H. Poritsky and H. Weil—1002
Metallographic study of diffusion interfaces, G. C. Kuczynski and B. H. Alexander—344
Metals, energy stored during cold-working of, Method for determining, M. B. Bever and L. B. Ticknow—1297(L)
Metals, Epitaxy of alkali chlorides on, G. W. Johnson—797
Metals, liquid, Surface tension of, N. R. Mukherjee—1215(L)
Microwave filters employing a single cavity excited in more than one mode, Wei-guan Lin—989
Microwave measurements of the dielectric properties of glass, George Birnbaum, S. J. Kryder, and Harold Lyons—95
Mixed gas flows, Generality of, Max M. Munk—524(L)

Natural width of a grain boundary in a metal, J. L. Snoek—109(L)
Necessary number of elements in a directional ring aerial, H. Lottrup Knudsen—1299
Negative coaxial cylindrical corona discharges in pure N_2, O_2, and mixtures thereof, Charles G. Miller and Leonard B. Loeb—614
Neutron distribution and critical size, Numerical computation of, A. S. Thompson—1223
New booklets—1249
Newtonian flow, Studies in. I. The dependence of the viscosity of liquids on temperature, Arthur K. Doolittle—1031
Newtonian flow, Studies in. II. The dependence of the viscosity of liquids on free-space, Arthur K. Doolittle—1471
Nickel-barium mixtures and rhenium when bombarded by electrons with energies from 50 to 8000 electron-volts, Secondary emission of, H. E. Farnsworth and M. J. Lun—77
Nickel single crystals, On the etched surfaces of, Shigeto Yamaguchi—983(L)
Nickel under tension, Initial susceptibility of, H. J. Peppiatt and B. N. Brockhouse—985(L)
Noble gas hot cathode diodes with negative arc drop, G. Medicus and G. Wehner—1388(L)
Noncontact temperature measuring device, J. E. Field and S. D. Gehman—106(L)
Nonlinear impedance element, Power spectrum of a narrow band noise passed through, John L. McLucas and Richard C. Raymond—1211
Nonlinear oscillator, Discrete energy levels of, James H. Moran—1355
Nonlinear vibration theory, Studies in, Stanley Fifer—1421
Nonspecular reflection of electromagnetic waves, Victor Twersky—825
Nuclear magnetic resonance study of transitions in polymers, L. V. Holroyd, R. S. Codrington, B. A. Mrowca, and E. Guth—696
Numerical computation of neutron distribution and critical size, A. S. Thompson—1223

Objective for use in the electron microscopy of ultra-thin sections, James Hillier—135
Observation of initial flow in a fluid obeying Darcy's law by radioactive-tracer techniques, F. T. Rogers, Jr., and L. E. Schilberg—233(L)
Offset wave-guide junction as a reactive element, L. D. Smullin and W. G. Glass—1124
Optimum source size for the Mach-Zehnder interferometer, F. D. Bennett—184
Oriented crystals in the rolled plates of alloys, Shigeto Yamaguchi—680(L)
Original authorship of formulas given in Clark and Deutsch's paper, M. Reiner and G. W. Scott Blair—236 (erratum)
Oscillations, Electron plasma, Gottfried Wehner—761
Oscillations of magnetic suspensions, Knox Millsaps and J. C. McPherson—429
Oscillations, Predominantly subharmonic, Carl A. Ludeke—1321
Oscillator, nonlinear, Discrete energy levels of, James H. Moran—1355
Oxide-coated cathode by x-ray diffraction method, Study of, Eiso Yamaka—1087(L)
Oxide-coated cathodes, Initial decay of, T. Hibi and K. Ishikawa—986(L)
Oxide replica for electron microscopy, Structure of, Shigeto Yamaguchi—1295(L)

Parallel plane diode, Theory of the, A. H. Taub and Nelson Wax—108 (erratum)
Parallelepipeds, almost cubic, Elastic vibrations of, H. Ekstein and T. Schiffman—1215(L)
Parametric excitation, N. Minorsky—49
Periodic statistical distortion of unidirectionally ordered diffractors, with application to collagen, Richard S. Bear and Orvil E. A. Bolduan—191
Permanent magnet lenses, John H. Reisner—561
Phase equilibria in an ordering alloy system, J. B. Newkirk, R. Smoluchowski, A. H. Geisler, and D. L. Martin—290
Photoconductivity of composite photoemissive cathodes, Serge Pakswer and William O. Reed—987(L)
Photoelasticity, Three-dimensional, R. C. O'Rourke—872
Physical entropy and information. II, L. Brillouin—338
Plane waves by soft obstacles, On the scattering of. I. Spherical obstacles, Robert W. Hart and Elliott W. Montroll—376
Plane waves, Scattering of, by soft obstacles. II. Scattering by cylinders, spheroids, and disks, Elliott W. Montroll and Robert W. Hart—1278
Plastic deformation of pure single crystals of lead and copper, Peter W. Neurath and James S. Koehler—621
Plasticity and conductivity, analogous flow phenomena in copper alloys, Rolland Sydney French—105(L)
Polystyrene capacitors, Electrical charge storage in, L. A. Matheson and V. J. Caldecourt—1176
Polystyrene particles in conjunction with shadow casting to the study of polished metallic surfaces, Applications of, I-Ming Feng—820
Portrait shadow-casting, Delbert E. Philpott—982(L)
Positive and negative coronas with coaxial geometry in pure N, pure O, and various mixtures at pressures from atmospheric to 27 mm, Starting potentials of, Charles G. Miller and Leonard B. Loeb—740
Positive coaxial cylindrical corona discharges in pure N_2, O_2, and mixtures thereof, Charles G. Miller and Leonard B. Loeb—494
Positive ion in cathode-ray tubes, Hollow cathode for studies, C. H. Bachman, Harold Eubank, and George Hall—1208
Positive-replica technique for electron microscopy, Modification of a, A. E. Austin and C. M. Schwartz—847(L)
Power spectrum of a narrow band noise passed through a nonlinear impedance element, John L. McLucas and Richard C. Raymond—1211
Precipitates of C and N in iron with an electron microscope, Study of, John Radavich and Charles Wert—367
Probe technique for the measurement of electron temperature, M. A. Easley—590
Production and stability of converging shock waves, Robert W. Perry and Arthur Kantrowitz—878
Propagation characteristics in a coaxial structure with two dielectrics, Alfredo Banos, Jr., David S. Saxon, and H. Gruen—117

Propagation in a compressible fluid of finite oblique disturbances with energy exchange and change of state, Frederick W. Ross—1414
Propagation of disturbances in one-dimensional accelerated electron streams, L. D. Smullin—1496
Propane-air flames, Comparison of quenching distance and inflammability limit data for, Dorothy Martin Simon—103(L)
Properties of evaporated gold and tungsten oxides, P. G. Wilkinson—226
Publication charge for Letters to the Editor—679
Pulp and paper, Dynamic measurements of physical properties of, by audiofrequency sound, M. Horio and S. Onogi—971
Pulse-annealing for the study of relaxation processes in solids, W. E. Parkins, G. J. Dienes, and F. W. Brown—1012
Pulse method of determining the energy distribution of secondary electrons from insulators, Kenneth G. McKay—89

Radiation from fast electron beams, Application of the, H. Motz—527
—— H. Motz—1217 (errata)
Radiation on materials, Effects of, J. C. Slater—237
Radio signals caused by scattering, Attenuation of, A. H. LaGrone, W. H. Benson, Jr., and A. W. Stratton—672
Radioactive gases in buried pipes, Leak location of, Andrew Gemant, Edward Hines, and E. L. Alexanderson—460
Radioactive tracers for rapid measurement of cutting tool life, M. Eugene Merchant and E. J. Krabacher—1507(L)
Radioactivity, A method of producing an electric current from, P. E. Ohmart—1504(L)
Radiofrequency mass spectrometer, Paul Schissel—680(L)
Radiowave propagation beyond the horizon, Effective earth's radius for, William Miller—55
Random noise in dielectric materials, J. H. Mason—235(L)
Random noise, low frequency, Generation and measurement of, R. R. Bennett and A. S. Fulton—1187
Random noise, Theory of. Phenomenological models. I, David Middleton—1143
—— David Middleton—1326 (errata)
Random noise, Theory of. Phenomenological models. II, David Middleton—1153
Ratio of the critical shear stresses, A. J. Opinsky and R. Smoluchowski—1508(L)
Reflecting surface to simulate an infinite conducting plane, S. J. Raff—610
Reflection and transmission, Note on, Bela A. Lengyel—263
Reflection and transmission at the surface of metal-plate media, Bela A. Lengyel—265
Refractory compounds as thermionic emitters, D. L. Goldwater and R. E. Haddad—70
Relation of tensile strength to brittle temperature in plasticized polymers, R. F. Boyer—723
Relations between initial and final orientations in rolling and annealing of silicon ferrite, B. F. Decker and David Harker—900
Representation of the electric and magnetic fields produced by currents and discontinuities in wave guides. I, N. Marcuvitz and J. Schwinger—806
Residual stress in wires by the layer removal method, Formulas for the determination of, W. T. Read, Jr.—415
Resistance ignitor in mercury, Behavior of the, W. W. Rigrod—787
Ring aerial, directional, Necessary number of elements in, H. Lottrup Knudsen—1299
Rubber and tissue strips, Free longitudinal vibrations of, Richard W. Lawton and Allen L. King—1340
Rubber, Visco-elasticity of, Robert B. Blizard—730
Rubbers, Stress-temperature studies of transitions in, Robert S. Witte and Robert L. Anthony—689
Scabbing of metals under explosive attack, Some quantitative data bearing on the, John S. Rinehart—555
Scaling circuit, Magnetic, Hellmuth Hertz—107(L)
Scattering and absorption of gamma-rays, M. S. Plesset and S. T. Cohen—350
Scattering phenomena in electron microscope image formation, C. E. Hall—655
Schwarz-Christoffel transformations as used in applied physics, Epitomization of the basic theory of the generalized, Thomas James Higgins—365(L)
Secondary emission of nickel-barium mixtures and rhenium when bombarded by electrons with energies from 50 to 8000 electron-volts, H. E. Farnsworth and M. J. Lun—77
Sedimentation equilibrium in concentrated polymer solutions, M. Wales—735
Selenium, Electrical properties of. I. Single crystals, H. W. Henkels—916
Selenium, Electrical properties of. II. Microcrystalline selenium, H. W. Henkels—1265
Selenium rectifiers after a voltage pulse in the blocking direction, Recovery of, K. Lehovec—934
Semiconductor bornite, C. W. Horton—364(L)
Semiconductor, zinc oxide, Some electrical properties of, E. E. Hahn—855
Semiconductors, intrinsic, Partial differential equations describing steady current flow in, R. C. Prim—1388(L)
Separation of variables in electromagnetic theory, Domina Eberle Spencer—386
Shaped-beam antennas, General formulation for calculation of, A. S. Dunbar—1217(L)
Shock-wave phenomena: Waterlike substances, R. J. Seeger and H. Polachek—640
Silicon ferrite, Relations between initial and final orientations in rolling and annealing of, B. F. Decker and David Harker—900
Spectral emissivity of coatings of thoria and other refractories as a function of temperature, F. H. Morgan—108(L)
Spectrum of isotropic temperature fluctuations in an isotropic turbulence, Stanley Corrsin—469
—— Stanley Corrsin—1292 (erratum)
Spheres, concentric, two, Scattering of electromagnetic waves from, Arthur L. Aden and Milton Kerker—1242
Stability of linear varying-parameter systems, Lotfi A. Zadeh—402
Static electrification of dust particles on dispersion into a cloud, John E. Coolidge and George Schulz—103(L)
Static electrification of dust particles on dispersion into a cloud, Wulf B. Kunkel—103(L)
Steel, 1020, at low temperature, Fracture and yield stress of, A. S. Eldin and S. C. Collins—1296(L)
Storage in three dimensions using magnetic cores, Digital information, Jay W. Forrester—44
Stress-function approaches of Boussinesq and Timpe to the axisymmetric problem of elasticity theory, E. Sternberg, R. A. Eubanks, and M. A. Sadowsky—1121
Stress-temperature studies of transitions in rubbers, Robert S. Witte and Robert L. Anthony—689
Stresses produced in a body by an exploding charge, Some experimental indications of, John S. Rinehart—1178
Surface condition of a sphere on its water-entry cavity, Effect of, Albert May—1219
Surface and grain boundary diffusion, Calculation of diffusion penetration curves for, J. C. Fisher—74
Surface-wave propagation over a coated plane conductor, Stephen S. Attwood—504
Susceptance of a thin iris in circular wave guide with the TM_{01} mode incident, Kenneth L. Dunning and Rufus G. Fellers—1316
Suspenoids in divergent electric fields, Motion and precipitation of, Herbert A. Pohl—869

Symmetric biconical antennas, General theory of, S. A. Schelkunoff—1330
Symmetrical electron lens, Investigation of field distribution, J. R. Shah and L. Jacob—1236
Synchronous conditions in the cylindrical magnetron space charge, Analysis of, H. W. Welch, Jr., and W. G. Dow—433

Teflon, Volume-temperature relationships for the room temperature transition in, Fred A. Quinn, Jr., Donald E. Roberts, and R. N. Work—1085(L)
Temperature function in a moving medium, R. H. Ritchie—1389(L)
Temperature measuring device, Noncontact, J. E. Field and S. D. Gehman—106(L)
Temporary enhancement of hysteresis in barium titanate samples, D. R. Young—523(L)
Theorem of Brouwer, H. F. Mathis—1084(L)
Theory of the circular diffraction antenna, Harold Levine and Charles H. Papas—29
Theory of the dynamic plastic deformation of a thin diaphragm, G. E. Hudson—1
Theory of the parallel plane diode, A. H. Taub and Nelson Wax—108 (erratum)
Thermal expansion coefficients and the melting point of cubic elements, D. van der Reyden—363(L)
Thermal expansion of Au-Cd alloys containing 47.5 atomic percent Cd, Coefficients of, Lo-ching Chang—525(L)
Thermal transpiration, Some measurements of, S. Chu Liang—148
Thermionic emitters, Certain refractory compounds as, D. L. Goldwater and R. E. Haddad—70
Thickness-shear and flexural vibrations of crystal plates, Raymond D. Mindlin—316
Thin films by electron diffraction, Studies of, N. R. Mukherjee and Oliver Row—681(L)
Thoria and other refractories as a function of temperature, Spectral emissivity of coatings of, F. H. Morgan—108(L)
Tracer experiments in closed steady-state systems, Mathematical basis of the interpretation of, C. W. Sheppard and A. S. Householder—510
Transit time effect in a cylindrical diode, Way Dong Woo—1333
Transitions in polymers, Nuclear magnetic resonance study of, L. V. Holroyd, R. S. Codrington, B. A. Mrowca, and E. Guth—696
Transitions in rubbers, Stress-temperature studies of, Robert S. Witte and Robert L. Anthony—689
Transmission-line equivalent of electronic traveling-wave systems, W. E. Mathews—310
Transmission line Kerr cell, J. W. Beams and H. S. Morton, Jr.—523(L)
Transmission of hydrogen through metals, H. B. Wahlin—1503(L)
Traveling wave tube, Amplification of the, Bernard Friedman—443
Tropospheric propagation beyond the horizon, J. Feinstein—1292(L)
Turbulence in a two-dimensional fluid and in a three-dimensional fluid, Difference between, T. D. Lee—524(L)

Ultrasonic propagation in liquids under high pressures: Velocity measurements on water, Gerald Holton—1407

V-Antennas, Theory of, Ronold King—1111
Vibrations, elastic, of almost cubic parallelepipeds, H. Ekstein and T. Schiffman—1215(L)
Variables in electromagnetic theory, Separation of, Domina Eberle Spencer—386
Viscoelastic behavior of certain polymeric systems, Application of Nutting's equation to, Rolf Buchdahl and Lawrence E. Nielsen—1344
Viscoelastic properties of several high polymers, M. Horio, S. Onogi, C. Nakayama, and K. Yamamoto—966
Viscoelasticity, Forced vibration of reed as a method of determining, M. Horio and S. Onogi—977
Visco-elasticity of rubber, Robert F. Blizard—730
Visual depiction of magnetic lines of force by means of a gas discharge, Improvements in, F. Blaha and J. A. Schedling—11
Volta potentials of the copper-nickel alloys and several metals in air, Herbert H. Uhlig—1399
Volume diffusion of metals, G. J. Dienes—848(L)
Volume-temperature relationships for the room temperature transition in Teflon, Fred A. Quinn, Jr., Donald E. Roberts, and R. N. Work—1085(L)

Water-entry cavity of a sphere, Effect of surface condition, Albert May—1219
Water movement induced by compaction of clastic sediments, Robert A. Howard and Carl E. Bleil—360(L)
Wave-guide field in terms of normal modes, Expandability of a, J. Van Bladel—68
Wave propagation on helical wires, William Sollfrey—905
Work-hardening of mild steel by explosive attack, John S. Rinehart—1086(L)

X-ray absorption correction for encased diffractors in the Debye-Scherrer technique, H. L. Ritter, R. L. Harris, and R. E. Wood—169
X-ray absorption in a crystal set at the Bragg angle, H. N. Campbell—1139
X-ray detection of long-range order in Ni_3Mn, B. L. Averbach—1088(L)
X-ray diffraction method for studying imperfections of crystal structure in polycrystalline specimens, Alfred J. Reis, Jerome J. Slade, Jr., and Sigmund Weissmann—665
X-ray measurement of long-range order in β AgZn, L. Muldawer—663
X-ray measurement of short-range order in Ag-Au, N. Norman and B. E. Warren—483

Zinc crystals produced by the Bridgman method, Orientations of, L. M. Slifkin—1216(L)
Zinc oxide semiconductor, Some electrical properties of, E. E. Hahn—855

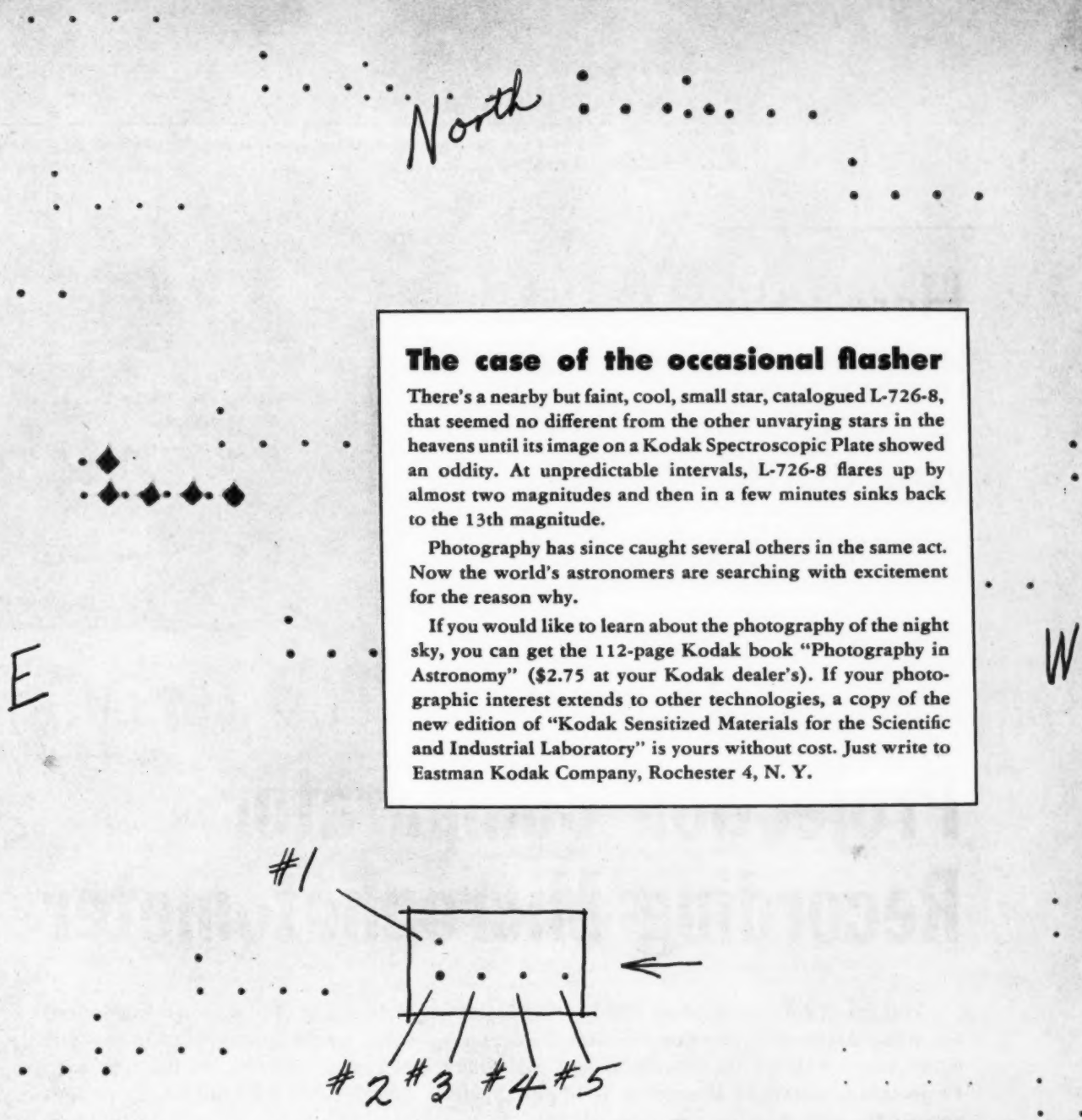

The case of the occasional flasher

There's a nearby but faint, cool, small star, catalogued L-726-8, that seemed no different from the other unvarying stars in the heavens until its image on a Kodak Spectroscopic Plate showed an oddity. At unpredictable intervals, L-726-8 flares up by almost two magnitudes and then in a few minutes sinks back to the 13th magnitude.

Photography has since caught several others in the same act. Now the world's astronomers are searching with excitement for the reason why.

If you would like to learn about the photography of the night sky, you can get the 112-page Kodak book "Photography in Astronomy" ($2.75 at your Kodak dealer's). If your photographic interest extends to other technologies, a copy of the new edition of "Kodak Sensitized Materials for the Scientific and Industrial Laboratory" is yours without cost. Just write to Eastman Kodak Company, Rochester 4, N. Y.

Multiple exposure by E. F. Carpenter with the 36-inch telescope of the University of Arizona on a Kodak Spectroscopic Plate, Type 103a-0. Five images of L-726-8 are marked. The very bright one is No. 2. Twenty minutes elapsed between the first and last; each exposure was two minutes.

Kodak

Here's the instrument you built!

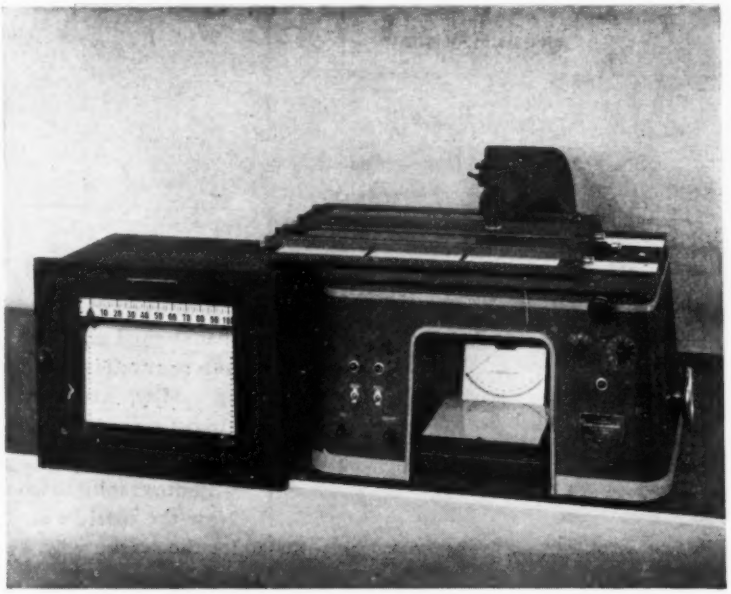

JACO BALANCED BEAM

Projection Comparator Recording Microphotometer

You asked for increased sensitivity and higher resolution . . . for a *proven* high speed recording device . . . for construction features that would speed your work and make it easier too. Now *all* these advantages—and many more—are here . . . in the new Jaco Projection Comparator Recording Microphotometer. Check these outstanding advantages against the work you are now doing:

★**Monitoring light beam eliminates effect of voltage fluctuations ● Adjustable entrance slits (as small as the equivalent of 1μ x 100μ at the plate) guarantee exceptional flexibility and resolution ● High speed (0.7 sec.) Brown Electronik chart recorder ● Stability achieved by use of double beam technique with single detector ● Reproducibility of ±1% ● Choice of 12 scanning speeds, either forward or reverse ● Linear measurement on plate or film to 0.01 mm.**

Other important features which space limits listing. For *all* the facts write for Catalogue M10-51R today.

JARRELL-ASH COMPANY
165 NEWBURY STREET, BOSTON 16, MASS.

BOSTON DETROIT CHATTANOOGA SAN FRANCISCO TORONTO

IF IT'S AN OPTICAL INSTRUMENT, THINK OF JARRELL-ASH

MAXIMUM PERFORMANCE at MINIMUM COST with the *Browning* OSCILLOSYNCHROSCOPES ON-5A ON-5X SYNCHROSCOPE P4-EX

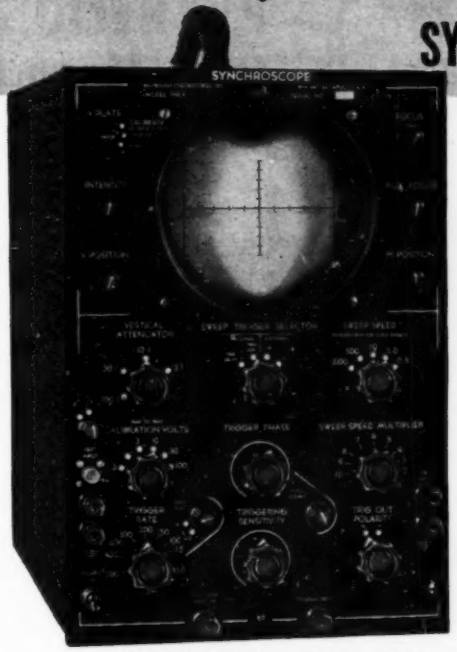

Models ON-5A and ON-5X are designed as basic, highly flexible laboratory instruments for general pulse work. Their specifications include:

- **High-gain vertical amplifiers.**
- **Triggered sweeps, if an external trigger is available.**
- **Recurrent sweeps, at a repetition rate of 10 to 100,000 per second.**
- **Vertical input delay of 0.45 microsecond (ON-5X).**

Model P4-EX is designed for applications requiring a triggered sweep, and where the signal levels met do not demand extremely high-gain amplification. Its many outstanding features include:

- **Internal trigger, at a repetition rate of 50 to 5000 per second, easily synchronized with an external trigger if desired.**
- **Output trigger, with the same range of repetition rates, which can be continuously phased to lead or lag the sweep start by a maximum of 500 microseconds**

Detailed specifications and performance data available promptly on your request.

These new instruments represent a high level of precision design and versatility of application at remarkably low cost. Major features that are common to all three instruments include:

- Type 5UP cathode-ray tube, operating at an accelerating potential of 2600 volts. P1, P7 and P11 screens are available.
- Sweep writing rate continuously variable from 1.0 to 25,000 microseconds per inch.
- Sweep calibration in microseconds per horizontal scale division, accurate to plus or minus 10%.
- Vertical amplifier flat within 3 db from 5 cycles to 5 megacycles.
- Vertical calibration voltages, at accuracy of plus or minus 5% for Model P4-EX, and plus or minus 10% for Models ON-5A and ON-5X.
- Vertical amplifier input step attenuator.
- CRT cathode connection externally available, for application of blanking or marker pulses.

NET PRICES, F.O.B. Winchester, Massachusetts:
P4-EX . . . $465.00 ON-5A . . . $485.00 ON-5X . . . $535.00

Write today for **FREE BULLETINS** giving detailed specifications and performance data.

BROWNING
Laboratories, Inc.
Winchester, Mass.
ENGINEERED FOR ENGINEERS

R C INTERVALOMETER

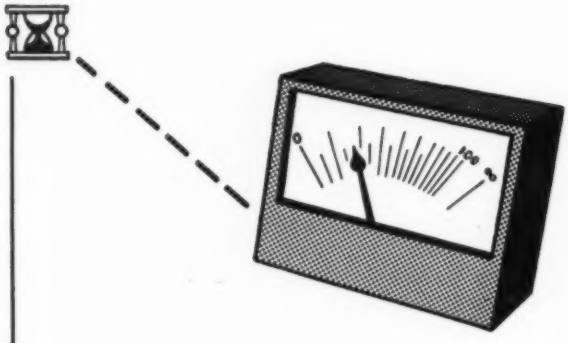

intervals

MEASURED PRECISELY!!

0.5μ SEC.

TO

0.1 SEC.

NELSON & STREET

P.O. BOX 4342 TAKOMA PARK

WASHINGTON 12, D.C.

EPLAB

PYRHELIOMETER

For the Measurement of SOLAR RADIATION

Eppley Pyrheliometers are used for solar radiation measurements at ninety-eight weather stations in the continental United States, Canada, Alaska, Greenland, Iceland, Caribbean Sea, and the Pacific Ocean. Sixty-two of these stations are under the direction of the United States Weather Bureau.

The Eppley Pyrheliometer was adopted as standard equipment by the Weather Bureau after considerable experimentation. It was found to be the best instrument so far tested by the Bureau.

Used in conjunction with a suitable recorder, the Eppley Pyrheliometer will provide an accurate and reliable record of total solar and sky radiation on a horizontal surface.

Bulletin No. 2 On Request

THE EPPLEY LABORATORY, INC.

Scientific Instruments

Newport, Rhode Island, U.S.A.

S. S. White MOLDED RESISTORS

The "All-Weather" Resistors

The resistors that give you

- *Inherent low noise level*
- *Good stability in all climates*

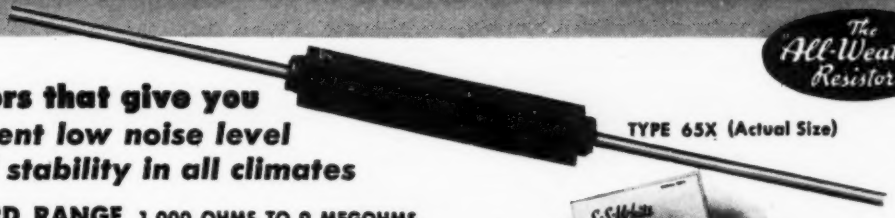

TYPE 65X (Actual Size)

STANDARD RANGE 1,000 OHMS TO 9 MEGOHMS

These resistors are used extensively in commercial equipment, including radio, telephone, telegraph, sound pictures, television, etc. They are also used in a variety of U.S. Navy equipment.

HIGH VALUE RANGE 10 TO 10,000,000 MEGOHMS

This unusual range of high value resistors has been developed to meet the needs of scientific and industrial control, measuring and laboratory devices — and of high voltage applications.

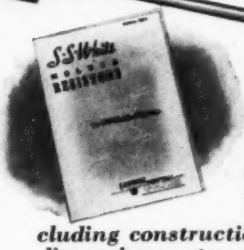

SEND FOR BULLETIN 4906

It gives details of Standard and High Value Resistors, including construction, characteristics, dimensions, etc. Also described are S. S. White 80X Resistors, designed for extremely high voltage equipment. Copy with Price List sent on request.

THE S. S. White INDUSTRIAL DIVISION

DENTAL MFG. CO. — Dept. F, 10 East 40th St. — NEW YORK 16, N. Y.

WESTERN DISTRICT OFFICE: TIMES BUILDING, LONG BEACH, CALIF.

NOW! **A HIGH-SENSITIVITY, HIGH-SPEED MICROOSCILLOGRAPH**

CENTRAL RESEARCH LABORATORIES MODEL 2

Signal-axis deflection factor only 0.2 volt per trace width!

Variation in signal-axis sensitivity less than 5 per cent from 0 to 10,000 megacycles!

Three beams, three independent deflecting systems, and direct photographic recording as in Model 1.

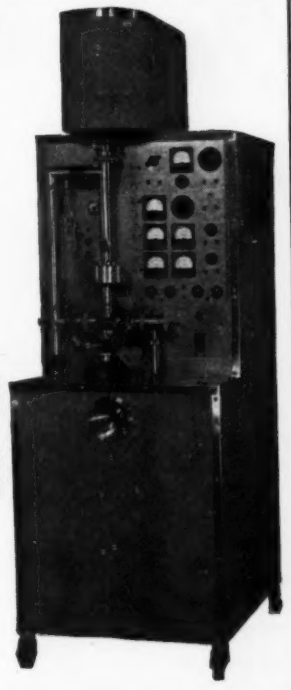

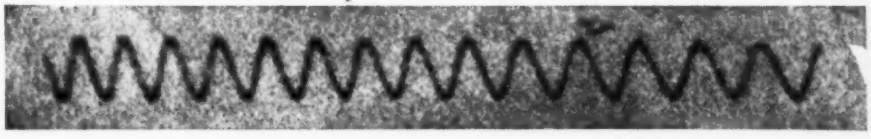

Unretouched single-sweep oscillogram, 3000-megacycle output of 2K41 Klystron into 50-ohm load (1.2 volts rms). Enlargement, 50 diameters.

Write us for prompt, complete information

CENTRAL RESEARCH LABORATORIES, INC., RED WING, MINN.

CREEP TEST INSTRUMENTS • TELESCOPES • TOOLMAKER MICROSCOPES • COMPARATORS • OPTICAL INSTRUMENTS • SPECTROMETERS **Gaertner** REFRACTOMETERS • MICROMETER SLIDES • INTERFEROMETERS • SPECTROPHOTOMETERS • LABORATORY SUPPORTS CATHETOMETERS • CHRONOGRAPHS • OPTICAL BENCHES • SPHEROMETERS • SPECTROSCOPES • DIVIDING MACHINES PHOTOELASTICITY POLARISCOPES • MICROSCOPES • SPECTROGRAPHS • POLARIMETERS • MONOCHROMATORS

PRECISION SPECTROMETER

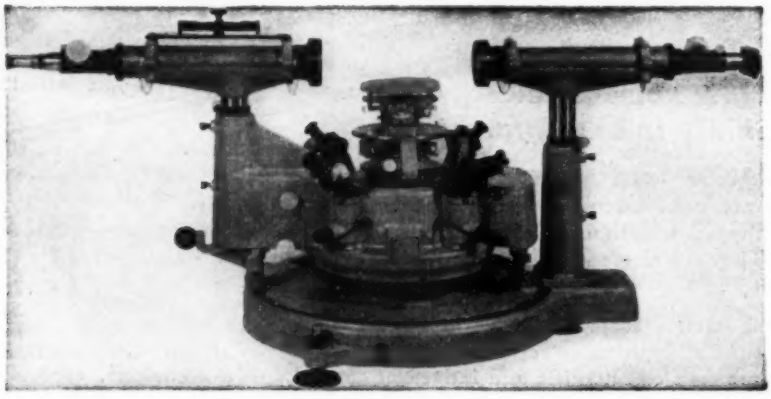

For highly accurate determinations of refactive indices and dispersion, measurement of prisms and wedge angles, and similar applications. Direct reading to 1 second. Polarizing and other attachments are available.

A completely new instrument incorporating many adjustments contributing to the attainment of high precision and operating convenience. Cat. No. L124.

Request Bulletin 165-50

THE GAERTNER SCIENTIFIC CORPORATION
1212 WRIGHTWOOD AVE. • CHICAGO 14 • U.S.A.

Only with CO-AX R.F. CABLES

AIR-SPACED ARTICULATED

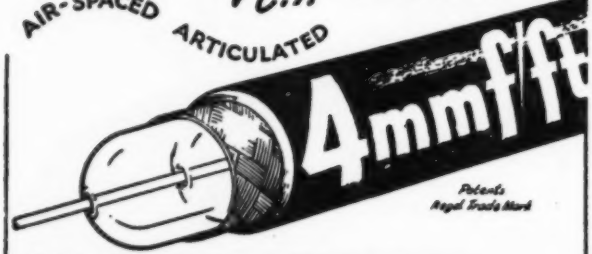

THE LOWEST EVER CAPACITANCE OR ATTENUATION

We are specially organised to give **SPOT DELIVERIES TO U.S.A**
Cable your rush order for shipment by air freight. Settlement by your own $ cheque

LOW ATTEN. TYPES.	IMPED OHMS	ATTEN. db/100ft at 1mg Mc/s.	LOADING Min. at 1mg Mc/s.	O.D."	
A1	74	1.7	0.11	0.36	
A2	74	1.3	0.24	0.44	
A34	73	0.6	1.5	0.88	HIGH POWER FLEXIBLE
LOW CAPAC TYPES.	**CAPAC. mmf/ft**	**IMPED. OHMS.**	**ATTEN. db/100ft 100Mc/s**	**O.D."**	
C1	7.3	150	2.5	0.36	
P.C.1	10.2	132	3.1	0.36	PHOTOCELL CABLE
C11	6.3	173	3.2	0.36	
C2	6.3	171	2.15	0.44	
C22	5.5	184	2.8	0.44	
C3	5.4	197	1.9	0.64	
C33	4.8	220	2.4	0.64	
C44	4.1	252	2.1	1.03	VERY LOW CAPACITANCE

TRANSRADIO LTD.
138A CROMWELL RD.
LONDON S.W.7. ENGLAND.
CABLEGRAMS TRANSRAD. LONDON

The 2550 Series

ELECTRONICALLY REGULATED POWER SUPPLIES

A high quality, heavy duty line of electronically regulated power supplies, specifically designed for broadcast, laboratory and production applications.

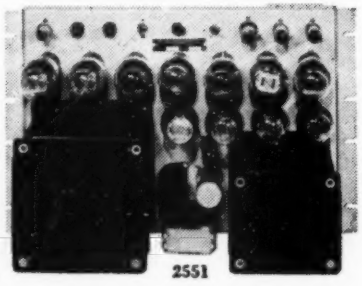

GENERAL SPECIFICATIONS

Output Voltage: 250 Volts DC, regulated • Regulation: 0.1% no load to full load • Ripple: Less than 2 mv peak • Stability: Approximately 0.1% volt change in output for line voltage variation from 105-125 V • Mounting: Standard 19" relay rack panel.

Type 2550: 0-250 mils at 250 volts DC. Panel Height 7" . . Price $225.00
Type 2551: 0-550 mils at 250 volts DC. Panel Height 12¼" Price $300.00
Type 2552: 0-650 mils at 250 volts DC. Panel Height 12¼" Price $350.00

• *Complete specifications available on request*

Manufacturers of a complete line of TV and Radar Test Equipment
Tel-Instrument Co. Inc.
50 PATERSON AVENUE • EAST RUTHERFORD, N. J.

2 New Instruments FOR THE INVESTIGATION OF Molecular Phenomena

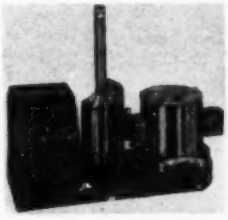

LIGHT-SCATTERING *Indicating & Recording* MICROPHOTOMETER

For the Measurement of:

Droplet size of aerosols . . . Purity of colloids . . . Particle size & concentration . . . Molecular aggregation in antigen-antibody reactions . . . Microfluorescence . . . Depolarization, turbidity and dissymmetry . . . Rate of minute precipitation, flocculation, and crystallization . . . Molecular weight of polymers.

Features

Excellent sensitivity . . . Completely a-c. operated . . . Outlet for recorder operation . . . Compact and accessible . . . Full-scale indication; 0.001 microamps . . . Meter indicates relative intensity, per cent transmission, density and photocurrent microamperes on five decade ranges without correction factors . . . Stable d-c, amplifier . . . Maladjustment of controls cannot damage unit . . . Removable slit and optical systems.

WRITE FOR BULLETIN 2182-W

PHOTOMULTIPLIER MICROPHOTOMETER

For the Precise Measurement and Comparison of Light Intensities at Selected Wavelengths

RANGE: Intensities from 20 micro-microlumens to 20 lumens; densities from 0 to 9.

SENSITIVITY: Full-scale meter readings are given with photomultiplier or phototube currents from 5 to 0.001 microamperes in five ranges.

DIRECT READING: Meter indicates relative intensity, per cent transmission, density and photocurrent microamperes covering five decades without correction factors.

WAVELENGTH SELECTION: Any filter two inches square may be positioned readily in the filter holder, either singly or in combinations up to 5/8 inch thick, also many other optical accessories for measurement at selected wavelengths.

Features

Outlet for recorder operation . . . A.C. operated and stabilized . . . Weight, only 11 lbs.

WRITE FOR BULLETIN 2190-W

AMERICAN INSTRUMENT CO., INC. AMINCO **Silver Spring, Maryland**

HIGH or LOW PRESSURE

High pressure or low, there is a Giannini precision pressure transmitter that meets your requirements for remote indication, recording or control.

From less than 1 up to 10,000 psi, with various types of resistance and inductive output values, Giannini precision pressure transmitters are designed to withstand extremes of acceleration, temperature, vibration, while at the same time retaining their accuracy and their fast response characteristics. "They are standard with the Leaders." Write for booklet.

G. M. Giannini & Co., Inc., Pasadena 1, California

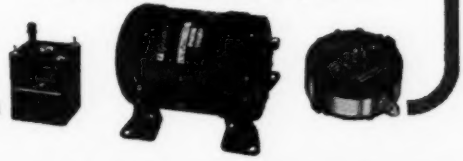

giannini

IMPORTANT IN

HIGH VACUUM WORK

APIEZON®

OILS, GREASES, WAXES

Apiezon products have the recognition of leading scientists who accord them top preference for high vacuum work. A bulletin just off the press describes the physical characteristics of a variety of special oils, greases and waxes for oil-diffusion pumps, sealing joints, stop cocks, etc. You should have a copy to augment your store of knowledge on the subject. Mailed free; simply ask for Bulletin 43-JP.

JAMES G. BIDDLE CO.

Electrical & Scientific Instruments

1316 ARCH STREET, PHILADELPHIA 7, PA.

WITHIN 2 DEGREES OF ABSOLUTE ZERO

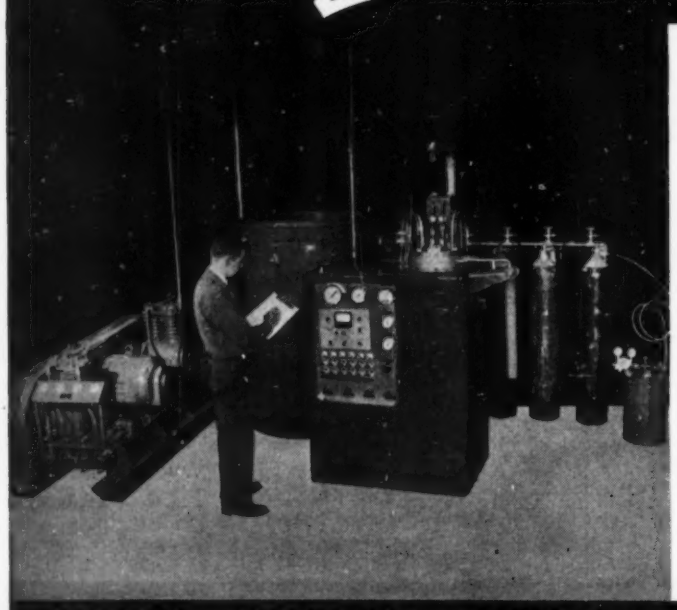

At −271°C. — where certain metals lose nearly all electrical resistance — where helium becomes a "fourth state of matter" — where near-perfect vacuum exists — research has been extremely difficult.

Now, with the ADL COLLINS HELIUM CRYOSTAT (a low-pressure helium liquefier), producing and maintaining temperatures down to −271°C. is no longer a problem. The Cryostat will produce 4 liters of liquid helium per hour and maintain temperatures from −100°C. to −271°C. It can be installed and in operation in three days' time. No special mounts or foundations are required.

Write for Illustrated Bulletin JAC-2

ARTHUR D. LITTLE, INC.
MECHANICAL DIVISION

30 MEMORIAL DRIVE, CAMBRIDGE 42, MASS.

RESEARCH · ENGINEERING · TECHNICAL ECONOMICS · ADVANCED EQUIPMENT

GEOPHYSICS

A Journal of General and Applied Geophysics

Published Quarterly by

SOCIETY OF EXPLORATION GEOPHYSICISTS

Box 7248 Tulsa 18, Oklahoma

- The official journal of the only international group of prospecting geophysicists
- Devoted to current problems in seismograph, gravity, magnetic and other methods of geophysical prospecting for oil and other minerals
- Covers geophysical instrumentation

SUBSCRIPTION RATES

ONE YEAR (4 issues) $9.00, foreign $9.50

Price list of back issues supplied on request

RESEARCH OPPORTUNITIES

Openings in the field of design of electronic equipment are available to MATHEMATICIANS, PHYSICISTS, and ENGINEERS at the University of Michigan's Willow Run Research Center.

PHYSICISTS and MATHEMATICIANS—with Bachelor's or Master's degrees, should also have a working knowledge of, and some experience in, electronics. Ph.D's with electronics experience are especially desired.

ENGINEERS—with experience in circuit development and design on analog or digital computers, telephone switching equipment or cathode ray displays are especially desired.

Researchers are offered the opportunity to complete the requirements for graduate degrees while employed at the Research Center.

Salaries are commensurate with training and experience. Applicants are invited to send a resume of education and experience to:

Personnel Office
UNIVERSITY OF MICHIGAN
Ann Arbor, Michigan

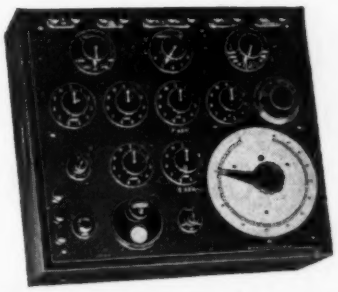

CAMBRIDGE UNIVERSAL BRIDGE

FOR THE MEASUREMENT OF D.C. RESISTANCE SELF AND MUTUAL INDUCTANCE, CAPACITANCE AND FREQUENCY

The Bridge is self-contained with battery and galvanometer detector for D.C. measurements, and with a reed vibrator and single telephone detector for A.C. measurements. Selector and range switches are fitted and the Bridge is direct reading for all quantities except frequency where a curve is provided.

For measurements at frequencies between 50 and 1500 cps. an external oscillator may be connected. With simple accessories tests can be made on iron-cored inductors carrying D.C.

Send for complete information

CAMBRIDGE INSTRUMENT COMPANY

3773 Grand Central Terminal, New York 17, N.Y.

PIONEER MANUFACTURERS OF PRECISION INSTRUMENTS

ENGINEERS PHYSICISTS

A major expansion of THE JACOBS INSTRUMENT COMPANY has made available a number of positions for men qualified to take responsibility as Section Heads. A minimum of five years of experience, plus an outstanding record of achievement, is required. Experience should be in high frequency circuit design, system studies, aircraft instruments, aerodynamics, servomechanisms, gyroscopes, optical instruments, missile guidance, fire control, digital or analog computers, or related fields.

These positions offer many unusual attractions including high salary, unusual opportunity in military and peacetime fields, security, employee benefits, and pleasant working conditions.

Qualified individuals interested in advancing themselves now should not overlook these opportunities.

JACOBS INSTRUMENT CO.

Bethesda 14, Maryland

150 KV—2 MA
150 P.S.I. GAS INSULATION!

A major atomic research center required a power supply of these specifications for use inside a Van de Graaff generator. All components had to withstand operation in a gas pressure of 150 pounds per square inch, and be contained in a confined volume less than 2 feet cubed.

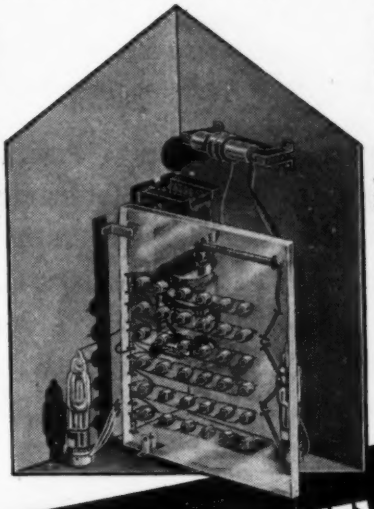

Model 2021

DESIGNED & BUILT BY BETA

High Voltage Power Supplies Built to Specifications

The Beta Electric Corp. is experienced in the design and construction of all types of power supplies for use inside the domes of Van de Graaff generators. Operation up to 400 P.S.I. pressure has been achieved successfully.

Major Specifications:

Input: 117 Volts, 400 Cycles
Output Voltage: 0-150,000 Volts DC, Positive grounded (H.V. Negative)
Output Current: 2ma
Ripple: Less than 0.5%
Regulation: Better than 5%
Size: 22" wide x 19" deep x 24" high

Our field engineers coast-to-coast are ready to discuss your problems. Write, wire or phone Today

BETA Electric Corporation
333 East 103rd St. • New York, 29
ENright 9-8520

ENGINEERS
DESIGNERS
PHYSICISTS

THE Aerophysics & Atomic Energy Research Division of North American Aviation, Inc. offers unparalleled opportunities in Research, Development, Design and Test work in the fields of Long Range Guided Missiles, Automatic Flight and Fire Control Equipment and Atomic Energy. Well-qualified engineers, designers and physicists urgently needed for all phases of work in

Supersonic Aerodynamics • Preliminary Design & Analysis • Electronics • Electro-Mechanical Devises • Instrumentation • Flight Test • Navigation Equipment • Controls • Servos • Rocket Motors • Propulsion Systems • Thermodynamics • Airframe Design • Stress & Structures

●

Salaries commensurate with training and experience.

Excellent working conditions.

Finest facilities and equipment.

Outstanding opportunities for advancement.

Write now — Give complete resume of education, background and experience

PERSONNEL DEPT

Aerophysics & Atomic Energy Research Division

North American Aviation, Inc.

12214 LAKEWOOD BLVD.
DOWNEY, CALIFORNIA

PROFESSIONALLY CHALLENGING RESEARCH POSITIONS for PHYSICISTS AND ENGINEERS

The Cornell Aeronautical Laboratory, Inc., an affiliate of Cornell University, has permanent positions open in the fields of pure and applied physics, electronics, instrument design, applied mathematics, and aeronautical sciences. Current and future work includes research and development on electronic computers, radar systems, atmospheric physics, physics of air flow (subsonic and supersonic), electro-mechanical and mechanical linkage analog computers, aircraft precision instrumentation, guidance systems for airplanes and missiles, and automatic landing systems.

The Laboratory occupies a position between those of universities and commercial research institutes and, we feel, combines many of the traditional advantages of both. Varied and stimulating programs include vital defense work and self-sponsored basic and applied research. In addition to maintaining industrial employee benefits and salary scales, professional development is encouraged through regular seminars, attendance at meetings of scientific societies, and frequent interchange of ideas and discussions with senior level scientists.

Confidential inquiries may be made by writing to the

Employment Manager

CORNELL AERONAUTICAL LABORATORY, INC.

P. O. Box 235, Buffalo 21, New York

Capehart

needs outstanding

RESEARCH PHYSICISTS
SR. ELECTRONIC ENGINEERS
SR. MECHANICAL ENGINEERS
ENGINEERING PHYSICISTS
CIRCUIT ENGINEERS
MICROWAVE ENGINEERS
TELEVISION ENGINEERS
VACUUM TUBE ENGINEERS
TEST EQUIPMENT ENGINEERS
FIELD ENGINEERS
ELECTRONIC TECHNICIANS

with Advanced Academic Training and Several Years' Experience for

RESEARCH AND DEVELOPMENT

in Radar, Servos, Computers, Receivers, Solid State Physics, Image Converters, Pulse and Timing Techniques, Special Purpose Tubes, Networks and Systems Design, Light and Electron Optics, Storage-Type Tubes, Photo-Electric Pickup Tubes and Related Test Equipment.

Our Long Range Programs and Steady Growth Assure Permanent Employment at Excellent Salaries for Competent and Qualified Personnel.

Interested Persons Are Invited to Submit Detailed Resumes of Experience and Education with Salary Requirements and Availability Date to:

The Employment Department
Capehart-Farnsworth Corporation
Fort Wayne 1, Indiana

PHYSICISTS AND SENIOR RESEARCH ENGINEERS

• • •

POSITIONS NOW OPEN

• • •

Senior Engineers and Physicists having outstanding academic background and experience in the fields of:

- Microwave Techniques
- Moving Target Indication
- Servomechanisms
- Applied Physics
- Gyroscopic Equipment
- Optical Equipment
- Computers
- Pulse Techniques
- Radar
- Fire Control
- Circuit Analysis
- Autopilot Design
- Applied Mathematics
- Electronic Subminiaturization
- Instrument Design
- Automatic Production Equipment
- Test Equipment
- Electronic Design
- Flight Test Instrumentation

are offered excellent working conditions and opportunities for advancement in our Aerophysics Laboratory. Salaries are commensurate with ability, experience and background. Send information as to age, education, experience and work preference to:

NORTH AMERICAN AVIATION, INC.
AEROPHYSICS LABORATORY
BOX NO. J4
12214 South Lakewood Blvd. Downey, California

PHYSICISTS

Mathematicians *Engineers*

with outstanding scholastic and experience records

SYLVANIA

OFFERS OPPORTUNITY

- **for rewarding work in fields where a fundamental approach is appreciated.**
- **for professional growth in fields which have a future.**
- **for evening graduate study at nearby universities.**
- **for work in modern Laboratories in pleasant surroundings overlooking Long Island Sound.**

Our Central Research Laboratories in Bayside, Long Island have underway, an expanding program in the research and development phases of new fields which include:

Solid State Physics
Applied Mathematics
Television
Navigation System Study and Development
Tube Development and Application
Radar Design and Development

Please Address Replies to
Manager of Personnel, Sylvania Electric Products, Inc., Bayside, N.Y.

RESEARCH OPPORTUNITIES

Theoretical and experimental research physicists interested in unusual opportunities for professional accomplishment and promotion are urged to investigate the variety of attractive openings in Battelle's expanding research organization. Engineering physics, solid state physics, mathematical physics, radiation physics, electronics, and many related fields offer attractive openings for present and future employment. Prompt and confidential handling of applications. Please address replies directly to

BATTELLE MEMORIAL INSTITUTE
505 King Avenue, Columbus 1, Ohio

ENGINEER—PHYSICIST

Graduate engineer with experience in High Vacuum technology; with knowledge of electrical, metallurgical, and chemical engineering wanted.

Responsible for development of industrial high vacuum equipment and application engineering.

Salary open. Company is of medium size, excellent reputation, and growing rapidly. Give full particulars in your first letter.

Address Box No. 1251A,
57 East 55 Street,
New York 22, New York

NEW SOUND LEVEL METER

Improved Design

Accurate · Simple to Use

The new Type 1551-A Sound-Level Meter is very easy to handle. It weighs only 11 pounds, including its battery power supply. It is simple to operate requiring only the switch selection of the appropriate response characteristic, and then the adjustment of a single attenuator switch until the indicating meter stays on scale. The sound level is the sum of the attenuator and meter readings.

When not in use, the microphone folds back into the instrument panel, automatically turning off filament and plate voltages.

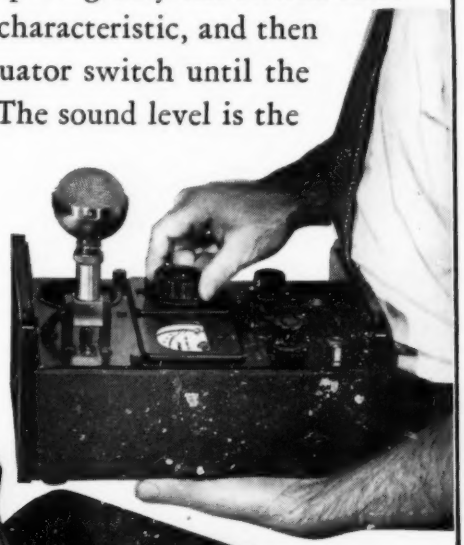

Type 1551-A
Sound-Level Meter . . $360.00

- **MEETS ALL STANDARDS** *of the American Standards Association, the A. I. E. E. and the Acoustical Society of America*
- **PORTABLE** — *weighs only 11 pounds, with batteries*
- **SIMPLE TO OPERATE** — *non-technical personnel can make just as accurate measurements as can anyone*
- **COMPLETE BATTERY OPERATION** *from standard batteries, readily available*
- **VERY WIDE RANGE** *of 24 to 140 db; will measure practically any noise level found in industry*
- **EXCELLENT STABILITY** — *improved negative feedback amplifier circuits*
- **NON-DIRECTIONAL CRYSTAL-DIAPHRAGM MICROPHONE**
- **TWO-SPEED INDICATING METER** *for steady or rapidly fluctuating sounds*
- **EXCELLENT ACCURACY** — *frequency response curves within current A.S.A.-specified tolerances; when amplifier sensitivity is standardized absolute accuracy of measurement is within ±1 db for average machinery noises*
- **INTERNAL CALIBRATING CIRCUIT** — *sensitivity can be standardized at any time from any 115-volt a-c line*
- **WIDE FREQUENCY RESPONSE** *of amplifier and panel meter — 20 cycles to 20 kilocycles*
- **LOW TEMPERATURE & HUMIDITY EFFECTS** — readings independent of both over normal room conditions (within 1 db)
- **READILY USED WITH ACCESSORY INSTRUMENTS** *such as graphic-level recorders, frequency and wave analyzers, magnetic-tape recorders*
- **MANY ACCESSORIES AVAILABLE** *for special applications; included are special microphones for high fidelity measurements, for reproducible standards and for use at end of long cable.*

STROBOSCOPES • VARIACS • SOUND-LEVEL METERS
VIBRATION METERS • IMPEDANCE BRIDGES
SIGNAL GENERATORS • OSCILLATORS
WAVE ANALYZERS • DISTORTION METERS
IMPEDANCE STANDARDS • VACUUM-TUBE
VOLTMETERS • FREQUENCY STANDARDS
BROADCAST MONITORS • PARTS AND ACCESSORIES

GENERAL RADIO Company

275 Massachusetts Avenue, Cambridge 39, Massachusetts, U. S. A.
90 West Street NEW YORK 6 · 920 S. Michigan Ave. CHICAGO 5 · 1000 N. Seward St. LOS ANGELES 38

Since 1915—Designers and Manufacturers of Electronic Test Equipment

DEMONSTRATION PROJECTION METER

Lecture demonstration of AC and DC measurements becomes a pleasure for both lecturer and audience with No. 72550 Projection Meter. Projected readings can be clearly seen by a large class. This meter is usable with projection lanterns of the horizontal slide or bellows type, and optical benches. The meter scale reads from 0 to 100 in 2 unit divisions with figures at every tenth division. DC movement has 100 ohms resistance; full-scale deflection is 1 milliampere or 100 millivolts. The AC full-scale deflection is 1 milliampere or 5 volts. External shunts, voltage multipliers and current transformers are available for wide ranges of AC and DC current and voltage readings.

Dimensions, 4⅛ x 4½ x 1½ inches.

Write for descriptive circular CNC-72

CENTRAL SCIENTIFIC COMPANY

Scientific Instruments • Laboratory Supplies

1700 Irving Park Road, Chicago 13

CHICAGO NEW YORK NEWARK BOSTON WASHINGTON DETROIT SAN FRANCISCO SANTA CLARA LOS ANGELES TORONTO MONTREAL VANCOUVER

LANCASTER PRESS, INC., LANCASTER, PA.